Journal of *Fungi*

Special Issue Reprint

Plant Pathogens and Mycotoxins

Edited by
Martín Gustavo Theumer and José Sebastián Dambolena

mdpi.com/journal/jof

MDPI

Plant Pathogens and Mycotoxins

Plant Pathogens and Mycotoxins

Guest Editors

Martín Gustavo Theumer
José Sebastián Dambolena

MDPI

Basel • Beijing • Wuhan • Barcelona • Belgrade • Novi Sad • Cluj • Manchester

Guest Editors

Martín Gustavo Theumer
Centro de Investigaciones en Bioquímica Clínica e Inmunología (CIBICI-CONICET-UNC)
Córdoba
Argentina

José Sebastián Dambolena
Instituto Multidisciplinario de Biología Vegetal (IMBIV, CONICET-UNC)
Universidad Nacional de Córdoba
Córdoba
Argentina

Editorial Office
MDPI AG
Grosspeteranlage 5
4052 Basel, Switzerland

This is a reprint of the Special Issue, published open access by the journal *Journal of Fungi* (ISSN 2309-608X), freely accessible at: https://www.mdpi.com/journal/jof/special_issues/Y3J3N03BDX.

For citation purposes, cite each article independently as indicated on the article page online and as indicated below:

Lastname, A.A.; Lastname, B.B. Article Title. *Journal Name* **Year**, *Volume Number*, Page Range.

ISBN 978-3-7258-8169-7 (Hbk)
ISBN 978-3-7258-8170-3 (PDF)
https://doi.org/10.3390/books978-3-7258-8170-3

© 2026 by the authors. Articles in this reprint are Open Access and distributed under the Creative Commons Attribution (CC BY) license. The reprint as a whole is distributed by MDPI under the terms and conditions of the Creative Commons Attribution-NonCommercial-NoDerivs (CC BY-NC-ND) license (https://creativecommons.org/licenses/by-nc-nd/4.0/).

Contents

About the Editors . . . . . **vii**

Preface . . . . . **ix**

Haiyang Li, Panpan Zhang, Xueqian Song, Huiying Li, Cong Chen, Limin Wang, et al.
T-DNA Mutagenesis Reveals FpPer1 as a Dual-Function Regulator of Virulence and Fungicide Resistance in *Fusarium pseudograminearum*
Reprinted from: *J. Fungi.* **2025**, *11*, 673, https://doi.org/10.3390/jof11090673 . . . . . **1**

Xiaoli Yu, Shuhan Yang, Panhong Su, Haiyao Bi, Yaxuan Li, Xingxing Peng, et al.
4-Propylphenol Alters Membrane Integrity in Fungi Isolated from Walnut Anthracnose and Brown Spot
Reprinted from: *J. Fungi.* **2025**, *11*, 610, https://doi.org/10.3390/jof11090610 . . . . . **13**

Amel Bennacer, Fatma Sahir-Halouane, Micaela Alvarez, Zahia Oukali, Nour El Houda Bennacer, Abdelhamid Foughalia and Josué Delgado
Talaromyces pinophilus Strain HD25G2 as a Novel Biocontrol Agent of *Fusarium culmorum*, the Causal Agent of Root and Crown Rot of Soft Wheat
Reprinted from: *J. Fungi.* **2025**, *11*, 588, https://doi.org/10.3390/jof11080588 . . . . . **31**

Zamir K. Punja, Sheryl A. Tittlemier and Sean Walkowiak
Fusarium Species Infecting Greenhouse-Grown Cannabis (*Cannabis sativa*) Plants Show Potential for Mycotoxin Production in Inoculated Inflorescences and from Natural Inoculum Sources
Reprinted from: *J. Fungi.* **2025**, *11*, 528, https://doi.org/10.3390/jof11070528 . . . . . **46**

Andrés G. Jacquat, Natalia S. Podio, María Carmen Cañizares, Pilar A. Velez, Martín G. Theumer, Vanessa A. Areco, et al.
The Growth, Pathogenesis, and Secondary Metabolism of *Fusarium verticillioides* Are Epigenetically Modulated by Putative Heterochromatin Protein 1 (FvHP1)
Reprinted from: *J. Fungi.* **2025**, *11*, 424, https://doi.org/10.3390/jof11060424 . . . . . **64**

Chun Wang, Liang Wang, Xuanjie Zhao, Lei Hou, Qingran Liu, Rui Ren, et al.
Functional Analysis of *FoCrpA* in *Fusarium oxysporum* Causing Rice Seedling Blight
Reprinted from: *J. Fungi.* **2025**, *11*, 317, https://doi.org/10.3390/jof11040317 . . . . . **89**

Holly P. Bartholomew, Christopher Gottschalk, Bret Cooper, Michael R. Bukowski, Ronghui Yang, Verneta L. Gaskins, et al.
Omics-Based Comparison of Fungal Virulence Genes, Biosynthetic Gene Clusters, and Small Molecules in *Penicillium expansum* and *Penicillium chrysogenum*
Reprinted from: *J. Fungi.* **2025**, *11*, 14, https://doi.org/10.3390/jof11010014 . . . . . **104**

Zhimin Yang, Huali Xue, Ye Han, Hui Ding and Ying Zhang
Research Progress and Management Strategies for the Common Mycotoxin Contamination of Traditional Chinese Medicines
Reprinted from: *J. Fungi.* **2025**, *11*, 411, https://doi.org/10.3390/jof11060411 . . . . . **130**

About the Editors

Martín Gustavo Theumer

Martín Gustavo Theumer is a career researcher at the Argentinian National Research Council (CONICET) and Professor of Food Microbiology in the Department of Clinical Biochemistry, Faculty of Chemical Sciences, National University of Córdoba, Argentina. He has participated in numerous research projects focused on plant defense mechanisms in the maize–*Fusarium verticillioides* and peanut–*Thecaphora frezii* pathosystems, as well as on the toxic effects of aflatoxin B1, fumonisin B1, and *T. frezii* extracts in animal cells.

José Sebastián Dambolena

José Sebastián Dambolena is a career researcher at the Argentinian National Research Council (CONICET) and Professor of Natural Products at the Faculty of Exact, Physical and Natural Sciences, National University of Córdoba, Argentina. His research focuses on phytopathogenic fungi, particularly *Fusarium* species affecting maize, and on the occurrence and regulation of mycotoxin biosynthesis, especially fumonisins. His work integrates fundamental and applied approaches to understand and control fungal contamination in crops, including the study of natural compounds and their effects on fungal growth and toxin production. He is currently involved in the study of mycoviruses as tools for controlling fungi and associated mycotoxins, as well as developing naturally derived pesticides for pest management in maize.

Preface

This reprint addresses phytopathogenic fungi, mycotoxin biosynthesis, and mycoviruses. It aims to compile recent advances on plant–fungal interactions, toxin regulation, and mycovirus–host relationships. Motivated by the need for sustainable disease control, it is addressed to researchers in plant pathology, mycology, and agricultural sciences.

Martín Gustavo Theumer and José Sebastián Dambolena
Guest Editors

Journal of *Fungi*

MDPI

Article

T-DNA Mutagenesis Reveals FpPer1 as a Dual-Function Regulator of Virulence and Fungicide Resistance in *Fusarium pseudograminearum*

Haiyang Li †, Panpan Zhang †, Xueqian Song †, Huiying Li, Cong Chen, Limin Wang, Zhifang Wang, Lingjun Hao, Yun Li, Xinlong Wang, Jiangang Kang, Honglian Li, Min Wang * and Shengli Ding *

College of Plant Protection, Henan Agricultural University, Zhengzhou 450046, China
* Correspondence: wangm@henau.edu.cn (M.W.); shengliding@henau.edu.cn (S.D.)
† These authors contributed equally to this article.

Abstract: *Fusarium* crown rot (FCR), caused by *Fusarium pseudograminearum*, is a devastating wheat disease leading to significant yield losses worldwide. However, the pathogenic mechanism of *F. pseudograminearum* and its resistance to fungicides remain poorly understood. In this study, we identified a hypothetical gene encoding GPI-anchored protein, designated FpPer1, by screening a T-DNA insertion mutant library of *F. pseudograminearum* for tebuconazole resistance. The Δ*Fpper1* mutant exhibited increased sensitivity to the triazole antifungal drugs and fludioxonil. Additionally, the deletion of *FpPER1* impaired fungal growth, conidiation, and pathogenicity in barley leaves and wheat coleoptiles. Furthermore, the Δ*Fpper1* mutant displayed enhanced susceptibility to various environmental stresses, including NaCl, CR, sorbitol, H_2O_2, and SDS. The mutant also showed reduced penetration peg formation and impaired reactive oxygen species (ROS) scavenging ability during infection. Subcellular localization analysis revealed that FpPer1-GFP co-localized with the endoplasmic reticulum (ER) marker RFP-HDEL in both conidia and hyphae, indicating its localization in the ER. In summary, our findings demonstrate that *FpPER1* plays an important role in pathogenicity and fungicide resistance in *F. pseudograminearum*. This study not only provides a theoretical foundation for understanding fungal virulence mechanisms but also offers practical insights for developing novel fungicide strategies.

Keywords: *Fusarium* crown rot; *Fusarium pseudograminearum*; *FpPER1*; pathogenicity; fungicide

1. Introduction

Wheat is one of the most important crops globally, with production steadily increasing due to advances in breeding techniques and agronomic management [1,2]. However, several factors hinder wheat production. *Fusarium* crown rot (FCR) caused by *F. pseudograminearum* is a soil-borne wheat disease, firstly reported in China by our research group [3]. *F. pseudograminearum* can infect wheat throughout its entire growth cycle, causing FCR through coleoptile and root infection or *Fusarium* head blight (FHB) via spike colonization, both of which significantly compromise grain yield and quality [4–6]. Recently, the lack of available resistant varieties [7], coupled with limited effective control measures, has led to an increase in FCR incidence, impacting approximately 3.3 million hectares in China's Huanghuai wheat area in 2024. Therefore, exploring the growth and development mechanisms, and pesticide resistance of *F. pseudograminearum* is crucial for

understanding the disease's occurrence and provides a theoretical basis for developing effective prevention and control strategies.

As FCR becomes a serious disease in wheat production, researchers are increasingly focusing on the molecular mechanisms that regulate the biological function in *F. pseudograminearum*. Recent studies have made significant progress in identifying key regulatory genes that influence pathogenicity in *F. peseudograminearum*. The key component of the Rpd3S complex, FpRco1, has been characterized to modulate vegetative growth and pathogenicity in *F. pseudograminearum* through mutant library screening [8]. Liu reported that FpZRA1 plays an important role in regulating fungal development, deoxynivalenol (DON) biosynthesis, and pathogenicity, with its expression induced by fungicides [9]. The transcription factor Fp487 is essential for growth and virulence in *F. pseudograminearum*, making it a potential RNAi target for RNA interference (RNAi) in managing FCR [10]. In addition, recent advances in pathogen-host interaction studies have identified and characterized two pathogen-associated molecular patterns (PAMPs), namely FpCDP1 and Fp00392 [11,12]. In summary, several key genes involved in the growth and pathogenicity of *F. pseudograminearum* have already been identified.

Targeting key genes that regulate fungal growth, development, and pathogenicity has emerged as a pivotal strategy for fungicide exploitation. Benzimidazole fungicides target fungal β-tubulin, effectively inhibiting microtubule assembly and disrupting essential cellular processes [13]. Similarly, phenamacril specifically binds to myosin I (MyoI), inhibiting its ATPase activity [14]. Sterol demethylation inhibitors (DMIs) block the demethylation process of ergosterol, leading to fungal cell death [15]. Succinic dehydrogenase inhibitors (SDHIs) block the activity of succinate dehydrogenase, ultimately disrupting fungal growth [16]. However, emerging studies have demonstrated that the long-term use of pesticides can lead to the development of fungicide resistance [17]. Ipconazole is an effective fungicide against *F. pseudograminearum*; however, the point mutation G464S of FpCYP51B has been found to confer resistance to ipconazole in the pathogen [18]. Therefore, identifying novel pesticide targets and understanding their resistance mechanisms are crucial for the development of new fungicide.

Glycosylphosphatidylinositol (GPI) is a posttranslational modification that plays an important role in anchoring cell-surface proteins to membranes via lipid modification in eukaryotes [19]. Numerous studies have indicated that GPI-anchored proteins are implicated in a wide range of cellular processes. It was found that the GPI-anchored protein ScPer1 was required for GPI-phospholipase A2 activity, and the mutant Δscper1 was functionally complemented by human ortholog PERLD1 [20]. In plant fungal pathogen *Cochlibolus heterostrophus*, the GPI ethanolamine phosphate transferase gene *ChGPI7* is critical for infection by regulating cell wall integrity and immune evasion [21]. These findings highlight the pivotal roles of GPI-anchored proteins across various biological functions.

Although some functions of the GPI-anchored proteins in pathogens have been elucidated, many issues remain unresolved. In this study, we employed a forward genetics approach to identify the genes targeted by fungicide via screening T-DNA insertion mutants. Our results determined that FpPer1 plays a crucial role in growth and pathogenicity, particularly in enhancing tolerance to fungicides, which may aid in the development of new pesticides in the future.

2. Materials and Methods

2.1. Strain and Culture Conditions

The wild-type *F. pseudograminearum* (WZ-8A), *Escherichia coli* (DH5α), and vectors pKOV21 containing the hygromycin phosphotransferase gene (*HPH*), pKNTG containing

the green fluorescent protein gene (*GFP*), and pKOV21-*HDEL-RFP* were used in this study. The following culture media were employed: PDA medium was used for the general culture of *F. pseudograminerum*; YEPD medium for mycelium collecting; Carboxymethyl cellulose (CMC) for spore collection of *F. pseudograminearum*; and LB medium was used for bacterial culture. All required primers were synthesized by Shanghai Bioengineering with some sequences presented in Table S1.

2.2. Knockout and Complementation of the FpPER1 Gene

The candidate gene *FpPER1* was deleted in *F. pseudograminearum* using split-marker methods. Initially, approximately 1.0 kb of the fragments of upstream L1 and downstream L2 were amplified using primers 1F/2R and 3F/4R, respectively, with the genome of WZ-8A strain serving as the template. Subsequently, using the fusion fragments L1, *HPH*, and L2 as templates, the fragments of L1H1 and L2H2 were amplified via primers 1F/HY-R and HY-F/4R, respectively. Finally, the mixed fragments of L1H1 and L2H2 were employed for PEG-mediated transformation to knock out the targeting gene (*FpPER1*) in WZ-8A. The primers utilized were shown in Table S1.

We conducted the complementation experiment on the mutant following the knockout experiment adhering to the aforementioned PEG-mediated protoplast transformation method. The *FpPER1* gene with its native promoter was cloned into the pKNTG vector. The complementation transformations of c*FpPer1* were screened using G418 resistance and confirmed by PCR with primers of NF/NR.

2.3. Biological Assays

The fungal growth rate was measured firstly, and the deletion mutant, complementation mutants, and wild-type (WZ-8A) were inoculated on PDA plates for 3 d at 25 °C. Subsequently, the diameters of the different strains were measured. For conidiation assays, fresh mycelial blocks were inoculated in CMC medium with shaking at 150 rpm for 5 d at 25 °C. Those experiments were performed in triplicate with three treatments each.

2.4. Pathogenicity Assay

Barley leaves, cultivated for 5 days, were used for inoculation with 5 mm fungal blocks. The fungal blocks were removed after 24 h of dark incubation. The plants were photographed after 3 d. Alternatively, when coleoptiles grew to 2–3 cm in length, wounds at the stem base were inoculated with 2 μL of conidial suspension at a concentration of 1.0×10^7/mL in ddH_2O after the apex was cut. The treatments were maintained at 25 °C in a moist chamber in the dark for 24 h, and then the plants were subsequently photographed after being cultured under light/night for one week.

2.5. Subcellular Localization of FpPer1

The wild-type strain of *F. pseudograminearum* was co-transformed with the pKNTG-*FpPER1* plasmid and the pKOV21-*RFP-HDEL* plasmid using the previously mentioned PEG-mediated method. The hyphae of the co-transformed strains were cultured and collected, and fluorescence localization of FpPer1 was observed in the co-transformed strains.

2.6. Sensitivity Assays to Different Fungicides

The technical-grade active ingredients of tebuconazole, difenoconazole, epoxiconazole, and fludioxonil were separately dissolved in 1 mL of acetone and then diluted with sterile water to prepare 5 ppm solutions. Under sterile conditions, an appropriate amount of the prepared pesticide solution was added to sterilize PDA medium in conical flasks to prepare PDA plates containing the corresponding fungicide concentrations (0.084 ppm

Tebuconazole, 0.4 ppm Difenoconazole, 0.1 ppm Epoxiconazole, and 0.05 ppm Fludioxonil), followed by thorough mixing. Then, 15 mL of the mixture was poured into 9 cm-diameter Petri dishes. Fresh mycelial plugs were inoculated onto the fungicide-containing plates and control plates for cultivation, and the inhibitory effects of the respective fungicides were calculated.

3. Results

3.1. Identification of Tebuconazole Resistance-Related Genes by Screening Mutant Library

Tebuconazole represents one of the most effective fungicides for controlling FCR. However, its precise mode of action against *F. pseudograminearum* remains incompletely understood. To investigate this, we screened our previously established T-DNA insertion mutant library [8] and identified significant variations in tebuconazole sensitivity among different mutants compared to the wild-type WZ-8A strain. Among them, the mutant W30 exhibited a markedly decreased resistance to tebuconazole (Figure 1). The T-DNA insertion position was confirmed within the FPSE_01026 gene in *F. pseudograminearum* via nested-PCR (Figure S1). The gene encodes the predicted protein with 331 amino acids. Functional domain analysis of the protein encoded by the FPSE_01026 gene revealed that this protein contains signal peptide in N terminal and Per1-like domain in C terminal (Figure 2A), consequently designating it as FpPer1. Phylogenetic analysis has uncovered that FpPer1 in *F. pseudograminearum* exhibits a relatively high affinity with *Fusarium austroamericanum* and *Fusarium graminearum*, compared to *Magnaporthe oryzae*, *Neurospora crassa*, *Colletotrichum tanaceti*, *Colletotrichum gloeosporioides*, *Sclerotinia sclerotiorum*, and *Botrytis cinerea* (Figure 2B).

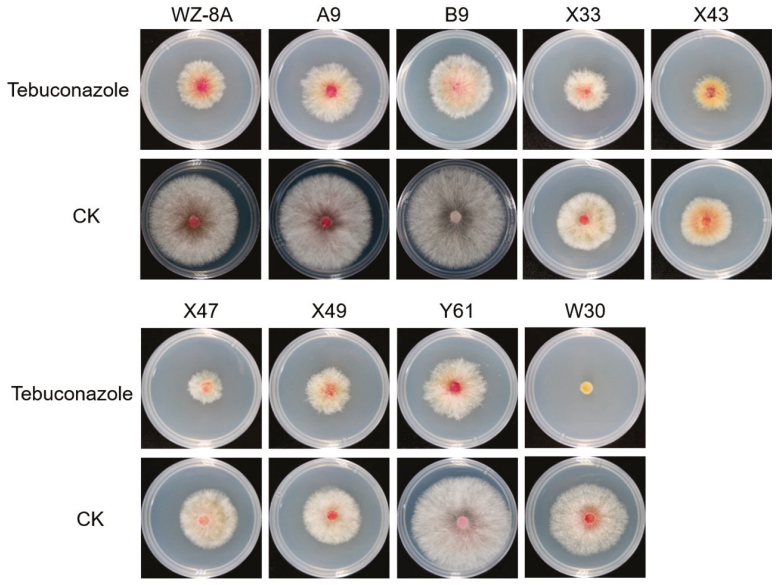


Figure 1. Identification of T-DNA insertion mutants associated with tebuconazole resistance. The top panel displays the mycelial growth of *F. pseudograminearum* on PDA plates supplemented with tebuconazole, while the bottom panels show the mycelial growth on PDA plates without tebuconazole (control). The colonies were measured and photographed two days post-inoculation on PDA plates. All experiments were conducted at least three times with independent biological replicates.

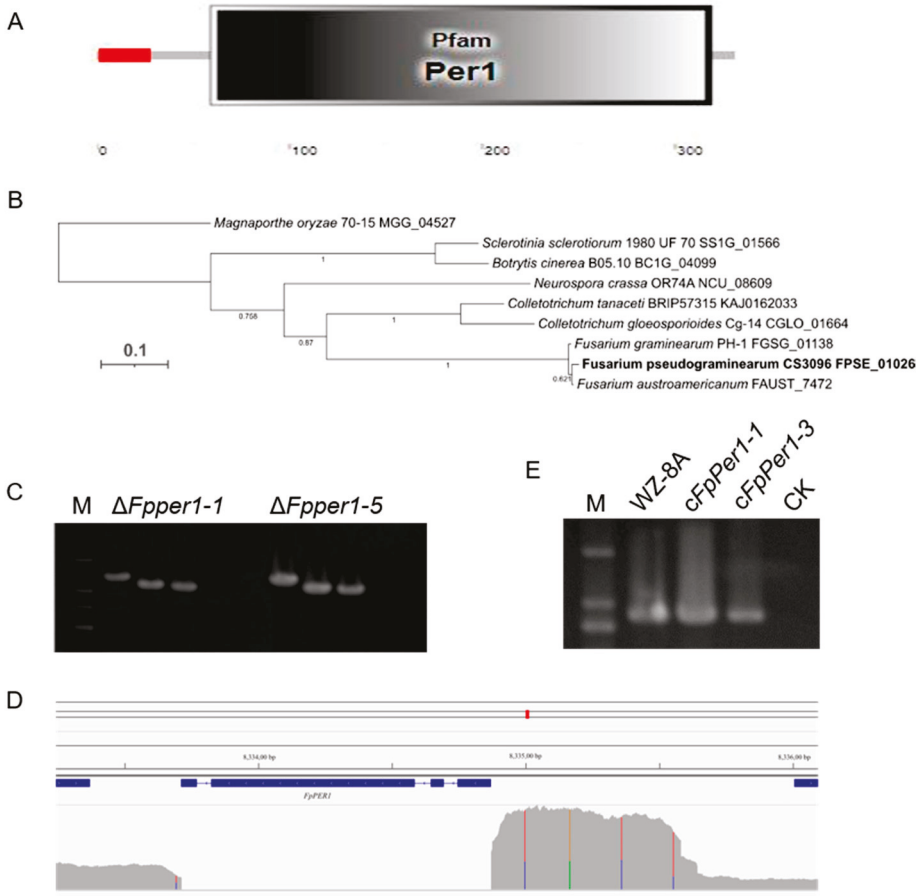


Figure 2. Deletion and complementation of *FpPER1* in *F. pseudograminearum*. (**A**), structural domain of FpPer1, predicted using Smart (http://smart.embl.de/) (accessed on 1 May 2019). The red square indicates signal peptide domains that direct protein transportation, while the gray square represents the Per1-like domain, a GPI-anchoring structure. (**B**), the phylogenetic evolutionary tree of FpPer1 (the bold text) and its orthologs, constructed using MrBayes v 3.1.2. (**C**), the agarose gel results of the PCR screening, revealing the products of in sizes of 1385 bp, 1053 bp, 971 bp, and 861 bp for the Δ*Fpper1-1* and Δ*Fpper1-5* mutants, using four pairs of primers: HYG-F/HYG-R, 1F/2R, 3F/4R, and NF/NR, respectively. (**D**), confirming the complete deletion of *FpPER1* in the genome of the Δ*Fpper1-1* mutant through genomic resequencing, which was performed using the WZ-8A genome as the reference. (**E**), the PCR screening products for WZ-8A, c*FpPer1-1* and c*FpPer1-3* obtained with primer NF/NR, resulting in a product size in 861 bp.

3.2. FpPER1 Is Involved in Growth and Conidia Production of F. pseudograminearum

To elucidate the function of FpPer1 in fungicides resistance and other biological processes, we generated *FpPER1* knockout using the split-marker method. Among the transformants obtained, the deletion of gene *FpPER1* in two transformants was verified by PCR (Figure 2C). Furthermore, the whole-genome resequencing of Δ*Fpper1-1* confirmed the complete deletion of the *FpPER1* locus form the *F. pseudograminearum* genome (Figure 2D). Additionally, we constructed complementary strain (c*FpPer1*) that reintroduced *FpPER1* under its native promoter (Figure 2E). Phenotypic characterization revealed that the Δ*Fpper1* mutant exhibited a significantly reduced growth rate and impaired aerial hyphae formation compared to both WZ-8A and complemented strains, indicating the critical role of *FpPER1* in vegetative growth (Figure 3A). Furthermore, the mutant displayed severe conidiation defects, including a reduction in conidial production and abnormal conidial morphology characterized by smaller size. Microscopic analysis revealed that the conidial septum decreased (Figure 3B–D). Regarding the decrease in sporulation, we observed that Δ*Fpper1* exhibited significant hyphal expansion in CMC medium (Figure 3E). Through observation

and analysis of sporulation, we determined that the *FpPER1* gene significantly influences the sporulation of *F. pseudograminearum*. In other words, the *FpPER1* gene impacts the reproduction of *F. pseudograminearum*.

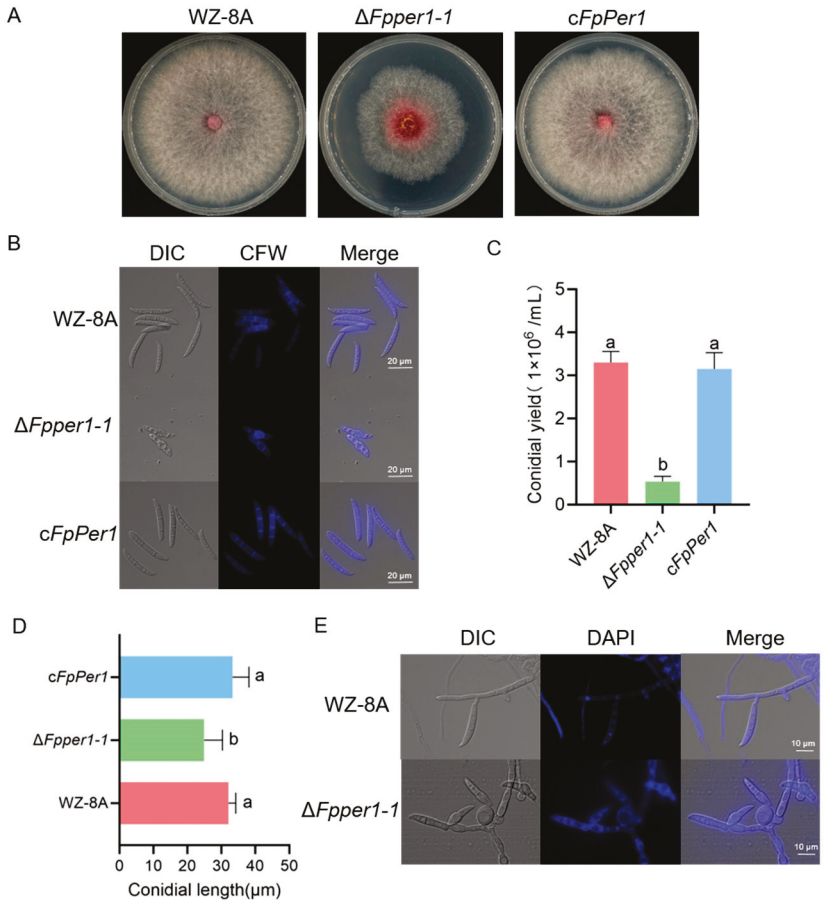


Figure 3. FpPer1 regulates the vegetative growth of *F. pseudograminearum*. (**A**), comparison of colony morphology among the strains WZ-8A, Δ*Fpper1-1*, and the c*FpPer1* on PDA plates. (**B**–**E**), *FpPER1* is involved in conidial formation in *F. pseudograminearum*. (**B**), WZ-8A, Δ*Fpper1-1*, and the complementary strain were cultured in CMC medium for 5 days, photographed using a microscope, and conidia were stained by calcofluor white (CFW) (scale bars = 20 μm). (**C**), the number of conidia was counted. (**D**), the length of conidia was measured. (**E**), the morphology of the mycelium was observed after culturing in CMC medium (scale bars = 10 μm). The mean values ± SD are presented, with lowercase letters (a, b) indicating groups of significant differences as determined by Duncan's multiple comparison procedures ($p < 0.05$). All experiments were conducted at least three times.

3.3. Deletion Mutant ΔFpper1 Shows Increased Sensitivity to Various Stress Conditions

During pathogen infection of the host, it encounters various environmental stresses, including oxidation, osmotic, and cell wall integrity stresses. To investigate the response of WZ-8A, Δ*Fpper1*, and the complementary strain under different stress conditions, these strains were cultured on PDA supplemented with NaCl, Congo Red (CR), sorbitol, H_2O_2, and SDS. Colony diameters were measured, and inhibition rates under different stress conditions were calculated. The results indicated that the deletion of *FpPER1* resulted in increased sensitivity to NaCl, CR, sorbitol, H_2O_2, and SDS compared to WZ-8A and complemented strains (Figure 4A,B). These findings demonstrated that *FpPER1* plays an important role in *F. pseudograminearum*'s adaptation to diverse environmental stresses.

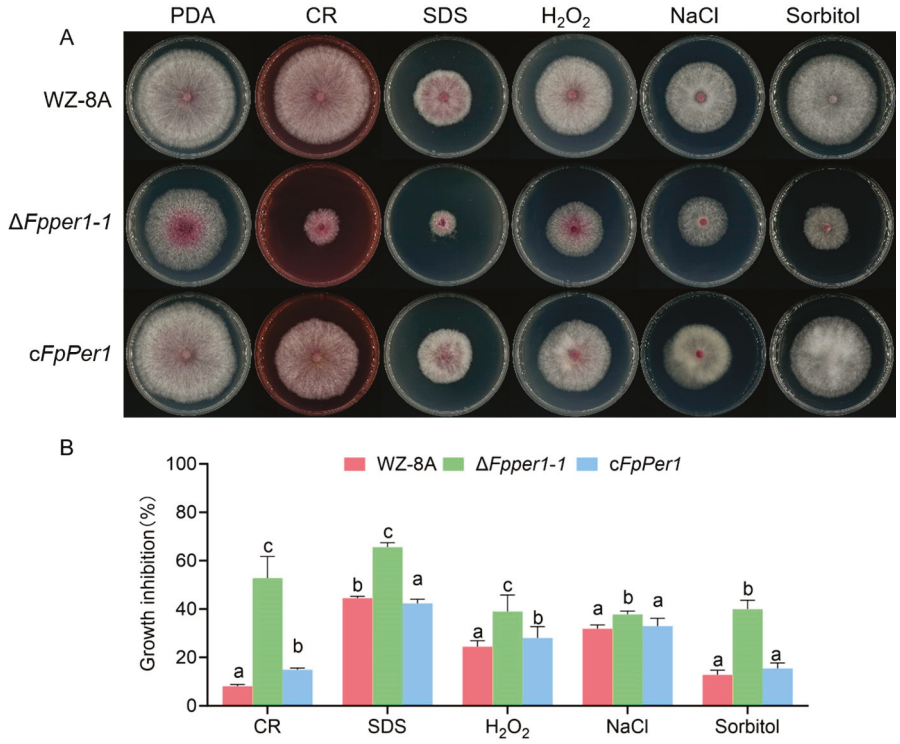


Figure 4. Sensitivity assays of the WZ-8A, Δ*Fpper1-1*, and c*FpPer1* strains under various stress conditions. (**A**), colonies of the strains on PDA medium, both without and with 0. 2 mg/mL Congo Red (CR), 0.025% SDS, 10 mM H_2O_2, 1 M NaCl, and 1.5 M Sorbitol. (**B**), colony diameters were measured, with the inhibition rates calculated under different stress conditions. The mean values ± SD from three repetitions are shown, with lowercase letters (a–c) indicating significantly different groups as calculated by Duncan's multiple comparison procedures ($p < 0.05$).

3.4. FpPER1 Is Essential for Full Virulence in F. pseudograminearum

To assess the pathogenicity of Δ*Fpper1*, conidial suspensions of WZ-8A, the Δ*Fpper1* mutant, and the complementary strain were inoculated onto the wounded wheat coleoptiles. The lesions caused by the Δ*Fpper1* mutant were significantly smaller than those caused by WZ-8A and complemented strain (Figure 5A). Similarly, pathogenic assays on barley leaves revealed that the Δ*Fpper1* mutant exhibited reduced virulence compared to the WZ-8A and complemented strains (Figure 5B). To investigate the underlying cause of this reduced pathogenicity of Δ*Fpper1*, we examined the infection process in wheat coleoptiles. Microscopic observations demonstrated that WZ-8A and complemented strains efficiently formed penetration pegs to facilitate host invasion, whereas Δ*Fpper1* exhibited a marked reduction in penetration peg formation (Figure 5C). Given that Δ*Fpper1* showed increased sensitivity to H_2O_2 in vitro, we further evaluated whether FpPer1 is important for scavenging reactive oxygen species (ROSs) during early infection. DAB staining revealed that stronger brown discoloration in Δ*Fpper1*-infected coleoptiles cells compared to those infected by the WZ-8A and complementary strain, suggesting higher ROS accumulation in the absence of *FpPER1* (Figure 5D,E). These results indicate that *FpPER1* regulates penetration peg formation, thereby affecting the pathogenicity of *F. pseudograminearum*, and also modulates host immunity by mitigating ROS accumulation.

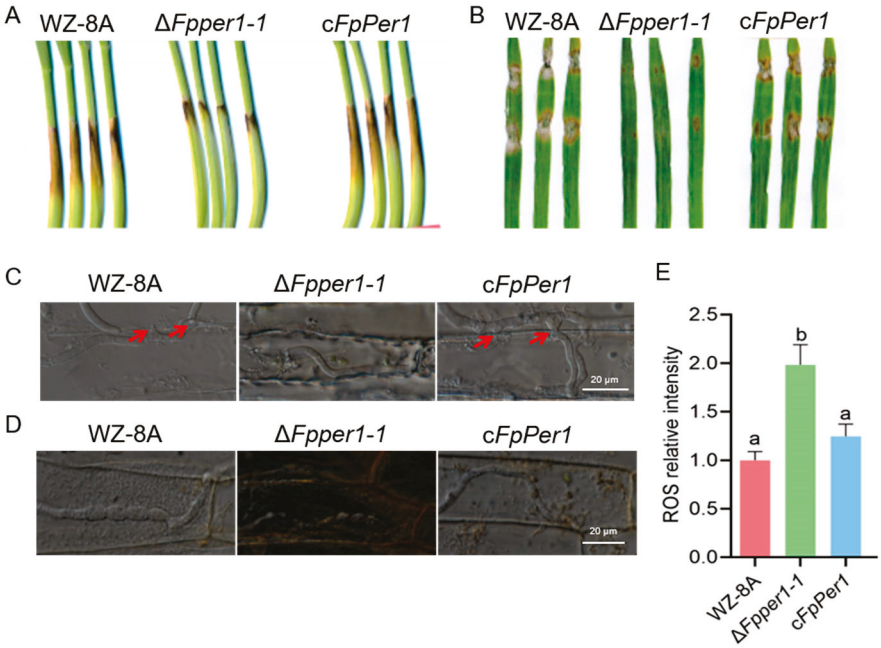


Figure 5. Pathogenicity assay of WZ-8A, Δ*Fpper1-1*, and c*FpPer1*. (**A**), the pathogenicity of these strains in coleoptiles inoculated with conidial suspension for 7 days. (**B**), the pathogenicity of the different strains in barley leaves with inoculated fresh fungal blocks for 3 days. (**C**), the infection process of the different strains in wheat coleoptile cell was observed under a microscope (scale bars = 20 μm), and the red arrow indicates the location of penetration peg formation. (**D**), ROS accumulation in infected coleoptiles was analyzed through DAB staining (scale bars = 20 μm). (**E**), the relative levels of reactive oxygen species (ROS) were measured in cells following infection with different strains. The mean values ± SD are presented, with letters (a, b) indicating groups of significant differences as determined by Duncan's multiple comparison procedures ($p < 0.05$). All experiments were performed in triplicate.

3.5. FpPer1 Locates in the Endoplasmic Reticulum in F. pseudograminearum

Previous studies have reported that the Per1 protein is typically located in the endoplasmic reticulum (ER), which is required for GPI-phospholipase A2 activity [20]. To explore the subcellular localization of FpPer1 in *F. pseudograminearum*, we co-transformed two vectors, encoding FpPer1-GFP and the ER marker RFP-HDEL into the wild-type strain. The results showed that the green fluorescent signal and red fluorescent signal completely merged in conidia, but did not merge with the blue signal, indicating that FpPer1 is localized in the ER, not the nucleus (Figure 6A). Furthermore, we observed identical ER localization patterns for FpPer1 during the hyphae stage (Figure 6B). These results demonstrate that FpPer1 functions in the endoplasmic reticulum of *F. pseudograminearum*.

3.6. FpPer1 Involves in Resistance to Pesticide in F. pseudograminearum

Having established FpPer1's involvement in tebuconazole resistance, we further investigated its potential role in conferring resistance to other fungicides. We selected three additional widely used fungicides that have demonstrated efficacy against *F. pseudograminearum*: difenoconazole, epoxiconazole, and fludioxonil. Interestingly, when the wild-type, Δ*Fpper1*, and complementary strain were cultured on PDA containing tebuconazole, difenoconazole, epoxiconazole, and fludioxonil, the mutant Δ*Fpper1-1* strain exhibits a stronger inhibition rate than that of the wild-type and complementary strain (Figure 7A,B). These consistent findings across multiple fungicide classes suggest that FpPer1 likely functions as a key regulator in a common resistance pathway targeted by diverse pesticides in *F. pseudograminearum*.

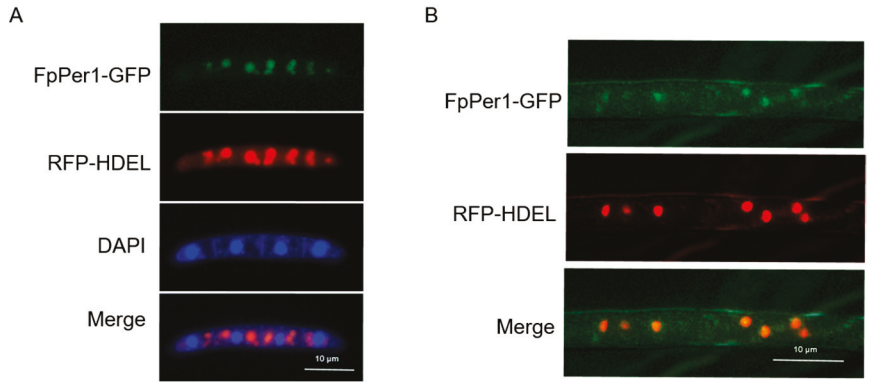


Figure 6. Subcellular localization of FpPer1 in *F. pseudograminearum*. (**A**), the fluorescence of FpPer1-GFP and RFP-HDEL in conidia, observed using a fluorescence microscope, with DAPI employed for nuclear staining (scale bars = 10 μm). (**B**), the fluorescence of FpPer1-GFP and RFP-HDEL in the hyphae of *F. pseudograminearum* was observed (scale bars = 10 μm). All experiments were conducted three times.

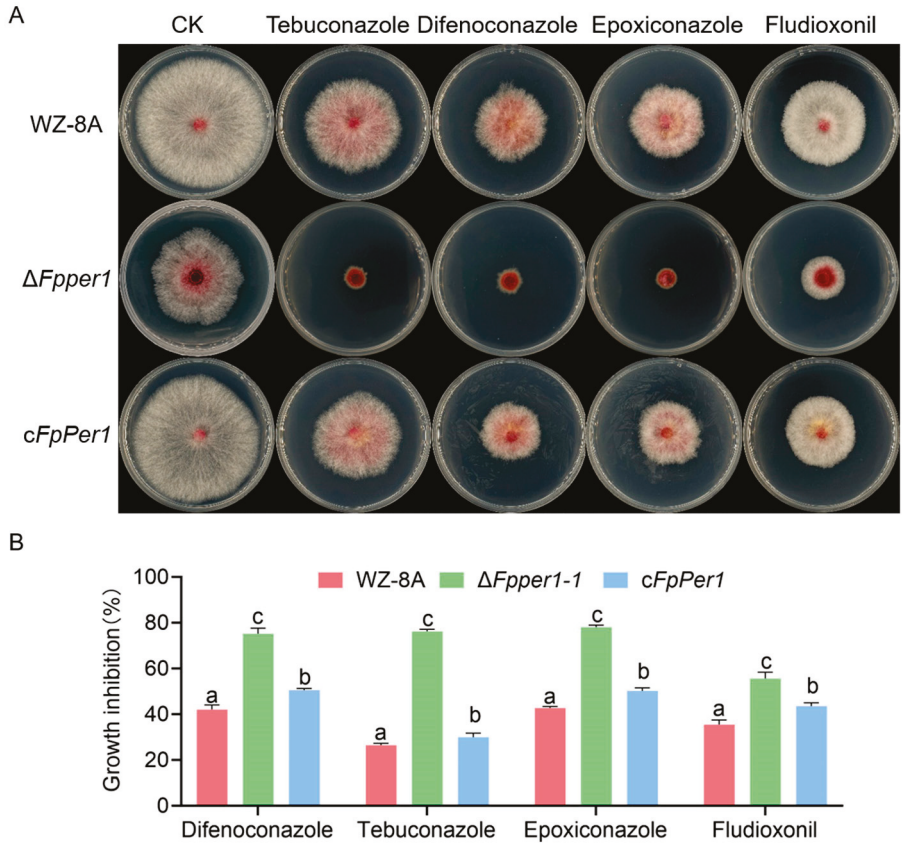


Figure 7. Sensitivity assays of WZ-8A, Δ*Fpper1-1*, and c*FpPer1* strains to various fungicides. (**A**), colonies of the strains grown on PDA medium with and without 0.084 ppm tebuconazole, 0.4 ppm difenoconazole, 0.1 ppm epoxiconazole, and 0.05 ppm fludioxonil. (**B**), colonies were photographed, and the inhibition rates were calculated for different fungicides. The mean values ± SD from three repetitions are presented. Lowercase letters (a–c) indicate significantly different groups as determined by Duncan's multiple comparison procedures ($p < 0.05$).

4. Discussion

Forward genetics, as a classical genetic approach that combines phenotypic screening with gene mapping, has been extensively validated as a powerful tool for identifying the functions of uncharacterized genes. In this study, we identified a GPI-anchored protein, FpPer1, involved in resistance to pesticides in *F. pseudograminearum* using a forward genetics

method. Through integrated genetic and biochemical approaches, we demonstrated that FpPer1 played an important role in both pathogenicity and response to various environmental stresses. Our research on the *FpPER1* gene highlights its promise as a target for novel fungicides. Disrupting *FpPER1* could desynchronize fungal growth, reproduction, and infection processes, providing a precise, sustainable strategy for crop disease management.

Emerging evidence suggests that long-term use of single-action fungicides can induce the development of fungicide resistance for pathogens. The risk can be substantially mitigated through the combined application of fungicides with different mechanisms of action. For instance, combined application of fluazinam with triazole enhances the synergistic activity against *F. pseudograminearum* [22]. Similarly, it is an effective way to control fungal leaf diseases using the mixtures of flutriafol and azoxystrobin [23]. These findings highlight the importance of identifying novel fungicide targets in *F. pseudograminearum*. Previous reports indicated that Per1 modulates resistance to triazole drugs in *Aspergillus fumigatus* and *M. oryzae* [24,25]. We found that FpPer1 regulates resistance not only to triazole drug but also to fludioxonil, suggesting that FpPer1 may modulate multiple signaling pathways involved in pesticide resistance. Probably, the incompleteness of the cell wall protein in the Δ*Fpper1* mutant may be contribute to its increased sensitivity to pesticides. Another possible reason is that Afper1 supports cell development by modulating UPR-mediated ER homeostasis in *A. flavus* [26]. Disturbed ER homeostasis may also explain the loss of fungicide resistance in the Δ*Fpper1* mutant of *F. pseudograminearum.* Our findings reveal that FpPer1 plays a critical role in pesticide resistance in *F. pseudograminearum*. Furthermore, the Δ*Fpper1* mutant exhibited heightened sensitivity to antifungal agents, suggesting that FpPer1 is a potential molecular target for new fungicides. In the future, combining novel FpPer1-targeting compounds with triazole fungicides could significantly improve the management of *Fusarium* crown rot.

Disruption of *FpPER1* resulted in defects in both growth and pathogenicity in *F. pseudograminearum*, which may be attributed to defects in cellular integrity. Given that cell wall and membrane integrity are vital for maintaining cellular morphology, responding to environmental stress, and defending against pathogens [27,28], the observed hypersensitivity of the Δ*Fpper1* mutant to various environmental stresses suggests underlying issues with cellular integrity. Furthermore, pathogenic fungi depend on specialized infection structures, such as appressoria and penetration pegs, for successful host invasion [29–32]. While *MoPER1* has been demonstrated to regulate appressorium formation in *M. oryzae* [25], our findings reveal that the deletion of *FpPER1* impairs penetration pegs formation in *F. pseudograminearum*, representing a significant factor contributing to its reduced pathogenicity. In addition, GPI anchoring of protein is a conserved post-translational modification that occurs in endoplasmic reticulum [33]. However, it remains unclear whether the ER-localized protein FpPer1 regulates biological processes via lipid remodeling in *F. pseudograminearum*, which requires further investigation.

In conclusion, this study establishes FpPer1 as a multifunctional regulator of pathogenicity and pesticide resistance in *F. pseudograminearum*. Our findings provide a theoretical basis for the development of new fungicides targeting the gene *FpPER1* and offer novel insights into adaptation mechanisms. Future research should focus on elucidating the molecular networks through which FpPer1 coordinates these diverse biological processes.

Supplementary Materials: The following supporting information can be downloaded at: https://www.mdpi.com/article/10.3390/jof11090673/s1, Figure S1: The sequences identified using nested-PCR; Table S1: The primers used in this study.

Author Contributions: Conceptualization, S.D., H.L. (Haiyang Li), and H.L. (Honglian Li); methodology, P.Z., X.S., software, P.Z., X.S., H.L. (Huiying Li) and H.L. (Haiyang Li); validation, P.Z., X.S., L.W. and J.K.; formal analysis, X.S., P.Z., and H.L. (Haiyang Li); investigation, P.Z., X.S., H.L. (Huiying Li), H.L. (Haiyang Li), C.C., Z.W., L.H., Y.L. and X.W.; resources, S.D., H.L. (Haiyang Li) and H.L. (Honglian Li); data curation, P.Z., X.S.; writing—original draft preparation, H.L. (Haiyang Li), P.Z.; writing—review and editing, H.L. (Haiyang Li), S.D., X.S. and P.Z.; visualization, H.L. (Haiyang Li), X.S. and P.Z.; supervision, M.W., H.L. (Haiyang Li); project administration, M.W., H.L. (Haiyang Li); funding acquisition, S.D., H.L. (Haiyang Li). All authors have read and agreed to the published version of the manuscript.

Funding: This research was supported by grants from the National Natural Science Foundation of China (32372511, 31901835), the Natural Science Foundation of Henan Province of China (242300421326), the National Key Research and Development Program of China [2024YFD1400400], the Open Project of the National Key Laboratory of Wheat Improvement (WIKF202410), and the Innovative Research Team (in Science and Technology) in University of Henan Province (25IRTSTHN031).

Data Availability Statement: The original contributions presented in this study are included in the article and Supplementary Material. Further inquiries can be directed to the corresponding authors.

Conflicts of Interest: The authors declare that they have no conflicts of interest.

References

1. Sandiswa, F.; Khayalethu, N.; Learnmore, M.; Tarekegn, T.; Tsilo, J.T.; Hussein, S. Breeding wheat for durable leaf rust resistance in southern Africa: Variability, distribution, current control strategies, challenges and future prospects. *Front. Plant Sci.* **2020**, *11*, 549. [CrossRef]
2. Zhu, Z.; Hao, Y.; Mergoum, M.; Bai, G.; Humphreys, G.; Cloutier, S.; Xia, X.; He, Z. Breeding wheat for resistance to Fusarium head blight in the Global North: China, USA, and Canada. *Crop J.* **2019**, *7*, 730–738. [CrossRef]
3. Li, H.L.; Yuan, H.X.; Fu, B.; Xing, X.P.; Sun, B.J.; Tang, W.H. First report of *Fusarium pseudograminearum* causing crown rot of wheat in Henan, China. *Plant Dis.* **2012**, *96*, 1065. [CrossRef]
4. Jin, J.; Duan, S.; Qi, Y.; Yan, S.; Li, W.; Li, B.; Xie, C.; Zhen, W.; Ma, J. Identification of a novel genomic region associated with resistance to Fusarium crown rot in wheat. *Theor. Appl. Genet.* **2020**, *133*, 2063–2073. [CrossRef] [PubMed]
5. Ma, G.; Wang, H.; Qi, K.; Ma, L.; Zhang, B.; Zhang, Y.; Jiang, H.; Wu, X.; Qi, J. Isolation, characterization, and pathogenicity of *Fusarium* species causing crown rot of wheat. *Front. Microbiol.* **2024**, *15*, 1405115. [CrossRef] [PubMed]
6. Xu, F.; Song, Y.L.; Yang, G.Q.; Wang, J.M.; Liu, L.L.; Li, Y.H. First Report of *Fusarium pseudograminearum* from wheat heads with Fusarium head blight in North China Plain. *Plant Dis.* **2015**, *99*, 156. [CrossRef] [PubMed]
7. He, X.L.; Zhou, H.F.; Yuan, H.X.; Shi, Y.; Sun, B.J.; Li, H.L. Genetic Diversity of *Fusarium pseudograminearum* collected from Henan and Hebei winter wheat regions. *Sci. Agric. Sin.* **2016**, *49*, 272–281.
8. Li, H.Y.; Zhang, Y.; Qin, C.C.; Wang, Z.F.; Hao, L.J.; Zhang, P.P.; Yuan, Y.Q.; Ding, C.P.; Wang, M.X.; Zan, F.F.; et al. Identification and characterization of FpRco1 in regulating vegetative growth and pathogenicity based on T-DNA insertion in *Fusarium pseudograminearum*. *J. Integr. Agric.* **2024**, *23*, 3055–3065. [CrossRef]
9. Jiang, J.; He, K.; Wang, X.; Zhang, Y.; Guo, X.; Qian, L.; Gao, X.; Liu, S. Transcriptional dynamics of *Fusarium pseudograminearum* under high fungicide stress and the important role of FpZRA1 in fungal pathogenicity and DON toxin production. *Int. J. Biol. Macromol.* **2024**, *276*, 133662. [CrossRef]
10. Yang, X.; Cao, S.; Sun, H.; Deng, Y.; Zhang, X.; Li, Y.; Ma, D.; Chen, H.; Li, W. The critical roles of the Zn_2Cys_6 transcription factor Fp487 in the development and virulence of *Fusarium pseudograminearum*: A potential target for Fusarium crown rot control. *Microbiol. Res.* **2024**, *285*, 127784. [CrossRef]
11. Liu, Z.R.; Wang, X.L.; Wang, Z.F.; Hao, L.J.; Qin, C.C.; Zhan, F.F.; Zhang, Y.; Meng, J.X.; Li, Y.; Chen, C.; et al. FpCDP1 from *Fusarium pseudograminearum* is recognized as a novel pathogen-associated molecular pattern that induces plant immunity. *Plant Cell Environ.* **2025**, *48*, 5699–5709.
12. Yang, Q.; Wang, J.; Sun, J.X.; Gao, S.J.; Zheng, H.; Pan, Y.M. A *Fusarium pseudograminearum* secreted protein Fp00392 is a major virulence factor during infection and is recognized as a PAMP. *J. Integr. Agric.* **2025**, *2*, 30.
13. Zhou, Y.J.; Xu, J.Q.; Zhu, Y.Y.; Duan, Y.B.; Zhou, M.G. Mechanism of action of the benzimidazole fungicide on: Interfering with polymerization of monomeric tubulin but not polymerized microtubule. *Phytopathology* **2016**, *106*, 807–813. [CrossRef] [PubMed]
14. Zhang, C.; Chen, Y.; Yin, Y.; Ji, H.H.; Shim, W.B.; Hou, Y.; Zhou, M.; Li, X.D.; Ma, Z. A small molecule species specifically inhibits Fusarium myosin I. *Environ. Microbiol.* **2015**, *17*, 2735–2746. [CrossRef]

15. Ma, B.; Tredway, L.P. Induced overexpression of cytochrome P450 sterol 14α-demethylase gene (CYP51) correlates with sensitivity to demethylation inhibitors (DMIs) in *Sclerotinia homoeocarpa*. *Pest Manag. Sci.* **2013**, *69*, 1369–1378. [CrossRef]
16. Shao, W.; Sun, J.; Zhang, X.; Chen, C. Amino acid polymorphism in succinate dehydrogenase subunit c involved in biological fitness of *Botrytis cinerea*. *Mol. Plant Microbe Interact.* **2020**, *33*, 580–589. [CrossRef]
17. Yin, Y.; Miao, J.; Shao, W.; Liu, X.; Zhao, Y.; Ma, Z. Fungicide resistance: Progress in understanding mechanism, monitoring, and management. *Phytopathology* **2023**, *113*, 707–718. [CrossRef]
18. Li, G.; Zhang, L.; Li, Y.; Li, X.; Gao, X.; Dai, T.; Miao, J.; Liu, X. Analysis of resistance risk and mechanism of the 14α-demethylation inhibitor ipconazole in *Fusarium pseudograminearum*. *Pestic. Biochem. Physiol.* **2024**, *199*, 105786. [CrossRef]
19. Sharom, F.J.; Lehto, M. Glycosylphosphatidylinositol-anchored proteins: Structure, function, and cleavage by phosphatidylinositol-specific phospholipase C. *Biochem. Cell Biol.* **2002**, *80*, 535–549. [CrossRef]
20. Fujita, M.; Umemura, M.; Yoko-o, T.; Jigami, Y. PER1 is required for GPI-phospholipase A_2 activity and involved in lipid remodeling of GPI-anchored proteins. *Mol. Biol. Cell* **2006**, *17*, 5253–5264. [CrossRef]
21. Hu, H.; Liu, T.G.; Xie, X.Y.; Li, F.Y.; Liu, C.Y.; Jiang, J.T.; Li, Z.G.; Chen, X.L. GPI anchoring controls cell wall integrity, immune evasion and surface localization of ChFEM1 for infection of *Cochlibolus heterostrophus*. *J. Integr. Agric.* **2024**. [CrossRef]
22. Zhou, F.; Li, G.L.; Li, J.B.; Zhang, S.; Liang, Y.H.; Gui, Y.J.; Li, W.G.; Liu, R.Q. Combined application of fluazinam with triazole fungicides results in synergistic activity against Fusarium Crown Rot. *Plant Pathol.* **2025**, *74*, 1560–1569. [CrossRef]
23. Silva, T.S.; da Fonseca, L.F.; Yamada, J.K.; Pontes, N.D. Flutriafol and azoxystrobin: An efficient combination to control fungal leaf diseases in corn crops. *Crop. Prot.* **2021**, *140*, 105394. [CrossRef]
24. Chen, Y.; Wu, X.Y.; Li, C.G.; Zeng, Y.B.; Tan, X.Q.; Zhang, D.Y.; Liu, Y. MoPer1 is required for growth, conidiogenesis, and pathogenicity in *Magnaporthe oryzae*. *Rice* **2018**, *11*, 64. [CrossRef] [PubMed]
25. Chung, D.; Thammahong, A.; Shepardson, K.M.; Blosser, S.J.; Cramer, R.A. Endoplasmic reticulum localized PerA is required for cell wall integrity, azole drug resistance, and virulence in *Aspergillus fumigatus*. *Mol. Microbiol.* **2014**, *92*, 1279–1298. [CrossRef]
26. Lv, Y.; Yang, H.; Wang, J.; Wei, S.; Zhai, H.; Zhang, S.; Hu, Y. Afper1 contributes to cell development and aflatoxin biosynthesis in *Aspergillus flavus*. *Int. J. Food Microbiol.* **2022**, *377*, 109828. [CrossRef]
27. Free, S.J. Fungal cell wall organization and biosynthesis. *Adv. Genet.* **2013**, *81*, 33–82.
28. Vaahtera, L.; Schulz, J.; Hamann, T. Cell wall integrity maintenance during plant development and interaction with the environment. *Nat. Plants* **2019**, *5*, 924–932. [CrossRef]
29. Jiao, W.; Yu, H.; Cong, J.; Xiao, K.; Zhang, X.; Liu, J.; Zhang, Y.; Pan, H. Transcription factor SsFoxE3 activating SsAtg8 is critical for sclerotia, compound appressoria formation, and pathogenicity in *Sclerotinia sclerotiorum*. *Mol. Plant Pathol.* **2022**, *23*, 204–217. [CrossRef]
30. Li, Y.; Wang, G.; Xu, J.R.; Jiang, C. Penetration peg formation and invasive hyphae development require stage-specific activation of MoGTI1 in *Magnaporthe oryzae*. *Mol. Plant Microbe Interact.* **2016**, *29*, 36–45. [CrossRef]
31. Park, G.; Bruno, K.S.; Staiger, C.J.; Talbot, N.J.; Xu, J.R. Independent genetic mechanisms mediate turgor generation and penetration peg formation during plant infection in the rice blast fungus. *Mol. Microbiol.* **2004**, *53*, 1695–1707. [CrossRef]
32. Pejenaute-Ochoa, M.D.; Tomas-Gallardo, L.; Ibeas, J.I.; Barrales, R.R. Row1, a member of a new family of conserved fungal proteins involved in infection, is required for appressoria functionality in *Ustilago maydis*. *New Phytol.* **2024**, *243*, 1101–1122. [CrossRef]
33. Fujita, M.; Jigami, Y. Lipid remodeling of GPI-anchored proteins and its function. *Biochim. Biophys. Acta* **2008**, *1780*, 410–420. [CrossRef]

Disclaimer/Publisher's Note: The statements, opinions and data contained in all publications are solely those of the individual author(s) and contributor(s) and not of MDPI and/or the editor(s). MDPI and/or the editor(s) disclaim responsibility for any injury to people or property resulting from any ideas, methods, instructions or products referred to in the content.

Journal of Fungi

MDPI

Article

4-Propylphenol Alters Membrane Integrity in Fungi Isolated from Walnut Anthracnose and Brown Spot

Xiaoli Yu [1,2,†], Shuhan Yang [3,†], Panhong Su [3,4], Haiyao Bi [3], Yaxuan Li [3], Xingxing Peng [1,2], Xiaohui Sun [1,2,*] and Qunqing Wang [3,4,*]

[1] Yantai Academy of Agricultural Sciences, Yantai 265500, China; yuxiaoli92jnjn@126.com (X.Y.)
[2] Yantai Key Laboratory of Wheat Resources Precise Evaluation and Biological Breeding, Yantai 265500, China
[3] Department of Plant Pathology, College of Plant Protection, Shandong Agricultural University, Tai'an 271018, China
[4] Qilu College, Shandong Agricultural University, Tai'an 271018, China
* Correspondence: nyswjs@yt.shandong.cn (X.S.); wangqunqing@sdau.edu.cn (Q.W.)
† These authors contributed equally to this work.

Abstract: Walnut anthracnose (*Colletotrichum gloeosporioides* and *C. siamense*) and brown spot (*Alternaria alternata*) cause severe yield losses globally. Conventional fungicides face the challenges of pathogen resistance and environmental toxicity. This study evaluates 4-propylphenol, a plant-derived phenolic compound, as an eco-friendly alternative against key fungal pathogens of walnut. In vitro assays determined EC_{50} values against target pathogens (29.11–31.89 mg·L^{-1}) via mycelial growth inhibition and conidial germination suppression (EC_{50} = 55.04–71.85 mg·L^{-1}). Mechanistic analyses confirmed membrane disruption through propidium iodide staining (9.5-to-14.0-fold fluorescence intensity increase), DNA leakage (77.82–85.15% at 250 mg·L^{-1}), and protein efflux (58.10–66.49%). In field trials, we implemented a phenology-driven strategy: 100 mg·L^{-1} ground/canopy spray at flowering to reduce primary inoculum, followed by 400 mg·L^{-1} canopy application at fruiting. This protocol achieved 86.67% control efficacy against disease complexes with negligible phytotoxicity (SPAD variation < 5%). 4-propylphenol provides a sustainable solution through membrane-targeting action, effectively overcoming fungicide resistance in woody crops.

Keywords: *Colletotrichum*; *Alternaria*; 4-propylphenol; anthracnose; botanical fungicide; membrane disruption; phenology-driven; sustainable agriculture; disease management

1. Introduction

Walnut (*Juglans regia* L.), a woody oilseed crop with significant economic value and ecological benefits, holds a prominent position in global agricultural trade due to its edible nuts and oil [1]. Fungal diseases have emerged as a critical constraint to sustainable walnut industrialization, with anthracnose representing one of the most devastating phytopathologies. The anthracnose pathogen complex (*Colletotrichum godetiae*, *C. gloeosporioides*, *C. fioriniae*, *C. nymphaeae*, and *C. siamense*) can infect up to 50% of fruits [2–7]. Disease onset typically occurs in early July, followed by exponential spread during August, culminating in over 35% infected fruits by early September [8]. Brown spot disease (alternatively termed brown apical necrosis), caused by *Alternaria* fungi, induces fruit browning, rot, and premature abscission, accounting for 30% of yield losses [9,10]. *Alternaria alternata* has been confirmed as the dominant pathogenic species in Shandong and Sichuan provinces of China [11,12].

Chemical control remains the predominant management strategy, but prolonged reliance on benzimidazoles and triazoles has precipitated a triple crisis: evolution of pathogen resistance [13], collateral damage to non-target organisms [14–16], and persistent environmental contamination [17]. This predicament underscores the urgent need for innovative green control technologies. Plant-derived fungicides, characterized by biodegradability, target specificity, and slower resistance development, have emerged as a pivotal strategy to overcome current control limitations [18–20]. Notably, existing research predominantly focuses on broad-spectrum antimicrobial secondary metabolites such as chitooligosaccharides [21], zedoary oil [22], and phenolic/terpenoid compounds [23], while systematic screening of plant-based agents against walnut-specific pathogens remains unexplored.

This study established a tripartite screening system for plant-derived fungicides against walnut fungal diseases, integrating activity-guided screening, membrane-targeted mechanism elucidation, and field-adaptive optimization. In vitro antimicrobial assays first revealed that 4-propylphenol exhibits significant inhibitory activity against Shandong's predominant walnut pathogens: *Colletotrichum gloeosporioides* (EC_{50} = 31.89 ± 1.26 mg·L^{-1}, half-maximal effective concentration), the newly identified *C. siamense* (EC_{50} = 31.06 ± 2.23 mg·L^{-1}), and *A. alternata* (EC_{50} = 29.11 ± 1.88 mg·L^{-1}). As a volatile plant secondary metabolite [24,25], this phenolic compound not only demonstrates previously reported antimicrobial spectra [26,27] but also disrupts pathogen membrane integrity [28,29], as mechanistically elucidated herein. A phenology-driven precision application protocol was implemented in field trials: whole-plant and ground spray (100 mg·L^{-1}) during flowering to reduce primary inoculum, followed by canopy-directed application (400 mg·L^{-1}) at the fruiting stage. This strategy achieved 86.67% control efficacy in combined anthracnose–brown spot incidence ($p < 0.05$), with chlorophyll SPAD analysis confirming negligible phytotoxicity (<5% variation vs. control). This work pioneers a comprehensive technical framework for plant-derived fungicide development in walnut protection, spanning in vitro screening, mechanistic validation, and field efficacy evaluation. The findings not only address critical gaps in eco-friendly walnut disease management but also establish a replicable paradigm for creating botanical pesticides in woody oilseed crops, advancing sustainable practices for specialty forest product industries.

2. Materials and Methods

2.1. Fungal Pathogens

The *C. gloeosporioides* strain (isolated from anthracnose-infected walnut fruits in Chongqing, China, 2019) was provided by Dr. Jian Gao (College of Plant Protection, Southwest University). The glyceraldehyde-3-phosphate dehydrogenase (*GAPDH*) gene was amplified with primers GDF1/GDR1 [30] and confirmed as *C. gloeosporioides* by BLASTn analysis (Query cover 100%, Ident 99.66% to GenBank accession KM053198.1).

The *A. alternata* strain (isolated from brown spot lesions on walnut fruits in Tai'an, Shandong, China, 2020) was provided by Prof. Hongyan Wang (College of Plant Protection, Shandong Agricultural University). The internal transcribed spacer (ITS) region was amplified with primers ITS4/ITS5 [31] and confirmed as *A. alternata* by BLASTn analysis (Query cover 100%, Ident 99.81% to GenBank accession OK036715.1).

The *C. siamense* strain HQ21 (GenBank accession: PV929873) was isolated from symptomatic anthracnose fruits in Tai'an, Shandong, China, 2021. Molecular characterization of *C. siamense* HQ21 is described in Sections 2.2 and 2.3.

Partial sequences of molecular markers for all strains were deposited in Supplementary File S1, including: the *GAPDH* gene fragment for *C. gloeosporioides*, the ITS region for *A. alternata*, and the *calmodulin* (*CAL*) gene fragment for *C. siamense* HQ21.

All strains were maintained on potato dextrose agar (PDA) slants at 4 °C in darkness with subculturing performed biannually.

2.2. Isolation and Identification of Pathogen HQ21 from Walnut Anthracnose Fruits

Symptomatic anthracnose fruits were collected and transported at 4 °C within 4 h. After surface sterilization with 75% ethanol (1 min), 1 cm^2 tissue fragments from lesion margins were excised, treated with 1% NaClO (30 s), rinsed three times with sterile water, and cultured on PDA plates containing 100 $mg \cdot L^{-1}$ streptomycin (25 °C, 5–7 days in darkness). Pathogens were purified through three rounds of single-spore isolation on potato dextrose agar (PDA), yielding strain HQ21.

2.3. Pathogenicity Validation and Characterization of HQ21

Pathogenicity assay: Detached leaves of *Juglans regia* 'Xiangling' were needle-inoculated with HQ21 mycelial plugs (5 mm, 7-day-old PDA). Controls received sterile plugs. The leaves were maintained at 25 °C/85% RH for 5 days. Pathogens were re-isolated from lesions to fulfill Koch's postulates.

Morphological characterization: Purified isolates were cultured on PDA plates at 25 °C for 7 days. Colony morphology and pigmentation were recorded, and conidioma dimensions were measured microscopically (Nexcope NE910-FLNingbo Yongxin Optics Co., Ltd., Ningbo, China, 400×).

Molecular identification: Genomic DNA was extracted using a modified CTAB protocol [32]. DNA purity was verified by the A260/A280 ratio (1.93) and A260/A230 ratio (1.86) using a NanoDrop 2000c spectrophotometer (Thermo Fisher Scientific, Wilmington, NC, USA). The *CAL* locus was amplified with primers CL1C (5′-GAATTCAAGGAGGCCTTCTC-3′) and CL2C (5′-CTTCTGCATCATGAGCTGGAC-3′), designed by Weir BS et al. [33], in 20 μL reactions containing 2× Rapid Taq Master Mix (Vazyme) 10 μL, Primers 0.5 μM each, and Template DNA 50 ng.

Thermocycling parameters: Amplifications were performed in a Bio-Rad T100 Thermal Cycler (Bio-Rad Laboratories, Inc., Hercules, CA, USA) with the following profile: initial denaturation at 94 °C (5 min); 35 cycles of 94 °C (30 s), 55 °C (45 s), and 72 °C (1 min); final extension at 72 °C (10 min). *CAL* DNA was purified using the SanPrep Column DNA Gel Extraction Kit (Sangon Biotech, Co., Ltd., Shanghai, China), and sequenced bidirectionally (Sangon Biotech, Shanghai, China).

Phylogenetic reconstruction: *CAL* sequences were BLASTN-searched against NCBI GenBank (GenBank accession: PV929873). Reference sequences from type strains were aligned using ClustalW in MEGA 11. The neighbor-joining tree was constructed with 1000 bootstrap replicates.

2.4. Dose–Response Analysis of 4-Propylphenol on Mycelial Growth

Based on preliminary screening of plant-derived phenolics against walnut pathogens, 4-propylphenol was selected for mechanistic and applied evaluation due to its superior antifungal potency and environmental safety profile. The compound (purity $\geq$ 98%, Sigma-Aldrich, St. Louis, MO, USA) was dissolved in methanol to prepare a 10,000 $mg \cdot L^{-1}$ stock solution (stored at 4 °C in darkness). Serial dilutions were performed to obtain amended PDA media with final concentrations of 20, 40, 60, 80, and 100 $mg \cdot L^{-1}$ (methanol concentration $\leq$ 1% v/v). Sterile methanol-amended PDA served as solvent control.

Mycelial plugs (5 mm diameter) from actively growing cultures of *C. gloeosporioides*, *C. siamense*, and *A. alternata* were inoculated onto amended plates. After 5 days of incubation

at 25 °C in darkness, colony diameters were measured using the cross-hair method [34]. Mycelial growth inhibition was calculated as

$$\text{Inhibition (\%)} = [(D_c - D_t)/(D_c - 5)] \times 100$$

where D_c and D_t represent colony diameters (mm) in control and treatment groups, respectively.

Probit regression analysis (SPSS 22.0) was employed to establish toxicological equations by correlating log-transformed concentrations (X) with inhibition probability units (Y). Half-maximal effective concentrations (EC_{50}) and 95% confidence intervals were derived from the dose–response relationships.

2.5. Effects of 4-Propylphenol on Conidial Germination

Conidial suspension preparation: Conidia from *C. gloeosporioides*, *C. siamense*, and *A. alternata* were harvested by scraping sporulating cultures into 10 mL sterile water containing 0.05% Tween-80, vortexed for 30 s, and filtered through quadruple-layer sterile gauze. After centrifugation (4 °C, 3000× *g*, 10 min), pellets were resuspended and adjusted to 1×10^5 CFU mL^{-1} using a hemocytometer.

Germination inhibition assay: 4-propylphenol was incorporated into 1.5% water agar (WA) at final concentrations of 15.625, 31.25, 62.5, 125, 250, and 500 mg·L^{-1}. Aliquots (100 μL) of conidial suspensions were spread evenly on WA plates, with methanol-equivalent controls. Following 24 h incubation (25 °C, darkness), germination rates were assessed by counting germinated conidia. For each replicate, ≥50 spores were counted across five random fields (400×, Olympus CX23, Evident Corporation, Tokyo, Japan). Germination rate (%) = (Germinated spores/Total spores) × 100, where germination was defined by germ tube length ≥ spore diameter. Three replicates per treatment (total ≥ 150 spores) were evaluated.

2.6. Membrane Integrity Assessment

Membrane integrity was assessed by propidium iodide (PI) staining according to Stocks, S.M. [35]. Mycelial blocks of *C. gloeosporioides*, *C. siamense*, and *A. alternata* were cultured in potato dextrose broth (PDB) containing 40 mg·L^{-1} 4-propylphenol for 72 h at 25 °C. Hyphae were collected, washed thrice with PBS (pH 7.4), and stained with 10 μg·mL^{-1} propidium iodide (PI; Sigma-Aldrich) for 15 min. Control groups received equivalent 4-propylphenol-free PDB treatments. Membrane integrity was visualized under fluorescence microscopy (Nexcope NE910-FL; excitation 535 nm; emission 615 nm). Three hyphal segments per treatment were randomly selected for fluorescence intensity quantification using ImageJ v1.53.

2.7. Quantification of Mycelial DNA Leakage

Mycelial suspensions (5 mL, 20 mg·mL^{-1} dry weight) of *C. gloeosporioides*, *C. siamense*, and *A. alternata* were homogenously dispersed in 100 mL PDB containing 4-propylphenol (15.625, 31.25, 62.5, 125, and 250 mg·L^{-1}) and incubated at 25 °C with shaking (120 rpm) for 24 h. After centrifugation (8000× *g*, 10 min, 4 °C), supernatants were filtered through 0.22 μm membranes. DNA leakage was quantified by measuring absorbance at 260 nm (A_{260}) using a NanoDrop 2000c spectrophotometer (Thermo Fisher Scientific, Wilmington, NC, USA), with sterile PDB as blank control.

$$\text{DNA leakage (\%)} = (A_t - A_c)/(A_m - A_c) \times 100$$

A_t: Absorbance of treatment group;
A_c: Absorbance of negative control (mycelia in 4-propylphenol-free PDB);

A_m: Maximum leakage absorbance from mechanically disrupted mycelia (sonicated at 20 kHz for 5 min).

Three replicates per group were analyzed via nonlinear regression (SPSS 22.0).

2.8. Protein Leakage from Conidia

Hemocytometer-calibrated conidial suspensions (1×10^5 conidia·mL^{-1}) of *C. gloeosporioides*, *C. siamense*, and *A. alternata* were aliquoted (5 mL) into 100 mL PDB containing 4-propylphenol (15.625–250 mg·L^{-1}, 2-fold dilution series). Following shaking incubation (25 °C, 150 rpm, 24 h), samples were centrifuged (8000× *g*, 10 min, 4 °C). Filtered supernatants (0.22 μm) were analyzed at 280 nm (A_{280}) using a NanoDrop 2000c.

$$\text{Protein leakage (\%)} = (A_t - A_c)/(A_m - A_c) \times 100$$

A_t: Absorbance of treated conidia;

A_c: Absorbance of untreated control (conidia in 4-propylphenol-free PDB);

A_m: Maximum leakage from sonicated conidia (20 kHz, 5 min).

Triplicate biological replicates were subjected to nonlinear regression analysis (SPSS 22.0).

2.9. Leaf Treatment and Pathogen Inoculation

Mature detached leaves (30 ± 2 days old) of *Juglans regia* 'Xiangling' were collected from field-grown trees. Three biological replicates per treatment group were established, with each replicate consisting of one leaf. Leaves were treated with 4-propylphenol solutions (15.625–500 mg·L^{-1}, containing 0.1% Tween-80 surfactant) via foliar spray. Negative controls received sterile water with 0.1% Tween-80. After air-drying, each leaf was needle-inoculated at midribs with 5 mm mycelial plugs of *C. siamense* (7-day-old cultures) and incubated in a humidity chamber (25 °C, 90% RH) for 7 days. To enhance lesion visibility by removing chlorophyll, leaves were decolorized by immersion in 75% (*v*/*v*) aqueous ethanol within a water bath maintained at 60 °C until complete chlorophyll removal was achieved. After rinsing with distilled water and blotting dry, lesion diameters (mm) were measured.

$$\text{Inhibition (\%)} = (D_c - D_t)/D_c \times 100,$$

where D_c and D_t denote lesion diameters (mm) in control and treated groups, respectively. Data from three biological replicates were pooled, and dose–response curves were fitted using SPSS 22.0 to determine EC_{50} values and 95% confidence intervals. Significant differences were analyzed via one-way ANOVA and Duncan's test ($\alpha = 0.01$).

2.10. Field Safety Evaluation

Field trials were conducted on 5 June 2022 (early fruit expansion stage) using ten-year-old *Juglans regia* 'Xiangling' trees with uniform growth characteristics. A randomized complete block design was employed with three replicates. Each replicate consisted of one experimental tree, serving as an individual block, resulting in three total trees. On each tree, twelve branches with uniform growth status (similar age, orientation, and diameter) were selected and randomly allocated into four treatment groups, with three branches per group. Treatments consisted of three concentrations of 4-propylphenol (100, 200, and 400 mg·L^{-1}) and a water-treated control. Directional foliar spraying was applied specifically to the assigned branch groups using a knapsack electric sprayer (0.3 MPa pressure, 0.4 mm nozzle diameter). The spray volume was calibrated to 500 L·ha^{-1} based on pre-trial optimization, ensuring complete leaf coverage on treated branches without runoff and implementing physical isolation to prevent spray drift between treatments. At 30 days post-treatment,

chlorophyll SPAD values were measured on a total of 30 mature leaves per treatment group (i.e., 10 leaves/replicate) using a handheld SPAD-502 m (Konica Minolta, Inc., Tokyo, Japan). Significant differences among treatments were determined by one-way ANOVA followed by Duncan's multiple range test ($\alpha = 0.05$) in SPSS 22.0.

2.11. Optimization of Field Application Strategies

Given that the key pathogens causing walnut fruit diseases—*C. gloeosporioides* and *C. siamense* (anthracnose), and *A. alternata* (brown spot)—primarily infect fruits and collectively result in direct economic losses, this trial shifted the evaluation focus from leaf lesions to comprehensive fruit disease assessment. A randomized block trial (3 replicates) was conducted in 2023 at Huangqian Town's standardized walnut orchard using *Juglans regia* 'Xiangling' trees. Three treatment regimens were evaluated (Table 1): T1: Initial infection control (100 mg·L^{-1} canopy spray at flowering; water spray at fruiting); T2: T1 protocol + ground spray (100 mg·L^{-1} canopy + ground application at flowering; water spray at fruiting); T3: T2 protocol + enhanced fruiting-stage treatment (400 mg·L^{-1} canopy spray at fruiting); CK: Water-only controls for both stages.

Table 1. Field application strategies of 4-propylphenol.

Treatment	May 5 (Flowering)	June 10 (Fruiting)
T1	100 mg·L^{-1} canopy	Water spray
T2	100 mg·L^{-1} canopy + ground	Water spray
T3	100 mg·L^{-1} canopy + ground	400 mg·L^{-1} canopy
CK	Water spray	Water spray

Applications were performed using a knapsack electric sprayer (0.3 MPa, 0.4 mm nozzle) with ~500 L·ha^{-1} volume for full coverage. n = 3 biological replicates per treatment.

Disease assessment: Fifteen days post-treatment, 30 fruits per group were graded:

0: No lesions;

1: 1–2 lesions;

2: 3–5 lesions;

3: >5 lesions or coalesced necrosis.

$$\text{Disease index } (DI) = \Sigma(\textit{Disease grade} \times \textit{fruit count})/(3 \times \textit{total fruits}) \times 100.$$

$$\text{Control efficacy } (\%) = (DI_{CK} - DI_{\text{treatment}})/DI_{CK} \times 100.$$

Data were analyzed using SPSS 22.0 with significance thresholds at $\alpha = 0.05$.

3. Results

3.1. Isolation, Identification, and Pathogenicity of Colletotrichum siamense in Huangqian Walnut Orchards

Walnut fruits exhibiting anthracnose symptoms were collected from Huangqian Town, Tai'an City (Figure 1A). Strain HQ21, isolated through single-spore purification, formed circular colonies (78.3 ± 1.5 mm diameter) on PDA after 5 days at 25 °C. Colonies displayed dense aerial mycelia with dark gray centers and cream-colored margins on the obverse side (Figure 1B), while reverse sides exhibited gray-green central pigmentation (Figure 1C). Hyphae appeared cylindrical with septa (Figure 1D), producing hyaline, aseptate conidia measuring (14.2 ± 1.3) × (4.2 ± 0.6) μm (Figure 1E). Pathogenicity assays induced characteristic anthracnose lesions on inoculated leaves within 5 days, mirroring field symptoms (Figure 1F), while the controls remained asymptomatic (Figure 1G). Re-isolation from diseased tissues yielded morphologically identical colonies to HQ21, fulfilling Koch's

postulates. Phylogenetic analysis of concatenated *CAL* sequences placed HQ21 within a highly supported *C. siamense* clade (Bootstrap = 98%; genetic distance $\leq$ 0.002) (Figure 2). Integrated morphological and molecular evidence confirmed HQ21 as *C. siamense* Prihastuti, L. Cai & K.D. Hyde. The *CAL* gene sequence is available in GenBank under accession number PV929873.

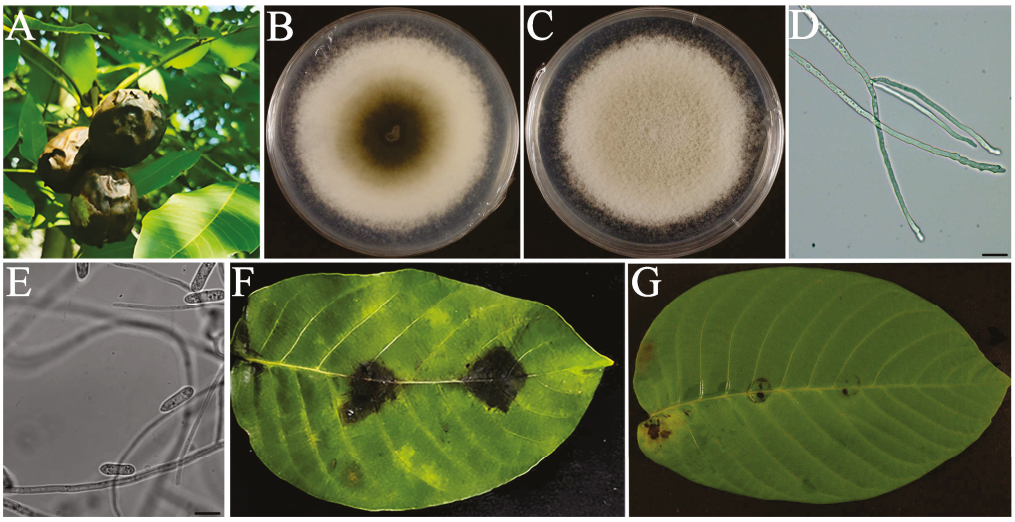


Figure 1. Isolation and pathogenicity determination of walnut anthracnose pathogen. (**A**): Field symptoms of walnut anthracnose on fruits. (**B**,**C**): Morphology of strain HQ21 on PDA, 5 days after inoculation (front and reverse view). (**D**): Hypha structure. (**E**): Conidia. (**F**): Disease progression in artificial inoculation assay (5 dpi). (**G**): Control leaf on PDA block inoculation. Scale bars: (**D**,**F**) = 20 μm.

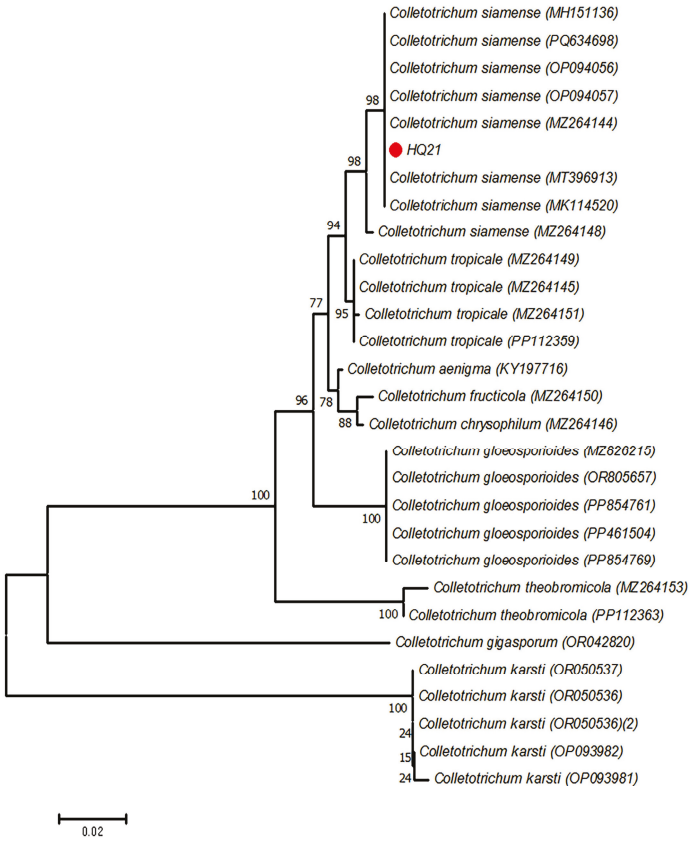


Figure 2. Phylogenetic analysis of strain HQ21 based on *CAL* gene sequences. The neighbor-joining tree was constructed using MEGA 11 software with 1000 bootstrap replicates. Sequences of reference strains (indicated by GenBank accession numbers) were retrieved from NCBI.

3.2. Virulence Analysis of 4-Propylphenol Against Target Pathogens

4-propylphenol exhibited significant dose-dependent inhibition of mycelial growth across all three pathogens. Serial dilutions (20–100 mg·L^{-1}) demonstrated significant dose–response relationships across all pathogens (R^2 = 0.827–0.948), with EC_{50} values of 31.893, 31.063, and 29.111 mg·L^{-1} for *C. gloeosporioides*, *C. siamense*, and *A. alternata*, respectively. Steep concentration–response profiles were evidenced by toxicity equation slopes (3.02–3.81) (Table 2 and Figure 3).

Table 2. Virulence regression parameters of 4-propylphenol against walnut pathogens.

Pathogen	Toxicity Regression Equation	R^2	EC_{50} (mg·L^{-1})	95% Confidence Interval (mg·L^{-1})
C. gloeosporioides	Y = −5.69 + 3.81X	0.827	31.89	8.16–49.25
C. siamense	Y = −4.80 + 3.22X	0.948	31.06	17.75–41.67
A. alternata	Y = −4.41 + 3.02X	0.882	29.11	9.52–42.63

Y: Inhibition probability units; X: Log-transformed concentrations. EC_{50} values derived from Probit analysis.

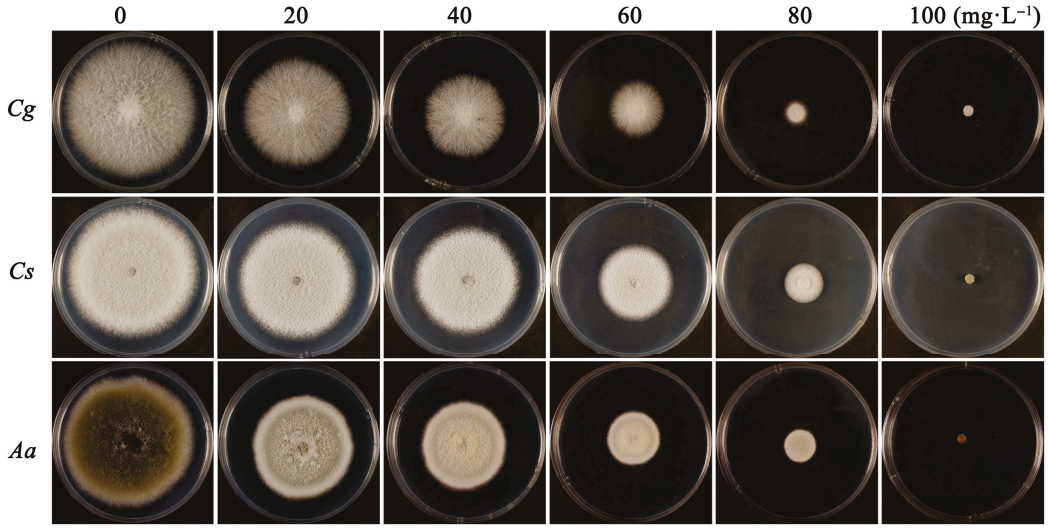


Figure 3. Dose-dependent inhibition of 4-propylphenol (0–100 mg·L^{-1}) on mycelial growth of *C. gloeosporioides* (Cg), *C. siamense* (Cs), and *A. alternata* (Aa).

3.3. Inhibitory Effects of 4-Propylphenol on Conidial Germination

As shown in Table 3 and Figure 4, 4-propylphenol exhibited significant concentration-dependent inhibition ($p < 0.01$) on conidial germination across all three pathogens. After 24 h treatment, the germination rates for *C. gloeosporioides*, *C. siamense*, and *A. alternata* were 80.00 ± 2.23%, 84.75 ± 2.91%, and 85.39 ± 3.18%, respectively. At 500 mg·L^{-1}, the germination rates decreased to 5.4 ± 1.7%, 7.5 ± 1.47%, and 9.2 ± 0.5%, corresponding to 89.22–93.25% suppression compared to controls. The EC_{50} values for conidial germination inhibition were 55.037, 71.854, and 64.414 mg·L^{-1} for *C. gloeosporioides*, *C. siamense*, and *A. alternata*, respectively.

Table 3. Virulence regression parameters of 4-propylphenol against walnut pathogen conidial germination.

Pathogen	Toxicity Regression Equation	R^2	EC_{50} ($mg \cdot L^{-1}$)	95% Confidence Interval ($mg \cdot L^{-1}$)
C. gloeosporioides	Y = −2.31 + 1.33X	0.966	55.037	44.148–67.138
C. siamense	Y = −2.82 + 1.52X	0.983	71.854	60.220–85.194
A. alternata	Y = −2.72 + 1.49X	0.956	64.414	41.959–93.571

Y: Inhibition probability units; X: Log-transformed concentrations. EC_{50} derived from Probit analysis.

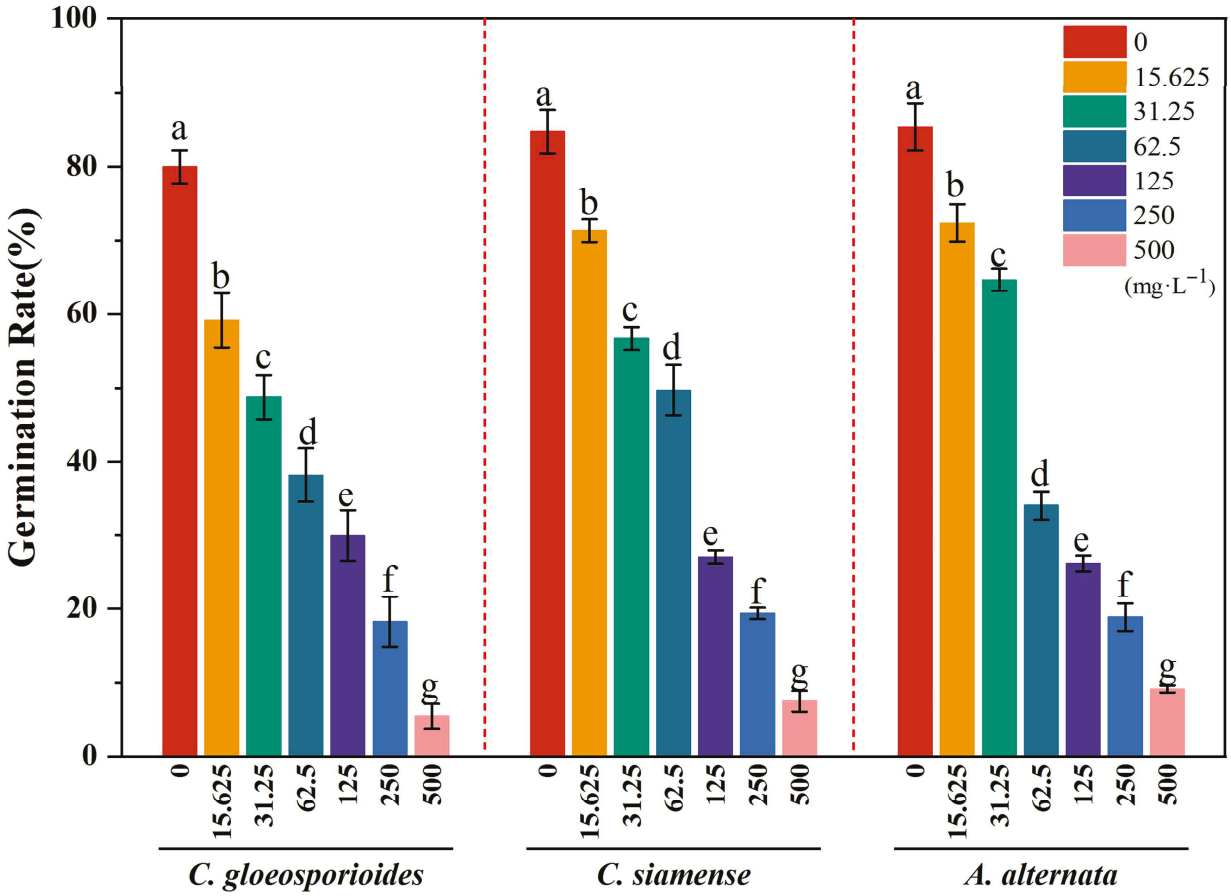


Figure 4. Inhibitory effects of 4-propylphenol on conidial germination of three pathogens. Column colors represent concentrations: 0, 15.625, 31.25, 62.5, 125, 250, and 500 $mg \cdot L^{-1}$. Different lowercase letters indicate significant differences ($p < 0.01$, Duncan's multiple range test).

3.4. Membrane Disruption Effects of 4-Propylphenol on Target Pathogens

Propidium iodide (PI) staining revealed significant membrane damage in 4-propylphenol-treated hyphae (Figure 5). The treatment groups exhibited intense red fluorescence signals (fluorescence intensity: *C. gloeosporioides* 55.74 ± 3.04 a.u., *C. siamense* 55.18 ± 6.54 a.u., and *A. alternata* 61.01 ± 8.13 a.u.), which were markedly higher than those in untreated controls (*C. gloeosporioides*: 3.98 ± 1.41 a.u.; *C. siamense*: 4.01 ± 1.00 a.u.; *A. alternata*: 6.45 ± 5.68 a.u.) ($p < 0.001$), representing 14.0-fold fluorescence intensity increases for *C. gloeosporioides*, 13.8-fold for *C. siamense*, and 9.5-fold for *A. alternata* compared to untreated controls. These results confirm that 4-propylphenol induces significant alterations in membrane permeability.

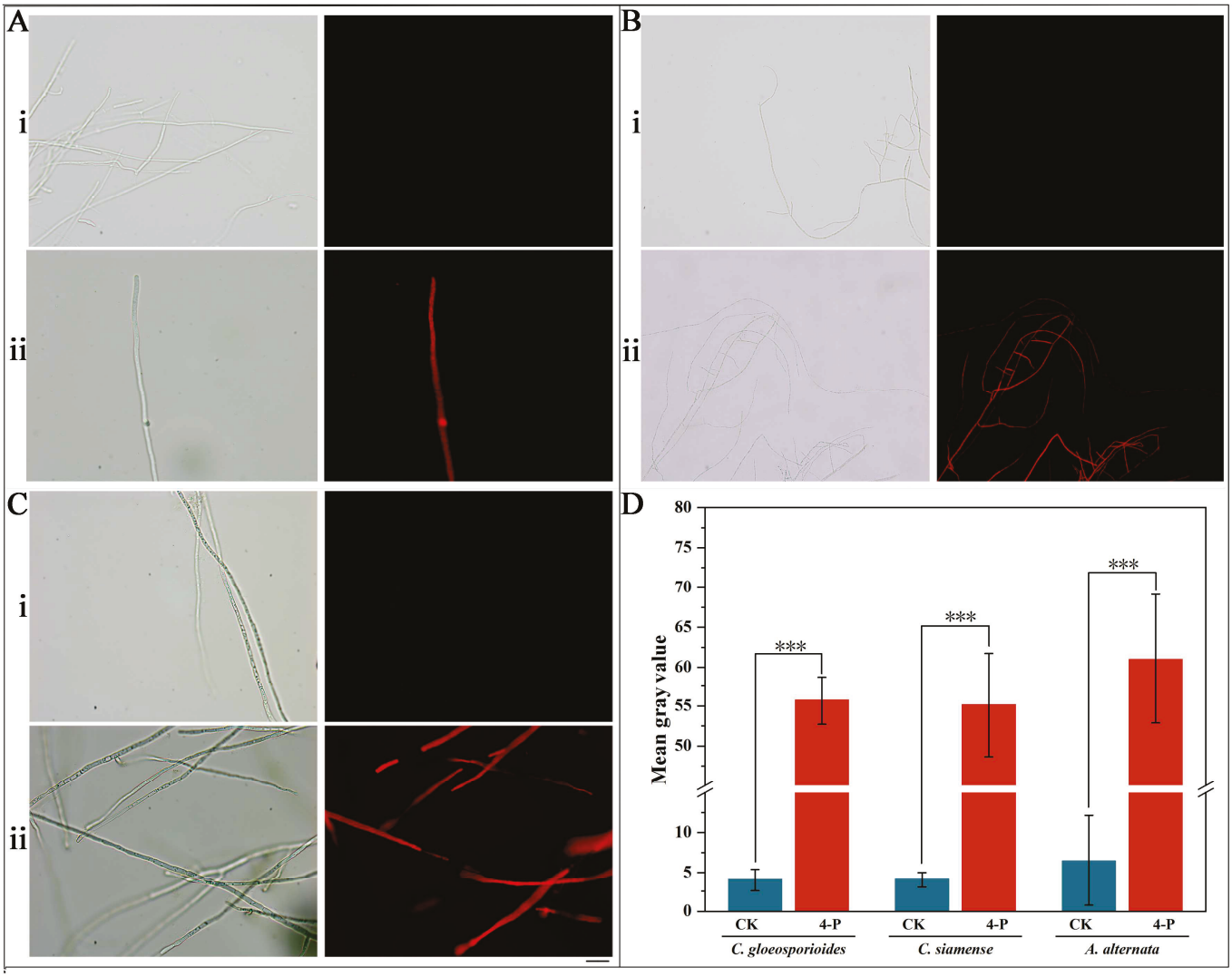


Figure 5. Effects of 4-propylphenol on membrane integrity of three pathogens. (**A**): *C. gloeosporioides* hyphae under bright-field (*left*) and PI fluorescence (**right**): (i) untreated control; (ii) 40 mg·L^{-1} 4-propylphenol treatment. (**B**): *C. siamense* hyphae under bright-field (*left*) and PI fluorescence (**right**): (i) untreated control; (ii) 40 mg·L^{-1} 4-propylphenol treatment. (**C**): *A. alternata* hyphae under bright-field (*left*) and PI fluorescence (**right**): (i) untreated control; (ii) 40 mg·L^{-1} 4-propylphenol treatment. (**D**): Quantitative analysis of PI fluorescence intensity showing 9.5-to-14.0-fold increases in treated hyphae. Scale bar = 200 μm (applicable to (**A**–**C**)). *** denote significant differences ($p < 0.001$, Duncan's multiple range test).

3.5. Dose-Dependent Induction of DNA Leakage by 4-Propylphenol

As illustrated in Figure 6, 4-propylphenol significantly increased DNA leakage from *C. gloeosporioides*, *C. siamense*, and *A. alternata* hyphae in a concentration-dependent manner (R^2 = 0.802–0.924). At 250 mg·L^{-1}, DNA leakage reached 77.82–85.15% of maximum saturation values achieved through mechanical disruption.

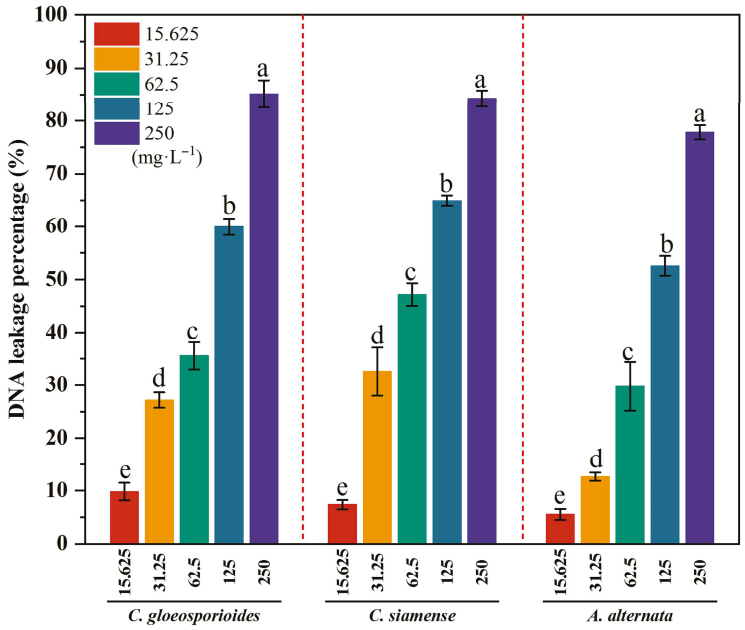


Figure 6. Dose-effect of 4-propylphenol on DNA leakage of three pathogens. Column colors represent concentrations: 15.625, 31.25, 62.5, 125, and 250 mg·L^{-1}. Different lowercase letters denote significant differences ($p < 0.01$, Duncan's multiple range test).

3.6. Protein Leakage Induced by 4-Propylphenol

As demonstrated in Figure 7, 4-propylphenol significantly compromised fungal membrane permeability, inducing dose-dependent protein leakage. Leakage levels exhibited strong positive correlations with compound concentrations (R^2 = 0.974–0.991). At 250 mg·L^{-1}, protein leakage reached 58.10–66.49% of maximum saturation values: *C. gloeosporioides* (65.02 ± 0.53%), *C. siamense* (58.10 ± 0.44%), and *A. alternata* (66.49 ± 1.05%).

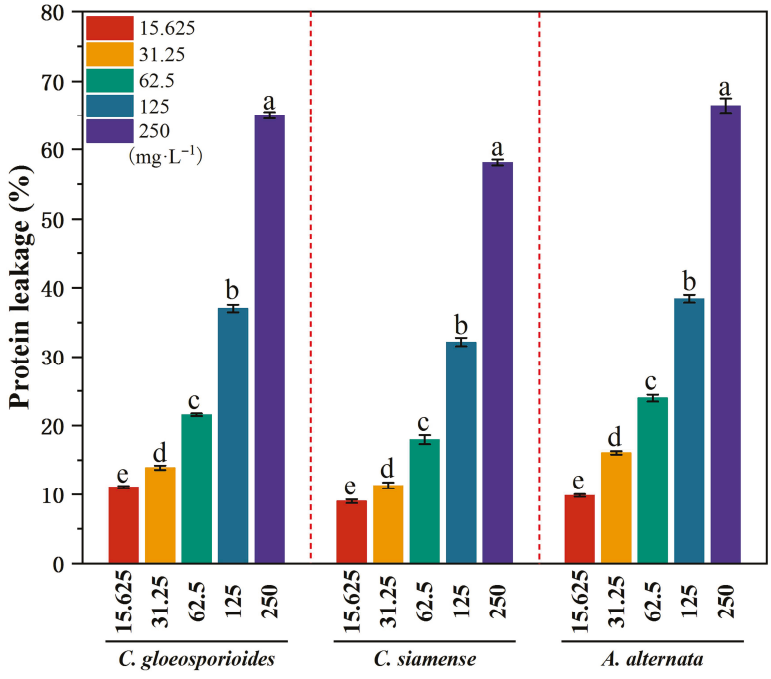


Figure 7. Dose-dependent protein leakage induced by 4-propylphenol in three pathogens. Column colors represent concentrations: 15.625, 31.25, 62.5, 125, and 250 mg·L^{-1}. Different lowercase letters indicate significant differences ($p < 0.01$, Duncan's multiple range test).

3.7. Protective Effects of 4-Propylphenol Against C. siamense Infection in Detached Walnut Leaves

Detached walnut leaves treated with 4-propylphenol (15.625–500 mg·L^{-1}) showed significant concentration-dependent suppression of *C. siamense* infection (R^2 = 0.99903). Visual assessment of disease progression revealed distinct phenotypic differences across treatment concentrations (Figure 8A), with complete inhibition of pathogen colonization observed at the highest concentration of 500 mg·L^{-1}. The dose–response relationship demonstrated progressive efficacy, achieving 47.52 ± 3.97% disease inhibition at 62.5 mg·L^{-1}, 84.67 ± 3.25% at 250 mg·L^{-1}, and 100% at 500 mg·L^{-1} (Figure 8C). Quantitative analysis through probit modeling determined the half-maximal effective concentration (EC_{50}) as 96.54 mg·L^{-1} (Figure 8B). Statistical comparison of inhibition rates across concentrations revealed significant differential efficacy ($p < 0.01$, Duncan's test), with distinct effectiveness groupings indicated by letter annotations in the histogram (Figure 8C). This comprehensive analysis confirms 4-propylphenol's potent capacity to protect foliar tissues against anthracnose pathogenesis, achieving complete pathogen suppression at the maximum tested concentration.

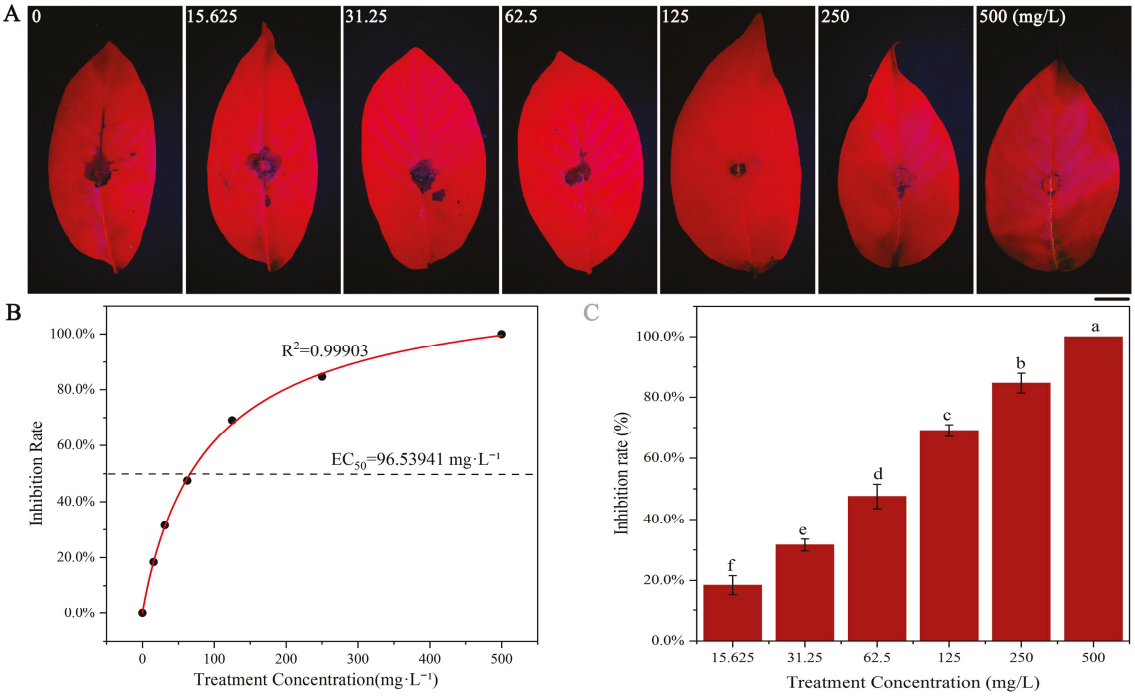


Figure 8. Protective effect of 4-propylphenol against *C. siamense* infection on detached walnut leaves. (**A**): Phenotypic comparison of detached walnut leaves treated with 4-propylphenol at different concentrations (0, 15.625, 31.25, 62.5, 125, 250, and 500 mg·L^{-1}) and inoculated with *C. siamense*. Images were captured 5 days post-inoculation after chlorophyll removal via ethanol decolorization. Scale bar = 2 cm. (**B**): Dose–response curve of *C. siamense* inhibition by 4-propylphenol. (**C**): Histogram of inhibition rates at tested concentrations. Columns labeled with different lowercase letters show statistically significant differences ($p < 0.01$, Duncan's multiple range test).

3.8. Field Safety Evaluation of 4-Propylphenol on Walnut Trees

Field trials evaluating the physiological safety of different 4-propylphenol concentrations on walnut trees demonstrated the following results (Figure 9): Foliar applications at 100, 200, and 400 mg·L^{-1} maintained leaf SPAD values at 43.6 ± 1.18, 44.4 ± 1.87, and 43.84 ± 1.96, respectively (Figure 9A). Compared to the water-treated control group (44.55 ± 1.39; Figure 9B), no significant differences ($p > 0.05$) in SPAD values were observed across treatments. Moreover, the 400 mg·L^{-1} treatment group (Figure 9C) exhibited no visible phytotoxicity symptoms. Based on comprehensive safety evaluation parameters (SPAD stability and foliar phenotypic integrity) and the potential enhancement of disease control

efficacy at higher concentrations, 400 mg·L^{-1} is recommended as the optimal application concentration to balance phytological safety and field efficacy.

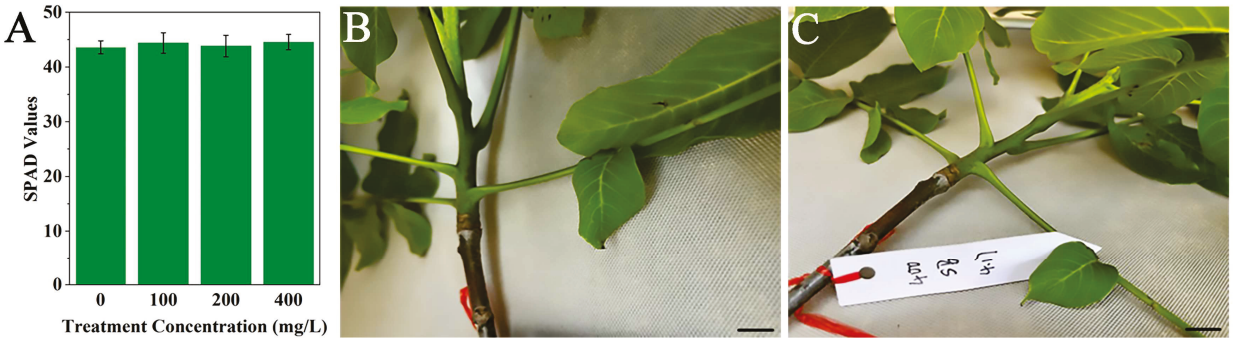


Figure 9. Evaluation of 4-propylphenol phytotoxicity in field-grown walnut trees (*Juglans regia*). (**A**): Leaf chlorophyll content (SPAD values) across experimental treatments (mean ± SD, n ≥ 30 leaves/treatment). (**B**): Representative foliage from water-treated control plants. (**C**): Foliar phenotype following 400 mg·L^{-1} 4-propylphenol application. Scale bar = 5 cm (applicable to (**B**,**C**)).

3.9. Integrated Application Strategies for Disease Control Efficacy

As shown in Figure 10E, 4-propylphenol demonstrated significant field efficacy against walnut fruit diseases. The T1 treatment (100 mg·L^{-1} canopy spray at flowering + water spray at fruiting; Figure 10B) achieved 47.78 ± 5.09% control efficacy with 28.89% diseased fruits. The T2 treatment (100 mg·L^{-1} canopy + ground spray at flowering + water spray at fruiting; Figure 10C) significantly enhanced overall efficacy to 80.00 ± 6.67% ($p < 0.01$; Figure 10E), reducing disease incidence to 12.22%. The T3 treatment (T2 + 400 mg·L^{-1} canopy spray at fruiting; Figure 10D) achieved optimal performance with 7.78% diseased fruits and 86.67 ± 3.33% control efficacy, significantly surpassing T1/T2 ($p < 0.01$; Figure 10E). Untreated controls (CK, Figure 10A) exhibited 56.67% disease incidence (Figure 10E).

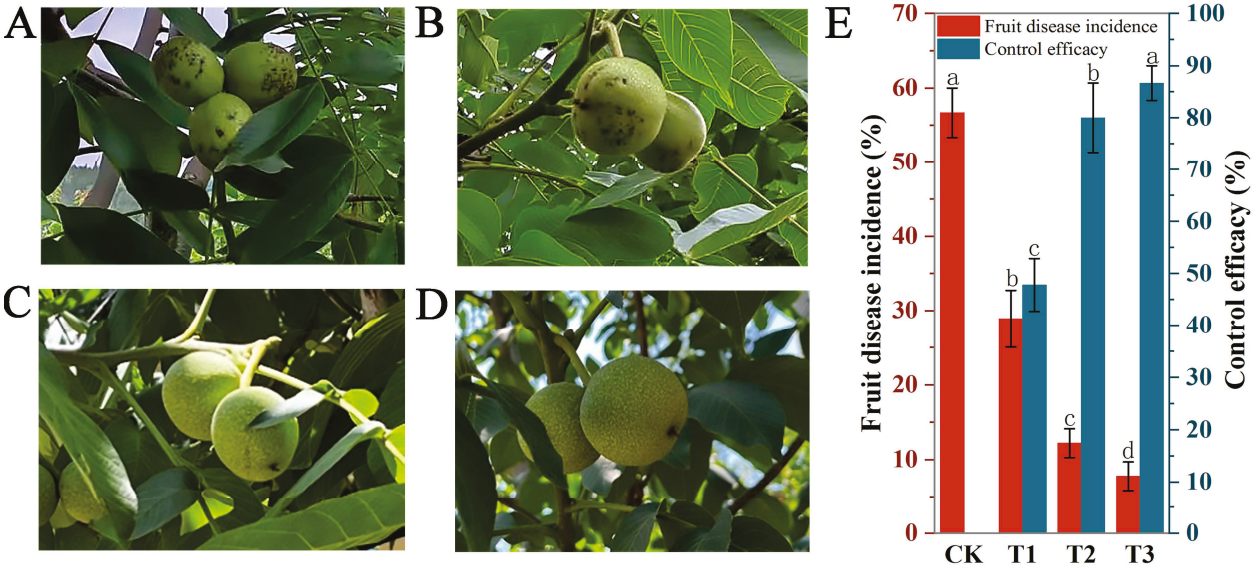


Figure 10. Field efficacy of 4-propylphenol application strategies against walnut diseases. (**A**). Untreated control (CK; water spray at both stages). (**B**). T1 treatment (100 mg·L^{-1} flowering canopy spray). (**C**). T2 treatment (100 mg·L^{-1} flowering canopy + ground spray). (**D**). T3 treatment (T2 + 400 mg·L^{-1} fruiting canopy spray). (**E**). Comparative disease incidence and control efficacy across treatments. Different lowercase letters denote significant differences ($p < 0.01$, Duncan's multiple range test).

4. Discussion

The pathogen diversity of walnut anthracnose and brown spot, coupled with their cross-host transmission characteristics, poses a persistent threat to the global walnut industry. Over 10 species of *Colletotrichum* spp. have been confirmed to infect walnuts [36–39], among which *C. siamense* has emerged as a critical pathogen due to its broad host adaptability and geographical dispersal capacity. The pathogenic strain of *C. siamense* identified in Tai'an, Shandong Province, further validates the expansion of this species in temperate woody crops. Notably, *C. siamense* exhibits a host range spanning at least 15 genera across seven plant families, including *Cornus* spp. [40], *Ixora chinensis* [41], *Persea Americana* [42], and *Citrus* spp. [43]. This polyphagous trait suggests potential cross-species transmission through host plant networks within agroecosystems, significantly amplifying the epidemiological complexity and control challenges of the disease.

This study is the first to elucidate the molecular mechanism by which 4-propylphenol exerts antifungal effects via targeted disruption of pathogen membrane integrity. Fluorescence staining revealed significant membrane damage, evidenced by 9.5-to-14.0-fold increases in propidium iodide (PI) staining intensity following treatment, consistent with the classical mode of phenolic compounds that alter membrane potential to induce ion homeostasis imbalance [44,45]. Unlike conventional fungicides (e.g., triazoles targeting enzyme inhibition) [46,47], this nonspecific membrane-targeting mechanism may theoretically reduce the risk of resistance development [48]. However, potential fungal adaptive mechanisms, such as MAPK signaling pathway-mediated dynamic regulation of membrane composition, warrant further investigation [49,50].

In bioactivity assessments, 4-propylphenol demonstrated EC_{50} values of 29.11–31.89 $mg \cdot L^{-1}$ against plant pathogens, comparable to the optimal eugenol derivative against *Botrytis cinerea* (EC_{50} = 31 $mg \cdot L^{-1}$) [51] and superior to 1-sulfonyloxy/acyloxy eugenol analogs against *Phytophthora capsica* (EC_{50} = 70.8 $mg \cdot L^{-1}$) [52]. Notably, its inhibition of conidial germination (EC_{50} = 55.04–71.85 $mg \cdot L^{-1}$) exhibited approximately 55-fold greater efficacy than ginseng stem-leaf total saponins (EC_{50} = 3037.7 $mg \cdot L^{-1}$) [53] and outperformed commercial biofungicides such as *Bacillus subtilis* lipopeptides (EC_{50} > 100 $mg \cdot L^{-1}$) [54]. The compound also displayed rapid (>90% inhibition within 24 h) and sustained antifungal activity, highlighting its unique advantages in plant disease management systems.

The proposed gradient application strategy (100 $mg \cdot L^{-1}$ ground spray (canopy and soil application) at the flowering stage; 400 $mg \cdot L^{-1}$ targeted canopy spraying at the fruiting stage) demonstrated high field efficacy in disease control while aiming at suppressing primary inoculum sources. This approach shares conceptual similarities with grape anthracnose management protocols (e.g., copper-based agents at bud break and microbial agents at flowering) [55], yet simplifies operational complexity through optimized concentration gradients of a single active ingredient. However, soil drenching may exert non-target effects on microbial communities. Metagenomic analysis is recommended to systematically evaluate impacts on soil microbial network structure and functional gene expression, thereby informing the development of ecologically sustainable application protocols.

5. Conclusions

This study established an integrated system encompassing membrane-targeting mechanism analysis and phenology-adapted application technology, providing an innovative framework for sustainable disease management in woody oil crops. Key findings include the following: (1) Novel antimicrobial mechanism: 4-propylphenol triggers cellular content leakage through membrane lipid disruption, demonstrating a resistance-avoidance mode that circumvents the mutation risks inherent in conventional fungicides targeting specific molecular sites. (2) Application strategy innovation: A hierarchical management strat-

egy, integrating flowering-stage ground disinfection and fruit-development-stage canopy protection, showed significant efficacy against walnut anthracnose, enabling chemical input reduction while maintaining eco-friendly orchard operations. Future research should prioritize three directions: molecular-level characterization of 4-propylphenol's specific binding sites with membrane lipids, establishment of regional pathogen resistance surveillance networks, and development of nano-encapsulated formulations to enhance residual activity. This integrated approach not only addresses critical challenges in walnut disease control but also provides replicable solutions for sustainable cultivation of other woody oil crops, including Chinese hickory (*Carya cathayensis*) and oil-tea camellia (*Camellia oleifera*). Through mechanism-driven technological innovation, this work achieves effective synergy between ecological safety and pathogen control, advancing the development of green control technologies in agricultural phytopathology.

Supplementary Materials: The following supporting information can be downloaded at: https://www.mdpi.com/article/10.3390/jof11090610/s1. File S1: Fungal DNA sequences in FASTA format.

Author Contributions: Conceptualization, Q.W. and X.S.; methodology, X.Y., P.S. and S.Y.; validation, Y.L. and H.B.; formal analysis, X.P. and S.Y.; investigation, X.Y., P.S. and Y.L.; resources, Q.W. and X.S.; data curation, H.B. and X.P.; writing—original draft preparation, X.Y. and S.Y.; writing—review and editing, P.S., Q.W. and X.S.; visualization, X.P. and Y.L.; supervision, Q.W. and X.S.; project administration, Q.W.; funding acquisition, Q.W., X.S., X.P. and X.Y. All authors have read and agreed to the published version of the manuscript.

Funding: This research was funded by the Key Research and Development Project of Shandong Province (the Agricultural Variety Improvement Project): 2023LZGC002; the Taishan Scholar Project, grant number tsqn202211093; the National Natural Science Foundation of China, grant numbers 32172387, 32172049 and 31701751; the Natural Science Foundation of Shandong Province, grant numbers ZR2024MC195, ZR2021YQ20, and ZR2024QC267; and the Shandong Province First-class Discipline Construction "811" Project, grant numbers SKL81121 and SKL81127. The Metabonomics Platform, Agronomy College of SDAU and Shandong Guocangjian Biotechnology Co., Ltd., provided technical support and suggestions for this research work.

Institutional Review Board Statement: This study complied with institutional guidelines for plant pathogen research. No endangered species were involved.

Informed Consent Statement: Not applicable.

Data Availability Statement: The data presented in this study are openly available in Zenodo, reference number 16245946.

Acknowledgments: We sincerely thank Jian Gao (College of Plant Protection, Southwest University) for providing *C. gloeosporioides* strains, and the research group of Hongyan Wang (College of Plant Protection, Shandong Agricultural University) for supplying *A. alternata* isolates. We acknowledge the technical support from the Metabonomics Platform of Agronomy College, Shandong Agricultural University, and Shandong Guocangjian Biotechnology Co., Ltd., for their analytical assistance and scientific suggestions. The authors alone are responsible for the content of this publication.

Conflicts of Interest: The authors declare no conflicts of interest. Shandong Guocangjian Biotechnology Co., Ltd., provided analytical assistance and scientific suggestions but had no role in the design of the study; in the collection, analyses, or interpretation of data; in the writing of the manuscript, and in the decision to publish the results. The funders had no role in the design of the study; in the collection, analyses, or interpretation of data; in the writing of the manuscript, or in the decision to publish the results.

References

1. Food and Agriculture Organization of the United Nations: Food and Agriculture Data. Available online: https://www.fao.org/faostat/en/#compare (accessed on 15 January 2025).
2. Lio, D.D.; Cobo-Díaz, J.F.; Masson, C.; Chalopin, M.; Kebe, D.; Giraud, M.; Verhaeghe, A.; Nodet, P.; Sarrocco, S.; Floch, G.L.; et al. Combined Metabarcoding and Multi-locus approach for Genetic characterization of *Colletotrichum* species associated with common walnut (*Juglans regia*) anthracnose in France. *Sci. Rep.* **2018**, *8*, 10765. [CrossRef] [PubMed]
3. Li, F.X.; Chen, J.W.; Chen, Q.; Liu, Z.Y.; Sun, J.Y.; Yan, Y.T.; Zhang, H.X.; Bi, Y. Identification, Pathogenicity, and Sensitivity to Fungicide of *Colletotrichum* Species That Causes Walnut Anthracnose in Beijing. *Agronomy* **2023**, *13*, 214. [CrossRef]
4. Savian, L.G.; Muniz, M.F.B.; Poletto, T.; Maculan, L.G.; Rabuske, J.E.; Blume, E.; Sarzi, J.S. First Report of *Colletotrichum nymphaeae* Causing Anthracnose on *Juglans regia* Fruits in Southern Brazil. *Plant Dis.* **2019**, *103*, 3287. [CrossRef]
5. Wang, Y.X.; Xu, X.W.; Cai, F.; Huang, F.X.; Chen, W.S.; Wang, Q.Z. First Report of *Colletotrichum nymphaeae* Causing Walnut Anthracnose in China. *Plant Dis.* **2022**, *106*, 2991. [CrossRef]
6. Wang, F.H.; Liu, C.; Zeng, Q.; Zhou, Y.J.; Liu, F.; Xu, X.L.; Yang, H.B.; Liu, Y.G.; Yang, C.L. Identification and pathogenicity analysis of leaf brown spot of *Juglans regia* in China. *Sci. Rep.* **2023**, *13*, 6599. [CrossRef]
7. Luongo, L.; Galli, M.; Garaguso, I.; Petrucci, M.; Vitale, S. First Report of *Colletotrichum fioriniae* and *C. nymphaeae* as Causal Agents of Anthracnose on Walnut in Italy. *Plant Dis.* **2022**, *106*, 327. [CrossRef]
8. Wang, Q.H.; Li, G.Q.; Liu, X.H.; Duan, C.H.; Zhang, Y.; Niu, S.G.; Zhu, W.C.; Qi, Y.K. Seasonal Epidemic Dynamics and Control Measurement of Walnut Anthracnose in Shandong Province. *J. West China For. Sci.* **2017**, *46*, 13–17. [CrossRef]
9. Belisario, A.; Maccaroni, M.; Coramusi, A.; Corazza, L.; Pryor, B.M.; Figuli, P. First Report of *Alternaria* Species Groups Involved in Disease Complexes of Hazelnut and Walnut Fruit. *Plant Dis.* **2004**, *88*, 426. [CrossRef]
10. Belisario, A.; Maccaroni, M.; Corazza, L.; Balmas, V.; Valier, A. Occurrence and etiology of brown apical necrosis on Persian (English) walnut fruit. *Plant Dis.* **2002**, *86*, 599–602. [CrossRef]
11. Yang, L.; Yang, S.Y.; Ma, W.J.; Zhou, J.H. Identification of Pathogen of Walnut Brown Spot and Investigation of the Disease Occurrence. *For. Res.* **2017**, *30*, 1004–1008. [CrossRef]
12. Qu, W.W.; Yang, K.Q.; Liu, H.X.; Wang, J.Y. Main diseases of walnut and integrated management in Shandong. *Plant Prot.* **2011**, *37*, 136–140. [CrossRef]
13. Chechi, A.; Stahlecker, J.; Dowling, M.E.; Schnabel, G. Diversity in species composition and fungicide resistance profiles in *Colletotrichum* isolates from apples. *Pestic. Biochem. Physiol.* **2019**, *158*, 18–24. [CrossRef]
14. Cheng, S.H.; Lin, R.H.; Wang, L.M.; Qiu, Q.Y.; Qu, M.M.; Ren, X.D.; Zong, F.L.; Jiang, H.; Yu, C.H. Comparative susceptibility of thirteen selected pesticides to three different insect egg parasitoid *Trichogramma* species. *Ecotoxicol. Environ. Saf.* **2018**, *166*, 86–91. [CrossRef]
15. Leite, F.G.; Sampaio, C.F.; Pires, J.A.C.; Oliveira, D.P.d.; Dorta, D.J. Toxicological impact of strobilurin fungicides on human and environmental health: A literature review. *J. Environ. Sci. Health B* **2024**, *59*, 142–151. [CrossRef] [PubMed]
16. Theenoor, R.; Ghosh, A.; Venkatesan, R. Harmonising control: Understanding the complex impact of pesticides on parasitoid wasps for enhanced pest management. *Curr. Opin. Insect Sci.* **2024**, *65*, 101236. [CrossRef]
17. Jiao, C.; Chen, L.; Sun, C.; Jiang, Y.; Zhai, L.M.; Liu, H.B.; Shen, Z.Y. Evaluating national ecological risk of agricultural pesticides from 2004 to 2017 in China. *Environ. Pollut.* **2020**, *259*, 113778. [CrossRef] [PubMed]
18. Brauer, V.S.; Rezende, C.P.; Pessoni, A.M.; Paula, R.G.D.; Rangappa, K.S.; Nayaka, S.C.; Gupta, V.K.; Almeida, F. Antifungal Agents in Agriculture: Friends and Foes of Public Health. *Biomolecules* **2019**, *9*, 521. [CrossRef] [PubMed]
19. Shuping, D.S.S.; Eloff, J.N. The Use of Plants to Protect Plants and Food Against Fungal Pathogens: A Review. *Afr. J. Tradit. Complement. Altern. Med.* **2017**, *14*, 120–127. [CrossRef]
20. Ayilara, M.S.; Adeleke, B.S.; Akinola, S.A.; Fayose, C.A.; Adeyemi, U.T.; Gbadegesin, L.A.; Omole, R.K.; Johnson, R.M.; Uthman, Q.O.; Babalola, O.O. Biopesticides as a promising alternative to synthetic pesticides: A case for microbial pesticides, phytopesticides, and nanobiopesticides. *Front. Microbiol.* **2023**, *14*, 1040901. [CrossRef]
21. Sun, Z.C.; Li, Q.L.; Zhang, J.W.; Sun, Z.H.; Wu, H.F.; Liang, H.Q.; Ma, M.; Huang, L.F.; Xu, X.D.; Ma, G.X. Phenolic constituents with antibacterial activity from *Eleutherine bulbosa*. *Fitoterapia* **2024**, *172*, 105787. [CrossRef]
22. Wang, B.; Liu, F.; Li, Q.; Xu, S.; Zhao, X.Z.; Xue, P.L.; Feng, X. Antifungal activity of zedoary turmeric oil against *Phytophthora capsici* through damaging cell membrane. *Pestic. Biochem. Physiol.* **2019**, *159*, 59–67. [CrossRef] [PubMed]
23. Zacchino, S.A.; Butassi, E.; Liberto, M.D.; Raimondi, M.; Postigo, A.; Sortino, M. Plant phenolics and terpenoids as adjuvants of antibacterial and antifungal drugs. *Phytomedicine* **2017**, *37*, 27–48. [CrossRef] [PubMed]
24. Füllemann, D.; Steinhaus, M. Characterization of Odorants Causing Smoky Off-Flavors in Cocoa. *J. Agric. Food Chem.* **2020**, *68*, 10833–10841. [CrossRef] [PubMed]
25. Lukić, I.; Jedrejčić, N.; Ganić, K.K.; Staver, M.; Peršurić, Đ. Phenolic and Aroma Composition of White Wines Produced by Prolonged Maceration and Maturation in Wooden Barrels. *Food Technol. Biotechnol.* **2015**, *53*, 407–418. [CrossRef]

26. Mohammed, M.A.; Saeed, Y.S.; Ali, J.F. Antibacterial activity of phenolic compounds of *Teucrium polium* L. *Pak. J. Pharm. Sci.* **2023**, *36*, 1435–1442. [CrossRef]
27. Sun, S.F.; Tang, N.W.; Han, K.; You, J.H.; Liu, A.R.; Wang, Q.Q.; Xu, Q. Antifungal Activity and Mechanism of 4-Propylphenol Against *Fusarium graminearum*, Agent of Wheat Scab, and Its Potential Application. *J. Agric. Food Chem.* **2024**, *72*, 5258–5268. [CrossRef]
28. Wan, Y.L.; Wang, X.W.; Yang, L.; Li, Q.H.; Zheng, X.T.; Bai, T.Y.; Wang, X. Antibacterial Activity of Juglone Revealed in a Wound Model of *Staphylococcus aureus* Infection. *Int. J. Mol. Sci.* **2023**, *24*, 3931. [CrossRef]
29. Anek, P.; Kumpangcum, S.; Roytrakul, S.; Khanongnuch, C.; Saenjum, C.; Phannachet, K. Antibacterial Activities of Phenolic Compounds in Miang Extract: Growth Inhibition and Change in Protein Expression of Extensively Drug-Resistant *Klebsiella pneumoniae*. *Antibiotics* **2024**, *13*, 536. [CrossRef]
30. Templeton, M.D.; Rikkerink, E.H.A.; Solon, S.L.; Crowhurst, R.N. Cloning and molecular characterization of the glyceraldehyde-3-phosphate dehydrogenase-encoding gene and cDNA from the plant pathogenic fungus *Glomerella cingulata*. *Gene* **1992**, *122*, 225–230. [CrossRef]
31. Schoch, C.L.; Seifert, K.A.; Huhndorf, S.; Robert, V.; Spouge, J.L.; Levesque, C.A.; Chen, W. Nuclear ribosomal internal transcribed spacer (ITS) region as a universal DNA barcode marker for Fungi. *Proc. Natl. Acad. Sci. USA* **2012**, *109*, 6241–6246. [CrossRef]
32. Allen, G.C.; Flores-Vergara, M.A.; Krasynanski, S.; Kumar, S.; Thompson, W.F. A modified protocol for rapid DNA isolation from plant tissues using cetyltrimethylammonium bromide. *Nat. Protoc.* **2006**, *1*, 2320–2325. [CrossRef]
33. Weir, B.S.; Johnston, P.R.; Damm, U. The *Colletotrichum gloeosporioides* species complex. *Stud. Mycol.* **2012**, *73*, 115–180. [CrossRef] [PubMed]
34. Edgington, L.V. Fungitoxic Spectrum of Benzimidazole Compounds. *Phytopathology* **1971**, *61*, 42. [CrossRef]
35. Stocks, S.M. Mechanism and use of the commercially available viability stain, BacLight. *Cytom. Part A J. Int. Soc. Anal. Cytol.* **2004**, *61*, 189–195. [CrossRef] [PubMed]
36. Zhang, L.; Zhao, L.L.; Liang, C.; Yu, L.H.; Zhang, Y. *Colletotrichum* species (*Glomerellales*, *Glomerellaceae*) causing walnut anthracnose in China. *MycoKeys* **2024**, *108*, 95–113. [CrossRef]
37. Cho, S.E.; Oh, J.Y.; Lee, D.H.; Kim, C.W. First Report of Anthracnose on *Juglans regia* Caused by *Colletotrichum siamense* in Korea. *Plant Dis.* **2022**, *107*, 218. [CrossRef]
38. Li, Y.X.; Lin, L.; Cao, J.; Gan, M.X.; Fan, X.L. Three new species of *Colletotrichum* (*Glomerellales*, *Glomerellaceae*) associated with walnut (*Juglans regia*) anthracnose from China. *MycoKeys* **2024**, *108*, 147–167. [CrossRef]
39. Zhang, L.; Yin, Y.Q.; Zhao, L.L.; Xie, Y.Q.; Han, J.; Zhang, Y. Two new species of *Colletotrichum* (*Glomerellaceae*, *Glomerellales*) causing walnut anthracnose in Beijing. *MycoKeys* **2023**, *99*, 131–152. [CrossRef]
40. Zhang, T.N.; Lv, B.S.; Zhang, T.; Luan, F.G. First Report of Anthracnose caused by *Colletotrichum siamense* and *C. gloeosporiodes* on *Cornus hongkongensis* in China. *Plant Dis.* **2022**, *106*, 2988. [CrossRef]
41. Qin, R.Y.; Zhang, Y.M.; Li, Q.L.; Huang, S.P.; Chen, X.L.; Guo, T.X.; Tang, L.H. Leaf Spot Caused by *Colletotrichum siamense*, *C. fructicola*, and *C. aeschynomenes* on *Ixora chinensis* in Guangxi, China. *Plant Dis.* **2023**, *108*, 225. [CrossRef]
42. Hofer, K.M.; Braithwaite, M.; Braithwaite, L.J.; Sorensen, S.; Siebert, B.; Pather, V.; Goudie, L.; Williamson, L.; Alexander, B.J.R.; Toome-Heller, M. First report of *Colletotrichum fructicola*, *C. perseae*, and *C. siamense* causing anthracnose disease of avocado (*Persea americana*) in New Zealand. *Plant Dis.* **2021**, *105*, 1564. [CrossRef]
43. Pérez-Mora, J.L.; Mora-Romero, G.A.; Beltrán-Peña, H.; García-León, E.; Lima, N.B.; Camacho-Tapia, M.; Tovar-Pedraza, J.M. First Report of *Colletotrichum siamense* and *C. gloeosporioides* Causing Anthracnose of *Citrus* spp. in Mexico. *Plant Dis.* **2020**, *105*, 496. [CrossRef]
44. Wang, Y.Y.; Xue, Y.; Bi, Q.Q.; Qin, D.K.; Du, Q.Z.; Jin, P. Enhanced antibacterial activity of eugenol-entrapped casein nanoparticles amended with lysozyme against gram-positive pathogens. *Food Chem.* **2021**, *360*, 130036. [CrossRef] [PubMed]
45. Nogueira, J.O.E.; Campolina, G.A.; Batista, L.R.; Alves, E.; Caetano, A.R.S.; Brandão, R.M.; Nelson, D.L.; Cardoso, M.D.G. Mechanism of action of various terpenes and phenylpropanoids against *Escherichia coli* and *Staphylococcus aureus*. *FEMS Microbiol. Lett.* **2021**, *368*, fnab052. [CrossRef]
46. Liang, Q.L.; Wei, L.X.; Xu, B.L.; Liu, J.; Zhang, S.W.; Liu, L.L. Induction of resistance of *Podosphaera xanthii* (hull-less pumpkin powdery mildew) to triazole fungicides and its resistance mechanism. *PLoS ONE* **2022**, *17*, e0263068. [CrossRef] [PubMed]
47. Wang, F.Y.; Yao, S.J.; Cao, D.T.; Ju, C.; Yu, S.M.; Xu, S.J.; Fang, H.; Yu, Y.L. Increased triazole-resistance and *cyp51A* mutations in *Aspergillus fumigatus* after selection with a combination of the triazole fungicides difenoconazole and propiconazole. *J. Hazard. Mater.* **2020**, *400*, 123200. [CrossRef]
48. Liu, X.L.; Li, H.; Qi, G.B.; Qian, Y.Y.; Li, B.W.; Shi, L.L.; Liu, B. Combating Fungal Infections and Resistance with a Dual-Mechanism Luminogen to Disrupt Membrane Integrity and Induce DNA Damage. *J. Am. Chem. Soc.* **2024**, *146*, 31656–31664. [CrossRef]
49. Wang, Q.; Wang, J.; Huang, Z.C.; Li, Y.; Li, H.; Huang, P.Y.; Cai, Y.Y.; Wang, J.Y.; Liu, X.H.; Lin, F.C.; et al. The endosomal-vacuolar transport system acts as a docking platform for the Pmk1 MAP kinase signaling pathway in *Magnaporthe oryzae*. *New Phytol.* **2025**, *245*, 722–747. [CrossRef]

50. Gao, X.Q.; Gao, G.G.; Zheng, W.F.; Liu, H.B.; Pan, W.B.; Xia, X.; Zhang, D.M.; Lin, W.W.; Wang, Z.H.; Feng, B.M. PARylation of 14-3-3 proteins controls the virulence of *Magnaporthe oryzae*. *Nat. Commun.* **2024**, *15*, 8047. [CrossRef]
51. Olea, A.F.; Bravo, A.; Martínez, R.; Thomas, M.; Sedan, C.; Espinoza, L.; Zambrano, E.; Carvajal, D.; Silva-Moreno, E.; Carrasco, H. Antifungal Activity of Eugenol Derivatives against *Botrytis Cinerea*. *Molecules* **2019**, *24*, 1239. [CrossRef]
52. Chen, G.Q.; Zhu, L.N.; He, J.X.; Zhang, S.; Li, Y.H.; Guo, X.L.; Sun, D.; Tian, Y.E.; Liu, S.M.; Huang, X.B.; et al. Combinatorial Synthesis of Novel 1-sulfonyloxy/acyloxyeugenol Derivatives as Fungicidal Agents. *Comb. Chem. High. Throughput Screen.* **2022**, *25*, 1545–1551. [CrossRef]
53. Salehan, N.M.; Meon, S.; Ismail, I.S. Antifungal activity of *Cosmos caudatus* extracts against seven economically important plant pathogens. *Int. J. Agric. Biol.* **2013**, *15*, 864–870.
54. Wang, J.; Guo, Q.G.; Su, Z.H.; Dong, L.H.; Wang, P.P.; Zhang, X.Y.; Lu, X.Y.; Zhao, W.S.; Qu, Y.H.; Li, S.Z.; et al. Effect of Fengycin Produced by *Bacillus subtilis* NCD-2 on the Conidial Germination and Microsclerotia Formation of *Verticillium dahliae*. *Acta Phytopathol. Sin.* **2020**, *50*, 739–747. [CrossRef]
55. Mochizuki, M.; Yamamoto, S.; Aoki, Y.; Suzuki, S. Isolation and characterization of *Bacillus amyloliquefaciens* S13-3 as a biological control agent for anthracnose caused by *Colletotrichum gloeosporioides*. *Biocontrol Sci. Technol.* **2012**, *22*, 697–709. [CrossRef]

Disclaimer/Publisher's Note: The statements, opinions and data contained in all publications are solely those of the individual author(s) and contributor(s) and not of MDPI and/or the editor(s). MDPI and/or the editor(s) disclaim responsibility for any injury to people or property resulting from any ideas, methods, instructions or products referred to in the content.

Journal of *Fungi*

MDPI

Article

Talaromyces pinophilus Strain HD25G2 as a Novel Biocontrol Agent of *Fusarium culmorum*, the Causal Agent of Root and Crown Rot of Soft Wheat

Amel Bennacer [1,2], Fatma Sahir-Halouane [1], Micaela Alvarez [3,*], Zahia Oukali [1], Nour El Houda Bennacer [4], Abdelhamid Foughalia [5] and Josué Delgado [2]

[1] Laboratory of Valorization and Conservation of Biological Ressources (VALCORE), Department of Biology, Faculty of Sciences, University of M Hamed Bougara, Boumerdes 35000, Algeria; a.bennacer@univ-boumerdes.dz (A.B.); fatmahalouane@yahoo.fr (F.S.-H.); oukaliz408@gmail.com (Z.O.)
[2] Grupo de Investigación Higiene y Seguridad Alimentaria, Instituto Universitario de Investigación de la Carne y Productos Cárnicos, Facultad de Veterinaria, Universidad de Extremadura, 10003 Cáceres, Spain; jdperon@unex.es
[3] Sección Departamental de Nutrición y Ciencia de los Alimentos, Facultad de Veterinaria, Universidad Complutense de Madrid, 28040 Madrid, Spain
[4] Laboratory of Water Environment and Sustainable Development, Faculty of Technology, University Blida 1, Blida 09000, Algeria; bennacer.noorelhouda@gmail.com
[5] Centre de Recherche Scientifique et Technique sur les Régions Arides (CRSTRA), BP 1682 RP, Biskra 07000, Algeria; hmadou.fou@gmail.com
* Correspondence: malvar54@ucm.es

Abstract: *Fusarium culmorum* is the causal agent of root rot and crown rot in soft wheat. The aim of this study was to investigate the control mechanism of *Talaromyces pinophilus* HD25G2 as a biocontrol agent against *F. culmorum*. This involved the isolation and molecular identification of *Fusarium* and *Talaromyces* strains from soft wheat. The assay included the inhibition test of *F. culmorum* mycelial growth on potato dextrose agar and soft wheat media at two water activity values (0.98 and 0.95), its production of mycotoxins, and the fungal cell wall-degrading enzymes implicated in the antagonistic effect of *T. pinophilus*. The results showed that *T. pinophilus* and its extract free of cells reduced the growth of *F. culmorum* by over 55%. Interestingly, the *T. pinophilus* HD25G2 showed high chitinase, protease, and cellulose production on solid media. In addition, chitinolytic and proteolytic activities were estimated at the values of 1.72 ± 0.02UI and 0.49 ± 0.01UI, respectively. However, the mycotoxin evaluation assay revealed that *F. culmorum* HD15C10 produced zearalenone (ZEA) and the biocontrol agent enhanced its production, but the early inoculation of *T. pinophilus*, before *F. culmorum* growth onset, inhibited 100% its growth and, therefore, prevented the presence of ZEA. Hence, this strain can be proposed as a biocontrol agent against *F. culmorum*, and it can be further investigated for biocontrol of *Fusarium* root and crown rot in vivo.

Keywords: antagonism; enzymatic activity; food security; mycelial growth; zearalenone

1. Introduction

The world's crop production experiences significant crop losses each year due to pathogens through reduced yield, productivity, and growth of many crops [1]. In this sense, *Fusarium* infection, a plant pathogenic fungus, is a global concern, causing economically severe crop losses and ranking among the most hazardous pathogens affecting cereals [2]. *Fusarium* encompasses a diverse group of fungal species, many of which are well-known

plant pathogens that have caused significant crop damage over the past two centuries. These fungi commonly colonise aerial parts of plants, either as natural components of the mycobiota or as aggressive pathogens, particularly affecting horticultural crops and cereal grains like maize, often rendering them unsuitable for consumption. *Fusarium* species are responsible for various plant diseases, including seedling blight, root and crown rot, as well as stalk and ear rot, and can infect plants at any developmental stage. The success of *Fusarium* infection depends on a series of complex and tightly regulated processes, beginning with host colonisation and culminating in disease manifestation [2,3]. Additionally, this genus poses a risk due to its ability to synthesise mycotoxins such as deoxynivalenol (DON), zearalenone (ZEA), and fumonisin B1. These mycotoxins are identified as some of the top five most significant mycotoxins [3]. Fusariosis has a significant economic impact across various countries and regions worldwide, including North and South America, Australia, Europe, North Africa (particularly Algeria), South Africa, and West Asia. Losses can reach up to 70% when infection conditions are favourable. They reduce yield by decreasing the germinative capacity of seeds, the grain count per spike, the weight of a thousand grains, and their overall quality [4]. Investigations have shown that strains of *Fusarium culmorum* are prevalent and highly aggressive on wheat seedlings along with *Fusarium graminearum* and *Fusarium pseudograminearum*, contributing to head blight (FHB), crown rot (FCR) and root rot (FRR) diseases in Algeria [5,6]. These diseases affect soft wheat (*Triticum aestivum*) worldwide, causing substantial yield losses, especially in dry climates and regions where conservation agriculture practices, such as minimal tillage and stubble retention, are applied. FCR is mainly spread through infected stubble [7], FRR is worsened by the use of infected seeds, and FHB is identified by the bleaching of spikelets [8,9]. Aside from causing yield losses, *F. culmorum* also leads to the build-up of diverse mycotoxins, mainly ZEA [10]. To control these hard-to-reach fungi, a range of strategies has been proposed, including crop rotation, the use of resistant varieties, or antifungal treatment. These are the main practical approaches used with limited effectiveness [11]. Plant protection treatments relying on synthetic chemicals are increasingly scrutinised owing to worries over human health, environmental impact, the development of resistant strains, and residue presence in harvested fruit [12]. Therefore, due to *Fusarium* dissemination and its persistence in the soil, its control seems limited to prophylactic measures [13]. However, in recent years, special attention has been given to methods of biological control. The use of microorganisms with antifungal activity is a promising alternative to the use of pesticides, due to the ubiquity of these microorganisms, their great diversity, and their dissemination in rhizospheric soils, and it is potentially beneficial to the health of consumers [14]. Previous research has shown that *Talaromyces pinophilus* (Hedgc.) Samson is prevalent in soil, compost, seeds, grains, the phyllosphere, and the phylloplane. Furthermore, it has been recognised as an endophytic fungus in several therapeutic plants [1,15,16]. It has been widely utilised for its ability to degrade cellulose and as a sustainable source of pigments and bioactive compounds [17,18]. Few studies have looked at *T. pinophilus*' antagonistic activity and mycoparasitic behaviour against *Rhizoctonia solani* [19,20]. The detailed mechanism of *T. pinophilus* mycoparasitism against *B. cinerea* was outlined by Abdel-Rahim and Abo Elyossr [21]. They concluded that the fungus's toxic metabolites, including extracellular wall-degrading enzymes, antibiotics, and volatile organic compounds (VOCs), contribute to the expression of its antagonistic activity [22,23].

This research aimed to evaluate the antagonistic effects of *T. pinophilus* on *F. culmorum*, the pathogen is responsible for *Fusarium* Root and *Fusarium* Crown Rot in soft wheat. This study focused on examining the inhibition of *F. culmorum* growth, mycotoxin production, as well as the enzymes that degrade the fungal cell wall, which play a role in the antagonistic

interaction. To the best of our knowledge, this is the first study worldwide to investigate these specific antagonistic mechanisms between *T. pinophilus* and *F. culmorum*.

2. Materials and Methods

2.1. Fungal Isolation and Identification

Fusarium sp. HD15C10 was isolated from samples of soft wheat seeds, harvested in the year 2020, from the Tizi-ouzou region (36.73601203227208, 3.9740759227314664) (Algeria), while the *Talaromyces* spp. HD25G2 was isolated from healthy, asymptomatic soft wheat seeds stored in the Constantine region (36.334561393967014, 6.714242306223273), Algeria.

The seed samples (1 Kg) were transferred into sterilised polyethene bags and promptly taken to the laboratory and refrigerated until isolation. Isolation was performed using PDA medium (TM Media, Delhi, India) enriched with chloramphenicol (250 mg/L) and rose Bengal (66.7 mg/L) (both from Sigma-Aldrich, St. Louis, MO, USA).

In order to isolate the fungi, soft wheat seeds from both samples were individually selected, surface-sterilised using 1% sodium hypochlorite, thoroughly rinsed with sterilised distilled water, and subsequently dried on a sterile filter paper. The sterilised seeds (5 grains per plate) were then placed on PDA plates and incubated at 25 °C for 7 days [24].

After incubation, the colonies were subsequently purified through a single-spore isolation technique. The monosporic colonies were further examined both macroscopically and microscopically [25,26].

Macroscopic characterisation involved evaluating morphological features such as colony growth rate, texture, and colour. Microscopic observations of *Talaromyces* spp. and *Fusarium* spp. isolates were carried out by examining the shape of phialides and conidia, as well as the positioning of chlamydospores, using a Motic BA210 model microscope (Fisher Scientific, Schwerte, Germany). The endophytic fungus *Talaromyces* spp. was initially identified through its colony morphology, growth texture, and micromorphological features on potato dextrose agar (PDA), glycerol nitrate 25% agar (GN25) at 25 °C, and Czapek yeast agar (CYA; Sigma-Aldrich) at 37 °C after 7 days of incubation. The fungi were subsequently stored in the laboratory's mycological collection for future use. The isolation was performed in triplicate.

2.2. Molecular Identification of Talaromyces spp. and Fusarium spp. Strains by PCR Assay

Molecular identification of the fungal isolate was achieved through PCR amplification targeting the internal transcribed spacer (ITS) region of ribosomal DNA. Fungal mycelium was harvested from potato dextrose agar (PDA) after 5 days of incubation at 28 °C, suspended in 100 µL of sterile distilled water, and stored at −80 °C. Genomic DNA was extracted utilising the NucleoSpin Plant II DNA Prep Kit (Macherey-Nagel, Düren, Germany), following the SDS/CTAB lysis method, with subsequent purification via phenol/chloroform extraction. PCR amplification and sequencing were performed at GLS Sidi Bel Abbes (Sidi Bel Abbès, Algeria) and Eurofins Scientific (Nantes, France). The ITS region was amplified using the primer pair ITS1 (5′-CTTGGTCATTTAGAGGAAGTAA-3′) and ITS4 (5′-TCCTCCGCTTATTGATATGC-3′), as described by Gardes and Bruns [27].

The PCR reaction mixture, with a total volume of 25 µL, contained 1 µL (20 ng) of fungal DNA, 2.5 µL of 10× EF-Taq buffer, 0.5 µL of 10 mM dNTPs, 1.0 µL of each forward and reverse primer (10 pmol), 0.25 µL of EF-Taq polymerase (2.5 U), and nuclease-free water to complete the volume. The PCR conditions included an initial denaturation at 95 °C for 5 min, followed by 35 cycles consisting of denaturation at 95 °C for 30 s, annealing at 55 °C for 30 s, and extension at 72 °C for 45 s, concluding with a final extension at 72 °C for 7 min. PCR products were visualised on an agarose gel under UV light (VWR-730 Avantor, Radnor, PA, USA). Specific bands were excised and purified using the NucleoSpin

Plant II kit (Fisher Scientific, Schwerte, Germany) following the manufacturer's protocol. The amplified ITS region from both strands was sequenced using the primers ITS1 and ITS4. The resulting sequences were analysed through the BLAST tool on the NCBI website (http://blast.ncbi.nlm.nih.gov/Blast.cgi).

Multiple sequence alignments were performed using CLUSTALW (https://www.genome.jp/tools-bin/clustalw), and phylogenetic relationships were determined using MegAlign software (version 5.01) with reference sequences from GenBank.

The sequences for *T. pinophilus* strain HD25G2 and *F. culmorum* HD15C10 were deposited in the GenBank nucleotide sequence database under accession numbers OM978188 and ON743052, respectively.

2.3. Antagonistic Activity

All assays were conducted on PDA and soft wheat simulating media. The 2% milled soft wheat agar media (SWA) was prepared and adjusted at two distinct water activities (a_w) values by adding glycerol until it achieved 0.98 (high water availability; SWA98) and 0.95 a_w (intermediate water stress; SWA95) according to Da Cruz Cabral et al. [28].

2.3.1. Dual Culture Test

A 6 mm diameter mycelial plug of actively growing *F. culmorum* was placed on one edge of a Petri dish containing PDA, SWA98 and SWA95, while a mycelial plug of *T. pinophilus* was placed on the opposite edge, 35 mm away. The plates were incubated at 25 °C until the morphological overgrowth interaction was observed. The pathogen *F. culmorum* was inoculated alone in the middle of the testing plates as a positive control [29]. To calculate the growth inhibition percentage (I%), the following equation was used:

$$I\% = [(RC - RT)/RC] \times 100 \quad (1)$$

In this formula, RC denotes the diameter of the pathogen's radial growth in the control treatment, while RT represents the diameter of radial growth when the pathogen is exposed to the biocontrol agent (BCA).

Additionally, after the results were obtained, an assay of direct confrontation was required. The mycelium close to the contact zone in dual cultures was observed microscopically. All the assays (antagonistic activity and dual culture as well as negative controls) in different media were performed in triplicate.

2.3.2. *Talaromyces pinophilus* Culture Filtrate Inhibition Test

The method involves adding culture filtrates from the antagonistic strain *T. pinophilus* into a culture medium, followed by inoculation with discs of the pathogen to evaluate its effectiveness against *F. culmorum* [28,29]. Three plugs from the *T. pinophilus* culture were transferred to Erlenmeyer flasks containing 150 mL of PDB or SWB (at two different a_w levels) and incubated on a rotary shaker at 150× *g* and 26 °C for 7 days. After incubation, the liquid culture was harvested by centrifugation at 9500× *g* for 10 min and subsequently filtered using a 0.45 µm syringe filter (RephiLe Bioscience, Philadelphia, PA, USA). A negative control was prepared, maintaining the same conditions. The resulting filtrates from PDB and SWB were incorporated into PDA and SWA98 or SWA95 media, respectively, at a 10% (*v*/*v*) concentration. Three 6 mm diameter agar plugs from the *F. culmorum* culture were placed at equal distances (35 mm apart) on the Petri dish, which was then incubated at 26 °C until the fungal colonies overlapped. The inhibition percentage (I%) was determined using the method described earlier.

2.4. Direct Confrontation Test

This test was used to evaluate the antagonistic interaction between BCA mycelium and *F. culmorum* mycelium in SWA98 and SWA95 media in direct contact, applying the BCA before the growth of *F. culmorum* [30,31]. In SWA plates at the two a_w, 100 µL of *T. pinophilus* strain (10^Q spore/mL) was inoculated on all the surfaces and incubated at 25 °C. After three days, a mycelium plug (6 mm diameter) from 4-day-old actively developing colonies of *F. culmorum* was seeded in the centre of the plates. The plates were observed daily (9th day after incubation). Negative controls of both strains were grown separately. The assays in different culture media, as well as the negative control, were conducted in triplicate.

2.5. Mycotoxin Production

Three plugs from *F. culmorum* mycelia close to the contact zones between moulds from the dual culture test in SWA media (Section 2.3.1) were collected. The mycotoxins were extracted and analysed following the methodology described by Galán et al. [31]. Briefly, acetonitrile, water, and acetic acid (79:20:1; *v*/*v*/*v*) were added to the sample at a ratio of 4 mL/g, and the solution was shaken for 90 min. Following extraction, a 0.5 mL aliquot of the extract was mixed with 0.5 mL of a different acetonitrile/water/acetic acid solution in a 20:79:1 (*v*/*v*/*v*) ratio and transferred into 1.5 mL vials. A 10 µL portion of the diluted extract was subsequently analysed using target metabolomics in a Q-Exactive Plus Orbitrap mass spectrometer (Thermo Fisher Scientific, Waltham, MA, USA).

2.6. Enzymes Qualitative Screening of T. pinophilus HD25G2

Protease, chitinase, and cellulase activities were evaluated on skim milk agar, Chitinase detection Medium (CDM), and Czapek-Mineral Salt agar medium supplemented with carboxy methyl cellulose (CMC). All the media cultures were maintained at pH 7 and incubated in the dark as described by Cherukupally et al. [32] and Reghmit et al. [33]. The results are observed according to the change in the media's colour:

- Clear zones around the disc indicate proteolytic activity.
- The chitin hydrolysis area changes colour from yellow to purple.
- The presence of a yellow opaque zone surrounding the colonies shows the presence of cellulases.

2.7. Quantitative Enzyme Assays

2.7.1. Determination of Protease Activity

To evaluate proteolytic activity, a liquid medium supplemented with 1% casein as the substrate was used, following the method described by Reghmit et al. [33]. The cultures were grown for 5 days at 28 °C, after which they were centrifuged at 9500× *g* for 15 min.

A 500 µL aliquot of the supernatant was then mixed with 1.25 mL of 1% casein prepared in phosphate buffer (pH 10) and incubated at 40 °C for 30 min. The reaction was terminated by adding 3 mL of 0.19 M trichloroacetic acid (Sigma-Aldrich), followed by a further incubation at 40 °C for 15 min. The mixture was then subjected to centrifugation at 9500× *g* for 10 min.

After the centrifugation process, 500 µL of the supernatant was combined with 2.5 mL of 0.4 M $NaCO_3$ and 250 µL of Folin–Ciocalteu's reagent (Sigma-Aldrich). The resulting solution's absorbance was measured at a wavelength of 660 nm to determine the concentration of released short peptides and free amino acids. Subsequently, enzyme activity was calculated based on the amount of enzyme required to release 1 µmol of tyrosine per minute, per mL of enzyme solution. A negative control (without inoculating the fungi) was also prepared, maintaining the same conditions.

2.7.2. Chitinase Hydrolytic Activity Assay

Following the method described by Reghmit et al. [33]. Two plugs from a 5-day-old *Talaromyces* culture were transferred into 50 mL of synthetic medium (SM). The culture was incubated and then centrifuged at 8000× *g* for 5 min. The supernatant, which served as the enzyme solution, was mixed in equal volume (1 mL) with 1% colloidal chitin prepared in 0.05 M sodium acetate buffer (pH 5). This mixture was incubated for 1 h at 37 °C under constant agitation. After the incubation, the reaction mixture underwent a second centrifugation at 5000× *g* for 15 min. To assess chitinase activity, 1 mL of the supernatant was mixed with 3 mL of dinitrosalicylic acid (DNS) reagent and boiled for 5 min. The absorbance of the solution was recorded at 585 nm. Chitinase activity was expressed as the amount of enzyme needed to release 1 µmol of N-acetylglucosamine (GlcNAc) per minute under the assay conditions. All experiments were performed in triplicate. A negative control (without inoculating the fungi) was also prepared, maintaining the same conditions.

2.8. Statistical Analysis

Values were analysed using two-way ANOVA with Tukey's HSD to study the interactions between the different media and treatments on growth inhibition and mycotoxins due to within the natural population, biological data generally follow a normal distribution. All the tests were carried out using IBM SPSS software version 25.0 (IBM Corp., Armonk, NY, USA). Cohen's term *d* was used to calculate the effect size index by using R software version 4.5.1. (https://www.r-project.org). Statistical significance was set at $p \leq 0.01$.

3. Results

3.1. Fungal Isolation and Identification

In this study, *F. culmorum* HD15C10 was isolated from soft wheat seed crops grown in Tizi-Ouzou, Algeria. Preliminary *F. culmorum* strain HD15C10 characterisation was carried out based on macroscopic colony traits and microscopic features. The following figure demonstrates the macroscopic and microscopic appearances (Figure 1A,B) and, in addition, the molecular phylogeny of *F. culmorum* strain HD15C10 with DNA sequences for reference strains (Figure 1C).

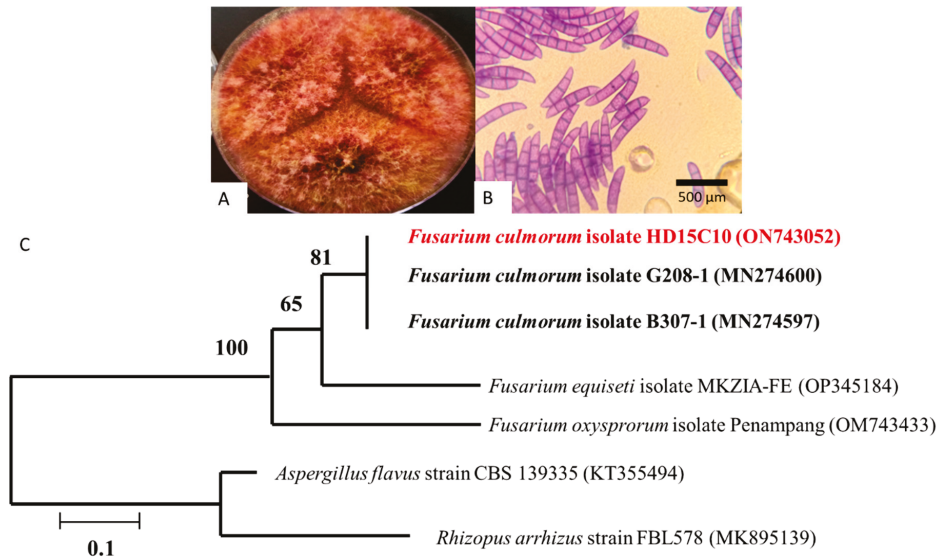


Figure 1. *Fusarium culmorum* strain HD15C10: (**A**) 7-day-old culture at 25 °C on potato dextrose agar (PDA) medium; (**B**) light microscopic analysis showing the fungal elements as conidiophores and conidia; (**C**) molecular phylogeny of *F. culmorum* strain HD15C10 with DNA sequences for reference strains of *F. culmorum* (bar indicates genetic distance due to sequence divergence).

Sequencing of the ITS region showed 99.4% similarity with *F. culmorum* isolate G208-1 (MN274600), and a phylogenetic tree was constructed using other closely related sequences of *F. culmorum* (Figure 1C).

Figure 2 represents the macroscopic and microscopic appearances (Figure 2A–D) and the molecular phylogeny of *T. pinophilus* HD25G2 with DNA sequences for reference strains (Figure 2E).

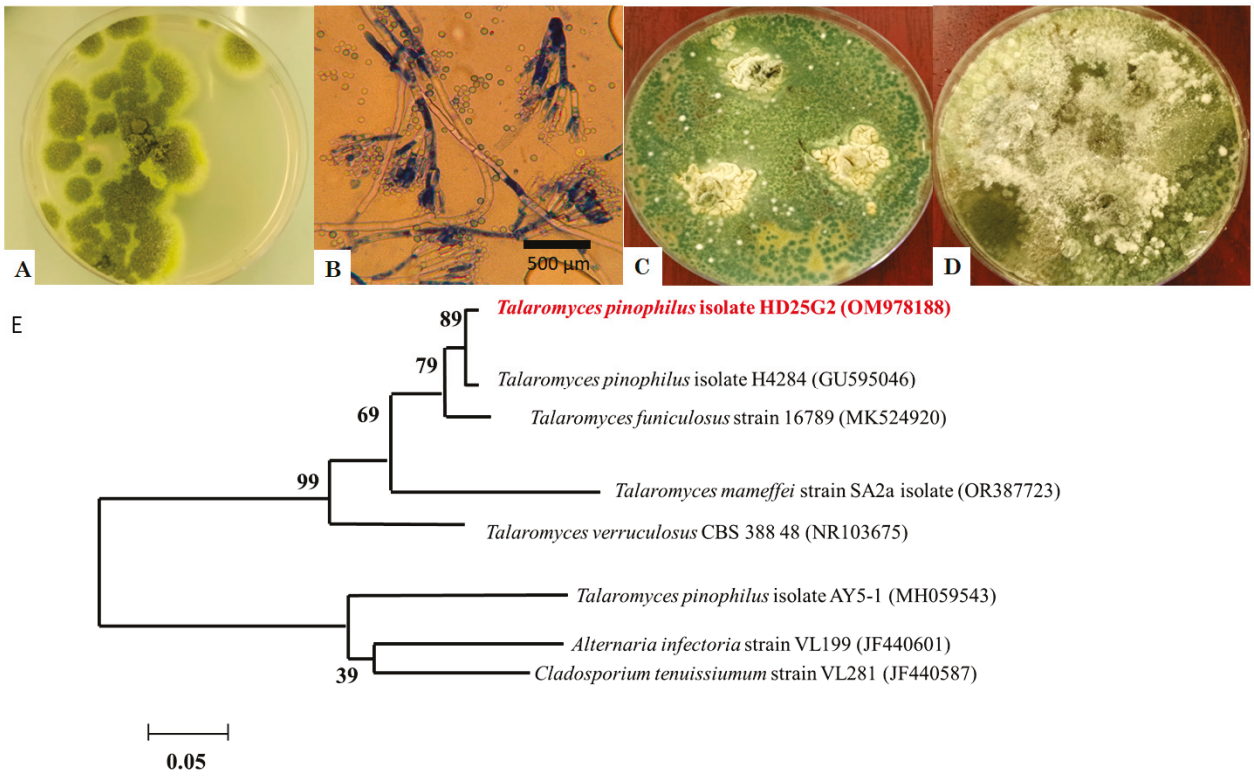


Figure 2. *Talaromyces pinophilus* strain HD25G2: (**A**) 7-day-old culture on PDA medium at 25 °C; (**B**) conidiophores with smooth walled elements, characteristically symmetrically biverticillate; (**C**) 7-day-old culture on GN25 medium at 25 °C; (**D**) 7-day-old culture on CYA medium at 37 °C; (**E**) molecular phylogeny of *T. pinophilus* strain HD25G2. with DNA sequences for reference strains of *Talaromyces* spp. (bar indicates genetic distance due to sequence divergence).

On PDA, colonies of *T. pinophilus* grew to 27–32 mm after 7 days of incubation at 25 °C, displaying a greyish-green to dull green colour with white and yellow mycelia (Figure 2A). When cultured on CYA and GN25 media, after 7 days of incubation at 37 °C (Figure 2C) and 25 °C (Figure 2D), the colonies appeared greyish-green, with a raised centre and flat, well-defined edges. The texture was floccose and funiculose, particularly in the central region (Figure 2A). The reverse side of the colonies exhibited a greyish-orange colouration. Conidiophores were smooth, symmetrically biverticillate, with stipes (150–200 × 2–3 µm) bearing three to six metulae (10–11 × 2.5–3 µm), which supported acerose phialides (8.5–12 × 2–3 µm) (Figure 2B). The conidia were smooth, globose to subglobose, with a diameter ranging from 2 to 3 µm. No ascomata were observed. Additionally, the ITS sequence of the *T. pinophilus* strain HD25G2 showed 99.5% similarity with *T. pinophilus* isolate H4284 (GU595046) (Figure 2E).

3.2. Mycelial Growth Inhibition

The biocontrol potential of the *T. pinophilus* isolate was in vitro assessed through different mechanisms against *F. culmorum*. The inhibition effect of *T. pinophilus* on the mycelial growth of *F. culmorum* in dual culture assay displayed a percentage of inhibition

around 72.59% (PDA), 73.7% (SWA98), and 72.01% (SWA95) after 7 days of incubation (Figure 3) compared to the untreated control (showing no activity) ($p < 0.01$; Table 1). The results demonstrated a large effect size when *T. pinophilus* was added concerning the untreated control, with Cohen's *d* values ranging from 7 to 21. No statistical differences were found between the same treatments in different media after the analyses using two-way ANOVA with Tukey's HSD ($p > 0.01$). Cohen's *d* values between media were in the range of −0.4 and 0.2 in the dual culture assay and between 0 and 0.1 in the filtrate culture. Importantly, BCA was most efficient in blocking 100% mycelial growth of *F. culmorum* HD15C10 when administered 3 days after the BCA in the direct confrontation test (Figure 3(A_4,B_4,C_4)).

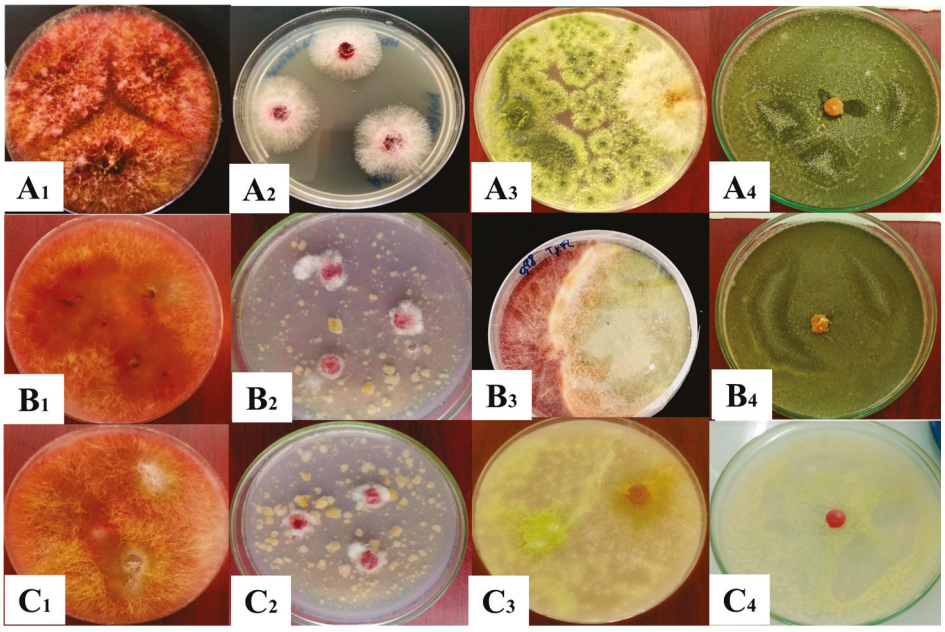


Figure 3. (**A_1–A_4**) Assays on potato dextrose agar media (image A_1 also shown in Figure 1A), (**B_1–B_4**) on soft wheat agar media a_w 0.98, and (**C_1–C_4**) on soft wheat agar media a_w 0.95 (1: *Fusarium culmorum* control, 2: filtrate assay, 3: direct confrontation assay, 4: direct confrontation (*Talaromyces pinophilus* was cultivated 2 days before *F. culmorum*)).

Table 1. Assessment of antagonistic activity of *Talaromyces pinophilus* HD25G2 against *Fusarium culmorum* HD15C10 on potato dextrose agar and on soft wheat stimulating media at two water activity (a_w) values.

Media	Assay	Percentage of Growth Inhibition of *F. culmorum* (%)
Potato dextrose agar	Dual culture	72.59 ± 0.37 *a
	Filtrate culture	61.48 ± 0.74 *a
Soft wheat simulating media a_w 0.98	Dual culture	73.7 ± 0.37 *a
	Filtrate culture	62.96 ± 3.70 *a
Soft wheat simulating media a_w 0.95	Dual culture	72.22 ± 2.12 *a
	Filtrate culture	59.99 ± 1.03 *a

* Statistical differences with the control group ($p < 0.01$). Statistical differences between the same treatment with different media indicated by letters.

The filtrate of *Talaromyces* demonstrated the ability to inhibit the growth of the pathogen (Table 1). This strain effectively restricted both radial and aerial growth. The

results suggest that the inhibition percentage is likely influenced by the concentration of *Talaromyces* filtrate and the quality of the bioactive molecules present (Figure 3(A_2,B_2,C_2)).

The microscopic evaluation of *F. culmorum* in contact with *T. pinophilus* is represented in Figure 4. The microscopical visualisation showed a denser mycelium from *F. culmorum* in the confrontation zone with the BCA (Figure 4B) with respect to the normal growth of the pathogen (Figure 4A). Furthermore, there was an increase in the exudate droplet production by the toxigenic mould when confronted with the BCA (Figure 4).

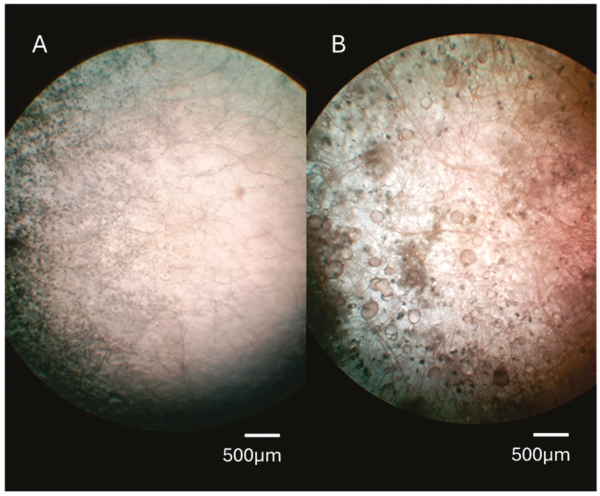


Figure 4. Microscopic evaluation of *Fusarium culmorum* HD15C10. (**A**): Normal growth of *F. culmorum* in soft wheat agar with 0.98 water activity (a_w). (**B**): *F. culmorum* growth close to the contact zone with *Talaromyces pinophilus* used as a biocontrol agent.

3.3. Mycotoxin Analysis

The analysis revealed that *F. culmorum* HD15C10 is a producer of ZEA. The results (Table 2) showed that the presence of the BCA triggered the ZEA production. Cohen's *d* showed a large effect size when adding the biocontrol agent (−3.40 at 0.95 a_w and −32.55 at 0.95 a_w).

Table 2. Mycotoxin production of *Fusarium culmorum* HD15C10 in soft wheat agar at 0.98 and 0.95 water activity in the presence of the biocontrol agent *Talaromyces pinophilus* HD25G2.

Water Activity (a_w)	Treatment	Zearalenone (ng/g)
0.98	Control	0.63 ± 0.84^{a}
	F. culmorum + *T. pinophilus*	104.19 ± 60.98^{b}
0.95	Control	8.33 ± 6.99^{c}
	F. culmorum + *T. pinophilus*	334.16 ± 17.76^{d}

Statistical differences are indicated with different letters $p \leq 0.01$.

3.4. T. pinophilus Extracellular Enzymes

Figure 5 represents the appearance of *T. pinophilus* on solid media for the enzymatic activity assays indicated by clear zones around the colony. The tested *T. pinophilus* strain showed the capacity to produce chitinases, proteases, and cellulases. The strain showed cellulase activity, as indicated by an 80 mm clear zone around the colonies after 3 days of incubation. It also exhibited notable protease activity, demonstrated by visible protein hydrolysis on skim milk agar (clear zone). Additionally, *T. pinophilus* displayed strong chitinase activity, evidenced by a purple zone with a diameter of 65 mm (Figure 5). Enzyme assays revealed that the proteolytic activity of *T. pinophilus* was 0.49 ± 0.01 IU at pH 10,

while its chitinase activity was 1.72 ± 0.02 IU compared to negative controls that showed no enzymatic activity.

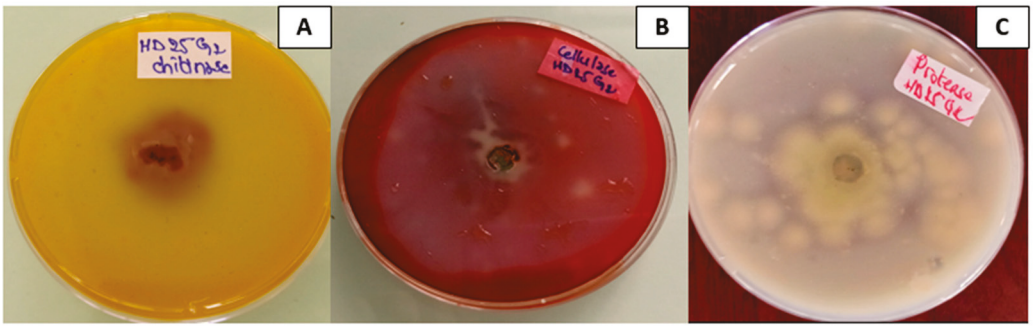


Figure 5. *Talaromyces pinophilus* HD25G2 production of extracellular enzymes on selective solid medium. Positive enzymatic activity indicated by a change in colour of the medium around the colony. (**A**): chitinase activity; (**B**): cellulase activity; (**C**): protease activity.

4. Discussion

Significant efforts have been made to replace chemical fungicides with environmentally friendly alternatives, particularly biological control agents (BCAs) [34,35]. A critical first step in biological control is the identification of effective antagonistic agents. However, research on the antagonistic potential of *T. pinophilus* as a BCA against phytopathogenic fungi remains limited [17,20,21]. Endophytes are microorganisms that reside within the tissues of plants that appear healthy and show no symptoms of infection [36].

To the best of our knowledge, this is the first study to investigate the endophytic fungus *T. pinophilus* as a biological control agent (BCA) against *F. culmorum*. Notably, the *T. pinophilus* strain HD25G2 was predominantly isolated from healthy, asymptomatic stored soft wheat seeds from the Constantine region in Algeria.

This study demonstrated for the first time the inhibition of *F. culmorum* mycelial growth by *T. pinophilus*. Dual culture techniques have been widely used in tests of antagonistic activities, showing useful in vitro results [33,37], such as those in Figure 3. Previous studies have indicated that *Talaromyces* species are commonly found in soil, air, and the seeds of various plants, with some strains showing potential for controlling plant diseases [38]. For instance, *Talaromyces flavus*, isolated from tomatoes, significantly reduced tomato blight caused by *Verticillium dahlia* [39]. Similarly, the Q2 strain of *T. purpureogenus* has demonstrated the ability to suppress the growth of 12 plant pathogens and mitigate soil-borne diseases, including bitter melon wilt, tobacco black shin disease, and potato stem rot, under controlled greenhouse conditions [40]. *T. muroii* TM28 demonstrated effective inhibition of *Fusarium pseudograminearum*, with an inhibition rate exceeding 50% [41]. Moreover, *T. pinophilus* has also been reported to exhibit inhibitory effects against *B. cinerea*, demonstrating mycoparasitic activity [21]. The sterile fermentation filtrate of *T. pinophilus* demonstrated a high inhibitory capacity on the mycelial growth of *F. culmorum* when cultured on both PDA and SWA media. This observed antagonism is likely attributed to the strain's production of various cell wall-degrading enzymes and catalytic activities (Figure 4). Previous research has recognised *Talaromyces* species as significant cellulose-degrading fungi, contributing significantly to biomass degradation processes [42,43]. These fungi possess a wide range of genes involved in encoding proteases, enzymes for secondary metabolite biosynthesis, and enzymes that degrade fungal cell walls [44–46]. The fungal cell wall is integral to several key processes, including fungal survival, morphogenesis, and pathogenicity [47], and its breakdown is a central mechanism through which antagonistic microorganisms exert their inhibitory effects [48]. Chitin and β-(1,3)-glucan, both critical components of the *Fusarium* cell wall, are synthesised by the enzymes chitin synthase and

β-(1,3)-glucan synthase [49]. Chitin plays an essential role in cell division and contributes to the pathogen's virulence [50]. *T. pinophilus* can produce chitinase, which appears to play a central role in the degradation of the *F. culmorum* cell wall. Previous studies have shown that *T. pinophilus* generates two types of chitinase enzymes, which have been demonstrated to degrade the cell walls of *Verticillium dahliae* and *Rhizoctonia solani*, as well as inhibit spore germination and germ tube elongation of *Alternaria alternata* [51]. However, chitinase alone is not solely responsible for fungal cell wall degradation; it operates synergistically with other hydrolytic enzymes, such as 1,3-β-glucanase, proteases, and lipases, to comprehensively dismantle the host cell wall [52]. In this context, the robust enzymatic activity exhibited by various mycoparasitic organisms has been recognised as a critical factor for the lysis of cell walls in phytopathogenic fungi [53]. In the present study, the *T. pinophilus* strain significantly impacted the mycelial growth of the phytopathogen *F. culmorum*. This finding is consistent with the work of Abdel-Rahim and Abo-Elyousr [21], who documented the mycoparasitic interaction of *T. pinophilus* with *B. cinerea.* A typical mycoparasitic interaction involves several stages, including host detection, attraction, attachment, coiling around the host, and the lysis of the host cell wall through the action of hydrolytic enzymes [54]. Additionally, it has been reported that diffusible compounds, proteins, or antibiotics produced by fungal strains can inhibit the growth of other microorganisms [55,56].

However, despite the successful growth inhibition observed, the BCA stimulated the ZEA production by *F. culmorum* when no total inhibition was achieved (aw 0.98: 114.19 and aw 0.95: 334.16 ng/g compared to the control, $p \leq 0.01$), demonstrating that the growth measure is not a proper indicator of the effectiveness of BCAs against toxigenic moulds [57,58]. The microscopic evaluation revealed that the mould morphology was also affected and could trigger the production of mycotoxins due to the stress caused by the presence of *Talaromyces*. Several studies have shown that in the presence of stress conditions, such as BCAs, provoking the inhibition of the pathogen's mycelial growth, the latter could boost the production of mycotoxins, directly affecting the genes responsible for the mycotoxin synthesis [59–61].

The ZEA overproduction at a common temperature on field and storage (25 °C) could lead to the discard of *T. pinophilus* as BCA. However, the early inoculation with the BCA prevented the appearance of the toxigenic mould. Therefore, the strategy to successfully counteract *F. culmorum* growth in soft wheat would be the inoculation of this BCA before any possibility of the toxigenic fungal growth onset. This strategy could be exerted both by inoculating crops before harvesting, since this strain is ubiquitous in this environment, or immediately after harvesting, to endow the soft wheat with BCA spores in case it is contaminated with the pathogen and the conditions are propitious for fungal growth. However, this further research step must be carried out in future studies to achieve the best strategy to prevent ZEA accumulation in soft wheat. The stimulation of mycotoxin production has been previously demonstrated in other toxigenic moulds using biocontrol agents and chemical fungicides at subinhibitory concentrations in different matrices. Therefore, the importance of proper application of antifungal agents and the possible need to reinoculate the crops is emphasised by the results of the present study [55,57,62,63].

Efforts should be focused on basic preventative measures such as the correct rate (%) of humidity, prevention of contact with soil, etc. However, the proposed strategy could be a cheap and easy preventative measure for developing countries to avoid the waste of soft wheat in case conditions favour fungal growth, and this wheat could be used for different purposes, such as animal feeding, or destination of the wheat for flour since the fungal growth would not mean mycotoxin production. This alternative would benefit the food safety and security of developing countries, given that it would prevent mycotoxin

contamination and food waste. The present study was designed as an exploratory and hypothesis-generating investigation, aiming to provide preliminary insights into the biocontrol potential of *T. pinophilus*, a strain that, to our knowledge, has not been previously evaluated in this specific context. To this end, we employed laboratory-based antagonism assays, enzymatic activity profiling, and co-culture mycotoxin quantification as initial screening tools to assess its potential efficacy. The use of parametric tests in this study is justified by the expectation that, within the natural population, such biological data generally follow a normal distribution, offering increased statistical power and precision. Given the early-stage nature of this work and the absence of data under agronomic or storage conditions, no specific recommendations for field application or commercial formulation can be proposed at this point yet.

5. Conclusions

In conclusion, this study provided evidence that the endophytic *T. pinophilus* holds potential as an effective BCA against *F. culmorum*, a producer of zearalenone (ZEA). The production of cell wall-degrading enzymes by *T. pinophilus* enhances its suitability as BCA, offering a promising alternative to chemical fungicides for managing fungal pathogens. The study also confirms that the mycotoxin production of toxigenic moulds must be evaluated when BCA is applied, although it reduces the growth of the pathogens, but does not fully inhibit them. Finally, the use of *T. pinophilus* as a BCA, being a cheap and easy preventive measure, may be proposed for crops with a high probability of suffering conditions that are prone to mould growth, although further research is necessary to measure the best strategy to minimise ZEA contamination. This strategy would positively impact the reduction in mycotoxin contamination and food waste.

Author Contributions: Conceptualization, A.B. and J.D. methodology, A.B., M.A., N.E.H.B., A.F. and Z.O.; formal analysis, A.B. and M.A.; investigation, A.B. and M.A.; resources, A.B., Z.O., N.E.H.B., A.F. and J.D.; data curation, A.B.; writing—original draft preparation, A.B.; writing—review and editing, M.A.; visualisation, M.A.; supervision, F.S.-H., M.A. and J.D.; project administration, F.S.-H. and J.D.; funding acquisition, J.D. All authors have read and agreed to the published version of the manuscript.

Funding: The Algerian Ministry of Higher Education and Scientific Research (MERS), General Directorate of scientific research and technological development (DGRSDT) and the University of Boumerdes supported this research (PRFU project entitled Développement d'une formulation à base de biochar associé à un consortium endophytique fongique: Application dans la stimulation et la régulation de pathosystéme Blé/Fusarium/Ver blanc, Code: D00L05UN350120230003). This research was funded by Junta de Extremadura-Consejería de Economía, Ciencia y Agenda Digital -, Fondo Europeo de Desarrollo Regional-"Una manera de hacer Europa" (grant number GR18056). Q-Exactive mass spectrometer for proteomic research was funded by the Spanish Ministerio de Economía y Competitividad (Ref. UNEX-AE-3394).

Institutional Review Board Statement: Not applicable.

Informed Consent Statement: Not applicable.

Data Availability Statement: The original contributions presented in the study are included in the article. Further inquiries can be directed to the corresponding author.

Acknowledgments: This work is also dedicated to the soul of my dear friend Maarouf Rahil, a student at the laboratory of ecology and natural ecosystems management, University Aboubaker Belkaid, Telmcen, Algeria.

Conflicts of Interest: The authors declare no conflicts of interest.

References

1. Gai, Y.; Wang, H. Plant Disease: A Growing Threat to Global Food Security. *Agronomy* **2024**, *14*, 1615. [CrossRef]
2. Ekwomadu, T.I.; Mwanza, M. Fusarium Fungi Pathogens, Identification, Adverse Effects, Disease Management, and Global Food Security: A Review of the Latest Research. *Agriculture* **2023**, *13*, 1810. [CrossRef]
3. Mielniczuk, E.; Skwaryło-Bednarz, B. *Fusarium* Head Blight, Mycotoxins and Strategies for Their Reduction. *Agronomy* **2020**, *10*, 509. [CrossRef]
4. Ferrigo, D.; Raiola, A.; Causin, R. *Fusarium* Toxins in Cereals: Occurrence, Legislation, Factors Promoting the Appearance and Their Management. *Molecules* **2016**, *21*, 627. [CrossRef]
5. Paulitz, T.C.; Schroeder, K.L.; Schillinger, W.F. Soilborne pathogens of cereals in an irrigated cropping system: Effect of tillage, residue management, and crop rotation. *Plant Dis.* **2010**, *94*, 61–66. [CrossRef]
6. Abdallah-Nekache, N.; Laraba, I.; Ducos, C.; Barreau, C.C.; Bouznad, Z.; Bouregheda, H. Occurrence of *Fusarium* head blight and *Fusarium* crown rot in Algerian wheat: Identification of associated species and assessment of aggressiveness. *Eur. J. Plant Pathol.* **2019**, *154*, 499–512. [CrossRef]
7. Smiley, R.W.; Gourlie, J.A.; Easley, S.A.; Patterson, L.-M.; Whittaker, R.G. Pathogenicity of fungi associated with the wheat crown complex in Oregon and Washington. *Plant Dis.* **2005**, *89*, 949–957. [CrossRef]
8. Xu, X.; Nicholson, P. Community ecology of fungal pathogens causing wheat head blight. *Annu. Rev. Phytopathol.* **2009**, *47*, 83–103. [CrossRef] [PubMed]
9. Moya-Elizondo, E.A.; Arismendi, N.; Montalva, C.; Doussoulin, H. First Report of *Fusarium sporotrichioides* Causing Foliar Spots on Forage Corn in Chile. *Plant Dis.* **2013**, *97*, 1113. [CrossRef] [PubMed]
10. Błaszczyk, L.; Ćwiek-Kupczyńska, H.; Hoppe Gromadzka, K.; Basińska-Barczak, A.; Stępień, Ł.; Kaczmarek, J.; Lenc, L. Containment of *Fusarium culmorum* and Its Mycotoxins in Various Biological Systems by Antagonistic *Trichoderma* and *Clonostachys* Strains. *J. Fungi* **2023**, *9*, 289. [CrossRef]
11. Corkley, I.; Fraaije, B.; Hawkins, N. Fungicide resistance management: Maximizing the effective life of plant protection products. *Plant Pathol.* **2022**, *71*, 150–169. [CrossRef]
12. Akrami, M.; Yousefi, Z. Biological Control of *Fusarium* wilt of Tomato (*Solanum lycopersicum*) by *Trichoderma* spp. as Antagonist Fungi. *Biol. Forum* **2015**, *7*, 887–892.
13. Arie, T. *Fusarium* diseases of cultivated plants, control, diagnosis, and molecular and genetic studies. *J. Pestic. Sci.* **2019**, *44*, 275–281. [CrossRef]
14. Berg, G.; Zachow, C.; Müller, H.; Philipps, J.; Tilcher, R. Next-Generation Bio-Products Sowing the Seeds of Success for Sustainable Agriculture. *Agronomy* **2013**, *3*, 648–656. [CrossRef]
15. Yao, Y.Q.; Lan, F.; Qiao, Y.M.; Wei, J.G.; Huang, R.S.; Li, L.B. Endophytic fungi harbored in the root of *Sophora tonkinensis* Gapnep: Diversity and biocontrol potential against phytopathogens. *Microbiol. Open* **2017**, *6*, e00437. [CrossRef]
16. Koul, M.; Meena, S.; Kumar, A.; Sharma, P.R.; Singamaneni, V.; Riyaz-Ul-Hassan, S.; Kong, W.L.; Rui, L.; Ni, H.; Wu, X.Q. Antifungal Effects of Volatile Organic Compounds Produced by *Rahnella aquatilis* JZ-GX1 Against *Colletotrichum gloeosporioides* in Liriodendron chinense × tulipifera. *Front. Microbiol.* **2020**, *11*, 1114. [CrossRef]
17. Nicoletti, R.; Trincone, A. Bioactive compounds produced by strains of *Penicillium* and *Talaromyces* of marine origin. *Mar. Drugs* **2016**, *14*, 37. [CrossRef]
18. Caro, Y.; Venkatachalam, M.; Lebeau, J.; Fouillaud, M.; Dufossé, L. Pigments and colorants from filamentous fungi. In *Fungal Metabolites*; Mérillon, J.-M., Ramawat, K.G., Eds.; Springer International Publishing: Cham, Switzerland, 2017; Volume 26, pp. 499–568.
19. Alagesaboopathi, C. Biological control of damping-off disease of cotton seedling. *Curr. Sci.* **1994**, *95*, 865–868.
20. Nicoletti, R.; De Stefano, M.; De Stefano, S.; Carella, A. Antagonism against *Rhizoctonia solani* and fungitoxic metabolite production by some *Penicillium* isolates. *Mycopathologia* **2004**, *158*, 465–474. [CrossRef] [PubMed]
21. Abdel-Rahim, I.R.; Abo-Elyousr, K.A.M. *Talaromyces pinophilus* strain AUN-1 as a novel mycoparasite of *Botrytis cinerea*, the pathogen of onion scape and umbel blights. *Microbiol. Res.* **2018**, *213*, 1–9. [CrossRef] [PubMed]
22. Yang, H.; Cui, S.; Wei, Y.; Li, H.; Hu, J.; Yang, K.; Wu, Y.; Zhao, Z.; Li, J.; Wang, Y.; et al. Antagonistic effects of *Talaromyces muroii* TM28 against *Fusarium* crown rot of wheat caused by *Fusarium pseudograminearum*. *Front. Microbiol.* **2004**, *14*, 1292885. [CrossRef]
23. Koul, M.; Meena, S.; Kumar, A.; Sharma, P.R.; Singamaneni, V.; Riyaz-Ul-Hassan, S.; Hamid, A.; Chaubey, A.; Prabhakar, A.; Gupta, P. Secondary metabolites from endophytic fungus *Penicillium pinophilum* induce ROS-mediated apoptosis through mitochondrial pathway in pancreatic cancer cells. *Planta Medica* **2016**, *82*, 344–355. [CrossRef]
24. Abdel-Hafez, S.I.I.; Abo-Elyousr, K.A.; Abdel-Rahim, I.R. Leaf surface and endophytic fungi associated with onion leaves and their antagonistic activity against *Alternaria porri*. *Czech Myco.* **2015**, *67*, 1–22. [CrossRef]
25. Chabasse, D.; Bouchara, J.P.; de Gentile, L.; Brun, S.; Cimon, B.; Penn, P. Les moisissures d'intérêt médical. Cahier de formation biologie médicale. In *Cahier de Formation Bioforma*, 1st ed.; Beddosa, A., Ed.; Bioforma: Paris, France, 2002; Volume 25, pp. 26–45.
26. Leslie, J.F.; Summerell, B.A. *The Fusarium Laboratory Manual*; Blackwell Publishing: Oxford, UK, 2006; p. 109.

27. Gardes, M.; Bruns, T.D. ITS primers with enhanced specificity for basidiomycetes—Application to the identification of mycorrhizae and rusts. *Mol. Ecol.* **1993**, *2*, 113–118. [CrossRef]
28. Da Cruz Cabral, L.; Delgado, J.; Patriarca, A.; Rodríguez, A. Differential response to synthetic and natural antifungals by *Alternaria tenuissima* in wheat simulating media: Growth, mycotoxin production and expression of a gene related to cell wall integrity. *Int. J. Food Microbiol.* **2019**, *292*, 48–55. [CrossRef] [PubMed]
29. Islam, M.M.; Hossain, D.M.; Rahman, M.M.E.; Suzuki, K.; Narisawa, T.; Hossain, I.; Harada, N. Native *Trichoderma* strains isolated from Bangladesh with broad spectrum antifungal action against fungal phytopathogens. *Arch. Phytopathol. Plant Prot.* **2016**, *49*, 75–93. [CrossRef]
30. Marques, E.; Martins, I.; Mello, S.C.M. Antifungal potential of crude extracts of *Trichoderma* spp. *Biota Neotrop.* **2017**, *18*, e20170418.
31. Galán, A.J.; Ruiz-Moyano, S.; Martín, A.; Delgado, J.; Álvarez, M.; López-Corrales, M. Implementation of netting system for production of 'Calabacita' dried figs: Effects on pest incidence, fruit quality and mycotoxin occurrence. *Sci. Hortic.* **2024**, *331*, 113099. [CrossRef]
32. Cherukupally, R.; Amballa, H.; Reddy, B.N. In vitro screening for enzymatic activity of *Trichoderma* species for biocontrol potential. *Ann. Plant Sci.* **2017**, *6*, 1784–1789. [CrossRef]
33. Reghmit, A.; Benzina-tihar, F.; Halouane-Sahir, F.; Oukali, Z.; Ghozali, N. *Trichoderma* spp. isolates from the rhizosphere of healthy olive trees in northern Algeria and their biocontrol potentials against the olive wilt pathogen, *Verticillium dahlia*. *Org. Agric.* **2021**, *11*, 639–657. [CrossRef]
34. Burcham, D.C.; Abarrientos, J.R.; Wong, J.Y.; Ali, M.I.M.; Fong, Y.K.; Schwarze, F.W. Field evaluation of *Trichoderma* spp. as a biological control agent to preventwood decay on Benin mahogany (*Khaya grandifoliola*) and rain tree (*Samanea saman*) in Singapore. *Biol. Control* **2017**, *114*, 114–124. [CrossRef]
35. Gotor-Vila, A.; Usall, J.; Torres, R.; Abadias, M.; Teixidó, N. Formulation of the biocontrol agent *Bacillus amyloliquefaciens* CPA-8 using different approaches: Liquid, freeze- drying and fluid-bed spray-drying. *Biol. Control* **2017**, *62*, 545–555. [CrossRef]
36. Jalgaonwala, R.E.; Mohite, B.V.; Mahajan, R.T. A review: Natural products from plant associated endophytic fungi. *J. Microbiol. Biotech. Res.* **2017**, *1*, 21–32.
37. Zandyavari, N.; Sulaiman, M.A.; Hassanzadeh, N. Molecular characterization and biocontrol potential of *Trichoderma* spp. against *Fusarium oxysporum* f. sp. dianthi in carnation. *Egypt. J. Biol. Pest Control* **2024**, *34*, 1. [CrossRef]
38. Dethoup, T.; Kaewsalong, N.; Songkumorn, P.; Jantasorn, A. Potential application of a marine-derived fungus, *Talaromyces tratensis* KUFA 0091 against rice diseases. *Bio. Control* **2017**, *119*, 1–6. [CrossRef]
39. Naraghi, L.; Heydari, A.; Rezaee, S.; Razavi, M.; Jahanifar, H. Study on antagonistic effects of *Talaromyces flavus* on *Verticillium albo-atrum*, the causal agent of potato wilt disease. *Crop Prot.* **2010**, *29*, 658–662. [CrossRef]
40. Tian, Y.H.; Peng, H.Y.; Wang, D.H.; Li, X.F.; He, B.L.; Gao, K.X. Biocontrol potential of *Talaromyces purpurogenus* and its regulation on soil microbial community. *J. App. Ecol.* **2020**, *31*, 3255–3266.
41. Bouanaka, H.; Bellil, I.; Khelifi, D. Multiple methods for varietal resistance assessment of durum wheat cultivars against *Fusarium culmorum* the causal agent of *Fusarium* head blight and crown rot in Algeria. *Physiol. Mol. Plant Pathol.* **2021**, *115*, 101683. [CrossRef]
42. Houbraken, J.; de Vries, R.P.; Samson, R.A. Modern taxonomy of biotechnologically important *Aspergillus* and *Penicillium* species. In *Advances in Applied Microbiology*; Gadd, G.M., Sariaslani, S., Eds.; Academic Press: Cambridge, MA, USA, 2013; pp. 119–249.
43. Fujii, T.; Hoshino, T.; Inoue, H.; Yano, S. Taxonomic revision of the cellulose degrading fungus *Acremonium cellulolyticus* nomen nudum to *Talaromyces* based on phylogenetic analysis. *FEMS Microbiol. Lett.* **2014**, *351*, 32–41. [CrossRef]
44. Haggag, W.M.; Kansoh, A.L.; Aly, A.M. Proteases from *Talaromyces flavus* and *Trichoderma harzianum*: Purification, Characterisation and Antifungal Activity Against Brown Spot Disease on Faba Bean. *Plant Pathol. Bull.* **2006**, *15*, 231–239.
45. Wang, B.; Guo, L.; Ye, K.; Wang, L. Chromosome-scale genome assembly of *Talaromyces rugulosus* W13939, a mycoparasitic fungus and promising biocontrol agent. *Mol. Plant-Microbe Interact.* **2020**, *33*, 1446–1450. [CrossRef]
46. Aggarwal, S.; Dorairaj, S.; Adlakha, N. Stoichiometric balance ratio of cellobiose and gentiobiose induces cellulase production in *Talaromyces cellulolyticus*. *Biotechnol. Biofuels Bioprod.* **2023**, *16*, 48. [CrossRef]
47. Kim, K.S.; Lee, Y.H. Gene expression profiling during conidiation in the rice blast pathogen *Magnaporthe oryzae*. *PLoS ONE* **2012**, *7*, e43202. [CrossRef]
48. Karthik, C.; Elangovan, N.; Kumar, T.S.; Govindharaju, S.; Barathi, S.; Oves, M. Characterization of multifarious plant growth promoting traits of rhizobacterial strain AR6 under chromium (VI) stress. *Microbiol. Res.* **2017**, *204*, 65–71. [CrossRef]
49. Li, D.; Chen, S.; Jing, L. Purification and partial characterization of two chitinases from the mycoparasitic fungus *Talaromyces flavus*. *Mycopathologia* **2005**, *159*, 223–229. [CrossRef]
50. Plaza, V.; Silva-Moreno, E.; Castillo, L. Breakpoint: Cell wall and glycoproteins and their crucial role in the phytopathogenic fungi infection. *Curr. Prot. Peptid. Sci.* **2020**, *21*, 227–244. [CrossRef] [PubMed]
51. Lenardon, M.D.; Munro, C.A.; Gow, N.A.R. Chitin synthesis and fungal pathogenesis. *Curr. Opin. Microbiol.* **2010**, *13*, 416–423. [CrossRef] [PubMed]

52. Benhamou, N.; Chet, I. Hyphal interactions between *Trichoderma harzianum* and *Rhizoctonia solani*: Ultrastructure and gold cytochemistry of the mycoparasitic process. *Phytopathology* **1993**, *83*, 1062–1071. [CrossRef]
53. Ting, A.S.Y.; Chai, J.Y. Chitinase and β-1, 3-glucanase activities of *Trichoderma harzianum* in response towards pathogenic and non-pathogenic isolates: Early indications of compatibility in consortium. *Biocatal. Agric. Biotechnol.* **2015**, *4*, 109–113. [CrossRef]
54. Pandey, V.; Shukla, A.; Kumar, J. Physiological and molecular signalling involved in disease management through *Trichoderma*: An effective biocontrol paradigm. In *Current Trends in Plant Disease Diagnostics and Management Practices*; Kumar, P., Gupta, V.K., Tiwari, A.K., Kamle, M., Eds.; Springer International Publisher: Cham, Switzerland, 2016; Volume 12, pp. 317–346.
55. Delgado, J.; Ballester, A.-R.; González-Candelas, L.; Núñez, F. Impact of the antifungal protein PgAFP on the proteome and patulin production of *Penicillium expansum* on apple-based medium. *Int. J. Food Microbiol.* **2022**, *363*, 109511. [CrossRef]
56. Reghmit, A.; Benzina-tihar, F.; Sahir-Halouane, F. Volatile organic compounds activities of *Trichoderma* species isolated from olive grove soil against the wilt pathogen, *Verticillium dahlia*. *Eur. J. Plant Pathol.* **2024**, *168*, 15.
57. Delgado, J.; Ballester, A.-R.; Núñez, F.; González-Candelas, L. Evaluation of the activity of the antifungal PgAFP protein and its producer mould against *Penicillium* spp postharvest pathogens of citrus and pome fruits. *Food Microbiol.* **2019**, *84*, 103266. [CrossRef]
58. Álvarez, M.; Rodríguez, A.; Núñez, F.; Silva, A.; Andrade, M.I. In vitro antifungal effects of spices on ochratoxin A production and related gene expression in *Penicillium nordicum* on a dry-cured fermented sausage medium. *Food Control* **2020**, *114*, 107222. [CrossRef]
59. Peromingo, B.; Sulyok, M.; Lemmens, M.; Rodríguez, A.; Rodríguez, M. Diffusion of mycotoxins and secondary metabolites in dry-cured meat products. *Food Control* **2019**, *101*, 144–150. [CrossRef]
60. Cebrián, E.; Rodríguez, M.; Peromingo, B.; Bermúdez, E.; Núñez, F. Efficacy of the combined protective cultures of *Penicillium chrysogenum* and *Debaryomyces hansenii* for the control of ochratoxin a hazard in dry-cured ham. *Toxins* **2019**, *11*, 710. [CrossRef] [PubMed]
61. Cebrián, E.; Núñez, F.; Gálvez, F.J.; Delgado, J.; Bermúdez, E.; Rodríguez, M. Selection and Evaluation of *Staphylococcus xylosus* as a Biocontrol Agent against Toxigenic Moulds in a Dry-Cured Ham Model System. *Microorganisms* **2020**, *8*, 793. [CrossRef]
62. Schmidt-Heydt, M.; Baxter, E.; Geisen, R.; Magan, N. Physiological relationship between food preservatives, environmental factors, ochratoxin and *otapksPV* gene expression by *Penicillium verrucosum*. *Int. J. Food Microbiol.* **2007**, *3*, 277–283. [CrossRef]
63. Álvarez, M.; Agostini, I.; Silva, S.; Dallemole-Giaretta, R.; Sulyok, M.; Sampaio, A.; Rodrigues, P. Mycotoxins and Other Secondary Metabolites Are Produced by *Gnomoniopsis smithogilvyi* When Confronted with Biological and Chemical Control Agents. *Agriculture* **2023**, *13*, 1166. [CrossRef]

Disclaimer/Publisher's Note: The statements, opinions and data contained in all publications are solely those of the individual author(s) and contributor(s) and not of MDPI and/or the editor(s). MDPI and/or the editor(s) disclaim responsibility for any injury to people or property resulting from any ideas, methods, instructions or products referred to in the content.

Journal of Fungi

MDPI

Article

Fusarium Species Infecting Greenhouse-Grown Cannabis (*Cannabis sativa*) Plants Show Potential for Mycotoxin Production in Inoculated Inflorescences and from Natural Inoculum Sources

Zamir K. Punja [1,*], Sheryl A. Tittlemier [2] and Sean Walkowiak [2]

[1] Department of Biological Sciences, Simon Fraser University, Burnaby, BC V5A 1S6, Canada
[2] Grain Research Laboratory, Canadian Grain Commission, Winnipeg, MB R3C 3G8, Canada; sean.walkowiak@grainscanada.gc.ca (S.W.)
* Correspondence: punja@sfu.ca

Abstract: Several species of *Fusarium* are reported to infect inflorescences of high-THC-containing cannabis (*Cannabis sativa* L.) plants grown in greenhouses in Canada. These include *F. graminearum*, *F. sporotrichiodes*, *F. proliferatum*, and, to a lesser extent, *F. oxysporum* and *F. solani*. The greatest concern surrounding the infection of cannabis by these *Fusarium* species, which cause symptoms of bud rot, is the potential for the accumulation of mycotoxins that may go undetected. In the present study, both naturally infected and artificially infected inflorescence tissues were tested for the presence of fungal-derived toxins using HPLC-MS/MS analysis. Naturally infected cannabis tissues were confirmed to be infected by both *F. avenaceum* and *F. graminearum* using PCR. Pure cultures of these two species and *F. sporotrichiodes* were inoculated onto detached inflorescences of two cannabis genotypes, and after 7 days, they were dried and assayed for mycotoxin presence. In these assays, all *Fusarium* species grew prolifically over the tissue surface. Tissues infected by *F. graminearum* contained 3-acetyl DON, DON, and zearalenone in the ranges of 0.13–0.40, 1.18–1.91, and 31.8 to 56.2 µg/g, respectively, depending on the cannabis genotype. In *F. sporotrichiodes*-infected samples, HT2 and T2 mycotoxins were present at 13.9 and 10.9 µg/g in one genotype and were lower in the other. In *F. avenaceum*-inoculated tissues, the mycotoxins enniatin A, enniatin A1, enniatin B, and enniatin B1 were produced at varying concentrations, depending on the isolate and cannabis genotype. Unexpectedly, these tissues also contained detectable levels of 3-acetyl DON, DON, and zearalenone, which was attributed to apre-existing natural infection by *F. graminearum* that was confirmed by RT-qPCR. Beauvericin was detected in tissues infected by *F. avenaceum* and *F. sporotrichiodes*, but not by *F. graminearum*. Naturally infected, dried inflorescences from which *F. avenaceum* was recovered contained beauvericin, enniatin A1, enniatin B, and enniatin B1 as expected. Uninoculated cannabis inflorescences were free of mycotoxins except for culmorin at 0.348 µg/g, reflecting pre-existing infection by *F. graminearum*. The mycotoxin levels were markedly different between the two cannabis genotypes, despite comparable mycelial colonization. Tall fescue plants growing in the vicinity of the greenhouse were shown to harbor *F. avenaceum* and *F. graminearum*, suggesting a likely external source of inoculum. Isolates of both species from tall fescue produced mycotoxins when inoculated onto cannabis inflorescences. These findings demonstrate that infection by *F. graminearum* and *F. avenaceum*, either from artificial inoculation or natural inoculum originating from tall fescue plants, can lead to mycotoxin accumulation in cannabis inflorescences. However, extensive mycelial colonization following prolonged incubation of infected tissues under high humidity conditions is required. Inoculations with *Penicillium citrinum* and *Aspergillus ochraceus* under these conditions produced no detectable mycotoxins. The mycotoxins

alternariol and tentoxin were detected in several inflorescence samples, likely as a result of natural infection by *Alternaria* spp. *Fusarium avenaceum* is reported to infect cannabis inflorescences for the first time and produces mycotoxins in diseased tissues.

Keywords: *Fusarium avenaceum*; *Fusarium graminearum*; bud rot; mycotoxins; post-harvest

1. Introduction

The commercial production of high-THC-containing plants of cannabis (*Cannabis sativa* L.) in Canada following legalization in 2018 for recreational and medicinal uses has been steadily increasing. Production occurs mostly in environmentally controlled indoor rooms and in greenhouses, although a small proportion of the production, approximately 10%, occurs outdoors. One of the major challenges to the large-scale production of cannabis plants is the potential exposure to infection by pathogens, which may originate from various sources. These sources include infected propagation materials, contaminated seeds, or inoculum from adjacent fields in which the pathogens may be infecting unrelated crops, which subsequently provide a source of inoculum for cannabis plants [1]. There is previously published evidence that a large number of fungal pathogens with wide host ranges are able to spread and infect cannabis plants under the appropriate environmental conditions [1,2].

There are currently no regulatory restrictions to prevent the spread of pathogens within or between cannabis crops or across geographical regions where cannabis production is permitted. Hence, the unregulated movement of plant materials from one region to another has been shown to result in the spread of a number of pathogens contained in that material [1]. Regulations are imposed on the occurrence of specific fungal pathogens that have the potential to produce mycotoxins within the cannabis inflorescences that are harvested and marketed for sale [3]. These regulations specify the tolerance levels for certain species of *Aspergillus* and *Penicillium* species and their associated mycotoxins. In some jurisdictions, these tolerance levels may be zero. There is currently little published information on the extent to which these mycotoxins may be present and the corresponding levels in different jurisdictions [3,4].

Recently, reports of infection by a range of mycotoxin-producing species of *Fusarium* on both greenhouse-grown cannabis plants as well as on field-grown hemp plants have raised concerns over the potential for mycotoxin production within the inflorescences, and hence their potential to cause harm to humans and animals exposed to these contaminating species [5–8]. In hemp plants grown outdoors, several mycotoxins produced by *Fusarium graminearum* have been reported to be present in inflorescences [7]. These plants were generally exposed to prolonged periods of wet weather outdoors that provided conducive conditions for growth of these pathogens. The sources of inoculum were identified to be adjacent wheat or cereal fields harboring these pathogens [6,8]. In greenhouse-grown cannabis plants in Canada, the occurrence of potential mycotoxin-producing species of *Fusarium* that include *F. graminearum* and *F. sporotrichiodes* has been reported [1,2,9], but there are no previous reports of the occurrence of associated mycotoxins in the infected inflorescences. In addition, the potential sources of inoculum of *Fusarium* species that are able to infect these tissues and the environmental conditions favoring disease development are unknown.

In 2024, cannabis plants showing pinkish-white mycelial growth on the inflorescences were observed in the greenhouse environment of a producer in British Columbia (Figure 1a,b). Samples of dried cannabis inflorescences after the drying process was com-

pleted and before packaging had occurred also showed evidence of infection. These samples showed pinkish-white mycelial growth indicative of the presence of a *Fusarium* sp. on the exterior of the sample as well as internally (Figure 1c,d). The objectives of this study were to (i) confirm the species of *Fusarium* that were present on these inflorescences and to determine if the tissues contained any mycotoxins; (ii) to conduct artificial inoculation studies to demonstrate pathogenicity of the isolates recovered and to determine if there were any mycotoxins produced; and (iii) to investigate possible sources of inoculum that could explain the occurrence of infection on greenhouse-grown inflorescences.

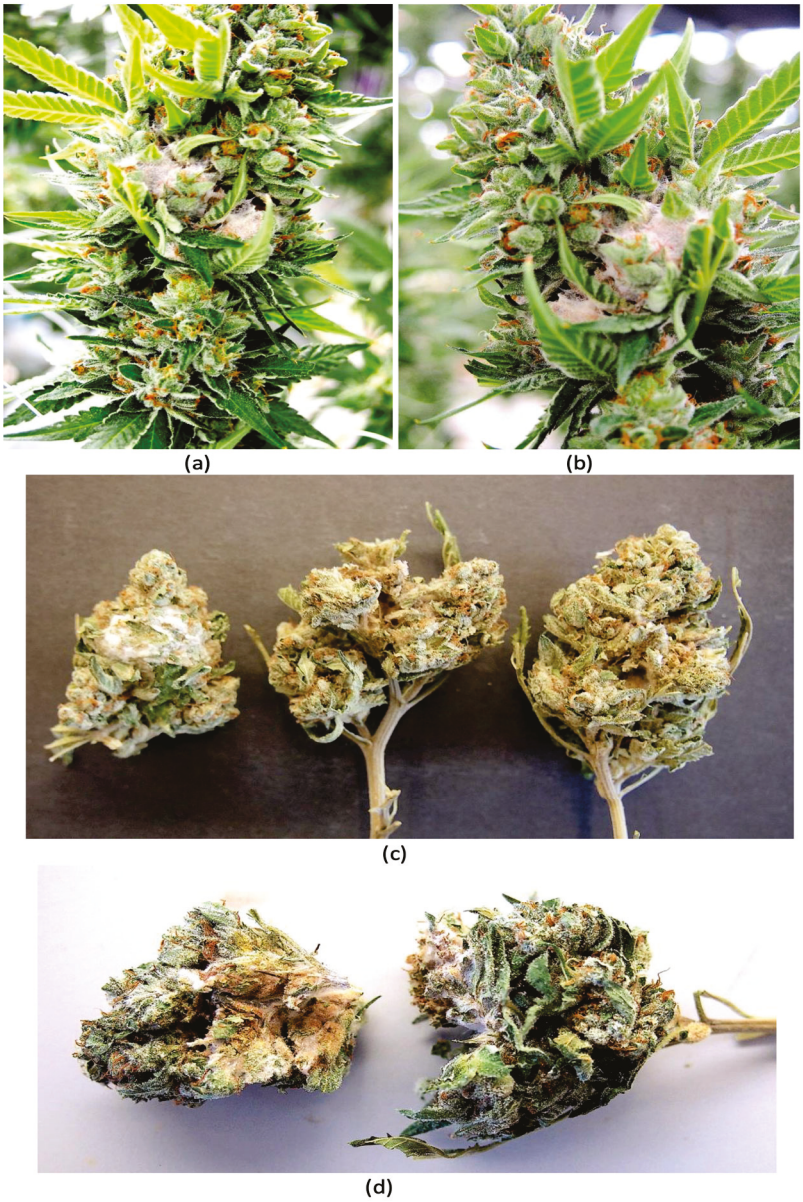


Figure 1. Observations of mycelium of *Fusarium* spp. growing on cannabis inflorescences. (**a**,**b**) Pinkish-white mycelial growth can be seen on inflorescences on plants in the greenhouse from natural infection. (**c**) Mycelial growth is evident on dried inflorescences from the same plants. (**d**) Pinkish-white mycelial growth can be seen inside and on the surface of dried buds. The presence of *Fusarium* spp. was confirmed by isolation in pure culture and molecular identification.

2. Materials and Methods

Plant and fungal sources. During July 2024, visible symptoms of infection of the inflorescences of cannabis plants of genotype AP were observed in a licensed commercial

greenhouse facility situated in the Fraser Valley region of British Columbia. The affected inflorescences developed a whitish-pink mycelium (Figure 1a,b) that was visibly different from that commonly caused by *Botrytis cinerea*, the gray mold pathogen that causes bud rot [5,6]. Small tissue pieces measuring 0.5 mm^2 were dissected from the affected inflorescences and surface-sterilized for 90 s in a 10% solution of household bleach (containing 5.25% NaOCl) followed by a 30 s dip in 70% EtOH and then rinsed thrice in sterile distilled water. The pieces were blotted dry and plated onto potato dextrose agar containing 130 mg/L of streptomycin sulfate (PDA+S) and incubated under ambient laboratory conditions (temperature range of 21–23 °C and 10–12 h/day fluorescent lighting) for 5–7 days. Emerging colonies were sub-cultured onto fresh media and kept for further identification using morphological and molecular criteria.

In August of 2024, samples of cannabis inflorescences of genotype AD from the same greenhouse facility were observed to contain a whitish-pink mycelium on the surface of the tissues as well as internally, causing visible decay (Figure 1c,d). These samples had been harvested and dried following commercial practices and were being sorted after trimming and before packaging. The tissues were subjected to the isolation procedure described above. Additional sampling was conducted during August of 2024 of the florets (inflorescences) of tall fescue (*Festuca arundinacea* Schreb.) plants that were growing outside the greenhouse in which diseased cannabis inflorescences were observed. These plants were situated at a distance of approximately 30 m away from the greenhouse (Figure 2a,b). Samples of inflorescences and leaves were obtained from these plants at random and surface-sterilized as above and plated onto PDA+S and select fungal colonies were transferred to fresh medium after 5–7 days. The weather conditions during sampling were overcast skies with a light drizzle and a temperature of 18 °C.

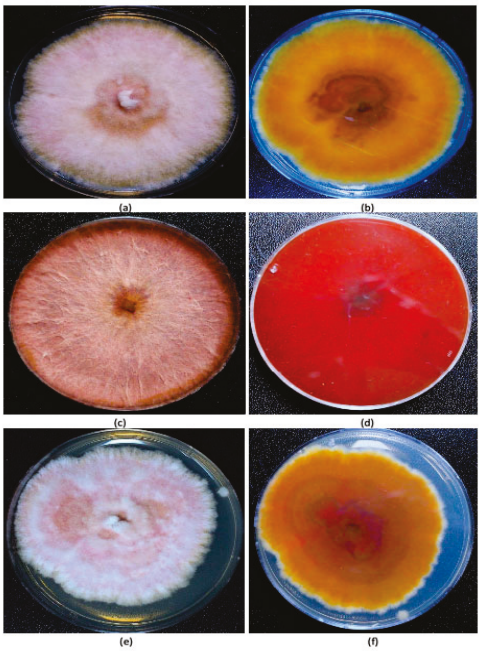


Figure 2. Colony morphology of two *Fusarium* spp. growing on potato dextrose agar for 2 weeks. (**a**,**b**) Top view and bottom view, respectively, of *Fusarium avenaceum* isolated from cannabis inflorescences shown in Figure 1a,b. (**c**,**d**) Top view and bottom view, respectively, of *Fusarium graminearum* isolated from cannabis inflorescences shown in Figure 1a,b. (**e**,**f**) Top view and bottom view, respectively, of *Fusarium avenaceum* isolated from tall fescue plants.

Molecular identification. A number of fungal colonies that were consistently recovered on Petri dishes from the tissue samples of cannabis and tall fescue inflorescences were

sub-cultured and examined for colony color and growth pattern. Most colonies produced a reddish-brown pigment and resembled *Fusarium* spp. Others were darkly pigmented and resembled *Alternaria* species. Six representative isolates of *Fusarium* spp. as well as three unidentified cultures from diseased inflorescences or leaves were transferred from hyphal-tipped colonies and sent to the University of Guelph Laboratory Services, Agriculture and Food Laboratory, Guelph, ON (www.guelphlabservices.com, accessed on 4 August 2024) for identification to the species level by PCR using the primers ITS1–ITS4 (ITS1-F CTTGGTCATTTAGAGGAAGTAA and ITS4 TCCTCCGCTTATTGATATGC). The elongation factor 1α (EF-1α) primer set EF-1 (5′ ATG GGT AAG GAG GAC AAG AC 3′) and EF-2 (5′ GGA GGT ACC AGT GAT CAT GTT 3′) [2] was also used for further speciation of *Fusarium* spp. as follows. Cultures of representative isolates from different tissue sources were grown in potato dextrose broth at room temperature for 7 days and DNA was extracted from harvested mycelium using the QIAGEN DNeasy Plant Mini Kit (QIAGEN, Montreal, QC, Canada). Aliquots of 1 µL containing 5–20 ng DNA were used for PCR in a 25 µL reaction volume consisting of 2.5 µL 10x buffer (containing 15 mM $MgCl_2$), 0.5 µL 10 mM dNTP, 0.25 µL Taq DNA Polymerase (Qiagen, Montreal, QC, Canada), 0.25 µL 10 mM forward and reverse primers, as well as 20.25 µL DNAse- and RNAse-free water (Invitrogen, Waltham, MA, USA). All PCR amplifications were performed in a MyCycler thermocycler (BioRad, Hercules, CA, USA) with the following program: 3 min at 94 °C; 30 s at 94 °C, 30 s at 60 °C, 3 min at 72 °C (35 cycles); and 7 min at 72 °C. PCR products were separated on 1% agarose gels and bands of the expected size (700 bp) were purified with the QIAquick Gel Extraction Kit (QIAGEN, Montreal, QC, Canada) and sent to Eurofins Genomics (Eurofins MWG Operon LLC 2016, Louisville, KY, USA) for sequencing. The resulting sequences were compared to the corresponding ITS1-5.8S-ITS4 or EF-1α sequences from the National Center for Biotechnology Information (NCBI) GenBank database (www.ncbi.nlm.nih.gov, accessed on 4 September 2024). Multiple sequence alignment of the respective isolates was performed using the CLUSTAL W program (http://www.genome.jp/tools/clustalw, accessed on 10 September 2024). Species identities were also confirmed with species-specific DNA markers following the methods as described by Bamforth et al. [10] for both DNA samples isolated from pure fungal cultures and from naturally and artificially infected plant tissues.

Pathogenicity tests. Following the identification of the fungal isolates to the species level, five *Fusarium* isolates representing two species were used for pathogenicity tests. The five isolates included three *F. avenaceum* isolates—two from cannabis inflorescences (fresh and dried, FB1 and FB2) and the other isolate from tall fescue inflorescences (FB3)—one isolate of *F. graminearum* from tall fescue plants (FG), and a *F. sporotrichiodes* isolate (FS) from a diseased cannabis inflorescence obtained in 2021 [2,9]. The five isolates were grown on PDA+S for 2 weeks and mycelial plugs (8 mm diameter) were placed mycelial side down onto freshly harvested detached cannabis inflorescences of two cannabis genotypes—AK and AD. The characteristic features of these two genotypes are described in Supplementary Figure S1. Three mycelial plugs were placed equidistant from one another on each inflorescence sample. The inflorescences were harvested from 7-week-old flowering plants in the same greenhouse facility. They were chosen at random but ensuring there were no visible signs of any fungal infection. They were placed inside plastic bags and transported to the laboratory and stored at 4 °C overnight. Two inflorescences were each placed inside plastic containers (25 cm × 12 cm) lined with wet paper towels. Following inoculation, the tissues were misted thrice with sterile distilled water from a hand-held spray bottle and the lids were closed. There were two containers for each of the five isolates (n = 4 per isolate) and they were incubated under ambient laboratory conditions. Control inflorescences were similarly misted but not inoculated. In addition to the five *Fusarium* isolates, an

isolate each of *Penicillium citrinum* and *Aspergillus ochraceous* was also inoculated onto a duplicate set of inflorescences and placed under the same conditions. These cultures were obtained from cannabis inflorescence tissues in a previous study [11]. All containers were examined at 4 and 7 days after inoculation, and each inoculated sample was photographed to show the extent of mycelial development of the respective fungi. The experiment was repeated a second time in September 2024 using a different set of inflorescences of the same two genotypes harvested from 7-week-old flowering plants and inoculated as described previously. Thus, each fungal isolate was tested for pathogenicity in 8 replications on cannabis inflorescences of 2 genotypes from 2 independent trials.

Mycotoxin analysis. After 7 days of incubation, all inflorescence samples were gently transferred to large trays and placed inside a forced air incubator set at 35 °C for 5 days or until all moisture had been removed and the samples felt dry to the touch. They were then transferred to Ziploc bags and sealed and stored inside a dark cabinet for 3 months. Prior to mycotoxin analysis, one inflorescence sample from each of the repeated experiments was combined to represent the specific fungal species inoculated. Control samples were combined in the same manner. The samples were crumbled by hand and tissue pieces were crushed using a mortar with a pestle until a comminuted mixture of small fragments was obtained. They were transferred into a 50 mL Falcon tube and stored for 2 weeks in darkness. The contents were thoroughly shaken by hand and a 5 g subsample was transferred to a small screw-cap vial and prepared for analysis for mycotoxins as described by Brown et al. [12]. A sub-sample of 0.1 g of the ground dried cannabis tissue was transferred to a 30 mL glass test tube to which 1 mL of acetonitrile was added. The tubes were capped and rolled vertically by hand for 30 s to completely coat and submerge the tissues with solvent, followed by sonication for 5 min. The tubes were rolled vertically by hand once again for 30 s, and the solvent was injected directly into an LC vial and subjected to the HPLC-MS/MS protocol described below.

A method based on high-performance liquid chromatography (HPLC) with tandem mass spectrometry (HPLC-MS/MS) was used for analyte (mycotoxin) determination [13]. The HPLC-MS/MS method covered 28 analytes, and the limits of quantitation are shown in Table 1. Stable isotope labeled ^{13}C internal standards were added to the diluted sample extract prior to HPLC-MS/MS analysis to mitigate the impact of matrix effects. Quality control samples were processed and analyzed alongside the 12 cannabis samples to monitor analytical method performance.

Analysis was performed on an AB Sciex 5500 TQ tandem mass spectrometer (AB Sciex, Concord, ON, Canada) coupled to a Waters Acquity I Class ultra-high-pressure liquid chromatography system consisting of an Acquity binary solvent manager, an Acquity FTN sample manager, and an Acquity column manager fitted with a Phenomenex Kinetex (Phenomenex, Torrance, CA, USA) 2.6 µm XB-C18 (50 × 2.1 mm) column held at 40 °C. A linear gradient HPLC program using 95.5% 5 mM ammonium acetate in water/0.5% acetic acid (v/v) and 95.5% 5 mM ammonium acetate in methanol with 0.5% acetic acid (v/v) as mobile phases A and B, respectively, separated the mycotoxin analytes shown in Table 1. The initial mobile phase was 98% A, changing to 30% A at 15 min and 2% A at 15.7 min. The mobile phase was changed back to the initial 98% A at 18.2 min and held there until the end of the run at 20 min. Mass spectrometric analysis was performed using electrospray ionization with polarity switching. The following mass spectrometer parameters were used: ion spray voltage of ±4500 V (depending on analyte), source temperature of 550 °C, curtain gas (N_2) at 25 psi, ion source gases (N_2) at 60 and 70 psi, and collision gas (N_2) at 9 psi. The transitions monitored and used to identify and quantify each of the mycotoxin analytes are described by Tittlemier et al. [13].

Table 1. Mycotoxin analytes and limits of quantitation (LOQs).

Mycotoxin	Abbreviation	LOQ (ug/kg)
Deoxynivalenol	DON	50
Deoxynivalenol-3-glucoside	D3G	50
3-acetyl deoxynivalenol	3ADON	50
15-acetyl deoxynivalenol	15ADON	50
Culmorin	CUL	20
Nivalenol	NIV	50
7-α hydroxy,15-deacetylcalonectrin	3ANX	80
7-α hydroxy, 3,15-dideacetylcalonectrin	NX	100
Zearalenone	ZEAR	24
Fumonisin B1	FB_1	24
Fumonisin B2	FB_2	24
Beauvericin	BEAU	2
Enniatin A	ENN A	2
Enniatin A1	ENN A1	5
Enniatin B	ENN B	20
Enniatin B1	ENN B1	16
HT-2 toxin	HT2	30
T-2 toxin	T2	20
Tentoxin	TENT	4
Alternariol methyl ether	AME	4
Altenuene	ALT	20
Alternariol	AOH	6
Aflatoxin B_1	AFB_1	1
Aflatoxin B_2	AFB_2	1
Aflatoxin G_1	AFG_1	1
Aflatoxin G_2	AFG_2	1
Ochratoxin A	OTA	1
Citrinin	CIT	3

Mycotoxin analytes were quantified using a calibration curve constructed from seven external standards. Peak areas from quantitation transitions were normalized to the peak area of ^{13}C-labeled internal standard during data analysis in order to counter matrix effects on quantitation prior to the interpolation of analyte concentration from the calibration curve. Isotope-labeled structural analogs were not commercially available for AOH, AME, ALT, TENT, BEAU, ENN A, ENN A1, ENN B, and ENN B1; therefore, peak areas from their quantitation transitions were normalized to $^{13}C_{34}$-FB_1. Analyte recoveries were calculated from pre-extraction fortified blanks analyzed with each sample batch. Mycotoxin concentrations in samples were corrected for recovery using the batch-specific recoveries determined for the pre-extraction fortified blanks. Analytes were considered to be identified and were quantified in samples when their retention time was within 0.1 min of the mean retention time in external standards used to construct the calibration curve, the ratio of qualifier to quantitation transition was within ±30% of the mean ratio in external standards used to construct the calibration curve, and the peak area signal-to-noise ratio was at least 10:1. Limits of quantitation were determined as the concentration in sample that produced a chromatographic peak with a signal-to-noise ratio of 10:1.

3. Results

Fungal isolation from plants and identification. Fungal colonies recovered from dried cannabis inflorescences and sub-cultured onto PDA+S were represented by two major morphological types. The first were slow-growing colonies with irregular margins and cottony aerial mycelia, and the underside of the colonies were beige with a tint of red (Figure 2a,b). The second type was represented by fast-growing red-pigmented colonies with some aerial mycelia (Figure 2c,d). Many fungal colonies recovered from tall fescue

plants, when sub-cultured to fresh medium, resembled these two colony types (Figure 2e,f), in addition to other colonies that were either pigmented red or black, or were not pigmented. The tall fescue plants sampled and the colonies recovered from them are shown in Figure 3. Among the six isolates of *Fusarium* spp. that were subjected to PCR of the ITS1-ITS4 region of rDNA and of the EF-1α region, two species were identified—*F. avenaceum* and *F. graminearum* (Figure 4). Both species were recovered from cannabis and tall fescue inflorescences, with homologies in the range of 99.4–99.6% for both gene regions according to BLAST analysis (https://blast.ncbi.nlm.nih.gov/Blast.cgi, accessed on 4 September 2024). Three additional cultures that were pigmented red or black were identified as *Epicoccum nigrum*, *Sordaria macrospora*, and *Alternaria alternata*, with 100%, 99.6%, and 99.4% homology, respectively, to the ITS region, and all of them were recovered from tall fescue leaves.

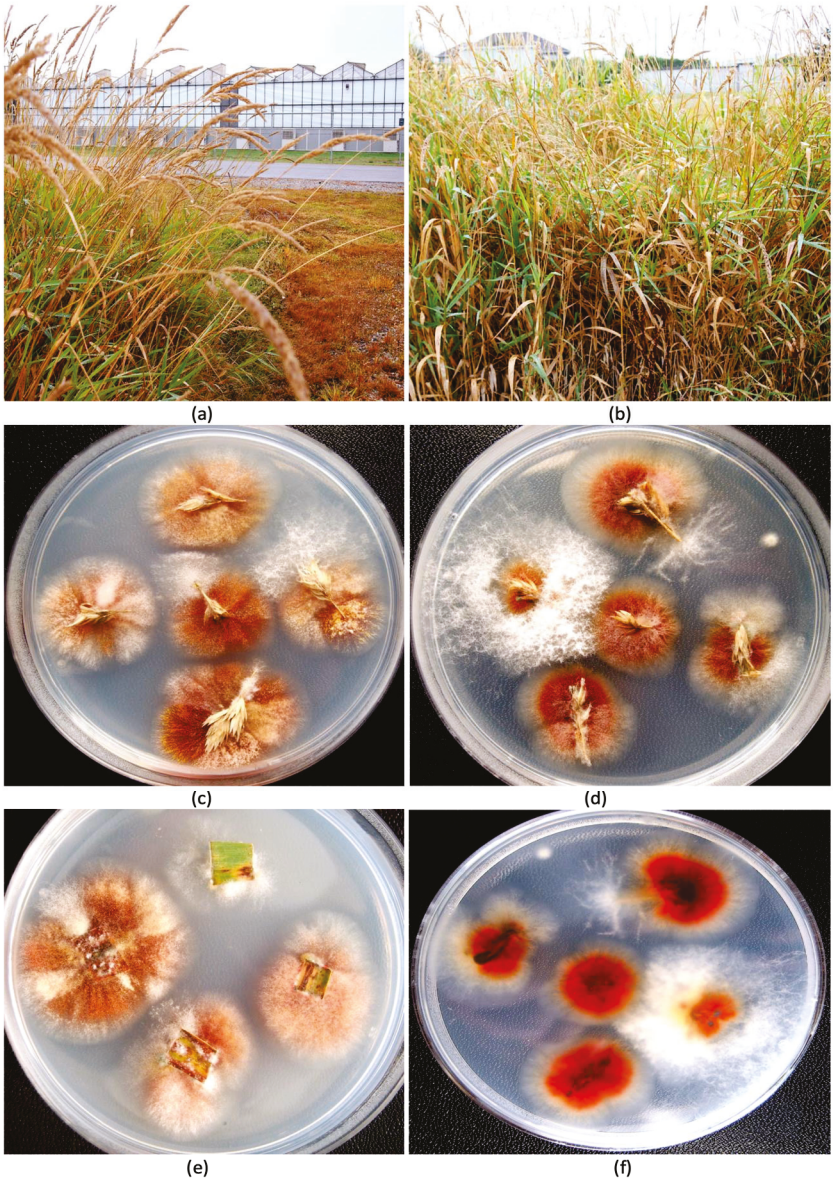


Figure 3. Recovery of fungal species from tall fescue plants growing adjacent to a cannabis greenhouse. (**a**,**b**) Tall fescue plants in the foreground with the cannabis greenhouse in the background. Photos were taken in August 2024 when the plants had developed abundant flowers. (**c**–**f**) Colonies of fungi recovered from inflorescence tissues plated onto potato dextrose agar. A high frequency of red-pigmented colonies was observed, which were identified as species of *Epicoccum* and *Fusarium*.

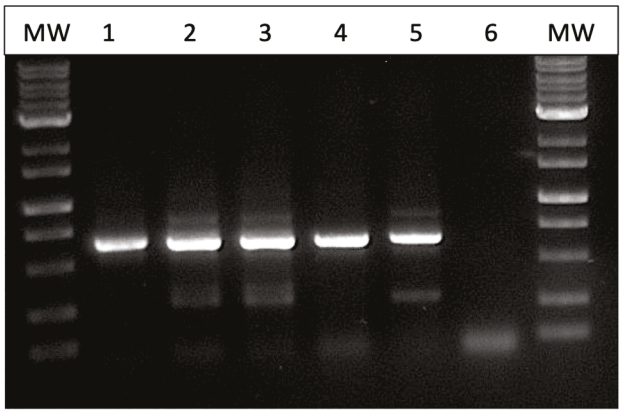


Figure 4. Electrophoresis gel following PCR using the EF-1a primer set of fungal colonies recovered from cannabis and tall fescue inflorescences. MW = molecular-weight ladder; lane 1 = positive control of *Trichoderma harzianum*; lanes 2 and 3 = *Fusarium avenaceum* from tall fescue plants; lane 4 = *Fusarium graminearum* from cannabis plants; lane 5 = *Fusarium avenaceum* from cannabis plants; lane 6 = control (no DNA).

Pathogenicity tests. Following the inoculation of freshly harvested detached cannabis inflorescences with mycelial plugs of *F. avenaceum* and *F. graminearum*, extensive mycelial growth was observed after 4 and 7 days on each of the two cannabis genotypes (AK, AD) due to the high humidity conditions within the sealed plastic containers (Figure 5). The *F. avenaceum* isolates from cannabis and tall fescue plants (FB1, FB2, FB3) grew similarly and there were no observable differences in the extent of mycelial colonization (Figure 5a–h). After 7 days, a ball of mycelium formed at each inoculation site. In contrast, inoculation with *F. graminearum* resulted in the complete colonization of the inflorescences after 7 days, resulting in a mummified appearance (Figure 5i–l). When these samples were dried, they retained the physical appearance of a mummified structure (Figure 6a). Inflorescences inoculated with *F. sporotrichiodes* were also covered by mycelial growth after 7 days, but to a much lesser extent compared to *F. graminearum* (Figure 6b). Inoculations with *A. ochraceus* and *P. citrinum* resulted in considerable sporulation by these species as shown in Figure 6c,d. These samples were similarly dried and used for mycotoxin analysis.

Mycotoxin occurrence. From the 8 samples of cannabis tissues that were naturally infected or artificially infected by 3 *Fusarium* species on 2 cannabis genotypes, a total of 14 mycotoxins were detected as shown in Table 2. From the naturally infected, dried cannabis inflorescences (buds) that were confirmed to contain *F. avenaceum* by isolation in pure culture and PCR identification, the mycotoxins BEAU and enniatins A1, B, and B1 were present at concentrations ranging from 0.063 to 1.78 μg/g. In cannabis inflorescences inoculated with an isolate of *F. graminearum* recovered from cannabis plants, the mycotoxins 3ADON and DON accumulated at levels of 0.34 and 1.91 μg/g, respectively, on cannabis genotype AK. In addition, ZEAR was present at a level of 56.2 μg/g (Table 2).

On cannabis genotype AD, these mycotoxin levels were 0.13, 1.18, and 31.8 μg/g, which were much lower than in genotype AK under the same conditions. In addition, the mycotoxin culmorin was present at a level of 0.38 μg/g in genotype AD.

In cannabis inflorescences inoculated with *F. avenaceum* originating from cannabis, the mycotoxins enniatins A, A1, B, and B1 were produced at varying levels. These levels were lower in tissues of genotype AD compared to AK, as observed previously with the mycotoxins 3ADON, DON, and ZEAR. In addition, BEAU was produced on genotype AD. In cannabis inflorescences inoculated with *F. avenaceum* originating from tall fescue spikes, the mycotoxins enniatins A, A1, B, and B1 were produced at varying levels, with higher levels detected in genotype AK compared to AD as before. BEAU was present in both

genotypes, with higher levels in genotype AD. Lastly, in *F. sporotrichiodes*-inoculated tissues, the mycotoxins HT2 and T2 accumulated at levels of 13.9 and 10.9 µg/g, respectively. In addition, BEAU was also present at 0.133 µg/g (Table 2).

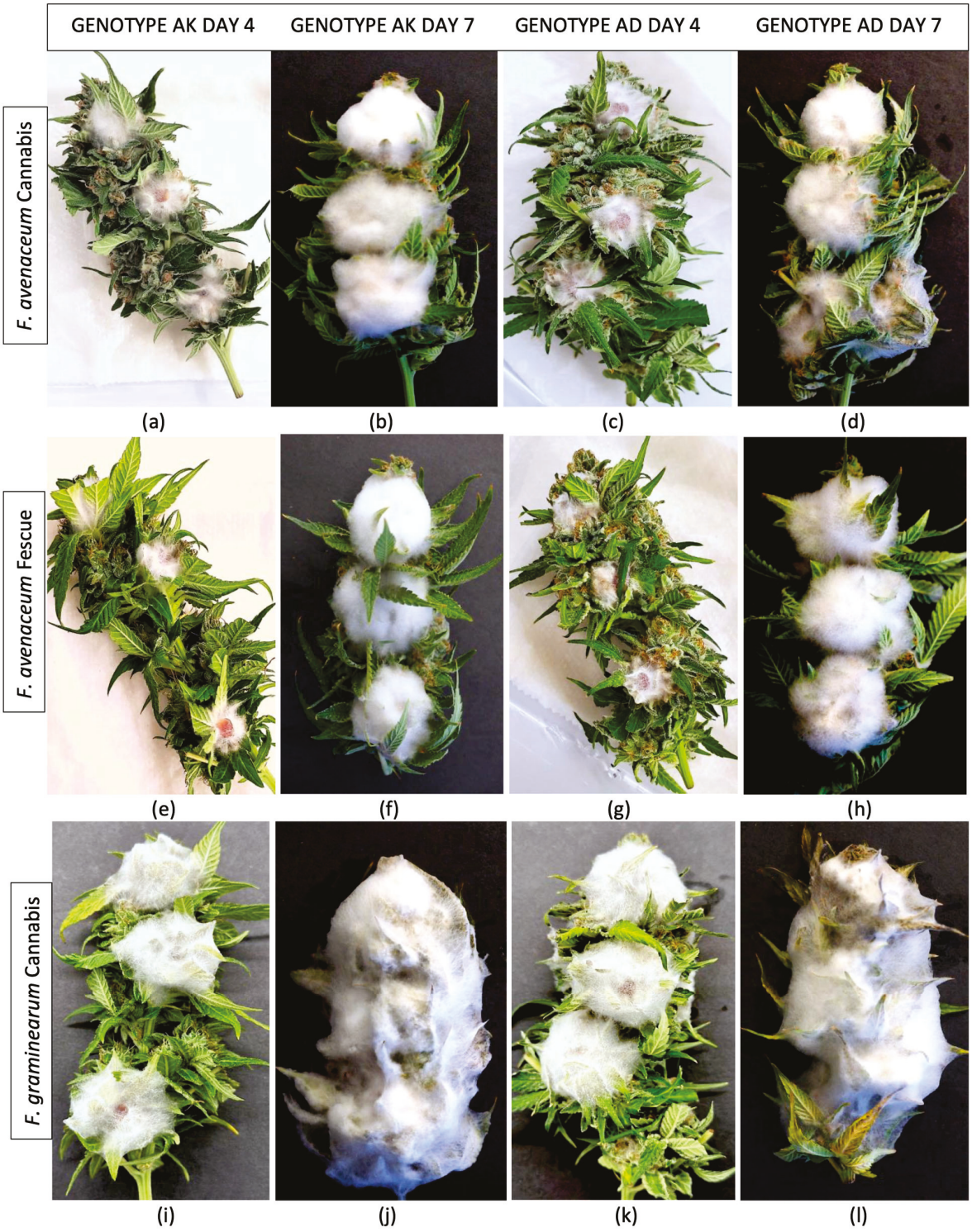


Figure 5. Mycelial colonization of detached cannabis inflorescences following inoculation with mycelial plugs of *Fusarium* spp. Two cannabis genotypes were included and photos were taken after 4 and 7 days of incubation under high humidity conditions in the laboratory. (**a**–**d**) Genotypes AK and AD inoculated with *Fusarium avenaceum* from cannabis. (**e**–**h**) Genotypes AK and AD inoculated with *Fusarium avenaceum* from tall fescue. (**i**–**l**) Genotypes AK and AD inoculated with *Fusarium graminearum* from cannabis.

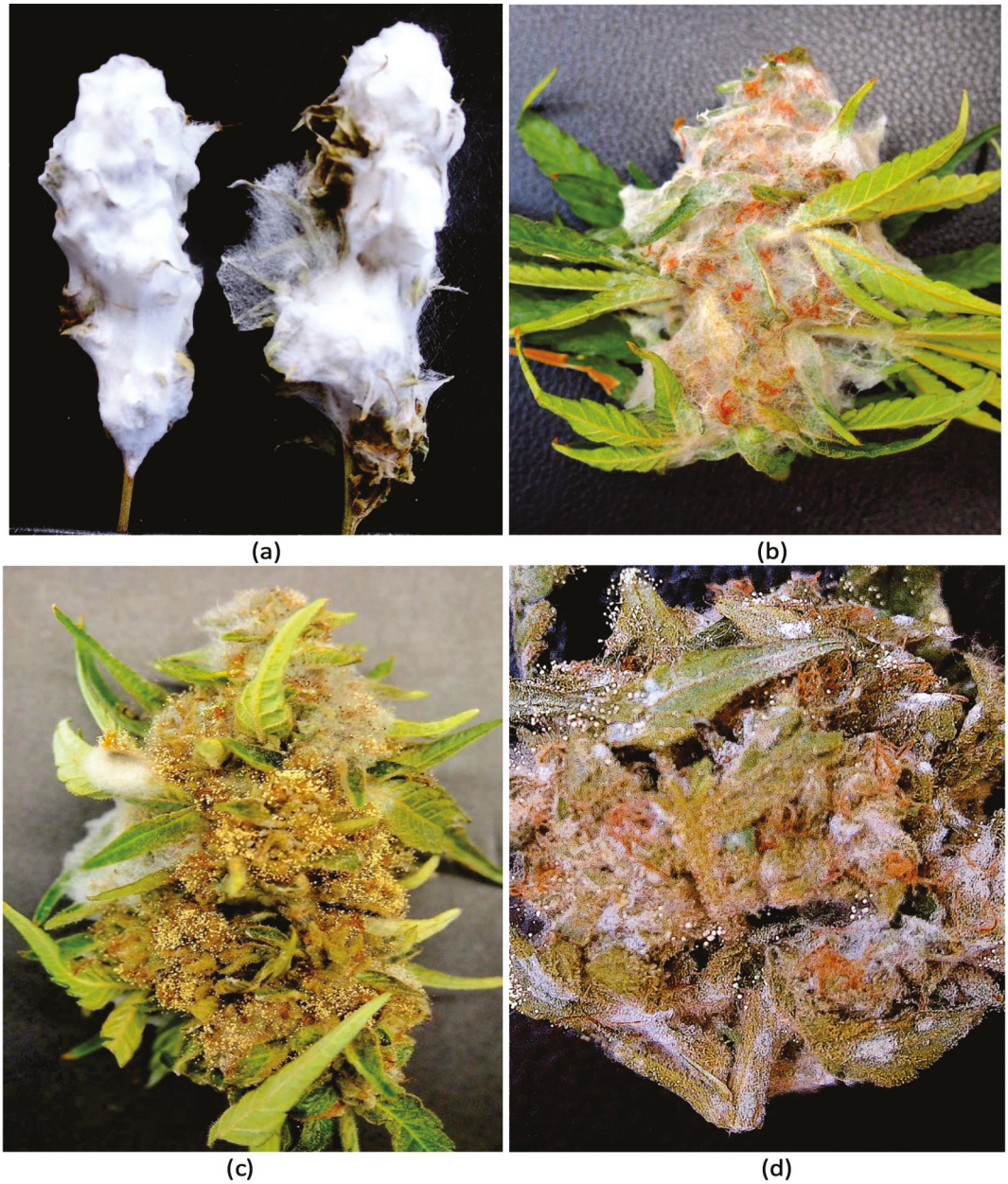


Figure 6. Colonization of detached cannabis inflorescences following inoculation with various fungi and incubation for 7 days. (**a**) Inoculation with *Fusarium graminearum* followed by drying of the tissues. (**b**) Inoculation with *Fusarium sporotrichiodes*. (**c**) Inoculation with *Aspergillus ochraceus*. (**d**) Inoculation with *Penicillium citrinum*.

There were some unexpected results regarding the mycotoxins that were detected. For example, the mycotoxin alternariol was present in tissues of cannabis genotype AK inoculated with *F. graminearum* (FG) and *F. avenaceum* FB3 from tall fescue. As well, the mycotoxin tentoxin was present in tissues of genotypes AK and AD inoculated with *F. avenaceum* from tall fescue. In addition, the mycotoxins 3ADON and DON were present in tissues of both cannabis genotypes inoculated with *F. avenaceum* isolates from cannabis (FB1, FB2) and tall fescue (FB3). Control (uninoculated) cannabis tissues were devoid of mycotoxins, except for culmorin that was present at 0.38 μg/g. Inflorescences inoculated with *A. ochraceus* contained no mycotoxins with those receiving *P. citrinum* containing 6.1 μg/g of BEAU.

To explain the possible causes of the unexpected results above, tissues from which the mycotoxins were obtained were subsequently used for DNA extraction and were subjected to RT-qPCR using species-specific primers for *F. graminearum* and *F. avenaceum* [10]. In tissues inoculated with these two species, the corresponding DNA sequences were present (Table 2). However, in tissues that were inoculated with *F. avenaceum* only, the presence of *F. graminearum* was confirmed, suggesting some background infection had potentially occurred from natural inoculum at the time the inflorescences were harvested for use in this study. These findings can explain the spurious presence of mycotoxins that were likely to be associated with incipient infections by *F. graminearum* in samples where the tissues were either not inoculated or were inoculated with a different species.

Table 2. Response of two genotypes of cannabis (AD, AK) to inoculation with three species of Fusarium isolated from two hosts (cannabis, fescue) with regard to mycotoxin accumulation in inflorescence tissues compared to naturally infected tissues. Mycotoxin levels were determined using an HPLC-MS/MS method.

	Naturally Infected Bud Tissues (*F. avenaceum*)	***Fusarium graminear.* (Cannabis)**	***Fusarium graminear.* (Cannabis)**	***Fusarium avenaceum* (Cannabis)**	***Fusarium avenaceum* (Cannabis)**	***Fusarium avenaceum* (Fescue)**	***Fusarium avenaceum* (Fescue)**	***Fusarium sporotrich.* (Cannabis)**
CANNABIS GENOTYPE	AD	AK	AD	AK	AD	AK	AD	AK
MYCOTOXINS DETECTED (μg/g)								
3-acetyl DON	-	0.34	0.13	-	-	**0.073 ***	-	-
Alternairol	-	0.159	-	-	-	0.151	-	-
DON	-	1.91 *	1.18 *	**0.142 ***	**0.03 ***	**0.51 ***	**0.08 ***	-
Zearalenone	-	56.2	31.8	-	-	-	-	-
Beauvericin	0.098	-	-	-	2.43	0.008	0.051	0.133
Culmorin	-	-	0.38 *	-	-	-	-	-
Enniatin A	-	-	-	0.028	0.019	0.042	0.011	-
Enniatin A1	0.063	-	-	0.621	0.358	0.714	0.181	-
Enniatin B	1.78	-	-	9.3	6.7	7.67	3.96	-
Enniatin B1	0.395	-	-	5.89	2.95	4.37	1.40	-
HT2	-	-	-	-	-	-	-	13.9
T2	-	-	-	-	-	-	-	10.9
Tentoxin	-	-	-	-	-	0.033	0.049	-

Control uninoculated cannabis inflorescences used in this study were found to be free of mycotoxins except for the detection of culmorin at 0.38 μg/g. * The presence of DNA of *F. graminearum* was confirmed in these samples by RT-qPCR using the methods described by Bamforth et al. [10]. The color coding reflects the characteristic mycotoxins produced by the representative *Fusarium* or *Alternaria* species. Light blue = *F. graminearum*; green = *F. avenaceum* and *F. sporotrichiodes*; yellow = *F. avenaceum* and *F. sporotrichiodes*; purple = *F. sporotrichiodes*; red = *Alternaria* species.

4. Discussion

Fusarium species are widespread pathogens of crop plants and cause a broad range of disease symptoms. Up to 16 species of *Fusarium* have been reported to be associated with cannabis plants and are classified in 6 species complexes: *Fusarium oxysporum, F. solani*, *F. incarnatum-equiseti, F. sambucinum, F. tricinctum*, and *F. fujikuroi*. Among these, a sub-set of the species that cause diseases on cereal crops are known to produce a range of mycotoxins that can cause problems following ingestion by humans and animals [14,15]. In particular, the *Fusarium* species causing head blight or scab symptoms on wheat are the most well characterized with regard to the range of mycotoxins produced [14–16]. On cannabis plants, infection by two cereal-infecting *Fusarium* species, namely *F. graminearum* and *F. sporotrichiodes*, has been previously reported [1,2,9]. However, the potential of these species to produce mycotoxins in cannabis tissues has not been previously investigated.

In the present study, isolates of *F. graminearum* and *F. sporotrichioides* and a species previously unreported from cannabis, *F. avenaceum*, all isolated from symptomatic fresh and dried inflorescences, were tested for mycotoxin production under controlled conditions. It should be noted that the inoculated cannabis tissues were incubated under high relative humidity (>90%) for a prolonged period (7 days) prior to mycotoxin analyses being conducted. Similarly, asymptomatic control tissues were exposed to these incubation conditions. Where present, these conditions would have allowed undetected incipient infections to progress before the assays were performed. Under normal greenhouse-growing conditions, these environmental conditions would not be expected to occur unless air circulation was compromised and temperature and relative humidity levels exceeded the normal range (55% relative humidity and temperatures in the range of 27–30 °C). Such conducive conditions (70% relative humidity and temperatures in the range of 34–36 °C) can occur in greenhouses at certain times of the year, resulting in outbreaks of diseases, such as Botrytis bud rot, caused by *B. cinerea*. This disease is favored by humid conditions that occur from July to October, resulting in disease outbreaks [17]. In the present study, the development of pinkish-white mycelium of *Fusarium* was observed on some plants growing under greenhouse conditions in late summer, suggesting the environmental conditions were conducive for infection to occur at these time periods. In addition, the relative humidity and temperature within inflorescences are reported to be higher than the ambient environment [10], indicating that microclimatic conditions may be conducive for infection by *Fusarium* spp. as they are for *B. cinerea* [17]. Such conditions can result in the development of *F. avenaceum* and *F. graminearum* in inflorescence tissues prior to packaging, a situation also similarly encountered with *B. cinerea* infections [17]. The incidence of visible infections due to *Fusarium*, however, appears to be less common on greenhouse-grown cannabis plants when contrasted with outdoor-grown hemp plants. Outdoors, *Fusarium* spp. were reported to infect inflorescences and produce mycotoxins, and prolonged periods of rain and high humidity (75–80%) were associated with outbreaks of disease [6–8]. The incidence of detection of various *Fusarium* spp. within these samples was 95%, indicating that the potential for contamination by mycotoxins in outdoor-grown hemp is significantly higher than for indoor-grown cannabis. In addition, the post-harvest drying and storage conditions for hemp can lead to the extensive growth of *Fusarium* spp. [6,8]. While the sources of inoculum for hemp may include spores from adjacent fields planted to cereal crops, the inoculum sources for indoor-grown cannabis have not been previously identified.

In the present study, tall fescue plants that were grown as a part of the urban landscape within a 30 m distance from the greenhouse were observed to harbor both *F. avenaceum* and *F. graminearum*. Isolates of both species recovered from spikelet tissues of this host were capable of infecting cannabis inflorescences under laboratory conditions and produced mycotoxins in these tissues. The mycotoxins accumulated were reflective of the infecting species, with some exceptions, and were produced at significant levels (Table 2). The importance of wild grass species, including tall fescue plants, growing adjacent to wheat fields in providing a source of inoculum for initiation of disease has been confirmed in several previous studies. At a field site located in Germany, Gerling et al. [18] reported that grasses belonging to *Lolium* spp. growing next to wheat production fields impacted the *Fusarium* species composition and mycotoxin accumulation in wheat plants, particularly those located adjacent to the grasses. The most prevalent species of *Fusarium* recovered from the grasses, and shown to be pathogenic on wheat plants, were *F. graminearum*, *F. culmorum*, and *F. sporotrichioides*. A low level of recovery of *F. avenaceum* was also reported. Wheat kernels produced on plants located next to the infected grasses had higher *Fusarium* abundance and mycotoxin accumulation compared to those located at further distances [18]. The use of irrigation enhanced the abundance of *Fusarium* spp. on both the grasses and on

the wheat plants when compared to non-irrigated sides of the field, with *F. graminearum* being recovered at the highest frequency. Sampling at various distances from the grasses revealed a gradient in percent recovery from the wheat plants, with the highest recovery observed at a 1 m distance and lowest at 33 m. These results demonstrate that the grasses can be a reservoir of inoculum for *Fusarium* spp. that subsequently spread into the wheat field [18].

Similar findings were obtained from field studies conducted in New York State, where *F. graminearum* was shown to be prevalent within spikes of various wild grass species, including tall fescue, especially in irrigated sites adjacent to agricultural fields [19]. *Fusarium avenaceum* was also recovered from a number of different grass species [20] and it has been shown to be seed-borne in tall fescue production sites in Oregon [21], and was shown to infect tall fescue and orchard grass plants grown for pasture [22]. These observations support the hypothesis that *Fusarium* inoculum produced in infected spikes on tall fescue plants growing adjacent to a cannabis greenhouse facility could potentially have spread and infected cannabis inflorescences within the greenhouse. While both *F. graminaearum* and *F. sporotrichioides* have been previously recovered from diseased cannabis and hemp inflorescences [5,6,9,10], they are not reported to infect other parts of the cannabis plant, such as roots and stems, and hence do not provide a potential source of inoculum. Since there are strict biosecurity protocols in place for indoor production of cannabis to meet regulatory guidelines [17], other inoculum sources of these cereal-infecting species, such as worker's clothing or boots, are unlikely. Air-borne inoculum from external sources is the most likely source, which can enter through open greenhouse vents.

In addition to the mycotoxins associated with the three *Fusarium* spp. included in this study, other mycotoxins were detected in dried cannabis inflorescences, such as alternariol and tentoxin, which were present in three samples. The likely source of these mycotoxins is from *Alternaria* spp., which are known to infect cannabis plants [23]; they are also commonly present in grain samples similarly colonized by this pathogen [13,24]. While the inflorescence samples collected for artificial inoculation studies did not show external symptoms due to any pathogen, pre-existing latent infections were likely to have been present that continued to progress during the high relative humidity conditions under which the tissues were incubated. Similar *Alternaria* toxins were also reported to be present at high concentrations in dried hop flowers [25] and in hemp seeds [26]. In hop flowers, DON accumulation from *Fusarium* spp. was detected in all the samples tested. Mycotoxins normally associated with *Aspergillus* or *Penicillium* species colonizing plant tissues, including aflatoxins and ochratoxins, were not detected in hop flowers. They were also absent in a large-scale sampling of dried cannabis flowers conducted in California [27].

In the present study, artificial inoculations conducted with isolates of *A. ochraceus* and *P. citrinum* derived from cannabis inflorescences did not give rise to any of the ochratoxins normally produced by these species [16,28] in the inoculated tissues, although additional studies may be needed to determine the mycotoxin potential of these species in cannabis. Other aflatoxin-producing species of *Aspergillus* were not included in this study as they were unavailable at the time this study was initiated. Currently, there is not a strong body of evidence to support that aflatoxins and ochratoxins are prevalent in cannabis samples originating from production sites that follow regulatory guidelines during production. However, these mycotoxins have attracted attention from regulatory agencies as their known carcinogenic properties can present potential risks to immunocompromised humans if exposed to levels that exceed certain thresholds [3]. There is a growing body of evidence, including data from the current study, which indicates that *Fusarium* and *Alternaria* toxins may actually be more ubiquitous in cannabis tissues. In future studies, these mycotoxins should receive more attention to determine their presence and if the establishment of

threshold limits is required and if monitoring for their presence in cannabis tissues should be enforced.

Incipient infections by *F. graminearum* were confirmed to be present in asymptomatic fresh inflorescences samples used for inoculation with *F. avenaceum* by RT-qPCR. Pathogen presence explains the unexpected detection of mycotoxins associated with this species. It should be noted that these tissues were tested for mycotoxin presence after 7 days of incubation under high relative humidity conditions. By this time, mycelial growth had encompassed the cannabis tissues, a situation not commonly observed in commercial growing environments. It is not certain whether natural infections would have proceeded to develop and accumulate mycotoxins under normal cultivation practices. In the absence of a known source of *Fusarium* inoculum, such as the tall fescue plants identified in the present study, the risk levels for mycotoxin accumulation would appear to be low. While *Fusarium* mycotoxins and various fungal metabolites were reported to be present in seized samples from illicit growing operations in Arizona and California [4], the growing environments depicted do not reflect the production environments encountered in legalized production sites.

In the future, a large-scale systematic study of cannabis inflorescences for the presence of *Fusarium* mycotoxins in licensed production facilities should shed light on the extent to which they accumulate in inflorescence tissues produced under greenhouse conditions. It also remains to be determined what levels of relative humidity conditions could promote the development of *Aspergillus* and *Penicillium* species to the level of colonization that would be associated with ochratoxin and aflatoxin accumulation. Based on the observations from the present study, the risks of contamination with these toxins remain low within licensed production facilities. The current findings, also supported by the recent published literature, suggest that the potential for *Alternaria* and *Fusarium* colonization of cannabis and hop tissues is more likely to lead to mycotoxin presence, and this could represent a moderate risk level. Some of these toxins—enniatins, BEAU, and *Alternaria* toxins—can be classified as "emerging mycotoxins", defined as "mycotoxins which are neither routinely determined nor legislatively regulated". However, the evidence of their incidence is rapidly increasing according to Chiotta et al. [16]. Future studies should target these groups of mycotoxins to determine whether or not the current regulations surrounding mycotoxins in cannabis should be modified to include them.

The two cannabis genotypes included in this study that were artificially inoculated produced comparable rates of tissue colonization by mycelium but differed in the levels of mycotoxins that were present, in some cases differing by as much as four-fold. These differences could be attributed to the different genetic backgrounds of these genotypes (Supplementary Figure S1), but the mechanism remains unexplained. However, they are highly interesting as they suggest there may be differences in the extent to which certain genotypes of cannabis may accumulate these mycotoxins, with some apparently showing lower levels. In wheat samples, differences in the accumulation of mycotoxins in harvested grains were reported to be influenced by the cultivar, fungal isolate, and geographic location, suggesting that the complex interactions between the pathogens, different cultivars, and the environment are important in determining disease outcomes and mycotoxin accumulation [13].

In summary, this study indicates the potential for disease development and mycotoxin accumulation in cannabis inflorescence tissues following infection by *Fusarium* species that commonly infect graminaceous hosts, including cereal crops and other grasses. In view of the findings from this study, there may be a need to develop best practices that limit the spread of inoculum and introduction of *Fusarium* species from neighboring alternate hosts. These may include the elimination of these hosts if they are adjacent to a greenhouse facility

to provide a clear buffer zone, as well as spore-monitoring studies to confirm inoculum presence. In addition, research is needed to better understand the interactions between cannabis cultivars and *Fusarium* fungal isolates, since there are known to be differences in cultivar responses to mycotoxin accumulation in cereal grains [29–31]. Furthermore, studies on the environmental conditions leading to disease development and mycotoxin accumulation in cannabis are needed, both in greenhouse-grown and outdoor-grown crops, since these factors can influence mycotoxin accumulation in cereal crops [29,32]. Lastly, targeted disease management approaches and assessing the potential for breeding for resistance to infection by *Fusarium* species and mycotoxin accumulation in cannabis and hemp should be explored to better manage this unique host–pathogen interaction.

Supplementary Materials: The following supporting information can be downloaded at: https://www.mdpi.com/article/10.3390/jof11070528/s1, Figure S1: Characteristics of cannabis genotypes AK and AD used for inoculation with *Fusarium* species and mycotoxin analysis in this study.

Author Contributions: Conceptualization, Z.K.P.; methodology, Z.K.P., S.A.T. and S.W.; formal analysis, Z.K.P., S.A.T. and S.W.; writing—original draft preparation, Z.K.P.; writing—review and editing, Z.K.P., S.A.T. and S.W.; supervision, Z.K.P., S.A.T. and S.W.; project administration, Z.K.P.; validation verification—Z.K.P., S.A.T. and S.W. All authors have read and agreed to the published version of the manuscript.

Funding: This research received no external funding.

Institutional Review Board Statement: Not applicable.

Informed Consent Statement: Not applicable.

Data Availability Statement: The original contributions presented in this study are included in the article; further inquiries can be directed to the corresponding author.

Acknowledgments: We thank the following individuals who provided technical assistance during various aspects of this study: Samantha Lung, Emily Frketich, and Barbara Wong, Simon Fraser University; Niradha Withana Gamage, Laboratory Service Biologist, and Angelique Parajas, Grain Research Laboratory, Canadian Grain Commission; and Kara B. Loudon, University of Manitoba.

Conflicts of Interest: The authors declare no conflicts of interest.

References

1. Punja, Z.K. Emerging Diseases of *Cannabis sativa* and Sustainable Management. *Pest Manag. Sci.* **2021**, *77*, 3857–3870. [CrossRef] [PubMed]
2. Punja, Z.K.; Ni, L. The Bud Rot Pathogens Infecting Cannabis (*Cannabis sativa* L., Marijuana) Inflorescences: Symptomology, Species Identification, Pathogenicity and Biological Control. *Can. J. Plant Pathol.* **2021**, *43*, 827–854. [CrossRef]
3. Gwinn, K.D.; Leung, M.C.K.; Stephens, A.B.; Punja, Z.K. Fungal and Mycotoxin Contaminants in Cannabis and Hemp Flowers: Implications for Consumer Health and Directions for Further Research. *Front. Microbiol.* **2023**, *14*, 1278189. [CrossRef] [PubMed]
4. Stephens, A.B.; Rivera, A.B.; Cahill, T.M.; Leung, M.C.K. Evaluation of *Fusarium* Mycotoxins and Fungal Metabolites in Seized Cannabis in Arizona and California, 2023–2024. *Environ. Health Perspect.* **2025**, *133*, 047701. [CrossRef] [PubMed]
5. Gwinn, K.D.; Hansen, Z.; Kelly, H.; Ownley, B.H. Diseases of *Cannabis sativa* Caused by Diverse *Fusarium* Species. *Front. Agron.* **2022**, *3*, 796062. [CrossRef]
6. Gauthier, N.; Szarka, D.; Smith, H.; Munir, M. Fusarium Bud Blight and Head Blight Contamination in Stored Hemp: Avoid Postharvest and Storage Molds. Beware of Mycotoxins. Available online: https://plantpathology.ca.uky.edu/files/hemp_disease_alert_postharvest_fusarium.pdf (accessed on 28 February 2025).
7. Kagan, I.A.; Smith, H.S.; Schendel, R.R.; Gauthier, N. Separation and Quantification of Mycotoxins in Floral Tissue of Hemp (*Cannabis Sativa*) Infected with *Fusarium graminearum*. *JSFA Rep.* **2025**, *5*, 140–148. [CrossRef]
8. Szarka, D.; Smith, H.S.; Dixon, E.; Munir, M.; Rahnama, M.; Gauthier, N.A. *Fusarium* Species Recovered from Postharvest Hemp Materials from Kentucky Fields. *Plant Health Prog.* **2023**, *24*, 468–474. [CrossRef]

9. Punja, Z.K. The Diverse Mycoflora Present on Dried Cannabis (*Cannabis sativa* L., Marijuana) Inflorescences in Commercial Production. *Can. J. Plant Pathol.* **2021**, *43*, 88–100. [CrossRef]
10. Bamforth, J.; Chin, T.; Ashfaq, T.; Gamage, N.W.; Pleskach, K.; Tittlemier, S.A.; Henriquez, M.A.; Kurera, S.; Lee, S.-J.; Patel, B.; et al. A Survey of *Fusarium* Species and ADON Genotypes on Canadian Wheat Grain. *Front. Fungal Biol.* **2022**, *3*, 1062444. [CrossRef] [PubMed]
11. Punja, Z.K.; Ni, L.; Lung, S.; Buirs, L. Total Yeast and Mold Levels in High-THC-Containing Cannabis (*Cannabis sativa* L.) Inflorescences are Influenced by Genotype, Environment, and Pre- and Post-Harvest Handling Practices. *Front. Microbiol.* **2023**, *14*, 1192035. [CrossRef] [PubMed]
12. Brown, A.K.; Xia, Z.; Bulloch, P.; Idowu, I.; Francisco, O.; Stetefeld, J.; Stout, J.; Zimmer, J.; Marvin, C.; Letcher, R.J.; et al. Validated Quantitative Cannabis Profiling for Canadian Regulatory Compliance-Cannabinoids, Aflatoxins, and Terpenes. *Anal. Chim. Acta* **2019**, *1088*, 79–88. [CrossRef] [PubMed]
13. Tittlemier, S.A.; Blagden, R.; Chan, J.; Gaba, D.; Mckendry, T.; Pleskach, K.; Roscoe, M. *Fusarium* and *Alternaria* Mycotoxins Present in Canadian Wheat and Durum Harvest Samples. *Can. J. Plant Pathol.* **2019**, *41*, 403–414. [CrossRef]
14. Munkvold, G.P. Fusarium Species and Their Associated Mycotoxins. In *Mycotoxigenic Fungi*; Moretti, A., Susca, A., Eds.; Methods in Molecular Biology; Springer: New York, NY, USA, 2017; Volume 1542, pp. 51–106. ISBN 978-1-4939-6705-6.
15. Munkvold, G.P.; Proctor, R.H.; Moretti, A. Mycotoxin Production in *Fusarium* According to Contemporary Species Concepts. *Annu. Rev. Phytopathol.* **2021**, *59*, 373–402. [CrossRef] [PubMed]
16. Chiotta, M.L.; Fumero, M.V.; Cendoya, E.; Palazzini, J.M.; Alaniz-Zanon, M.S.; Ramirez, M.L.; Chulze, S.N. Toxigenic Fungal Species and Natural Occurrence of Mycotoxins in Crops Harvested in Argentina. *Rev. Argent. Microbiol.* **2020**, *52*, 339–347. [CrossRef] [PubMed]
17. Buirs, L.; Punja, Z.K. Integrated Management of Pathogens and Microbes Affecting Greenhouse-Cultivated Cannabis *(Cannabis sativa* L.). *Plants* **2024**, *13*, 786. [CrossRef] [PubMed]
18. Gerling, M.; Petry, L.; Barkusky, D.; Büttner, C.; Müller, M.E.H. Infected Grasses as Inoculum for *Fusarium* Infestation and Mycotoxin Accumulation in Wheat with and Without Irrigation. *Mycotoxin Res.* **2023**, *39*, 19–31. [CrossRef] [PubMed]
19. Fulcher, M.R.; Winans, J.B.; Quan, M.; Bergstrom, G.C. The Incidence of *Fusarium Graminearum* in Wild Grasses Is Associated with Rainfall and Cumulative Host Density in New York. *Plant Dis.* **2020**, *104*, 2681–2687. [CrossRef] [PubMed]
20. Fulcher, M.R.; Oladipo, E.D.; Winans, J.B.; Quan, M.; Bergstrom, G.C. Structure and Diversity of *Fusarium* Communities Inhabiting Non-Cultivated Grass Inflorescences in New York State. *Can. J. Plant Pathol.* **2021**, *43*, 48–55. [CrossRef]
21. Ocamb, C.M.; Alderman, S.C. *Fusarium* Species Associated with Tall Fescue Seed Production in Oregon. *Plant Health Prog.* **2004**, *5*, 7. [CrossRef]
22. Yates, S.G.; Tookey, H.L.; Ellis, J.J. Survey of Tall-Fescue Pasture: Correlation of Toxicity of *Fusarium* Isolates to Known Toxins. *Appl. Microbiol.* **1970**, *19*, 103–105. [CrossRef] [PubMed]
23. Roberts, A.J.; Punja, Z.K. Pathogenicity of Seedborne *Alternaria* and *Stemphylium* Species and Stem-Infecting *Neofusicoccum* and *Lasiodiplodia* Species to Cannabis (*Cannabis sativa* L., Marijuana) Plants. *Can. J. Plant Pathol.* **2022**, *44*, 250–269. [CrossRef]
24. Tittlemier, S.A.; Blagden, R.; Chan, J.; Roscoe, M.; Pleskach, K. A Multi-Year Survey of Mycotoxins and Ergosterol in Canadian Oats. *Mycotoxin Res.* **2020**, *36*, 103–114. [CrossRef] [PubMed]
25. Sarkanj, I.D.; Vahcic, N.; Markov, K.; Haramija, J.; Ursulin-Trstenjak, N.; Hajdek, K.; Sulyok, M.; Krska, R.; Sarkanj, B. First Report on Mycotoxin Contamination of Hops (*Humulus lupulus* L.). *Toxins* **2024**, *16*, 293. [CrossRef] [PubMed]
26. Lanzanova, C.; Giorni, P.; Bulla, G.; Locatelli, S.; Montanari, M.; Alberti, I.; Leni, G.; Abate, A.; Bertuzzi, T. Investigation on the Presence of Mycotoxins in Seed Hemp Varieties. *Food Addit. Contam. Part A* **2024**, *41*, 400–409. [CrossRef] [PubMed]
27. Jameson, L.E.; Conrow, K.D.; Pinkhasova, D.V.; Boulanger, H.L.; Ha, H.; Jourabchian, N.; Johnson, S.A.; Simeone, M.P.; Afia, I.A.; Cahill, T.M.; et al. Comparison of State-Level Regulations for Cannabis Contaminants and Implications for Public Health. *Environ. Health Perspect.* **2022**, *130*, 097001. [CrossRef] [PubMed]
28. Perdoncini, M.R.F.G.; Sereia, M.J.; Scopel, F.H.P.; Formigoni, M.; Rigobello, E.S.; Beneti, S.C.; Cardoso, F.A.R.; Marchi, L.B.; Junior, C.G.D.S.; Fernandes, P.G.M.; et al. Growth of Fungal Cells and the Production of Mycotoxins. In *Cell Growth*; IntechOpen: London, UK, 2019; pp. 1–14. [CrossRef]
29. Amarasinghe, C.C.; Simsek, S.; Brûlé-Babel, A.; Fernando, W.G.D. Analysis of Deoxynivalenol and Deoxynivalenol-3-Glucosides Content in Canadian Spring Wheat Cultivars Inoculated with *Fusarium graminearum*. *Food Addit. Contam. Part A* **2016**, *33*, 1254–1264. [CrossRef] [PubMed]
30. Aureli, G.; Amoriello, T.; Belocchi, A.; D'Egidio, M.G.; Fornara, M.; Melloni, S.; Quaranta, F. Preliminary Survey on the Co-Occurrence of DON and T2 + HT2 Toxins in Durum Wheat in Italy. *Cereal Res. Commun.* **2015**, *43*, 481–491. [CrossRef]

31. Ruan, Y.; Babonich, R.; Clarke, J.M.; Hucl, P.J.; Clarke, F.R.; Knox, R.E.; Bokore, F.E.; Pozniak, C.J. Differential Reaction of Hexaploid and Tetraploid Wheat to *Fusarium graminearum* Chemotypes in a Controlled Environment. *Can. J. Plant Pathol.* **2021**, *43*, 760–768. [CrossRef]
32. Walkowiak, S.; Bonner, C.T.; Wang, L.; Blackwell, B.; Rowland, O.; Subramaniam, R. Intraspecies Interaction of *Fusarium graminearum* Contributes to Reduced Toxin Production and Virulence. *Mol. Plant Microbe Interact.* **2015**, *28*, 1256–1267. [CrossRef] [PubMed]

Disclaimer/Publisher's Note: The statements, opinions and data contained in all publications are solely those of the individual author(s) and contributor(s) and not of MDPI and/or the editor(s). MDPI and/or the editor(s) disclaim responsibility for any injury to people or property resulting from any ideas, methods, instructions or products referred to in the content.

Journal of *Fungi*

MDPI

Article

The Growth, Pathogenesis, and Secondary Metabolism of *Fusarium verticillioides* Are Epigenetically Modulated by Putative Heterochromatin Protein 1 (FvHP1)

Andrés G. Jacquat [1,2], Natalia S. Podio [3], María Carmen Cañizares [4], Pilar A. Velez [5,6], Martín G. Theumer [5,6], Vanessa A. Areco [7], María Dolores Garcia-Pedrajas [4,*] and José S. Dambolena [1,2,*]

1 Facultad de Ciencias Exactas Físicas y Naturales (FCEFyN), Universidad Nacional de Córdoba (UNC), Córdoba X5016GCA, Argentina; andresgjacquat@gmail.com
2 Instituto Multidisciplinario de Biología Vegetal (IMBIV), Consejo Nacional de Investigaciones Científicas y Técnicas (CONICET), Avenida Vélez Sarsfield 1611, Córdoba X5016GCA, Argentina
3 Instituto de Ciencia y Tecnología de Alimentos Córdoba (ICYTAC), Consejo Nacional de Investigaciones Científicas y Técnicas (CONICET), and Universidad Nacional de Córdoba (UNC). Bv. Dr. Juan Filloy s/n, Cdad. Universitaria, Córdoba X5016BMB, Argentina; npodio@fcq.unc.edu.ar
4 Instituto de Hortofruticultura Subtropical y Mediterránea "La Mayora", Universidad de Málaga, Consejo Superior de Investigaciones Científicas (IHSM—UMA—CSIC), Estación Experimental "La Mayora", Avenida Dr. Wienberg s/n, Algarrobo-Costa, 29750 Málaga, Spain; carmen.canizares@eelm.csic.es
5 Departamento de Bioquímica Clínica, Facultad de Ciencias Químicas (FCQ), Universidad Nacional de Córdoba (UNC), Córdoba X5000HUA, Argentina; pilarvelez@fcq.unc.edu.ar (P.A.V.); mgtheumer@unc.edu.ar (M.G.T.)
6 Centro de Investigaciones en Bioquímica Clínica e Inmunología (CIBICI), Consejo Nacional de Investigaciones Científicas y Técnicas (CONICET), Haya de la Torre y Medina Allende—Ciudad Universitaria, Córdoba X5000HUA, Argentina
7 Instituto Multidisciplinario de Investigación y Transferencia Agroalimentaria y Biotecnológica (IMITAB, CONICET-UNVM), Villa María X5900LQC, Argentina; vareco@unvm.edu.ar
* Correspondence: mariola@eelm.csic.es (M.D.G.-P.); jdambolena@imbiv.unc.edu.ar (J.S.D.)

Abstract: *Fusarium verticillioides* is a globally prevalent phytopathogenic fungus responsible for multiple diseases in maize and a major producer of the mycotoxin fumonisin B1 (FB1), a highly toxic fungal secondary metabolite (FSM). The histone code, which includes reversible modifications such as acetylation and methylation, plays a critical role in regulating chromatin structure and gene expression. In fungi, di- and tri-methylation of histone H3 at lysine 9 (H3K9me2/3) serves as a key epigenetic mark associated with heterochromatin formation and transcriptional repression. In this study, we identified and characterized a putative heterochromatin protein 1 (HP1) family member in *F. verticillioides*, designated FvHP1, based on conserved domain architecture and phylogenetic analyses. FvHP1 retains essential residues required for H3K9me2/3 recognition, supporting its functional conservation within the HP1 protein family. Phenotypic analysis of the ΔFvHP1 mutant revealed impaired vegetative growth, reduced conidiation and virulence, and altered FB1 mycotoxin production. Additionally, the accumulation of red pigment in the mutant was linked to the deregulation of secondary metabolism, specifically the overproduction of fusarubin-type naphthoquinones, such as 8-O-methylnectriafurone. These results support the role of FvHP1 in facultative heterochromatin-mediated repression of sub-telomeric biosynthetic gene clusters, including the pigment-associated PGL1 cluster. Our findings provide new insights into the epigenetic regulation of fungal pathogenicity and metabolite production, as well as the first evidence of a functional HP1 homolog in *F. verticillioides*.

Keywords: *Fusarium verticillioides*; phytopathogenic; fumonisin B1; fungal secondary metabolite; histone code; epigenetic; heterochromatin; heterochromatin protein 1 (HP1); fusarubin-type naphthoquinones; 8-O-methylnectriafurone

1. Introduction

Fusarium verticillioides (Sacc.) Nirenberg (teleomorph: *Gibberella fujikuroi* Mating Population A) is a highly prevalent soil-inhabiting filamentous fungus found in the most important cereal crops globally, such as maize (*Zea mays* L., *Poaceae*) [1]. This fungus exhibits both endophytic and pathogenic/parasitic behavior, causing several diseases throughout the maize biological cycle (seedling blight, stalk rot, ear rot) and resulting in crop yield losses [2–5]. Global corn production losses caused by F. verticillioides are estimated to be 10%, reaching 30% to 50% in severely affected areas. Moreover, it is a major producer of mycotoxins called fumonisins, which pose a significant problem due to their toxicological implications for humans and farm animals [6–9]. Therefore, given its negative economic impact and its implications for human and animal health, *Fusarium verticillioides* and its secondary metabolites are under continuous study.

The polyketide fumonisin B type 1 (FB1) is the most important fungal secondary metabolite (FSM) produced by *F. verticillioides* due to its high toxicity and prevalence in cereals [8,10]. In addition to FB1, *F. verticillioides* produces other polyketide secondary metabolites such as the naphthoquinone pigment bikaverin [11,12] and black perithecial pigments [11,13]. The compound 8-O-methylnectriafurone was identified as one of several fusarubin-type naphthoquinones produced by Fusarium fujikuroi. These compounds are synthesized through a non-reducing polyketide synthase (NR-PKS) pathway. They are red pigments that contribute to the pigmentation and structural integrity of perithecia, the sexual fruiting bodies of the fungus [13]. Fungal secondary metabolites are intermediates or end products of genus- or species-specific metabolic pathways, whose complete biosynthetic pathways are generally encoded in a biosynthetic gene cluster (BGC) [14–16]. This genetic organization is presumed to be the consequence of evolutionary pressure, as it would facilitate both the coordinated transcriptional regulation (co-regulated genes) and the horizontal transfer among strains of all the genetic elements required for the production of a specific secondary metabolite [17,18]. In *F. verticillioides*, BGCs for FB1 and the dark perithecial pigment comprise 15 [19] and 7 genes [11], respectively.

The synthesis of FSMs is tightly regulated by both pathway-specific and broad-domain transcription factors (TFs), as well as by epigenetic mechanisms, including the chemical modification of histones [16,20]. The reversible covalent modifications of histones have an impact on chromatin structure, specifically the facultative heterochromatin region, being an important mechanism to regulate BGCs expression. It is worth mentioning that chromatin presents two main functional and structurally well-defined states: the highly compacted heterochromatin associated with gene silencing, and the unfolded euchromatin associated with gene expression [21]. This transcriptional regulation by the conformational state of chromatin involves the histone code, which refers to the specific pattern of post-translational covalent modifications, such as methylation, acetylation, and phosphorylation, on specific lysine (K), serine (S), and arginine (R) residues of the N-terminus tail of the H3 and H4 histones. Each pattern is linked to a specific biological function, and can be heritable [16,21–23]. Specifically, the di-/tri-methylation (me2/3) on lysine 9 of the N-terminal tail of H3 histone (H3-K9me2/3) is among the best-understood post-translational modifications involved in heterochromatin formation and gene repression [24]. The main protein implicated in heterochromatin formation by recognizing and attaching to the H3-K9me2/3

epigenetic mark is heterochromatin protein 1 (HP1) [16,25]. HP1 is a highly conserved eukaryotic heterochromatin-associated non-histone chromosomal protein that contains two major conserved domains: the CHRomatin Organization MOdifier (CHROMO) domain and the CHROMO Shadow domain (CD and CSD, respectively). These domains are separated by a hinge sequence [26,27]. This molecular structure allows HP1 to adopt different spatial conformations, giving it great functional versatility and the capability to interact with many other types of molecules. These include interactions with itself, forming HP1 homodimers, as well as with H3 histone, non-histone chromosomal and non-chromosomal proteins, single and double-stranded DNA, and RNA molecules [28]. Although a wide range of functions have been attributed to HP1 proteins, they are best known for their fundamental role in establishing, propagating, and maintaining the heterochromatic state promoting gene silencing through transcriptional restriction [24,28–31].

Previously, a lysine histone methyltransferase (KHMTase) encoded by the *FvDim5* (NCBI accession code FVEG_08911) gene was associated with heterochromatin formation in *F. verticillioides* [32]. The biological processes regulated by the expression of the *FvDim5* gene include vegetative growth, microconidia production, pathogenic behavior, and pigmentation (FSM) of the fungal colony [32]. The functional characterization of HP1 in several filamentous fungi has identified it as a major modulator of FSM production, as well as influencing both vegetative and pathogenic behaviors [33–36]. Nevertheless, no homologous HP1 proteins have been studied in *F. verticillioides* yet. The aim of the present study was to identify and annotate the functional and structural characteristics of the putative HP1 protein encoded by *F. verticillioides*, a reader protein of the epigenetic mark H3K9me2/3, which is catalyzed by the KHMTase FvDim5. Our in silico approach resulted in a unique protein sequence that possesses all the hallmarks of members of the HP1 family. This was considered a putative HP1 protein of *F. verticillioides* and was tentatively named FvHP1 (in non-italics), which is encoded by the *FvHP1* (in italics) gene. Then, our deletion mutant-based approach suggests that FvHP1 plays a significant role in regulating vegetative growth, pathogenicity, and the production of FMSs, such as FB1 and pigments. Although the pathways of FB1 biosynthesis are well-established, this study enhances our understanding of the epigenetic mechanisms that regulate FB1 biosynthesis, as little is known about this aspect. Additionally, we contribute to the structural diversity of fungal pigments by discovering a previously unknown metabolite. Finally, we advance the understanding of the transition to pathogenic and parasitic behavior mediated by epigenetic regulators.

2. Materials and Methods

Fungal strains, growth conditions and conidia production

Fusarium verticillioides M3125 (FGSC #7600), provided by Dr. Robert Proctor (USDA, Agricultural Research Service, National Center for Agricultural Utilization Research, Peoria, IL, USA), served as the wild-type (WT) strain and the parental strain for the deletion mutant used in this study. Fungal strains were grown on Potato Dextrose Agar (PDA) (VWR Chemicals BDH®, Leuven, Belgium) or Czapek Dox Agar (CDA) (OXOID, Basingstoke, Hants, UK), in the dark at 25 °C. Czapek Dox Broth (CDB), either commercial (OXOID, Basingstoke, Hants, UK) or homemade (3.0% P/V sucrose, 0.2% $NaNO_3$, 0.1% KH_2PO_4, 0.04% $MgSO_4$ $7H_2O$, 0.05% KCl and 0.0016% Fe(II)SO_4 $2H_2O$), YEPS (2.0% sacarose, 1.0% yeast extract, 2.0% peptone), and GYAM (0.24 M glucose, 0.05% yeast extract, 8 mM L-asparagine, 5 mM malic, acid, 1.7 mM NaCl, 4.4 mM K_2HPO_4, 2 mM $MgSO_4$, and 8.8 mM $CaCl_2$; pH 3.0) were used for liquid cultures. For the selection of transformants and their subsequent growth, the media were supplemented with 250 μg/mL of Nourseothricin (NTC) (Jena Bioscience, Jena, Deutschland).

Bioinformatic analyses

The Basic Local Alignment Search Tool (BLAST) [36] of the NCBI (National Center for Biotechnology Information, U.S. National Library of Medicine, Bethesda, MD, USA) was used for protein sequence searches through the online server at https://blast.ncbi.nlm.nih.gov/Blast.cgi (accessed on 9 March 2024) [37]. The search for domain-level homologies was conducted using the NCBI Conserved Domain Search (CDS) software as implemented at https://www.ncbi.nlm.nih.gov/Structure/cdd/wrpsb.cgi (accessed on 9 March 2024). [38]. Protein alignment was conducted using the probabilistic consistency-based progressive multiple alignment, which incorporates 3D conformational constraints information. This multiple structure-sequence alignment was implemented through the PROMALS3D software (http://prodata.swmed.edu/promals3d/promals3d.php (accessed on 9 March 2024)) [39,40]. For the protein phylogenetic relationships, an unrooted Maximum Likelihood tree of protein sequences was constructed using IQ-TREE multicore version 1.6.11 [41] and displayed with MEGA X version 10.1.5 software [42]. The best-fit substitution model was determined by the ModelFinder program [43]. The alignment was displayed with Unipro UGENE v. 42.0 software [44].

Production of deletion mutants

For the deletion of FvHP1 in *F. verticillioides*, a deletion vector compatible with *Agrobacterium tumefaciens*-mediated transformation (ATMT) was constructed using the OSCAR method [45]. Approximately 1200 bp of the 5′ and 3′ flanking regions of the gene corresponding to accession code FVEG_01876 were independently amplified by polymerase chain reaction (PCR) using Phusion® High-Fidelity DNA Polymerase (Thermo Fisher Scientific, Waltham, MA, USA) (Figure 1a) [46]. Then, a BP Clonase (BP Clonase™ II, Gateway™, Exime Mix, Invitrogen™, Thermo Fisher Scientific, MA, USA) reaction was performed, combining both amplified gene flanks with the binary vector pOSCAR and a vector providing the resistant marker for the selection of fungal transformants. As resistance marker vector we used pA-NTC^R-OSCAR, which contains a nourseothricin acetyltransferase (*nat1*) gene conferring resistance to nourseothricin (NTC). The BP clonase reaction was used to transform One Shot™ OmniMAX™ 2 T1R Chemically Competent *E. coli* (Invitrogen, Carlsbad, CA, USA) following the commercial manual's instructions. The correct construct in *E. coli* colonies was verified by restriction enzyme digestion (Figure 1b). The deletion construct was then transferred to *A. tumafaciens* strain AGL1, using a standard electroporation method, in preparation for fungal transformation. The ATMT of *F. verticillioides* was performed according to previously described protocols [41]. Fungal transformants were confirmed based on their resistance to NTC (250 μg/mL supplemented CDA medium), negative PCR amplification with FvHP1-specific primers, and negative Southern blot hybridization using an FvHP1-specific probe labelled with digoxigenin–dUTP, DNA probe labeling, hybridization, and detection were performed using the DIG High Prime I DNA Labeling and Detection Starter Kit (Roche, Mannheim, Germany). From the total pool of transformant colonies, three were selected and designated as ΔHP1#6, ΔHP1#15, and ΔHP1#17. To confirm stable deletion, transformants were transferred several times to fresh CDA plates supplemented with 250 μg/mL of NTC. Results were displayed in Figure 1, where the PCR product patterns (Figure 1c) and Southern blot analysis (Figure 1d) were consistent with a targeted replacement event in which the ORF of the putative FvHP1 encoding gene (FVEG_0187) was replaced by the expression cassette of the *nat1* gene (NTC resistance-conferring gene). A transformant with a random ectopic integration of the deletion construct was also selected. This strain was designated as ECT. The primers used to amplify the ORF of the FVEG_0187 gene were Hep1F (5′-CCTGCTCTTAGTGACGAGG-3′) and Hep1R (5′-GAGGACTCCAACTCTTCGC-3′). The primers for amplifying the *nat1* gene were NatF (5′-ATGACCACTCTTGACGACACG-3′) and NatR (5′-TTGACGTTGGTGACCTCCAG-3′).

To amplify the 5′ flanks of the putative *FvHP1* gene ORF (1329 bp), the primers used were FvHP1-attB2r (5′-ggggacagctttcttgtacaaagtggaaCAGCCAACGACATCTCATCTCTG-3′) and FvHP1-attB1r (5′-ggggactgctttttgtacaaacttgtACTAACGTGTGCTAGTCTACGTTG-3′). For amplifying the 3′ flanks of the putative *FvHP1* gene ORF (1187 bp), the primers were FvHP1-attB4 (5′-ggggacaactttgtatagaaaagttgttCGAGACGCAGCCATATAAGGT-3′) and FvHP1-attB3 (5′-ggggacaactttgtataataaagttgtAGAGACGAGCTTCCAGATACC-3′). Lowercase indicates the sequence attached to the end of each primer for recognition by BP clonase.

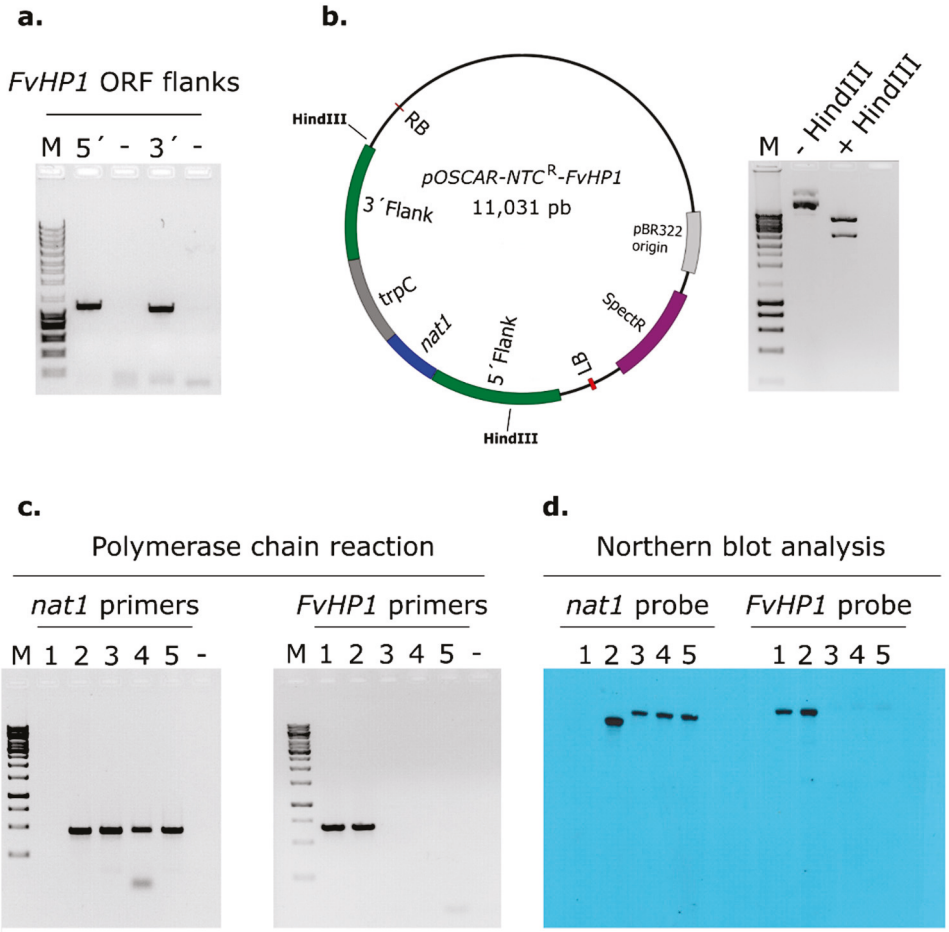


Figure 1. Generation of deletion mutants for *FvHP1* in F. verticillioides. (**a**) Electrophoretic analysis of the *FvHP1* 5′ and 3′ flanks amplified by PCR. (**b**) Map of pOSCAR-NTC^R-FvHP1 deletion construct (HindIII restriction sites are indicated). The colored boxes indicate functional regions: LB: T-DNA left border; RB: T-DNA right border; nat1: nourseothricin acetyl transferase gene; trpC: promoter region of the Aspergillus nidulans gpdA gene; SpectR: spectinomycin resistance gene; pBR322: replication origin. The electrophoretic gel on the right shows the HindIII digestion pattern of the pOSCAR. (**c**) Confirmation of *FvHP1* deletion by PCR in selected transformants using primer pairs for *FvHP1* gene ORF and nat1 (NTC^R) gene. (**d**) Southern blot analysis of selected transformants using probes complementary to the *FvHP1* gene ORF and the nat1 gene. Wells labeled with 1, 2, 3, 4, and 5 in panels c and d indicate WT, ECT, and deletion mutant strains ΔHP1#6, ΔHP1#15, and ΔHP1#17, respectively. Wells labeled with "-" in panels (**a**,**c**) indicate PCR negative water control, and in panels (**a**–**c**), well "M" indicates molecular weight marker (1Kbp, NZYDNA Ladder III, NZYTech®, Paço do Lumiar, Lisboa, Portugal)). All electrophoretic analyses were performed on 0.8% *w*/*v* agarose gels stained with ethidium bromide. Bands were revealed under UV light (UVP, LLC, Analytik Jena US LLC, Upland, CA, USA).

Lag phase, growth rate, and conidiation

To assess fungal vegetative growth, PDA Petri dishes were inoculated at the center with 5 µL of a conidia suspension (1.0×10^6 conidia/mL) from each strain and incubated

in the dark at 25 ± 1 °C until the colonies completely covered the surface of the plate. For each colony, two diameter measurements were recorded daily using a Vernier scale caliper. The two diameter measurements were taken perpendicular to each other, and an average was recorded. The lag phase was estimated using a nonlinear regression curve derived from a non-modified Gompertz model [47,48] fitted to the colony growth over an 8-day incubation period. This vegetative colonial feature represents the time (in hours) it takes for the colony to reach an area of 13.4 mm^2 (equivalent to a diameter of 5 mm). Mathematically, the lag phase was determined by solving for the time ("t") variable when "A" = 13.4 (Equation (1)). The growth rate was estimated from the slope of the linear regression curve fitted to data derived from the linear vegetative growth phase. To determine microconidia production, 5 mL of YEPS liquid medium was inoculated with 10 µL of a conidia suspension (1.0×10^6 conidia/mL) in 50 mL glass tubes. The tubes were placed on an orbital shaker in the dark at 28 ± 1 °C for four days. Then, the culture was filtered through Miracloth membranes, and the microconidia were counted using a hemocytometer.

$$A = \alpha \times e^{[-\beta \times e\hat{}(-\gamma \times t)]} \quad (1)$$

where "A" is the area variable (mm^2), "t" is the time variable (hours), "e" is the mathematical constant ~2.718, and "α", "β" and "γ" are the statistics of the Gompertz equation. In all assays, "α", "β" and "γ" significantly explained the observed variables at a significance level of 0.05.

Pathogenicity assays

Fungus–maize interaction assays were conducted under two different culture regimes: hydroponic–phytotron and soil–greenhouse. They were designated as experimental schemes A and B, respectively. In addition to these, an in vitro assay was performed to evaluate radicle development. In all experiments, kernels were disinfected with a NaClO solution (3.0 mg Cl/mL) and subjected to thermal treatment at 60 °C for 5 min [49]. For experimental scheme A, maize seeds (hybrid ACA 474 VT3Pro MG-RR2, Argentina) were soaked in a conidia suspension or sterile water (mock inoculation) for 10 min. Then, the grains were placed on Petri dishes containing 2% water agar (WA) medium and incubated in darkness at 25 ± 1 °C for three days. Upon germination, seeds were transferred to hydroponic culture with a 12/12 h photoperiod, a temperature of 25 ± 1 °C, and a relative humidity of 75 ± 10%. The irrigation regime and the concentrations of the macro and micronutrients in the hydroponic solution were set according to the method described by Zörb et al. [50]. Stem heights were measured at 6, 10, and 14 days post-infection (DPI). The experiment was conducted once with 10–12 plants per treatment. For experimental scheme B, seeds (hybrid Golden Bantam sweet corn, Rocalba S.A., Girona, Spain) were incubated in sterile distilled water overnight in darkness at 25 ± 1 °C to induce germination. Then, they were individually planted in 1 L plastic pots containing a mixture of non-autoclaved substrate, coconut fiber, and vermiculite. The pots were then placed in the greenhouse, where they were exposed to natural photoperiod, relative humidity ranging from 60% to 95%, and temperatures ranging from 15 °C to 28 °C. At 10 days post-planting (DPP), seedlings were infected with a suspension of 1.0×10^6conidia/mL injected into the stem. At this point (10 DPP), the height of the seedlings (h0) was measured. At 10 days post-inoculation (DPI) or 20 DPP, seedling height (h1) was measured again to calculate the "post-infection seedling relative growth" parameter as a general plant health estimator. The equation implemented was $(h1 - h0) \times (h0)^{-1}$ and the result was expressed as a percentage. Three replicates of the assay were performed, with 7–14 seedlings per treatment in each replicate.

Radicle growth was used as another general plant health estimator. For this assay, 12 to 15 corn seeds (ACA 474 VT3Pro MG-RR2, Pergamino, Buenos Aires, Argentina) for each treatment were immersed in a 1.0×10^6conidia/mL suspension in PBS buffer with

1.5% Tween-20 for 10 min. A 1.5% Tween-20 in PBS buffer without conidia was used as the negative control. Then, they were placed in glass Petri dishes (90 × 15 mm) containing 1.5% WA medium and kept in darkness at 25 ± 1 °C for three days. They were symmetrically arranged around the periphery of the dish, with the kernel tips facing towards the center of the dish. The entire experiment was carried out twice.

FB1 production

To investigate the impact of the gene deletion on FB1 production, two different culture media were employed: GYAM and CDB. In *F. verticillioides* WT strains, FB1 synthesis is induced in GYAM medium but not in CDB medium. Liquid cultures were prepared by inoculating 50 mL of GYAM or CDB with 0.5 mL of conidia suspension (1.0×10^6 conidia/mL). After seven days of incubation in an orbital shaker at 200 rpm at a temperature of 28 ± 1 °C in the dark, a 1 mL sample was taken from each culture and centrifuged at 9000 RCF for 15 min to remove fungal cells. The supernatants were transferred to a fresh tube and diluted with HPLC-grade acetonitrile (Sintorgan, Villa Martelli, Buenos Aires, Argentina) at a 1:1 ratio. The FB1 content was determined using high-performance liquid chromatography (HPLC) (PerkinElmer Inc., Waltham, MA, USA) coupled with a fluorescence detector [51]. The quantification of FB1 was carried out by comparing the peak areas with those obtained from samples containing FB1 analytical standards (PROMEC Unit, South African Medical Research Council, Francie van Zijl Drive, Tygerberg Hospital, Parow, Tygerberg 7505, Cape Town, South Africa). The experiment was repeated twice, and five independent cultures were analyzed for each strain.

Production, isolation, and identification of fungal metabolites

Fungal metabolites were extracted and purified from a 7-day CDB culture (200 RPM orbital shaking in dark at 25 ± 1 °C) after removing fungal cells by centrifugation and filtration (0.45 PVDF filters). Solid-phase extraction C-18 cartridges (500 mg, 6 mL, 40 μm) conditioned with 10 mL of methanol and 10 mL of water were used. Filtrates were eluted from the columns using 2 mL of HPLC-grade acetonitrile and stored at −70 °C for further characterization. The metabolites were analyzed by chromatography coupled to mass spectrometry (HPLC-MS) using an Agilent Technologies 1200 Series UHPLC (Agilent, Santa Clara, CA, USA) equipped with a gradient pump (Agilent G1312B SL Binary), solvent degasser (Agilent G1379B), and an autosampler (Agilent G1367D SL þ WP). The chromatographic separation was achieved on a C18 column (5 mm, 100 mm × 4.60 mm i.d.) (Agilent, Santa Clara, CA, USA) at 40 °C using an Agilent G1316B column heater module. The mobile phase consisted of a solution of 5 mM ammonium acetate and 0.4% formic acid (solvent A) and a solution of 5 mM ammonium acetate and 0.4% formic acid in methanol (solvent B). The solvent gradient started with 5% B for 1 min and then changed to 50% B over 3 min. This was followed by a second ramp to 65% B over 6 min and a third ramp to 98% B over 12 min. The solvent remained in this state for 7 min. Then, an 8 min washing and stabilization step was used before the next run. The flow rate was set at 0.3 mL/min, and the injection volume was 10 μL. The HPLC system was connected to a photodiode array detector (PAD SL, Agilent G1315C) in conjunction with an ESI source and Q-TOF mass spectrometer (micrOTOF-QII Series, Bruker Daltonics Inc., Billerica, MA, USA). UV-vis spectra were recorded from 200 to 700 nm. Mass spectra were recorded in positive ion mode from m/z 80 to 1200. The working conditions for the ionization source were as follows: a capillary voltage of 4500 V, a nebulizer gas pressure of 4.0 bar, a drying gas flow of 8.0 L/min, and a drying gas temperature of 200 °C. Nitrogen was used as the nebulizer/dryer gas, while argon was used as the collision gas. The instrument was operated in full-scan mode. The exact mass was verified by introducing a sodium formate solution (40 mM) at the end of each chromatographic run using the multipath valve of the Micro-QTOF II. Metabolite identification was based on an accurate m/z ratio

(mass error $\leq$ 5 ppm) and fragmentation pattern (MS/MS spectrum with collision energies of 10.0, 15.0, and 20.0 eV). Data acquisition and spectrum processing were performed using Compass 3.1 and DataAnalysis 4.1, respectively (BrukerDaltonics, Billerica, MA, USA). Molecular features (pairs m/z; retention time) were extracted from the raw spectra using ProfileAnalysis 2.3 software (BrukerDaltonics, MA, USA). LC-MS analyses were processed using the Find Molecular Features (FMF) function with S/N = 10 for peak detection. Background subtraction and time alignment were also performed. Advanced bucket generation was used, with a retention time range of 1–30 min, a mass range of 80–1200 m/z, and each bucket (spectral bin) was formed with a resolution of 0.3 min and 10 m/z mDa without normalization. The generated bucket table was exported to Excel, and a blank subtraction step was performed. The final feature matrix was normalized by summing the peak areas for univariate analysis (volcano plot, $p < 0.05$ and Fold Change ≥ 2) and Pareto scaled for multivariate supervised statistical modeling (OPLS-DA) using MetaboAnalyst 5.0 online software.

Statistical analyses

Statistical analyses of fungal growth (*Lag phase, growth rate, and conidiation*), fumonisin B1 production data and phytopathogenicity assay data were performed by one-way analysis of variance (ANOVA) ($p \leq 0.05$). The normality and homogeneity of variance were tested. Data are presented as mean $\pm$ standard error and differences between means were considered significant if probability (p) ≤ 0.05. DGC test was used for means comparisons. All statistical analyses were performed using InfoStat v2020 software.

3. Results

3.1. Identification of a Putative HP1 Protein in Fusarium verticillioides

We scanned the NCBI Protein Reference Sequences (NCBI RefSeq_protein) database for putative HP1 proteins using a *F. verticillioides*-limited (taxid:117187) BLASTp search. The HP1 protein from *F. graminearum* (NCBI accession number XP_011319962.1) served as the query. The best hit showed 100% query coverage, 70.52% identity, and an e-value of 3.0×10^{-116} with the protein sequence recorded under NCBI accession code: XP_018744913.1. Two other hits displayed 31% and 32% query coverage, 35.53% and 37.04% identity, and e-values of 2.0×10^{-10} and 3.0×10^{-05}, respectively. We proceeded with the analysis of the top BLASTp result, due to its highly favorable characteristics, indicating it as the most likely homologous protein, as detailed below. The hypothetical protein XP_018744913.1 consists of 246 amino acid (aa) residues. NCBI's Conserved Domain Search (CDS) tools indicated the presence of two evolutionarily conserved domains among HP1 family members: the amino-terminal chromo domain (CD) and the carboxyl-terminal chromo shadow domain (CSD) [26]. The CD spans positions 62 to 113 aa, while the CSD spans positions 176 to 229 aa. A multiple structure-sequence alignment (Figure 2a), which includes several previously characterized HP1 proteins, demonstrated that the CD and CSD of the *F. verticillioides* XP_018744913.1 protein exhibit a high degree of similarity to the well-defined CD and CSD of Su(var)205 isoform A (NCBI accession code: NP_476755.1) [29,52,53], Swi6 (NP_593449.1) [54], BcHP1 (NCBI accession code: ATZ56699.1; Old locus tag: BC1G_06432) [55], NcHP1 [56], and FgHP1 [35] proteins. Furthermore, the candidate *F. verticillioides* HP1 (XP_018744913.1) was found to contain three aromatic residues (phenylalanine 62, tryptophan 84, and tyrosine 87) and three non-aromatic residues (threonine 94, glutamate 96, and asparagine 100) at homologous sites. These residues have been determined to be key for recognizing the H3K9me2/3 mark [57] (see Supplementary Figure S1). The protein phylogenetic reconstruction showed that XP_018744913.1 (from *F. verticillioides*) and FgHP1 (from *F. graminearum*) share a recent common ancestor (Figure 2b). In summary, the similarities of the CD and CSD regions and

the evolutionary relationships with other well-characterized members of the HP1 protein family provide sufficient evidence to propose that the amino acid sequence recorded by *F. verticillioides* under the NCBI accession code XP_018744913.1 is homologous to HP1 proteins, hereafter referred to as FvHP1 (non-italic letters). The coding nucleotide sequence, recorded under the NCBI accession code FVEG_01876, will be hereafter referred to as *FvHP1* (italic letters).

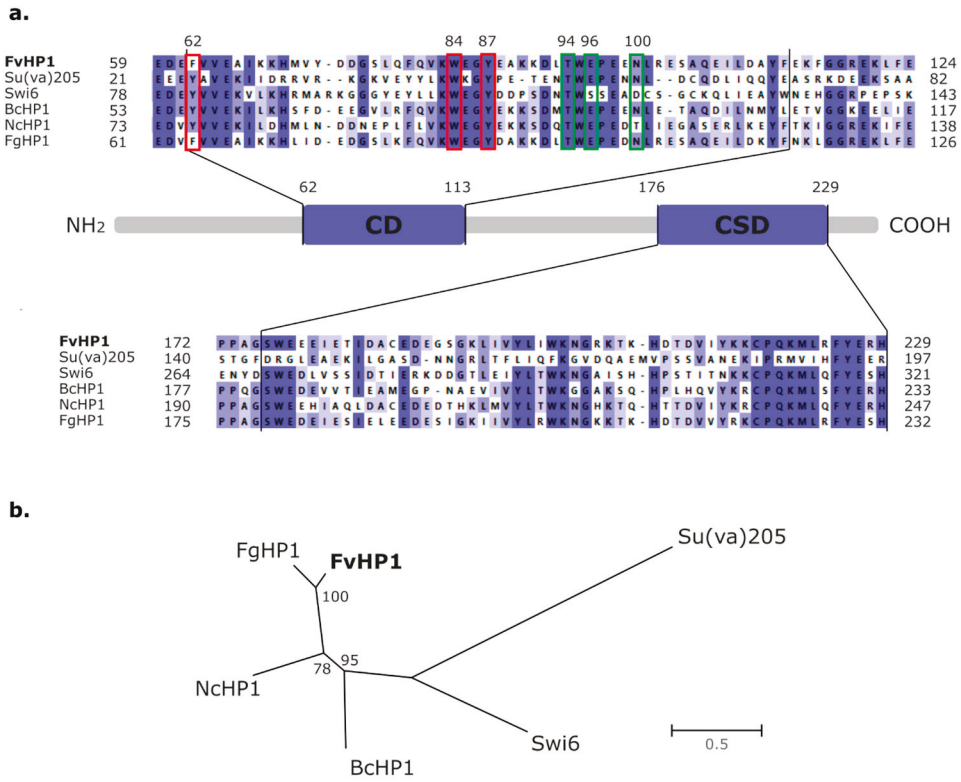


Figure 2. FvHP1 Functional-structural annotation, sequence comparison, and phylogenetic relationship. (**a**) A box diagram representing the complete amino acid sequence of the FvHP1 protein shows the CD and CSD, indicated by amino acid residue positions, along with the respective segmented PROMALS3D alignment. Color intensity indicates the percentage of identity for each site. Key sites for identifying the H3K9me2/3 histone mark are highlighted in red (aromatic) and green (non-aromatic) frames, with their corresponding amino acid residue position indicated. (**b**) Unrooted maximum likelihood phylogenetic tree of the complete aa sequence of orthologous HP1 proteins. Alignment: PROMALS3D. Best-fit amino acid substitution model: VT + F + G4. Scale bar: average number of substitutions per site.

3.2. Deletion of FvHP1 Gene Affects the Growth, Asexual Reproduction, and Pigment Production

To analyze the plausible functions of the *F. verticillioides* HP1 protein, we obtained three independent stable NTC-resistant transformants. These were single-spore sub-cultured (monosporic culture) and designated as Δ*FvHP1* #6, Δ*FvHP1* #15, and Δ*FvHP1* #17 strains (Figure 1c). An NTC-resistant transformant with a random ectopic integration of the deletion construct, referred to as the ECT strain, was included, in our experiments, as a control alongside the parental WT strain. This helped to rule out any potential effects of the *nat1* gene product or other alterations induced during the transformation process on the fungus phenotype. Interestingly, in contrast to the light-colored colonies of the WT and ECT strains, the three Δ*FvHP1* strains exhibited dark, deep red pigmentation when grown on solid media (Figure 3a). This strong pigment accumulation was also observed and measured in liquid CDB medium, as described later. These observations indicate that the FvHP1 protein participates in pigment production in *F. verticillioides*.

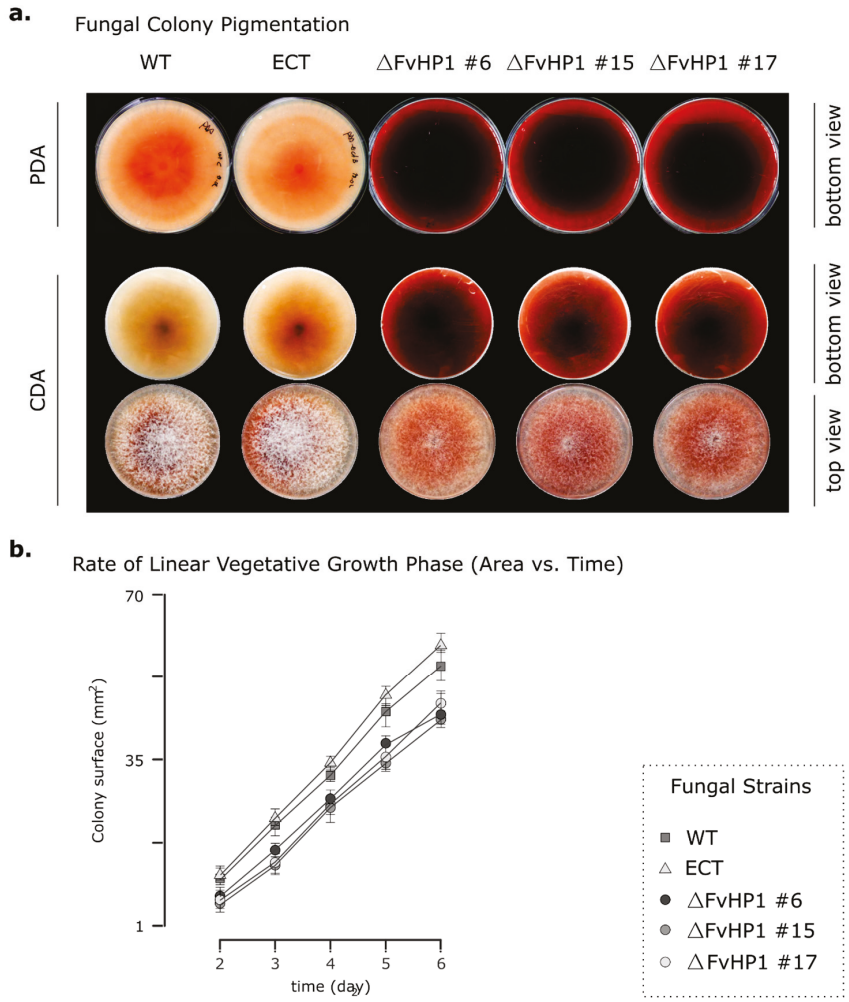


Figure 3. Effect of *FvHP1* deletion on colony pigmentation and vegetative growth. (**a**) Colony pigmentation. Photographs show bottom and top views of colonies. Strains were grown in CDA (OXOID™) and PDA (VWR Chemicals BDH®) media for 35 days in darkness at 25 °C. (**b**) Vegetative growth. Dots represent the mean area (mm^2) of *F. verticillioides* WT and mutant colonies during their linear growth state at different incubation times, from 2 to 6 days. Whiskers indicate the standard deviation. Strains were incubated on PDA in the dark at 25 ± 1 °C. Values having different letters are significantly different from each treatment according to DGC test of multiple range ($p \leq 0.05$). Experiments were performed twice with 5 replicates for each strain.

All three deletion strains exhibited a lower rate of vegetative growth compared to the WT and ECT strains (Figure 3b), suggesting that the FvHP1 protein may play a key role in vegetative behavior. For a comprehensive evaluation of the effect of *FvHP1* deletion on the colony's vegetative characteristics such as lag phase, growth rate, and conidiation, we selected one of the mutant strains, the *F. verticillioides* Δ*FvHP1* #6, for all subsequent evaluations. The lag phase of the deletion mutant was significantly longer (38 h; 95% CI 30–41) compared to that of the WT (23 h; 95% CI 15–27) and ECT (24 h; 95% CI 19–27) strains (Table 1). Besides, the growth rate of the Δ*FvHP1* #6 strain was significantly slower than that of the WT and ECT strains, with the mutation affecting the growth rate by approximately 15.9% and 11.4%, respectively. On the other hand, no significant difference in growth rate was found between the WT and ECT strains (Table 1). As expected, the extended lag phase and reduced growth rate resulted in significant differences in colony size. This difference was clearly observed at 5 days post-inoculation, showing a significant reduction in growth area compared to WT and ECT strains (25.7% and 31.7%, respectively). Additionally, the mutation had a negative effect on the production of microconidia (Table 1).

Δ*FvHP1* #6 produced significantly fewer conidia than the WT (66.7%) and ECT (55.5%) strains under conditions that stimulate conidia production. Taken together, these results indicate that FvHP1 protein plays an important role in regulating the vegetative growth of *F. verticillioides.*

Table 1. Effect of *FvHP1* gene deletion on fungal vegetative features.

Strain	Lag Phase (95% CI) [1]	Growth Rate [2]	Colony Size at 5 Days of Incubation (mm^2) [3]	Conidiation (Conidia/mL) [4]
Δ*FvHP1* #6	38 (30–41)	412 ± 7 a	1841 ± 110 a	$4 \pm 2 \times 10^7$ a
ECT	24 (19–27)	466 ± 7 b	2695 ± 104 b	$9 \pm 1 \times 10^7$ b
WT	23 (15–27)	490 ± 9 b	2477 ± 104 b	$12 \pm 1 \times 10^7$ c

[1] Time (hours) with a 95% confidence interval (CI) (lower limit—upper limit). Time was estimated from a nonlinear regression fitted to the Gompertz model (see "Materials and Methods") using colony size (area) data from 0 to 8 days of incubation (in darkness at 25 ± 1 °C) after point inoculation, at the center of a 90 × 15 Petri dish, with PDA (Britania S.A., Ciudad Autónoma de Buenos Aires, Argentina, Buenos Aires, Argentina) medium. Five cultures were made for each strain. [2] The growth rate was calculated based on the slope (mm^2/day ± standard error) derived from a linear regression during the linear growth phase. This phase encompassed the incubation period (in darkness at 25 ± 1 °C) from 2 to 6 days after point inoculation, at the center of a 90 × 15 Petri dish, with PDA (Britania S.A.) medium. [3] Colony size was recorded at the end of a 5-day incubation period (in darkness at 25 ± 1 °C) after point inoculation, at the center of a 90 × 15 Petri dish, with PDA (Britania S.A.) medium. [4] Conidia production was determined in YEPS liquid medium. Values having different letters are significantly different from each treatment according to DGC test of multiple range ($p \leq 0.05$). Data obtained from 5 independent fungal cultures.

3.3. FvHP1 Protein Is Required for Normal Fumonisin B1 Production

The effect of deleting the *FvHP1* gene on the production of fumonisin B1 (FB1) was also assessed using two different media: GYAM medium, which induces FB1synthesis, and CDB, which does not induce the synthesis of this mycotoxin. CDB medium was used to determine if *FvHP1* deletion would result in FB1 production under non-inducing conditions. At 3 days post-inoculation, all three fungal strains evaluated exhibited comparable levels of FB1 production in GYAM medium (Figure 4). However, at 7 days post-inoculation, the amount of FB1 produced by the deleted strain was significantly lower than that produced by the control strains: 3.97 ± 1.45 μg/mg compared to 8.95 ± 1.62 μg/mg (WT) and 10.80 ± 1.62 μg/mg (ECT). These results indicate a positive role for FvHP1 protein in regulating FB1 production. On the other hand, none of the evaluated strains showed FB1 production in CDB medium.

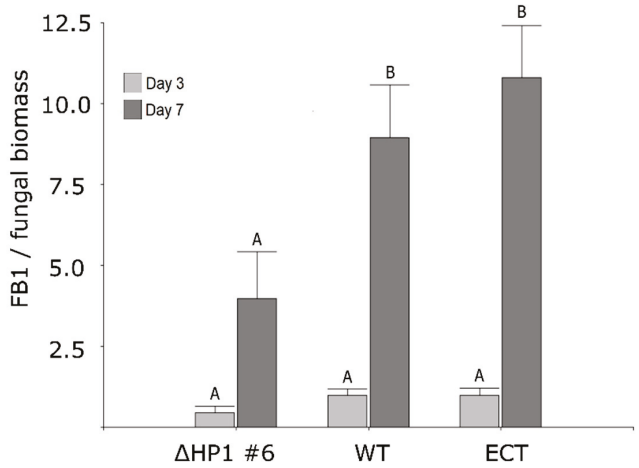


Figure 4. Effect of FvHP1 deletion on fumonisin B1production. Values are expressed as means (μg of FB1/mg of mycelium biomass), and whiskers represent the standard error. Bars with different letters are statistically different from each other according to DGC test of multiple range ($p \leq 0.05$), for the same incubation time (3 and 7 days).

3.4. FvHP1 Plays a Role in the Pathogenicity of F. verticillioides

When present in the soil or crop residues, *F. verticillioides* hyphae can colonize maize root tissues and the mesocotyl within a few days of seed germination [3]. Moreover, they can directly penetrate the grain's pericarp shortly after sowing [3,58]. Given this, we estimated the virulence of *F. verticillioides* by measuring radicle growth rate and stem growth rate under well-controlled laboratory conditions. The radicle growth rate (Figure 5a) and stem growth rate (Figure 5b) were used here as general indicators of plant health. For these experiments, maize seeds were infected by immersing them in conidia suspensions. Subsequently, one group was designated for radicle length measurements, while another group was transferred to hydroponic irrigation in a growth chamber. Additionally, we assessed the pathogenicity of the deletion mutants under other maize infection and cultivation conditions. This involved inducing an infection by directly injecting a conidial suspension into the stem of a 10-day post-planting (DPP) seedling grown in a pot. At 20 DPP, we evaluated the stem growth from the day of infection (10 days post-infection: 10 DPI) (Figure 5c) and assessed the extent of necrotic lesions on the leaves (Figure 5d).

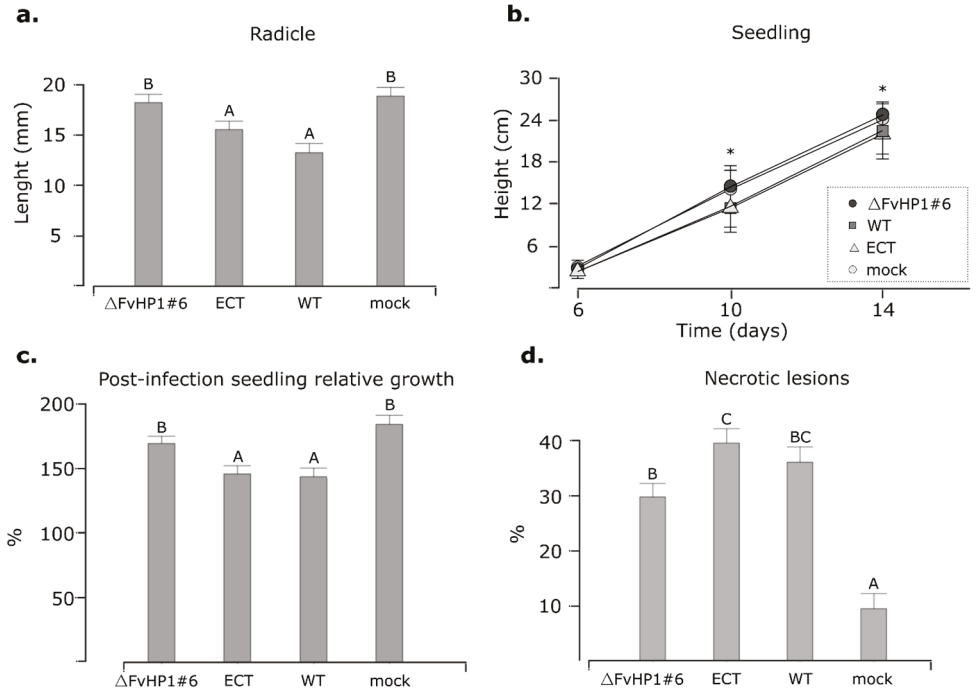


Figure 5. Effect of *FvHP1* gene deletion on F. verticillioides pathogenicity towards maize. (**a**) Radicle development assay. Corn seeds were surface-infected and incubated in a Petri dish with WA medium for 3 days, after which the radicle length was recorded. Values are expressed as mean with standard deviation (whiskers). Two experimental replicates were conducted, with 12–15 seeds per treatment in each replicate. (**b**) Hydroponic-phytotron assay (experimental schemes A): Height measurements are expressed as the mean, with whiskers indicating the standard deviation. Asterisk indicates significant differences between treatments (DMRT; $\alpha = 0.05$). The experiment was conducted once with 10–12 plants per treatment. (**c**,**d**) Greenhouse pathogenicity assay (experimental schemes B). These panels represent data from three experimental replicates and 7–14 seedlings per treatment in each replicate. The "post-infection seedling relative growth" parameter was calculated as the percentage increase in stem length at 10 DPI relative to the initial stem length (10 DPP). The "Necrotic lesions" parameter, defined as leaves with at least one coalescing and/or localized necrotic region, was assessed at 10 DPI and quantified as the percentage of leaf area with lesions per seedling (Supplementary Figure S2). In panels a, c, d, different letters among treatments indicate statistical differences according to DGC test of multiple range ($p \leq 0.05$).

The infection with the WT strain resulted in statistically significant differences in radicle growth rate, seedling growth rate in the hydroponic–phytotron assay, post-infection seedling relative growth in soil-greenhouse assays and necrotic lesions when compared to the non-infected plants (mock treatment). Consequently, these quantitative parameters were utilized to estimate the degree of pathogenicity of the mutant strains, with the WT and mock treatment serving as reference values. In panels "a", "b" and "c" of Figure 5, the results showed that deletion mutant Δ*FvHP1*#6 acquired values that resembled the mock treatment with respect to the WT and ECT infection. The similar results observed between infections with the WT strain and the ECT strain suggest that the random ectopic integration of the *nat1* gene expression cassette did not significantly modify the pathogenic behavior of the parental strain. Analyzing each experiment specifically, the Δ*FvHP1*#6 strain did not generate any significant effect on radicle growth compared to the seeds treated with sterile water. In the phytotron–hydroponic plant culture system, where seeds were superficially infected with conidia (Figure 5b), the growth of seedlings infected with the ECT and WT strains did not differ statistically from each other, but it was lower than that of seedlings infected with the deletion strain and non-infected seedlings. The differences became significantly more pronounced at 10 and 14 days post-infection (DPI). Similarly, in the greenhouse plant culture system (Figure 5, panels c and d), where the infection was generated by injecting conidia directly into the stem, a similar result was observed. The post-infection seedling relative growth generated by the deleted strain was statistically equivalent to that of non-infected plants. In the analysis of necrotic lesions, the fungal disease signature was not completely abolished in the Δ*FvHP1* #6 strain. The visible damage induced by infection with this strain was significantly higher than that observed in the uninfected control seedlings with respect to the percentage of leaves with necrotic lesions (Figure 5d). Necrotic lesions in seedlings infected with the Δ*FvHP1* #6 strain were not significantly smaller than those observed in seedlings infected with WT and ECT strains. The results of the pathogenicity assays suggest that the putative FvHP1 protein is associated with the pathogenic development of *F. verticillioides* in maize; however, its involvement is not entirely determinative of virulent behavior.

3.5. FvHP1 Is a Negative Regulator of Naphthoquinone Pigment Synthesis in F. verticillioides

The pigmentation observed in cultures of the deleted strain was analyzed. Out of 44 total metabolites present in both the Δ*FvHP1* #6 strain and ECT strain culture medium (CDB), 29 exhibited significant differences in concentration. A multivariate OPLS-DA analysis was conducted to identify the most important metabolites differentiating the profiles of the two strains. The scores plot (Figure 6) shows clear discrimination between the samples being evaluated. The validation parameters demonstrated that a satisfactory model was obtained, with R2Y and Q2 values of 0.987 and 0.983, respectively (Figure S3B). R2Y and Q2 parameters greater than 0.5 and close to 1 reveal the strong correlation (R2Y) and predictive power (Q2) of the model for discriminating fungal samples [59]. To ensure that the difference explained by the OPLS-DA model was the result of a real effect caused by the defining factor, rather than a random effect, a permutation test using 2000 permutations was performed (Figure S3C). The test demonstrated that the model was not statistically different from any of the permuted models ($p < 0.05$), indicating no overfitting of the data. In addition, the areas under the curve (AUC) of the receiver operating characteristic (ROC) curve were used to evaluate the overall predictive power of the OPLS-DA models (Figure S3D). Significantly high AUC values (AUC = 1) were obtained, validating the predictive power of the OPLS-DA.

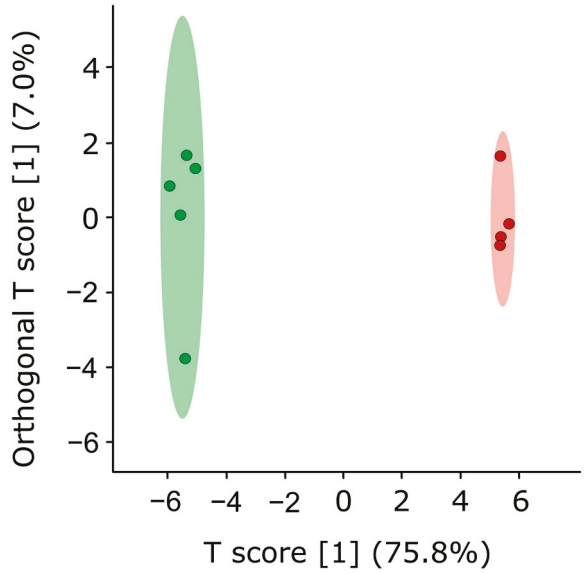


Figure 6. OPLS-DA Scores plot. This Orthogonal Partial Least Squares Discriminant Analysis (OPLS-DA) scores plot discriminates between the metabolite profiles of fungal strains. Samples were normalized by sum and Pareto scaled. Green and red dots indicate samples from ECT and Δ*FvHP1* #6 strains, respectively.

According to the OPLS-DA analysis, twenty metabolites showed a VIP value greater than 1 (Figure S3E). Then, an S-Plot analysis was used to identify metabolites that were statistically significant and potentially biologically relevant, considering their contributions to the model and their reliability. In total, six metabolites were highlighted in the S-Plot (Figure S3F). Finally, both univariate (Volcano Plot) and multivariate (VIP and S-Plot) metrics were considered to identify the most significant metabolites for discriminating between extracts of Δ*FvHP1* #6 and ECT strains. A total of 5 metabolites were selected: V3, V8, V16, V24, and V29. Four of them were produced at significantly higher levels in the deleted mutant compared to the ECT strain, while one metabolite showed decreased production in the deletion mutant (Figure S4). The selected compounds were tentatively identified based on their exact mass, isotope patterns, mass fragmentation patterns, UV–Vis spectra, and information from literature and online databases (Table 2).

Metabolite V3 showed a precursor ion at m/z 421.1085 [M + H]+. This compound was assigned to level IV of identification [60] as it is an unknown metabolite not previously reported in the literature. Its UV spectrum (Figure S5) showed absorption maximums at 227 and 271 nm, and its isotopic profile indicated the presence of a Zn atom. The molecular formula of this compound is $C_{20}H_{24}N_2O_4Zn$. The MS/MS spectrum showed a first fragment at m/z 377.12 [M+ H − 44]+ corresponding to the loss of CO_2. The next fragment at m/z 351.13 [M + H − 70]+ indicated the loss of CO_2 + C_2H_2.

Metabolite V8 was assigned to level II of identification (Figure S6). This compound showed a UV-Vis spectrum with maximums at 253, 318, and, 444 nm, and a precursor ion at m/z 319.0797 [M + H]+. Its isotopic profile and mass exact allowed identifying its molecular formula ($C_{16}H_{16}O_7$). The MS/MS spectrum shows a first fragment at m/z 301.07 [M + H − 18]+ (loss of H_2O) and a second fragment at m/z 286.04 [M + H − 33]+ (loss of H_2O + CH_3•). Besides, fragments at m/z 304.05 ([M + H − CH_3•]+), 289.03 ([M + H − CH_3• − CH_3•]+) and 272.06 ([M + H − H_2 − HO• − CO]+) were also registered. A similar metabolite was reported by Studt et al. [13] in *F. fujikuroi*. Thus, this metabolite was tentatively identified as 8-O-Methylnectriafurone.

Table 2. Metabolite identification.

Metabolite	RT [1] (min)	Experimental [2] [M + H]+ *m*/*z*	Calculated [3] [M + H]+ *m*/*z*	Tentative M. Formula	Δm [4] (ppm)	# Sigma [5]	MS Fragmentation (Intensity) [6]	MS2 Fragmentation (Intensity) [7]	l (nm) [8]	Putative Compound	MSI [9]
V3	8.18	421.1085	421.1071	C20H24N2O4Zr	3.7	5.5	421 (16); 377 (25); 351 (100); 260 (20); 242 (6)		224; 271		IV
V8	9.80	319.0797	319.0812	C16H14O7	4.7	4.6	319 (42); 304 (41); 301 (100); 289 (36); 286 (81); 273 (35); 272 (53); 261 (19); 258 (25); 257 (35); 249 (14); 243 (40); 229 (10)	301 → 303 (52); 289 (18); 288 (70); 273 (100); 270 (13); 261 (48); 260 (26); 259 (41); 245 (56); 246 (33); 243 (7); 233 (37); 229 (11)	224; 258sh; 304; 444	8-O-Methylnectriafurone	II
V16	11.08	301.0699	301.0707	C16H12O6	2.7	66.4	303 (7); 301 (5); 289 (14); 288 (100); 287 (17); 273 (72); 257 (11); 245 (23); 243 (9); 229 (6)	303 → 303 (62); 289 (15); 288 (80); 273 (100); 261 (38); 260 (35); 259 (61); 246 (25); 245 (42); 233 (46) 288 -> 289 (35); 288 (13); 274 (89); 271 (51); 256 (33); 247 (93); 246 (91); 245 (32); 244 (44); 243 (100); 233 (34); 231 (66); 229 (70)	268; 344; 506	Naphthoquinone	III
V24	12.00	436.1012	436.1013	C23H17NO8	3.6	2.6	436 (100); 421 (49); 420 (33); 408 (12); 403 (10); 393 (39); 379 (13); 375 (48); 358 (6); 347 (11); 330 (11); 304 (19); 286 (41); 258 (8)		223		IV

Table 2. *Cont.*

Metabolite	RT [1] (min)	Experimental [2] [M + H]+ *m*/*z*	Calculated [3] [M + H]+ *m*/*z*	Tentative M. Formula	Δm [4] (ppm)	# Sigma [5]	MS Fragmentation (Intensity) [6]	MS2 Fragmentation (Intensity) [7]	l (nm) [8]	Putative Compound	MSI [9]
V29	13.57	301.0705	301.0707	C16H12O6	0.4	16.3	301 (22); 303 (10); 288 (100); 286 (23); 273 (71); 272 (40); 258 (36); 257 (93); 245 (21); 243 (96); 242 (32); 229 (45)		265; 344; 514	Naphthoquinone	III

[1] RT: retention time, [2] Experimental [M + H]+ m/: Experimental mass of the protonated molecular ion, [3] Calculated [M + H]+ *m*/*z*: Calculated mass of the protonated molecular ion, [4] Δm: Mass deviation (ppm), difference between the experimental mass and the theoretical mass, expressed in parts per million (ppm). [5] # Sigma: It represents the deviation of the experimental mass from the theoretical mass in terms of standard deviations (σ). [6] MS fragmentation (intensity): Relationship between the ion fragments generated during analysis and the intensity of their signals in the mass spectrum. Energy of fragmentation equal to 15 eV except metabolite V24 (20 eV). [7] MS2 fragmentation (intensity): Ion fragments generated in the second stage of tandem mass spectrometry (MS/MS or MS^2). [8] l (nm): Wavelength of maximum absorption (nm). [9] MSI: Mass Spectrometry Imaging identification level.

Metabolites V16 and V29 showed a similar precursor ion at *m*/*z* 301.070 ([M + H]+) and a similar UV-Vis spectrum (Figures S7 and S8). Their isotopic profiles and mass exact indicated a molecular formula of $C_{16}H_{12}O_6$. These metabolites also showed a similar fragmentation pattern, with fragments at *m*/*z* 288.060 ([M + 3H − CH_3•]+), 273.037 ([M + H − C_2H_4]+), 257.043 ([M + H − C_2H_4 − C_2H_4]+), 245.041 ([M + H − C_2H_4 − CO]+), 243.061 ([M + 3H − CH_3CO_2H]+), and 229.047 ([M + 3H − CH_3CO_2H − CH_2]+). These fragments were also observed in the MS2 spectrum (*m*/*z* 301.070) of the metabolite V8 (Figure S6), suggesting that metabolites V16 and V29 could be isomers of this fragment. Both V16 and V29 were assigned to level III of identification, belonging to the naphthoquinones family.

Finally, metabolite V24 showed a precursor ion at *m*/*z* 436.1012 [M + H]+. This compound was assigned to level IV of identification. Its UV spectrum (Figure S9) showed maximum absorption at 223 nm, and its isotopic profile and mass exact indicated the molecular formula $C_{23}H_{17}NO_8$. MS/MS spectrum showed a first fragment at *m*/*z* 421.075 [M + H − CH_3•] + and a second fragment at 408.101 [M + H − CO] +. Fragments at *m*/*z* 393.080 ([M + H − CH_3• − CO] +) and 375.070 ([M + H − CH_3• − CO − H_2O]+) were also observed. In total, five metabolites (V3, V8, V16, V24, and V29) are reported for the first time for *F. verticillioides* in this work. Three of them are naphthoquinone pigments produced at high levels by the Δ*FvHP1* #6 strain.

4. Discussion

The histone code, which involves the reversible acetylation, methylation, ubiquitination, and phosphorylation patterns on the N-terminal tails and globular domains of histones H2B, H3, and H4, influences the dynamics between heterochromatin and euchromatin, consequently affecting various cellular functions [22]. In fungi, methylation and acetylation patterns on lysine 9 of the N-terminal tail of H3 histone (H3K9) are one of the most extensively studied epigenetic marks within the histone code [16]. A histone methyltransferase (HMT) catalyzes the specific di-/tri-methylation (me2/3) of H3K9. This specific H3K9 me2/3 modification binds to an HP1 protein, resulting in a non-covalent

H3K9me2/3-HP1 interaction. This event triggers a cascade of changes in the conformation of the heterochromatin state [24,25]. In this context, an H3K9 HMT, named FvDim5, was characterized in *F. verticillioides* [32]. However, to the best of our knowledge, no putative HP1 protein has been characterized in this species until now. In this study, we identified the protein sequence registered under the NCBI-RefSeq accession number XP_018744916.1, encoded by the annotated gene FVEG_01876, as a putative HP1 protein in *F. verticillioides*. We refer to this as the FvHP1 protein (Figure 7), and our phylogenetic evidence suggests it is an orthologous protein to the HP1 of *F. graminearum*. The aa sequence of FvHP1 shows a high similarity with the two typical domains shared by all members of the HP1 family: the CD and CSD protein motifs. Moreover, their aa sequence contains the conserved sites most significant for recognizing the H3K9me2/3 histone epigenetic mark, as reported by Nielsen et al. [57]. That is, the FvHP1 CD domain has three aa residues in homologous sites to *Mus musculus* (Mm) HP1b protein (Y21, W42, and F45), which are necessary to maintain the hydrophobic pocket structure for recognizing H3K9me2/3. The W residue at position 84 aa of FvHP1 is conserved with respect to the homologous MmHP1b W42 site, a site that does not permit point substitution to preserve CD functionality [57]. However, two point mutations were recorded at the other two essential sites for CD functionality. Specifically, the FvHP1 protein has two amino acid substitutions at the homologous Y21 and F45 sites of MmHP1b: Y62F and F87Y mutations in FvHP1 (see Supplemental Figure S1). These substitutions, Y by F and vice versa (both amino acid residues with a hydrophobic aromatic ring), presumably do not significantly affect CD domain activity as they do not alter the properties of the hydrophobic pocket, according to Nielsen et al. [57]. Thus, Y62F and F87Y are evolutionarily admissible point substitutions. Moreover, three other side-chain amino acids essential for interacting with H3K9me2/3, namely T51, E53, and N57 in MmHP1b protein [57], are also found at homologous sites on the FvHP1 protein (T94, E96, and N100, respectively; see Supplemental Figure S1). On the other hand, our phylogenetic reconstruction indicated that the predicted FvHP1 protein shares a recent common ancestor with FgHP1 protein, the HP1 family member encoded by *F. graminearum*. This result is consistent with the close evolutionary relationship of these fungal species [61,62]. Our analyses, based on sequence similarity and phylogenetic reconstruction, strongly suggest that FvHP1 is a putative protein belonging to the HP1 family and is orthologous to the HP1 protein of *F. graminearum*. This report provides the first characterization of a member of the HP1 family in *F. verticillioides*.

The sequence analysis performed in the present study shows that FvHP1 retains the aa residues necessary to ensure CD functionality, at least for recognizing histones epigenetic marks. However, its specific role in *F. verticillioides* metabolism needs to be elucidated. While a basal function can be attributed to all members of the protein family, HP1 appears to have a species-specific role that depends on the molecular environment at the chromosomal level [24,28,63], a phenomenon reflected across different fungal species. We found that deleting the *FvHP1* gene impairs the vegetative growth of the fungus and its clonal reproduction, specifically the production of microconidia. This is in agreement with what was reported by Freitag et al. [56], who demonstrated a similar role for HP1 in the vegetative growth of *Neurospora crassa*. Furthermore, our results are consistent with those obtained by Gu et al. [32], which showed that the KHMTase FvDim5, responsible for methylating the K9 residues in histone 3 (allowing the FvHP1 protein to recognize the epigenetic mark), plays a role in normal vegetative growth and microconidia production in *F. verticillioides* [32]. In contrast, only a slight reduction in radial growth was observed when the HP1 encoded gene was deleted in *Epichloë festucae* [64], and no defect in vegetative growth was discernible in HP1 deletion mutants in *F. graminearun* [35], *Aspergillus nidulans* [34], and *Botrytis cinerea* [55]. The reduced vegetative behavior was accompanied by a decrease

in the fungal virulence of *F. verticillioides* in its natural host. All quantitative infection signs evaluated in our study (root and stem growth, and leaf lesions) indicated that pathogenic behavior appears to be impaired with the deletion of the *FvHP1* gene. In agreement with this result, it was determined that the normal expression of the *FvDim5* gene is necessary to maintain the pathogenic behavior of *F. verticillioides* [32]. Our experimental approaches allowed us to evaluate the natural colonization capability of fungi on maize tissues. The radicle length assay and stem growth rate under phytotron-hydroponic conditions were conducted to simulate fungal infection by allowing microconidia to adhere to the kernel surface. The germination of the conidia likely occurred outside the plant tissues, with hyphae colonizing interstitial and cellular spaces and breaking physical plant barriers to initiate a systemic infection. In the greenhouse assay, we focused on the infection caused by the massive germination of conidia within the plant tissues. Here, infection was facilitated because the hyphae did not have to penetrate the cuticles and plant epidermises. Both infection strategies resulted in significantly reduced pathogenic behavior. This likely stems from the impaired vegetative growth and reduced microconidia production. The ability of *F. verticillioides* to behave as an endophyte or pathogen/parasite depends on its growth mode in the host, which in turn depends on the genotype of both the specimens and the environment [3,58,65].

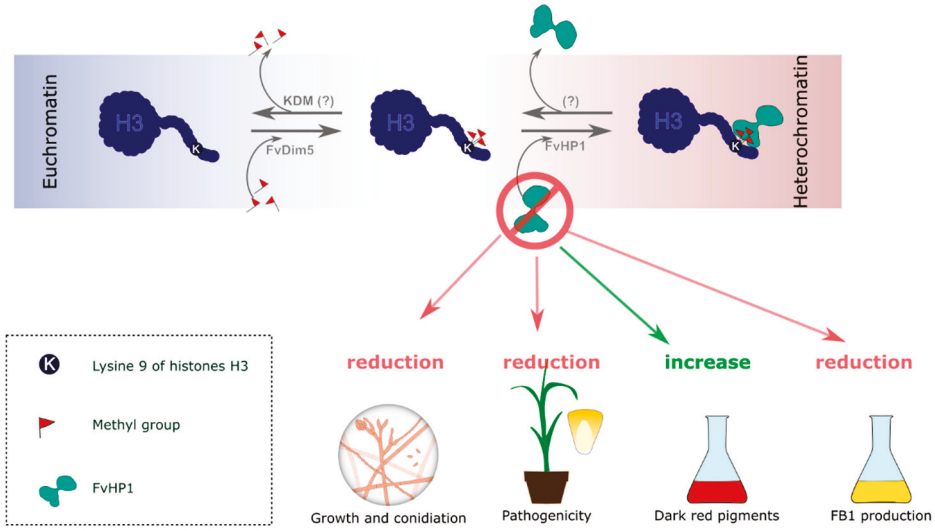


Figure 7. Schematic representation of the role of putative FvHP1 in heterochromatin formation and the biological effects of its absence. In the euchromatin state, the di- and tri-methylation of the deacetylated K9 of histone H3 is catalyzed by the specific methyltransferase FvDim5. This epigenetic mark is recognized by the putative FvHP1 protein, which contributes to chromatin compaction. The deletion of *FvHP1* negatively affects vegetative growth, conidiation, virulence, and FB1 production, while simultaneously increasing the accumulation of dark red pigments.

Mycotoxins are regarded as species-specific FSM and their role in pathogenic behavior has been previously established in *F. verticillioides* through the production of fumonisins, with FB1 being a key factor involved in its pathogenicity [66–69]. We investigated the effect of deleting the *FvHP1* gene on FB1 production. As expected, the deleted strain showed no FB1 production under non-FB1-inductive conditions (CDB medium), but reduced production was observed under FB1-inductive conditions (GYAM medium). Visentin et al. [70] revealed that histone acetylation acts as a positive regulator of the *FUM1* and *FUM21* genes by utilizing a standard histone deacetylase inhibitor (trichostatin A, TSA) in the fungus cultured on CDB medium. It is pertinent to remember that a hyperacetylated state of chromatin is related to its euchromatin form (non-compact and transcriptionally active chromatin). However, no increase in FB1 production was recorded since the *FUM8*

gene, which encodes an aminotransferase required to form the biologically active FB1, was downregulated under TSA treatment [70]. The non-production of FB1 measured in CDB medium in both experimental studies (ours and 65) suggests that FB1 BGC is under another regulatory mechanism and the chromatin state is of secondary relevance in this specific non-inducing condition. Other regulatory mechanisms could be involved, such as the broad-domain transcription factor PAC1, which is implicated in the repression of FB1 synthesis under alkaline conditions like CDB medium [71]. On the other hand, the results obtained under FB1-inducing medium demonstrated that the deletion of FvHP1 had a negative effect on FB1 production. This effect was unexpected because the presumed chromatin state in our deleted fungus would be lax and transcriptionally active. This result, however, is in line with the decrease in virulence observed in mutant *F. verticillioides*. Corn tissues create a conducive environment for hyphal growth and promote the production of fumonisins, similar to the GYAM medium (in vitro method). Therefore, despite the lack of quantification of FB1 in plant tissue (no assay performed), it is known that FB1 is produced by *F. verticillioides* whether it behaves as a parasite or endophyte [58].

In contrast to our findings, Gu et al. [32] demonstrated that the deletion of *FvDim5* had a positive effect on FB1 production in maize kernels. However, this discrepancy could be due to the fact that FB1 evaluation was performed under different environmental conditions (GYAM medium and maize kernels). To assess the impact of *FvHP1* deletion on the chromatin conformation and methylation level near the promoters of genes in the FB1 BGC, a chromatin immunoprecipitation assay should be conducted. Nevertheless, we preliminarily demonstrate that the production of FB1 is partially regulated by FvHP1, which aligns with the previously mentioned decrease in virulence. To fully understand the regulation of FB1 biosynthesis, it is essential to conduct an in-depth study of the interactions between specific and broad-domain transcription factors, as well as the acetylation and methylation patterns of the K9 residue on the H3 protein. Ultimately, our results achieve the goal of phenotypically characterizing the absence of the *FvHP1* gene and assessing the functionality of the FvHP1 protein at the organismal level in *F. verticillioides*, particularly concerning FB1 biosynthesis.

The intense red pigmentation observed in Δ*FvHP1* strains suggested that the synthesis of certain secondary metabolites in *F. verticillioides* might be regulated by conformational/condensation state of the chromatin. It is necessary to emphasize that the BGC responsible for producing these deep red pigments appears to be primarily regulated by the chromatin conformation, unlike the cluster responsible for synthesizing FB1. The role of reversible histone modifications affecting chromatin structure in the regulation of the synthesis of various FSMs, such as fungal pigments, has been demonstrated in other fungal species [35]. To date, two different types of pigments have been reported in *F. verticillioides*: bikaverin and the uncharacterized fusarubin-type naphthoquinones associated with perithecium dark pigmentation [11,13] Here, we delved deeper into elucidating the chemical nature of these red pigments. In total, we found that three naphthoquinone-like pigments were highly accumulated in *F. verticillioides* Δ*FvHP1* grown in CDB medium. On the other hand, bikaverin was not detected under these growth conditions. This is not surprising because CDB is an alkaline medium, and bikaverin biosynthesis is known to be repressed in alkaline conditions by the regulatory factor PAC1 [72,73]. Analysis of the accurate m/z ratio (mass error ≤ 5 ppm), fragmentation pattern, and absorption spectra of the three metabolites enabled us to identify 8-O-methylnectriafurone as one of the pigments highly accumulated in the Δ*FvHP1* strain. Although the other two naphthoquinone-like metabolites that highly accumulated in the *FvHP1* gene deletion mutant could not be fully identified, their accurate m/z ratio and fragmentation patterns were similar to that of 8-O-methylnectriafurone. These results suggest that they are structurally related to 8-O-

methylnectriafurone. Prior to the present report, the production of 8-O-methylnectriafurone by *F. verticillioides* had not been documented, to the best of our knowledge. However, this metabolite was previously found to be a component of pigments in the perithecium of *F. fujikuroi* [13]. In this work, we provide the first evidence regarding the chemical structure of the perithecium dark pigments in *F. verticillioides*.

The perithecium pigments of *F. fujikuroi* and *F. graminearum* are different. They belong to the chemical family of fusarubins and bostrycoidins, respectively. The similarity between the chemical structures of the perithecium pigments found in this study and those reported for *F. fujikuroi* suggests that the perithecium pigments in *F. verticillioides* are fusarubins and originate from the seven-member gene cluster named PGL1. Bioinformatic studies using genomic data could further support this hypothesis. Sequence alignment by Frandsen et al. [74] showed that the putative PGL1 BGC of *F. verticillioides* exhibited high similarity to those of *F. fujikuroi* and *F. graminearum*. Specifically, a synteny region exists in the PGL1 BGCs of *F. verticillioides* and *F. fujikuroi,* where the six homologous core genes of the cluster conserve both their relative positions and orientations in the two species [74]. One of these core genes, *PGL1*, encodes a seven-domain non-reducing polyketide synthase (NR-PKS) highly conserved in *F. verticillioides* and *F. fujikuroi* [13]. These NR-PKSs are predicted to form a fusarubin-type naphthoquinone structure by condensing seven acetyl-CoA units, which constitutes the chemical backbone of 8-*O*-methylnectriafurone [11,13]. On the other hand, in *F. graminearum*, there is an extra gene in its PGL1 BGC, the *PglL* gene, which is absent from the homologous region in the *F. fujikuroi* and *F. verticillioides* PGL BGCs [74]. Consequently, in the case of *F. graminearum,* the intermediate metabolite produced by the NR-PKS of the PGL BGC, 6-O-demethylfusarubinaldehyde, undergoes different secondary chemical modifications, leading to the formation of bostrycoidins instead of fusarubin structures.

Finally, although the chemical structure of the perithecium pigments of *F. verticillioides* has not been completely determined, our identification of 8-O-methylnectriafurone and related chemical compounds, combined with evidence from bioinformatic studies using genomic data from evolutionarily related species, provides sufficient evidence to propose their origin in the fusarubin chemical pathway coded by the PGL1 BGC. This pathway appears to be regulated by the FvHP1-mediated conformational state of the chromatin. The PGL1 BGC of *F. verticillioides* is located sub-telomerically, meaning it is expected to be transcriptionally repressed by facultative heterochromatin during the vegetative state. The identification of these pigments as highly accumulated in the Δ*FvHP1* strain provides evidence to support the hypothesis that in *F. verticillioides,* the PGL1 BGC is repressed during vegetative growth through the formation of facultative heterochromatin mediated by FvHP1 activity. In agreement with our results, a previous study reported by Reyes-Dominguez et al. [35] demonstrated the involvement of FgHP1 in the negative regulation of aurofusarin biosynthesis by *F. graminearum.*

Given that in other fungal species these pigments, fusarubin-type naphthoquinones, including 8-O-methylnectriafurone, have been associated with perithecium pigmentation [13,74] and the protection of ascospores (inside the perithecium) from ultraviolet light and the reactive oxygen species [75], the involvement of FvHP1 in regulating these fusarubins metabolites found in our work suggests that changes in chromatin conformation could play a role in regulating the sexual state in *F. verticillioides* (or *Gibberella fujikuroi* MP A, its teleomorph state). This hypothesis aligns with the findings of Cam et al. [14], who discovered that proteins homologous to HP1 are strongly associated with mating in *Schizosaccharomyces pombe*. Additionally, this corresponds with the observation that these pigments not only color the perithecia but are also believed to play a role in maintaining the structural integrity of perithecia in *F. fujikuroi* [13]. Furthermore, this is in agreement

with the findings reported by Gu et al. [32], who showed that the *FvDim5* deletion mutant exhibited a lack of perithecial formation in *Gibberella fujikuroi* MP A. To our knowledge, the finding of 8-O-methylnectriafurone red pigment production by *F. verticillioides* reported in the present paper represents the first characterization of perithecial pigments in this fungal species. Although it is not directly shown to be part of perithecia, there is sufficient evidence to strongly support this hypothesis. Experiments on the role of HP1 in perithecia pigmentation are currently being conducted.

In several organisms, including fungi, certain epigenetic marks are inherited during mitotic and meiotic cell division, allowing specific gene expression states to remain stable across successive cell generations [76–80]. This phenomenon is not implausible and merits further investigation, particularly in the context of chromatin compaction states in filamentous fungi.

Supplementary Materials: The following supporting information can be downloaded at: https://www.mdpi.com/article/10.3390/jof11060424/s1, Figure S1: Chromo domain sequences pair alignment (NCBI MSA Viewer v1.20.1) of FvHP1 (this study) and mouse HP1β (also known as MOD1 or M31). Figure S2: Signs of necrosis on a maize seedling leaf. Figure S3: Orthogonal Partial Least Squares Discriminant Analysis (OPLS-DA) to discriminate metabolite fungal strain. Figure S4: Box Plot of the most important metabolites to discriminate between ΔFvHP1 and FvECT strains. Figure S5: UV-Vis, MS, and MSMS spectrums of Metabolite V3. Figure S6: UV-Vis, MS and MSMS spectrums of Metabolite V8. MS 2 spectrums were also included. Figure S7: UV-Vis, MS, and MSMS spectrums of Metabolite V16. Figure S8: UV-Vis, MS, and MSMS spectrums of Metabolite V24. Figure S9: UV-Vis, MS, and MSMS spectrums of Metabolite V29.

Author Contributions: M.D.G.-P. and J.S.D. conceived and designed the experiments and, with the collaboration of A.G.J. and M.C.C. performed the production of deletion mutants. A.G.J. and M.G.T. performed the bioinformatic analyses. A.G.J. and V.A.A. performed the mycotoxins quantification. N.S.P. performed the secondary metabolites identification. A.G.J., P.A.V. and M.G.T. performed the pathogenicity assays. M.D.G.-P., J.S.D. and A.G.J. analyzed the data. M.D.G.-P., J.S.D., A.G.J. and M.G.T. wrote the paper. All authors have read and agreed to the published version of the manuscript.

Funding: Grant PID2022-143320OB-I00, Ministry of Science, Innovation and Universities, State Research Agency (MCIN/AEI/10.13039/501100011033), Spain, Grant PICT2019-03300, National Agency for Scientific and Technological Promotion, Argentina, and Grant 33620230100243CB, Secretariat of Science and Technology (SECyT-UNC), Argentina.

Institutional Review Board Statement: Not applicable.

Informed Consent Statement: Not applicable.

Data Availability Statement: The original contributions presented in this study are included in the article/Supplementary Material. Further inquiries can be directed to the corresponding authors.

Acknowledgments: JS Dambolena, MG Theumer, NS Podio and VA Areco are Career Members of CONICET. AG Jacquat has a fellowship from CONICET. MD García-Pedrajas is a Career Member of CSIC. Cañizares MC research contract was funded through Grant PID2022-143320OB-I00.

Conflicts of Interest: The authors declare no conflict of interest.

References

1. Blacutt, A.A.; Gold, S.E.; Voss, K.A.; Gao, M.; Glenn, A.E. *Fusarium verticillioides*: Advancements in Understanding the Toxicity, Virulence, and Niche Adaptations of a Model Mycotoxigenic Pathogen of Maize. *Phytopathology* **2018**, *108*, 312–326. [CrossRef] [PubMed]
2. Bacon, C.W.; Hinton, D.M. Symptomless Endophytic Colonization of Maize by *Fusarium moniliforme*. *Can. J. Bot.* **1996**, *74*, 1195–1202. [CrossRef]
3. Oren, L.; Ezrati, S.; Cohen, D.; Sharon, A. Early Events in the *Fusarium verticillioides*—Maize Interaction Characterized by Using a Green Fluorescent Protein-Expressing Transgenic Isolate. *Appl. Environ. Microbiol.* **2003**, *69*, 1695–1701. [CrossRef]

4. Oldenburg, E.; Höppner, F.; Ellner, F.; Weinert, J. Fusarium Diseases of Maize Associated with Mycotoxin Contamination of Agricultural Products Intended to Be Used for Food and Feed. *Mycotoxin Res.* **2017**, *33*, 167–182. [CrossRef]
5. Gai, X.; Dong, H.; Wang, S.; Liu, B.; Zhang, Z.; Li, X.; Gao, Z. Infection Cycle of Maize Stalk Rot and Ear Rot Caused by *Fusarium verticillioides*. *PLoS ONE* **2018**, *13*, e0201588. [CrossRef]
6. Glenn, A.E. Mycotoxigenic *Fusarium* Species in Animal Feed. *Anim. Feed Sci. Technol.* **2007**, *137*, 213–240. [CrossRef]
7. Presello, D.A.; Botta, G.; Iglesias, J.; Eyhérabide, G.H. Effect of Disease Severity on Yield and Grain Fumonisin Concentration of Maize Hybrids Inoculated with *Fusarium verticillioides*. *Crop Prot.* **2008**, *27*, 572–576. [CrossRef]
8. Braun, M.S.; Wink, M. Exposure, Occurrence, and Chemistry of Fumonisins and Their Cryptic Derivatives. *Comp. Rev. Food Sci. Food Safe* **2018**, *17*, 769–791. [CrossRef] [PubMed]
9. Kamle, M.; Mahato, D.K.; Devi, S.; Lee, K.E.; Kang, S.G.; Kumar, P. Fumonisins: Impact on Agriculture, Food, and Human Health and Their Management Strategies. *Toxins* **2019**, *11*, 328. [CrossRef]
10. Nelson, P.E.; Plattner, R.D.; Shackelford, D.D.; Desjardins, A.E. Production of Fumonisins by *Fusarium moniliforme* Strains from Various Substrates and Geographic Areas. *Appl. Environ. Microbiol.* **1991**, *57*, 2410–2412. [CrossRef]
11. Brown, D.W.; Butchko, R.A.E.; Busman, M.; Proctor, R.H. Identification of Gene Clusters Associated with Fusaric Acid, Fusarin, and Perithecial Pigment Production in *Fusarium verticillioides*. *Fungal Genet. Biol.* **2012**, *49*, 521–532. [CrossRef] [PubMed]
12. Achimón, F.; Krapacher, C.R.; Jacquat, A.G.; Pizzolitto, R.P.; Zygadlo, J.A. Carbon Sources to Enhance the Biosynthesis of Useful Secondary Metabolites in *Fusarium verticillioides* Submerged Cultures. *World J. Microbiol. Biotechnol.* **2021**, *37*, 78. [CrossRef] [PubMed]
13. Studt, L.; Wiemann, P.; Kleigrewe, K.; Humpf, H.-U.; Tudzynski, B. Biosynthesis of Fusarubins Accounts for Pigmentation of *Fusarium fujikuroi* Perithecia. *Appl. Environ. Microbiol.* **2012**, *78*, 4468–4480. [CrossRef]
14. Cam, H.P.; Sugiyama, T.; Chen, E.S.; Chen, X.; FitzGerald, P.C.; Grewal, S.I.S. Comprehensive Analysis of Heterochromatin- and RNAi-Mediated Epigenetic Control of the Fission Yeast Genome. *Nat. Genet.* **2005**, *37*, 809–819. [CrossRef]
15. Palmer, J.M.; Keller, N.P. Secondary Metabolism in Fungi: Does Chromosomal Location Matter? *Curr. Opin. Microbiol.* **2010**, *13*, 431–436. [CrossRef] [PubMed]
16. Strauss, J.; Reyes-Dominguez, Y. Regulation of Secondary Metabolism by Chromatin Structure and Epigenetic Codes. *Fungal Genet. Biol.* **2011**, *48*, 62–69. [CrossRef]
17. Khaldi, N.; Collemare, J.; Lebrun, M.-H.; Wolfe, K.H. Evidence for Horizontal Transfer of a Secondary Metabolite Gene Cluster between Fungi. *Genome Biol.* **2008**, *9*, R18. [CrossRef]
18. Tralamazza, S.M.; Rocha, L.O.; Oggenfuss, U.; Corrêa, B.; Croll, D. Complex Evolutionary Origins of Specialized Metabolite Gene Cluster Diversity among the Plant Pathogenic Fungi of the *Fusarium graminearum* Species Complex. *Genome Biol. Evol.* **2019**, *11*, 3106–3122. [CrossRef]
19. Proctor, R.H.; Brown, D.W.; Plattner, R.D.; Desjardins, A.E. Co-Expression of 15 Contiguous Genes Delineates a Fumonisin Biosynthetic Gene Cluster in Gibberella Moniliformis. *Fungal Genet. Biol.* **2003**, *38*, 237–249. [CrossRef]
20. Yu, J.-H.; Keller, N. Regulation of Secondary Metabolism in Filamentous Fungi. *Annu. Rev. Phytopathol.* **2005**, *43*, 437–458. [CrossRef]
21. Grewal, S.I.S.; Jia, S. Heterochromatin Revisited. *Nat. Rev. Genet.* **2007**, *8*, 35–46. [CrossRef] [PubMed]
22. Strahl, B.D.; Allis, C.D. The Language of Covalent Histone Modifications. *Nature* **2000**, *403*, 41–45. [CrossRef] [PubMed]
23. O'Kane, C.J.; Hyland, E.M. Yeast Epigenetics: The Inheritance of Histone Modification States. *Biosci. Rep.* **2019**, *39*, BSR20182006. [CrossRef]
24. Eissenberg, J.C.; Elgin, S.C.R. HP1a: A Structural Chromosomal Protein Regulating Transcription. *Trends Genet.* **2014**, *30*, 103–110. [CrossRef] [PubMed]
25. Machida, S.; Takizawa, Y.; Ishimaru, M.; Sugita, Y.; Sekine, S.; Nakayama, J.; Wolf, M.; Kurumizaka, H. Structural Basis of Heterochromatin Formation by Human HP1. *Mol. Cell* **2018**, *69*, 385–397.e8. [CrossRef]
26. Eissenberg, J.C.; Elgin, S.C. The HP1 Protein Family: Getting a Grip on Chromatin. *Curr. Opin. Genet. Dev.* **2000**, *10*, 204–210. [CrossRef]
27. Lomberk, G.; Wallrath, L.; Urrutia, R. The Heterochromatin Protein 1 family. *Genome Biol.* **2006**, *7*, 228. [CrossRef]
28. Kumar, A.; Kono, H. Heterochromatin Protein 1 (HP1): Interactions with Itself and Chromatin Components. *Biophys. Rev.* **2020**, *12*, 387–400. [CrossRef]
29. Eissenberg, J.C.; Morris, G.D.; Reuter, G.; Hartnett, T. The Heterochromatin-Associated Protein HP-1 Is an Essential Protein in Drosophila with Dosage-Dependent Effects on Position-Effect Variegation. *Genetics* **1992**, *131*, 345–352. [CrossRef]
30. Fanti, L.; Berloco, M.; Piacentini, L.; Pimpinelli, S. Chromosomal Distribution of Heterochromatin Protein 1 (HP1) in *Drosophila*: A Cytological Map of Euchromatic HP1 Binding Sites. *Genetica* **2003**, *117*, 135–147. [CrossRef]
31. Tortora, M.M.C.; Brennan, L.D.; Karpen, G.; Jost, D. HP1-Driven Phase Separation Recapitulates the Thermodynamics and Kinetics of Heterochromatin Condensate Formation. *Proc. Natl. Acad. Sci. USA* **2023**, *120*, e2211855120. [CrossRef] [PubMed]

32. Gu, Q.; Ji, T.; Sun, X.; Huang, H.; Zhang, H.; Lu, X.; Wu, L.; Huo, R.; Wu, H.; Gao, X. Histone H3 Lysine 9 Methyltransferase FvDim5 Regulates Fungal Development, Pathogenicity and Osmotic Stress Responses in *Fusarium verticillioides*. *FEMS Microbiol. Lett.* **2017**, *364*, fnx184. [CrossRef] [PubMed]
33. Bok, J.W.; Noordermeer, D.; Kale, S.P.; Keller, N.P. Secondary Metabolic Gene Cluster Silencing in *Aspergillus nidulans*. *Mol. Microbiol.* **2006**, *61*, 1636–1645. [CrossRef]
34. Reyes-Dominguez, Y.; Bok, J.W.; Berger, H.; Shwab, E.K.; Basheer, A.; Gallmetzer, A.; Scazzocchio, C.; Keller, N.; Strauss, J. Heterochromatic Marks Are Associated with the Repression of Secondary Metabolism Clusters in *Aspergillus nidulans*: Heterochromatin Regulation of Secondary Metabolism. *Mol. Microbiol.* **2010**, *76*, 1376–1386. [CrossRef] [PubMed]
35. Reyes-Dominguez, Y.; Boedi, S.; Sulyok, M.; Wiesenberger, G.; Stoppacher, N.; Krska, R.; Strauss, J. Heterochromatin Influences the Secondary Metabolite Profile in the Plant Pathogen *Fusarium graminearum*. *Fungal Genet. Biol.* **2012**, *49*, 39–47. [CrossRef]
36. Nishitani, A.; Hiramatsu, K.; Kadooka, C.; Mori, K.; Okutsu, K.; Yoshizaki, Y.; Takamine, K.; Tashiro, K.; Goto, M.; Tamaki, H.; et al. Expression of Heterochromatin Protein 1 Affects Citric Acid Production in *Aspergillus luchuensis* Mut. *kawachii*. *J. Biosci. Bioeng.* **2023**, *136*, 443–451. [CrossRef]
37. Altschul, S.F.; Gish, W.; Miller, W.; Myers, E.W.; Lipman, D.J. Basic Local Alignment Search Tool. *J. Mol. Biol.* **1990**, *215*, 403–410. [CrossRef]
38. Marchler-Bauer, A.; Bryant, S.H. CD-Search: Protein Domain Annotations on the Fly. *Nucleic Acids Res.* **2004**, *32*, W327–W331. [CrossRef]
39. Pei, J.; Grishin, N.V. PROMALS: Towards Accurate Multiple Sequence Alignments of Distantly Related Proteins. *Bioinformatics* **2007**, *23*, 802–808. [CrossRef]
40. Pei, J.; Kim, B.-H.; Grishin, N.V. PROMALS3D: A Tool for Multiple Protein Sequence and Structure Alignments. *Nucleic Acids Res.* **2008**, *36*, 2295–2300. [CrossRef]
41. Nguyen, L.-T.; Schmidt, H.A.; Von Haeseler, A.; Minh, B.Q. IQ-TREE: A Fast and Effective Stochastic Algorithm for Estimating Maximum-Likelihood Phylogenies. *Mol. Biol. Evol.* **2015**, *32*, 268–274. [CrossRef] [PubMed]
42. Kumar, S.; Stecher, G.; Li, M.; Knyaz, C.; Tamura, K. MEGA X: Molecular Evolutionary Genetics Analysis across Computing Platforms. *Mol. Biol. Evol.* **2018**, *35*, 1547–1549. [CrossRef] [PubMed]
43. Kalyaanamoorthy, S.; Minh, B.Q.; Wong, T.K.F.; Von Haeseler, A.; Jermiin, L.S. ModelFinder: Fast Model Selection for Accurate Phylogenetic Estimates. *Nat. Methods* **2017**, *14*, 587–589. [CrossRef]
44. Okonechnikov, K.; Golosova, O.; Fursov, M.; the UGENE team. Unipro UGENE: A Unified Bioinformatics Toolkit. *Bioinformatics* **2012**, *28*, 1166–1167. [CrossRef]
45. Paz, Z.; García-Pedrajas, M.D.; Andrews, D.L.; Klosterman, S.J.; Baeza-Montañez, L.; Gold, S.E. One Step Construction of Agrobacterium-Recombination-Ready-Plasmids (OSCAR), an Efficient and Robust Tool for ATMT Based Gene Deletion Construction in Fungi. *Fungal Genet. Biol.* **2011**, *48*, 677–684. [CrossRef]
46. Mullins, E.D.; Chen, X.; Romaine, P.; Raina, R.; Geiser, D.M.; Kang, S. *Agrobacterium*-Mediated Transformation of *Fusarium oxysporum*: An Efficient Tool for Insertional Mutagenesis and Gene Transfer. *Phytopathology* **2001**, *91*, 173–180. [CrossRef]
47. Ochoa-Velasco, C.E.; Navarro-Cruz, A.R.; Vera-López, O.; Palou, E.; Avila-Sosa, R. Growth Modeling to Control (in Vitro) *Fusarium verticillioides* and *Rhizopus stolonifer* with Thymol and Carvacrol. *Rev. Argent. Microbiol.* **2018**, *50*, 70–74. [CrossRef] [PubMed]
48. Di Rienzo, J.A.; Casanoves, F.; Balzarini, M.G.; Gonzalez, L.; Tablada, M.; Robledo, C.W. InfoStat Versión 2020. Centro de Transferencia InfoStat, FCA, Universidad Nacional de Córdoba, Argentina. 2020. Available online: http://www.infostat.com.ar (accessed on 1 July 2020).
49. Bacon, C.W. A Corn Seedling Assay for Resistance to *Fusarium moniliforme*. *Plant Dis.* **1994**, *78*, 302. [CrossRef]
50. Zörb, C.; Geilfus, C.-M.; Mühling, K.H.; Ludwig-Müller, J. The Influence of Salt Stress on ABA and Auxin Concentrations in Two Maize Cultivars Differing in Salt Resistance. *J. Plant Physiol.* **2013**, *170*, 220–224. [CrossRef]
51. Shephard, G.S.; Sydenham, E.W.; Thiel, P.G.; Gelderblom, W.C.A. Quantitative determination of fumonisins B1 and B2 by high-performance liquid chromatography with fluorescence detection. *J. Liq. Chromatogr.* **1990**, *13*, 2077–2087. [CrossRef]
52. Eissenberg, J.C.; James, T.C.; Foster-Hartnett, D.M.; Hartnett, T.; Ngan, V.; Elgin, S.C. Mutation in a Heterochromatin-Specific Chromosomal Protein Is Associated with Suppression of Position-Effect Variegation in Drosophila Melanogaster. *Proc. Natl. Acad. Sci. USA* **1990**, *87*, 9923–9927. [CrossRef] [PubMed]
53. Elgin, S.C.R.; Reuter, G. Position-Effect Variegation, Heterochromatin Formation, and Gene Silencing in Drosophila. *Cold Spring Harb. Perspect. Biol.* **2013**, *5*, a017780. [CrossRef] [PubMed]
54. Lorentz, A.; Ostermann, K.; Fleck, O.; Schmidt, H. Switching Gene Swi6, Involved in Repression of Silent Mating-Type Loci in Fission Yeast, Encodes a Homologue of Chromatin-Associated Proteins from Drosophila and Mammals. *Gene* **1994**, *143*, 139–143. [CrossRef]
55. Zhang, X.; Liu, X.; Zhao, Y.; Cheng, J.; Xie, J.; Fu, Y.; Jiang, D.; Chen, T. Histone H3 Lysine 9 Methyltransferase DIM5 Is Required for the Development and Virulence of *Botrytis cinerea*. *Front. Microbiol.* **2016**, *7*. [CrossRef]

56. Freitag, M.; Hickey, P.C.; Khlafallah, T.K.; Read, N.D.; Selker, E.U. HP1 Is Essential for DNA Methylation in Neurospora. *Mol. Cell* **2004**, *13*, 427–434. [CrossRef]
57. Nielsen, P.R.; Nietlispach, D.; Mott, H.R.; Callaghan, J.; Bannister, A.; Kouzarides, T.; Murzin, A.G.; Murzina, N.V.; Laue, E.D. Structure of the HP1 Chromodomain Bound to Histone H3 Methylated at Lysine 9. *Nature* **2002**, *416*, 103–107. [CrossRef]
58. Bacon, C.W.; Yates, I.E.; Hinton, D.M.; Meredith, F. Biological Control of *Fusarium moniliforme* in Maize. *Environ. Health Perspect.* **2001**, *109*, 325–332. [CrossRef]
59. Ramos, M.; Ghosson, H.; Raviglione, D.; Bertrand, C.; Salvia, M.-V. Untargeted Metabolomics as a Tool to Monitor Biocontrol Product Residues' Fate on Field-Treated Prunus Persica. *Sci. Total Environ.* **2022**, *807*, 150717. [CrossRef] [PubMed]
60. Sumner, L.W.; Amberg, A.; Barrett, D.; Beale, M.H.; Beger, R.; Daykin, C.A.; Fan, T.W.-M.; Fiehn, O.; Goodacre, R.; Griffin, J.L.; et al. Proposed Minimum Reporting Standards for Chemical Analysis: Chemical Analysis Working Group (CAWG) Metabolomics Standards Initiative (MSI). *Metabolomics* **2007**, *3*, 211–221. [CrossRef]
61. Ma, L.-J.; van der Does, H.C.; Borkovich, K.A.; Coleman, J.J.; Daboussi, M.-J.; Di Pietro, A.; Dufresne, M.; Freitag, M.; Grabherr, M.; Henrissat, B.; et al. Comparative Genomics Reveals Mobile Pathogenicity Chromosomes in *Fusarium*. *Nature* **2010**, *464*, 367–373. [CrossRef]
62. Watanabe, M.; Yonezawa, T.; Lee, K.; Kumagai, S.; Sugita-Konishi, Y.; Goto, K.; Hara-Kudo, Y. Molecular Phylogeny of the Higher and Lower Taxonomy of the *Fusarium*genus and Differences in the Evolutionary Histories of Multiple Genes. *BMC Evol. Biol.* **2011**, *11*, 322. [CrossRef] [PubMed]
63. Casale, A.M.; Cappucci, U.; Piacentini, L. Unravelling HP1 Functions: Post-Transcriptional Regulation of Stem Cell Fate. *Chromosoma* **2021**, *130*, 103–111. [CrossRef] [PubMed]
64. Chujo, T.; Lukito, Y.; Eaton, C.J.; Dupont, P.-Y.; Johnson, L.J.; Winter, D.; Cox, M.P.; Scott, B. Complex Epigenetic Regulation of Alkaloid Biosynthesis and Host Interaction by Heterochromatin Protein I in a Fungal Endophyte-Plant Symbiosis. *Fungal Genet. Biol.* **2019**, *125*, 71–83. [CrossRef]
65. Lanubile, A.; Ferrarini, A.; Maschietto, V.; Delledonne, M.; Marocco, A.; Bellin, D. Functional Genomic Analysis of Constitutive and Inducible Defense Responses to *Fusarium verticillioides* Infection in Maize Genotypes with Contrasting Ear Rot Resistance. *BMC Genom.* **2014**, *15*, 710. [CrossRef]
66. Glenn, A.E.; Zitomer, N.C.; Zimeri, A.M.; Williams, L.D.; Riley, R.T.; Proctor, R.H. Transformation-Mediated Complementation of a *FUM* Gene Cluster Deletion in *Fusarium verticillioides* Restores Both Fumonisin Production and Pathogenicity on Maize Seedlings. *Mol. Plant-Microbe Interact.* **2008**, *21*, 87–97. [CrossRef] [PubMed]
67. Brown, D.W.; Busman, M.; Proctor, R.H. *Fusarium verticillioides SGE1* Is Required for Full Virulence and Regulates Expression of Protein Effector and Secondary Metabolite Biosynthetic Genes. *Mol. Plant-Microbe Interact.* **2014**, *27*, 809–823. [CrossRef]
68. Arias, S.L.; Mary, V.S.; Otaiza, S.N.; Wunderlin, D.A.; Rubinstein, H.R.; Theumer, M.G. Toxin Distribution and Sphingoid Base Imbalances in *Fusarium verticillioides*-Infected and Fumonisin B1-Watered Maize Seedlings. *Phytochemistry* **2016**, *125*, 54–64. [CrossRef]
69. Otaiza-González, S.N.; Mary, V.S.; Arias, S.L.; Bertrand, L.; Velez, P.A.; Rodriguez, M.G.; Rubinstein, H.R.; Theumer, M.G. Cell Death Induced by Fumonisin B1 in Two Maize Hybrids: Correlation with Oxidative Status Biomarkers and Salicylic and Jasmonic Acids Imbalances. *Eur. J. Plant Pathol.* **2022**, *163*, 203–221. [CrossRef]
70. Visentin, I.; Montis, V.; Döll, K.; Alabouvette, C.; Tamietti, G.; Karlovsky, P.; Cardinale, F. Transcription of Genes in the Biosynthetic Pathway for Fumonisin Mycotoxins Is Epigenetically and Differentially Regulated in the Fungal Maize Pathogen *Fusarium verticillioides*. *Eukaryot. Cell* **2012**, *11*, 252–259. [CrossRef]
71. Picot, A.; Barreau, C.; Pinson-Gadais, L.; Caron, D.; Lannou, C.; Richard-Forget, F. Factors of the *Fusarium verticillioides* -Maize Environment Modulating Fumonisin Production. *Crit. Rev. Microbiol.* **2010**, *36*, 221–231. [CrossRef]
72. Flaherty, J.E.; Pirttilä, A.M.; Bluhm, B.H.; Woloshuk, C.P. *PAC1*, a pH-Regulatory Gene from *Fusarium verticillioides*. *Appl. Environ. Microbiol.* **2003**, *69*, 5222–5227. [CrossRef] [PubMed]
73. Wiemann, P.; Willmann, A.; Straeten, M.; Kleigrewe, K.; Beyer, M.; Humpf, H.; Tudzynski, B. Biosynthesis of the Red Pigment Bikaverin in *Fusarium fujikuroi*: Genes, Their Function and Regulation. *Mol. Microbiol.* **2009**, *72*, 931–946. [CrossRef] [PubMed]
74. Frandsen, R.J.N.; Rasmussen, S.A.; Knudsen, P.B.; Uhlig, S.; Petersen, D.; Lysøe, E.; Gotfredsen, C.H.; Giese, H.; Larsen, T.O. Black Perithecial Pigmentation in *Fusarium* Species Is Due to the Accumulation of 5-Deoxybostrycoidin-Based Melanin. *Sci. Rep.* **2016**, *6*, 26206. [CrossRef] [PubMed]
75. Proctor, R.H.; Butchko, R.A.E.; Brown, D.W.; Moretti, A. Functional Characterization, Sequence Comparisons and Distribution of a Polyketide Synthase Gene Required for Perithecial Pigmentation in Some *Fusarium* Species. *Food Addit. Contam.* **2007**, *24*, 1076–1087. [CrossRef] [PubMed]
76. Zhang, Y.; Yu, W.; Lu, Y.; Wu, Y.; Ouyang, Z.; Tu, Y.; He, B. Epigenetic Regulation of Fungal Secondary Metabolism. *J. Fungi* **2024**, *10*, 648. [CrossRef]
77. Lamka, G.F.; Harder, A.M.; Sundaram, M.; Schwartz, T.S.; Christie, M.R.; DeWoody, J.A.; Willoughby, J.R. Epigenetics in Ecology, Evolution, and Conservation. *Front. Ecol. Evol.* **2022**, *10*, 871791. [CrossRef]

78. Herman, J.J.; Sultan, S.E.; Horgan-Kobelski, T.; Riggs, C. Adaptive Transgenerational Plasticity in an Annual Plant: Grandparental and Parental Drought Stress Enhance Performance of Seedlings in Dry Soil. *Integr. Comp. Biol.* **2012**, *52*, 77–88. [CrossRef]
79. Sakashita, A.; Ooga, M.; Otsuka, K.; Maezawa, S.; Takeuchi, C.; Wakayama, S.; Wakayama, T.; Namekawa, S.H. Polycomb Protein SCML2 Mediates Paternal Epigenetic Inheritance through Sperm Chromatin. *Nucleic Acids Res.* **2023**, *51*, 6668–6683. [CrossRef]
80. Reardon, R.M.; Walsh, A.K.; Larsen, C.I.; Schmidberger, L.H.; Morrow, L.A.; Thompson, A.E.; Wellik, I.M.; Thompson, J.S. An Epigenetically Inherited UV Hyper-Resistance Phenotype in Saccharomyces Cerevisiae. *Epigenetics Chromatin* **2022**, *15*, 31. [CrossRef]

Disclaimer/Publisher's Note: The statements, opinions and data contained in all publications are solely those of the individual author(s) and contributor(s) and not of MDPI and/or the editor(s). MDPI and/or the editor(s) disclaim responsibility for any injury to people or property resulting from any ideas, methods, instructions or products referred to in the content.

Journal of Fungi

MDPI

Article

Functional Analysis of *FoCrpA* in *Fusarium oxysporum* Causing Rice Seedling Blight

Chun Wang [1,2,†], Liang Wang [1,†], Xuanjie Zhao [1], Lei Hou [1], Qingran Liu [1], Rui Ren [1], Anqi Lv [1], Xinyang Liu [1], Tianliang Xiong [1], Peng Guo [1], Xiaofeng Xu [1], Zhe Ni [1], Chunlai Liu [2] and Junhua Zhang [1,*]

[1] College of Plant Protection, Northeast Agricultural University, Harbin 150030, China; chunharbin@aliyun.com (C.W.)
[2] Institute of Plant Protection, Heilongjiang Academy of Agricultural Sciences/Scientific Observing and Experimental Station of Crop Pests in Harbin, Ministry of Agriculture and Rural Affairs, Harbin 150086, China
* Correspondence: podozjh@163.com
† These authors contributed equally to this work.

Abstract: *Fusarium oxysporum* is one of the main pathogens causing rice seedling blight disease. Revealing its pathogenic mechanism is of great significance for formulating prevention and control strategies for rice seedling blight disease. Copper transporting P-type ATPases (Cu-ATPase) is a large class of proteins located on the plasma membrane that utilize the energy provided by ATP hydrolysis phosphorylation to transport substrates across the membrane. It plays a crucial role in signal transduction, the maintenance of cell membrane stability, and material transport. The main function of Cu-ATPase is to maintain the homeostasis of copper in cells, which is essential for the normal growth and development of organisms. This study utilized the ATMT-mediated gene knockout method to obtain the knockout mutant Δ*FoCrpA* and the complementation strain Δ*FoCrpA-C*, which are highly homologous to the P-type heavy metal transport ATPase family in *F. oxysporum*. The results showed that, compared with the wild-type strain, the knockout mutant Δ*FoCrpA* had a lighter colony color; a reduced tolerance to copper ion, osmotic, and oxidative stress; a weakened ability to penetrate glass paper; and decreased pathogenicity. However, there was no significant difference in pathogenicity and other biological phenotypes between the complementation strain Δ*FoCrpA-C* and the wild-type strain. In summary, the *FoCrpA* gene is involved in osmotic and oxidative stress, affecting the invasion and penetration ability and pathogenicity of *F. oxysporum*, laying a theoretical foundation for understanding the development and pathogenic mechanism of *F. oxysporum*.

Keywords: *Fusarium oxysporum*; rice seedling blight; copper-transporting phosphorylating ATPase; pathogenicity

1. Introduction

Rice seedling blight poses a significant threat to global rice production, resulting in substantial losses in yield and quality [1,2]. This disease, which is among the most important rice seedling diseases, is caused by a diverse array of pathogens, including *Fusarium* spp. [3,4], *Burkholderia plantarii* [5], *Rhizoctonia solani* [6], *Marasmius graminum* [7], *Pythium aristosporum* [8], and *Cochliobolus carbonum* [9]. In Northeast China, *Fusarium oxysporum* has emerged as the predominant pathogen responsible for rice seedling blight [10]. Given the scarcity of effective resistant rice varieties, chemical fungicides have become one of the most widely used methods for controlling this disease [11]. However, the prolonged application of chemical fungicides has led to the development of drug resistance in

F. oxysporum [12–15]. Consequently, investigating the functions of pathogenesis-related genes in *F. oxysporum* is essential for elucidating its pathogenic mechanisms and developing sustainable control strategies.

Copper is an essential micronutrient for the normal physiological activities of living organisms. It serves as a component and active site in various redox reaction proteins, such as superoxide dismutase and cytochrome C oxidase, and is involved in numerous biological processes and metabolic activities, including photosynthesis, electron transfer, protein synthesis, and the alleviation of oxidative stress [16]. Copper ions play a crucial role in maintaining the metabolism and normal development of organisms [17]. Both copper deficiency and excess can be detrimental; copper ion deficiency can impair the activity of enzymes that rely on copper ions as a cofactor, thereby affecting cell survival [18]. In contrast, excessive copper ions can cause lipid and protein peroxidation, generating large amounts of reactive oxygen species that disrupt cell structure, impair cell division, and damage enzymatic systems [19]. Additionally, excess copper ions can react with cellular thiols, displacing other metals in proteins and causing oxidative damage at the nucleic acid level [20]. Cu-ATPase, a large class of membrane proteins located on the plasma membrane, utilizes the energy from ATP hydrolysis to transport substrates across the membrane. It plays a vital role in signal transduction, maintaining cell membrane stability, and facilitating substance transport [21]. Cu-ATPase comprises five subfamilies that transport different substrates. Among them, the P1B-type ATPase (Heavy Metal ATPase, HMA) is a subfamily of P-type ATPase that selectively absorbs and transports essential metal ions such as Cu^{+}, Cu^{2+}, Zn^{2+}, Co^{2+}, and Cd^{2+} [22]. The primary function of Cu-ATPase in HMA is to maintain cellular copper homeostasis, which is critical for normal growth and development [23]. In some pathogenic fungi, Cu-ATPase is required for normal growth, reproduction, and effective host invasion. For instance, in the filamentous plant pathogen *Cochliobolus heterospira*, mutation of the *ChCcc2* gene significantly affects its growth rate, pigmentation, spore count, and colony morphology [24]. In the pathogen *Colletotrichum lindemuthianum*, a knockout mutant of the *clap1* gene exhibited similar nutritional growth and spore formation as the wild type but displayed lighter pigmentation, fewer appressoria, and no disease symptoms [25]. In the ubiquitous fungus *Aspergillus flavus,* the deletion of *CrpA* and *CrpB* resulted in reduced toxicity to mice and a diminished colonization ability on corn seeds treated with copper fungicides [26]. Despite these findings, the role of Cu-ATPase in the pathogenicity of *F. oxysporum* remains poorly understood, necessitating further investigation into its specific mechanisms and impact on virulence.

Previously, we identified multiple pathogenesis-related genes, including *FoCrpA*, using a T-DNA insertion mutant library of the rice seedling blight fungus *F. oxysporum*. Through integrated bioinformatics characterization of the *FoCrpA*-encoded protein and functional validation via *Agrobacterium tumefasciens*-mediated transformation (ATMT)-based homologous recombination, this study systematically investigated the biological role of *FoCrpA* in *F. oxysporum*. Our approach enabled comprehensive evaluation of *FoCrpA* influence on fungal adaptive mechanisms, particularly focusing on stress response pathways and virulence regulation. These findings advance our understanding of *F. oxysporum* pathogenicity determinants, reveal promising molecular targets for next-generation antifungal agents, and provide theoretical foundation for developing novel disease management strategies against rice seedling blight.

2. Materials and Methods

2.1. Fungal Strains, Rice Variety, Plasmids

The *F. oxysporum* wild-type strain Fo21, originally isolated from symptomatic rice seedlings exhibiting rice seedling blight in Heilongjiang Province, China, served as the

progenitor for genetic manipulation. All fungal strains including WT Fo21, Δ*FoCrpA* mutants, and complemented strain Δ*FoCrpA-C* were maintained on potato dextrose agar (PDA: 200 g/L potato, 20 g/L glucose, 15 g/L agar). The rice cultivar Longjing 31 (*O. sativa* subsp. *japonica*), provided as pathologically certified seeds by the Phytopathology Laboratory of Northeast Agricultural University (Harbin, China). *Agrobacterium tumefaciens* AGL-1 was gifted by Professor Zhang Shihong of Jilin University. *Escherichia coli* DH5α was gifted by Professor Qin Qingming of Jilin University. The plasmid pXEH was gifted by Professor Li Guihua from Jilin University, which contains the hygromycin B resistance gene and is used for gene knockout. The plasmid pSUL was gifted by Professor Zhang Shihong from Jilin University, which contains the resistance gene Chlorpyriprone and is used for gene complementation.

2.2. Protein Sequence Analysis and Phylogenetic Reconstruction

The coding sequence of *FoCrpA* (GenBank accession: XP_018237293.1) was retrieved from the NCBI RefSeq database. Functional domain architecture was resolved through complementary analyses usingNCBI Conserved Domain Database (CDD) and SMART. Orthologous *CrpA* sequences from 15 taxonomically diverse Ascomycete fungi were downloaded from GenBank. Multiple sequence alignment and the maximum-likelihood phylogenetic tree was reconstructed in MEGA7.0 with 1000 bootstrap replications.

2.3. Targeted Gene Disruption and Complementation

Gene knockout and complementation were performed via *Agrobacterium tumefaciens*-mediated transformation (ATMT) using the binary vector system [27,28]. *FoCrpA* disruption mutant was generated by amplifying upstream and downstream flanking regions of *FoCrpA* from wild-type Fo21 genomic DNA using primers FoCrpA-UP-F/R and FoCrpA-DN-F/R. The plasmid pXEH was linearized with *EcoRI,* and the upstream fragment was ligated into the *EcoRI* site via ligation-independent cloning (Takara Bio). Recombinant plasmid pXEH-CUP was transformed into *E. coli* DH5α and validated by colony PCR (primers FoCrpA-UP-F/Hup-R). The downstream fragment was subsequently inserted into the *SalI* site of pXEH-CUP, yielding the final knockout vector pXEH-C. Following *Agrobacterium tumefaciens* AGL-1-mediated transformation with Fo21 conidia (1×10^6 spores/mL), transformants were selected on PDA containing 80 μg/mL hygromycin B, 300 μg/mL carbenicillin, and 150 μg/mL cefotaxime. Putative mutants were subcultured thrice and validated via multiplex PCR: HPH integration (Hyg-F/R, 1.2 kb), homologous recombination junctions (Cup-F/Hup-R: 800 bp; Hdn-F/Cdn-R: 750 bp), and *FoCrpA* knockout confirmation (FoCrpA-F/R, no amplification).

The complementation fragment C-*FoCrpA* (4880 bp), encompassing the full-length *FoCrpA* gene, was amplified using primers C-FoCrpA-F/R and purified. Plasmid pSUL was digested with *BamHI*, and the C-*FoCrpA* fragment was ligated into the *BamHI* site. The resultant complementation vector pSUL-C was validated through colony PCR, *BamHI* restriction digestion, and sequencing. pSUL-C was introduced into *Agrobacterium tumefaciens* AGL-1 and co-cultivated with Δ*FoCrpA* conidia. Transformants were selected on chlorimuron-ethyl-supplemented medium and verified by PCR amplification using primers FoCrpA-F/R. Successfully complemented strains, designated Δ*FoCrpA-C*, were confirmed by restored *FoCrpA* amplification. Mutants were verified by PCR and qRT-PCR. PCR amplification was performed in a 10 μL reaction volume containing: 5 μL 2 × Taq PCR Master Mix, 0.4 μL *FoCrpA*-F, 0.4 μL *FoCrpA*-R, 0.4 μL strains DNA, 3.8 μL ddH_2O to adjust the final volume. PCR (Bio-rad T100, Hercules, CA, USA) amplification was conducted under the following thermocycling conditions: initial denaturation at 94 °C for 5 min,

followed by 30 cycles of denaturation (94 °C, 30 s), annealing (55 °C, 30 s), and extension (72 °C, 1 min), with a final elongation step at 72 °C for 10 min. The ChamQ Universal SYBR qPCR Master Mix (Vazyme, Nanjing, China) was used to perform quantitative real-time PCR (qRT-PCR), and qRT-PCR assays ran on a QuantStudio^{TM}5 real-time PCR system. qRT-PCR reaction system was performed in a 20 µL reaction volume containing: 2xFast qPCR Master Mixture(Green) 10 µL, Actin-F/*FoCrpA*-F 0.5 µL, Actin-R/*FoCrpA*-R 0.5 µL, DNA template 1 µL, DEPC-ddH_2O 8 µL. qPCR amplification was conducted under the following thermocycling conditions: initial denaturation at 94 °C for 2 min, followed by 40 cycles of denaturation (94 °C, 15 s), annealing (60 °C, 15 s), and extension (72 °C, 45 s). Data analysis was carried out using the delta delta-CT ($2^{-\Delta\Delta Ct}$) method outlined by Livak and Schmittgen [29]. The primer sequences used are shown in Table 1.

Table 1. Primers used in this study.

Primer Name	Primer Sequence
Hyg-F	TCGCCCTTCCTCCCTTTATTTCAG
Hyg-R	CTACACAGCCATCGGTCCAGAC
SuR-F	CTCTCCGTTGCTTATCCTTGCCTA
SuR-R	CGCCATCACTACGCCTTGTCTT
FoCrpA-UP-F	GATCTTCACTAGTGGGAATTCCCCGTGATGATTTGCCCAATGAAT
FoCrpA-UP-R	TTGGGTACCGAGCTCGAATTCCGCCATGTTGACTGCTGTGAGA
FoCrpA-DN-F	TGGGGATCCTCTAGAGTCGACTGGTATTGGCAGTGGTAGTGTTGG
FoCrpA-DN-R	CTTGCATGCCTGCAGGTCGACCCGACGGAGGATCAAGATGTAAGC
Hup-R	TGCTCACCGCCTGGACGACTAA
Hdn-F	TGGACCGATGGCTGTGTAGAAGT
Cup	AGGCTTGGAGGAGAATGGTTGG
Cdn	AAGCCTTCCTTACGCCTGATGATG
FoCrpA-F	TGCTCACCGCCTGGACGACTAA
FoCrpA-R	TGGACCGATGGCTGTGTAGAAGT
C-*FoCrpA*-F	CCGGGTACCGAGCTCGAATTCCCGTTGCTCTGCCGTATCTTGAA
C-*FoCrpA*-R	AGCTGTCAAACATGAGAATTCAAGCCTTCCTTACGCCTGATGATG
Actin-F	GTTGCCTGAGACTTGACGACGAT
Actin-R	CTCCTCCGAACCATCCGCTACA

2.4. Phenotype Analysis

Mycelial plugs (5 mm diameter) from Fo21, Δ*FoCrpA*, and Δ*FoCrpA-C* were placed on PDA plates. For colony morphology, plates were incubated in the dark at 25 °C for 7 days, and then colony diameter and morphology were measured [11]. For mycelial dry weight and culture color, mycelial plugs were inoculated into 100 mL PDB medium and incubated at 180 rpm at 25 °C for 2 days. Culture color was observed, and hyphae were collected by centrifugation at 10,000 rpm for 15 min, dried at 80 °C to constant weight, and weighed. For copper ion stress, mycelial plugs were incubated on PDA plates with 0 mM, 0.25 mM, 0.5 mM, and 1 mM $CuSO_4$ in the dark at 25 °C for 5 days. For conidial production and germination, mycelial plugs were inoculated into 50 mL PDB medium incubated at 180 rpm at 25 °C for 2 days. Then, 100 µL suspension (1×10^8 spores/mL) was inoculated into 40 mL germination medium (GM: 20 g Sucrose, 1 g $NaNO_3$, 0.5 g KH_2PO_4, 0.5 g NaCl, and 0.5 g $MgSO_4$ in 1 L of distilled water) in a shaker at 180 rpm at 25 °C for 6 h, 9 h, and 12 h to calculate percentage of conidial germination. For stress response, mycelial plugs were placed on PDA plates amended with 1 M sorbitol, 0.5 M NaCl, 0.03% SDS, 1 mM Congo red, and 10 mM H_2O_2 and incubated in the dark at 25 °C for 5 days. For penetration capacity evaluation, cellophane membranes were overlaid on PDA plates. Post 48 h colonization, membranes were aseptically removed to assess substrate penetration through residual colony development during extended incubation

(24 h). The colony diameters were measured after being incubated and the inhibition rates of various stress factors were calculated. Each experiment was repeated three times.

2.5. Toxicity Assays with Culture Filtrates and Pathogenicity Assay

Next, 5 mm mycelial plugs from Fo21, Δ*FoCrpA*, and Δ*FoCrpA-C* strains were cultured in 100 mL PDB medium (25 °C, 100 rpm, 7 d). The culture was filtered, centrifuged (4000 rpm, 15 min), and the supernatant filtered through 0.22 μm membranes to obtain crude toxin extract. The surface-sterilized (70% ethanol, immersed for 1 min) rice seeds were incubated with the extract (PDB medium as control) under 25 °C light for 5 d. Germination rate and shoot lengths were determined using three biological replicates, each containing fifty rice seeds. For germination assessment, seeds with radicle emergence $\geq$ 2 mm were considered germinated. Shoot length was measured from coleoptile base to tip using digital calipers.

Rice seeds were surface-sterilized with 70% ethanol for 1 min, rinsed 3 times with sterile water, and subjected to germination pretreatment on sterile filter paper at 25 °C for 2 days. Spore suspensions of Fo21, Δ*FoCrpA*, and Δ*FoCrpA-C* strain were prepared, and conidial concentrations were adjusted to 1×10^6 conidia/mL. Germinated seeds were soaked in the conidial suspensions for 30 min, with sterile water as the control, then sown in pots on top of potting soil (vermiculite/soil ratio of 1:2) and covered with autoclaved sterile soil. Disease progression was observed after 14 days of incubation at 25 °C. Each treatment consisted of 50 rice plants with three replicates. Disease index was calculated based on rice seedling blight grading standards from previous research using a scale from 0 to 4, defined as follows [30]: 0 = no symptoms; 1 = a few small lesions below 1/4 of the stem circumference; 2 = large lesions occupying 1/4–1/2 of stem circumference; 3 = large lesions occupying 1/2–3/4 of stem circumference; 4 = lesions occupying all stem circumference and plant die. The disease index was calculated as follows: $\sum$(No.of diseased plants $\times$ relative grade) $\times$ 100/(total No. of investigated plants $\times$ the highest grade).

2.6. Statistical Analysis

All experiments were performed at least thrice using independent assays. One-way analysis of variance (ANOVA) was conducted using SPSS (version 22.0 for windows, 2013, IBM, Armonk, NY, USA). The statistical significance of data comparisons was performed between the wild type Fo21 and the deletion mutants with one-way analysis of variance (ANOVA), followed by Duncan's multiple range test. Values of $p < 0.05$ were labeled as statistically significant.

3. Results

3.1. Identification of FoCrpA from F. oxysporum

Bioinformatic analysis of *FoCrpA* using the NCBI Conserved Domain Database (CDD) identified its C-terminal region (residues 371–1081) as a canonical member of the P-type ATPase superfamily (PF00122), specifically classified as a heavy metal-transporting ATPase (HM-ATPase). Subsequent SMART analysis further resolved three conserved functional modules: (i) N-terminal HMA domain (PF00403, aa 45–86): A ββαβ metal-binding fold critical for heavy metal ion recognition and chelation. (ii) Central E1-E2_ATPase domain (PF00122, aa 210–450): Characteristic catalytic core of P-type ATPases, comprising E1 ATP-binding subdomain (aa 210–320) with conserved DKTGT phosphorylation motif and E2 transmembrane ion translocation subdomain (aa 350–450) containing CPC metal coordination residues; (iii) C-terminal Hydrolase_3 domain (PF13343, aa 500–620): A HAD-family phosphatase module potentially regulating ATPase autoinhibition (Figure 1A). Phylogenetic reconstruc-

tion using maximum-likelihood methods (MEGA7.0) of 15 ascomycete orthologs revealed strong clustering of *F. oxysporum FoCrpA* with *F. oxysporum* f. sp. *lycopersici* (XP_018237293.1, 99% identity), forming a distinct clade from *Fusarium odoratissimum* (XP_031071559.1) and *Fusarium redolens* (XP_046053860.1), while the protein from other fungi displays low similarity with homologous proteins (Figure 1B). This phyletic pattern suggests vertical inheritance of *FoCrpA* within the *Fusarium* genus, with functional conservation in metal homeostasis.

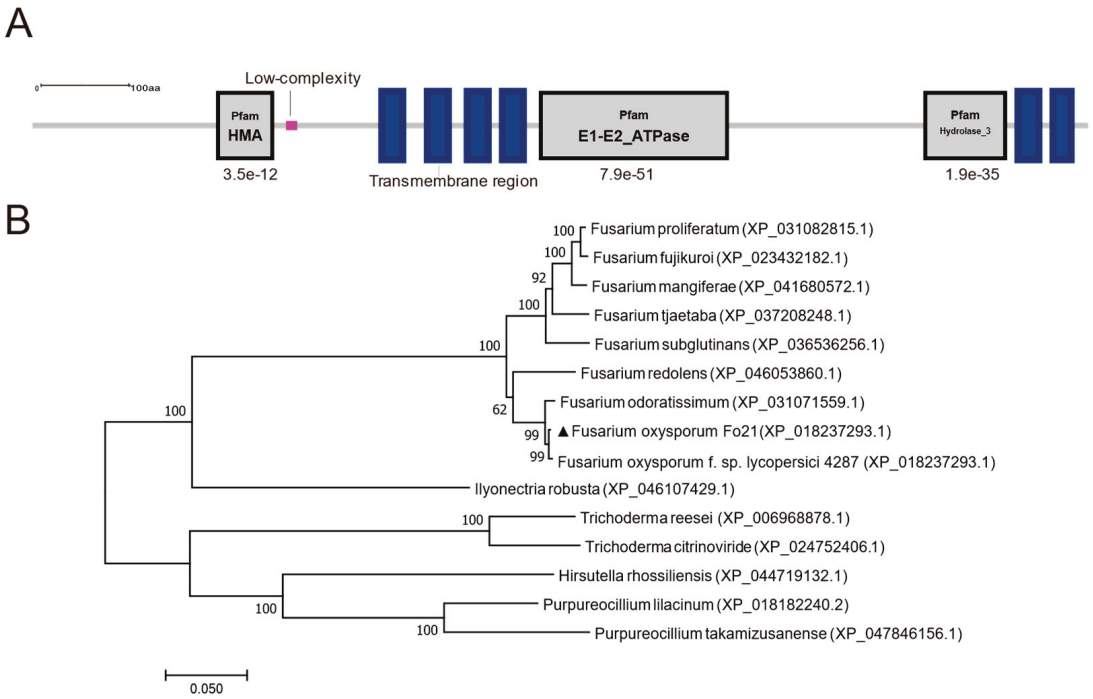


Figure 1. Functional domain architecture and phylogenetic analysis of *FoCrpA* in *F. oxysporum*. (**A**) Domain prediction of FoCrpA via the SMART database identified three conserved motifs: 1. Pfam: HMA (Heavy Metal-Associated) domain (aa 45–86): A β-sandwich fold critical for heavy metal ion binding and transport, conserved across prokaryotic and eukaryotic metal transporters. 2. Pfam: E1-E2_ATPase (aa 210–450): Characteristic of P-type ATPases, featuring an ATP hydrolysis module (E1, aa 210–320) for energy release and a transmembrane ion translocation module (E2, aa 350–450). 3. Pfam: Hydrolase_3 (HAD-like) (aa 500–620): A haloacid dehalogenase superfamily domain catalyzing phosphatase/hydrolase reactions, potentially linked to metal cofactor metabolism. (**B**) Maximum-likelihood phylogenetic tree of *FoCrpA* homologs across 9 *Fusarium* species and 6 other fungal species, reconstructed with MEGA7.0 (1000 bootstrap replicates).

3.2. Generation of FoCrpA Deletion Mutants and Complementation Assay

FoCrpA was deleted using a homologous recombination strategy (Figure 2A). The gene knockout vector pXEH-C was transferred into *Agrobacterium tumefaciens* AGL-1 to transform the wild-type Fo21 strain. The *FoCrpA* gene in *F. oxysporum* was replaced with the hygromycin resistance gene via homologous recombination (Figure 2A). Four primer pairs (Hyg-F/Hyg-R, Cup-Hup-R, Hdn-F/Cdn, *FoCrpA*-F/*FoCrpA*-R) were used to validate the knockout mutant over three generations (Figure 2B). The results showed that two mutants successfully integrated the hygromycin resistance gene (detected by Hyg-F/Hyg-R). The upstream (1531 bp) and downstream (1102 bp) fragments of *FoCrpA* were correctly integrated in two mutants (validated by Cup-Hup-R and Hdn-F/Cdn). Three mutants lacked the *FoCrpA* gene (confirmed by *FoCrpA*-F/*FoCrpA*-R). These results confirmed the successful knockout of the *FoCrpA* gene, and the mutant was named Δ*FoCrpA*.The *FoCrpA* locus (4880 bp) was cloned from Fo21 into pSUL via *BamHI,* generating complementation vector pSUL-C (PCR/restriction-verified). *Agrobacterium tumefasciens*-mediated transformation of pSUL-C into Δ*FoCrpA* restored the target fragment (867 bp PCR-amplified in complemented

strain Δ*FoCrpA-C* and WT, absent in Δ*FoCrpA*), confirming genetic complementation (Figure 2C). Transcriptional validation via qRT-PCR using the internal reference gene β-actin as a control demonstrated complete abolition of *FoCrpA* expression in Δ*FoCrpA* (expression level <0.01% of wild-type Fo21, normalized to 1), with full transcriptional restoration observed in the complemented strain Δ*FoCrpA-C* (Figure 2D). This indicates that *FoCrpA* was disrupted successfully in Δ*FoCrpA* and reintegrated in Δ*FoCrpA-C*.

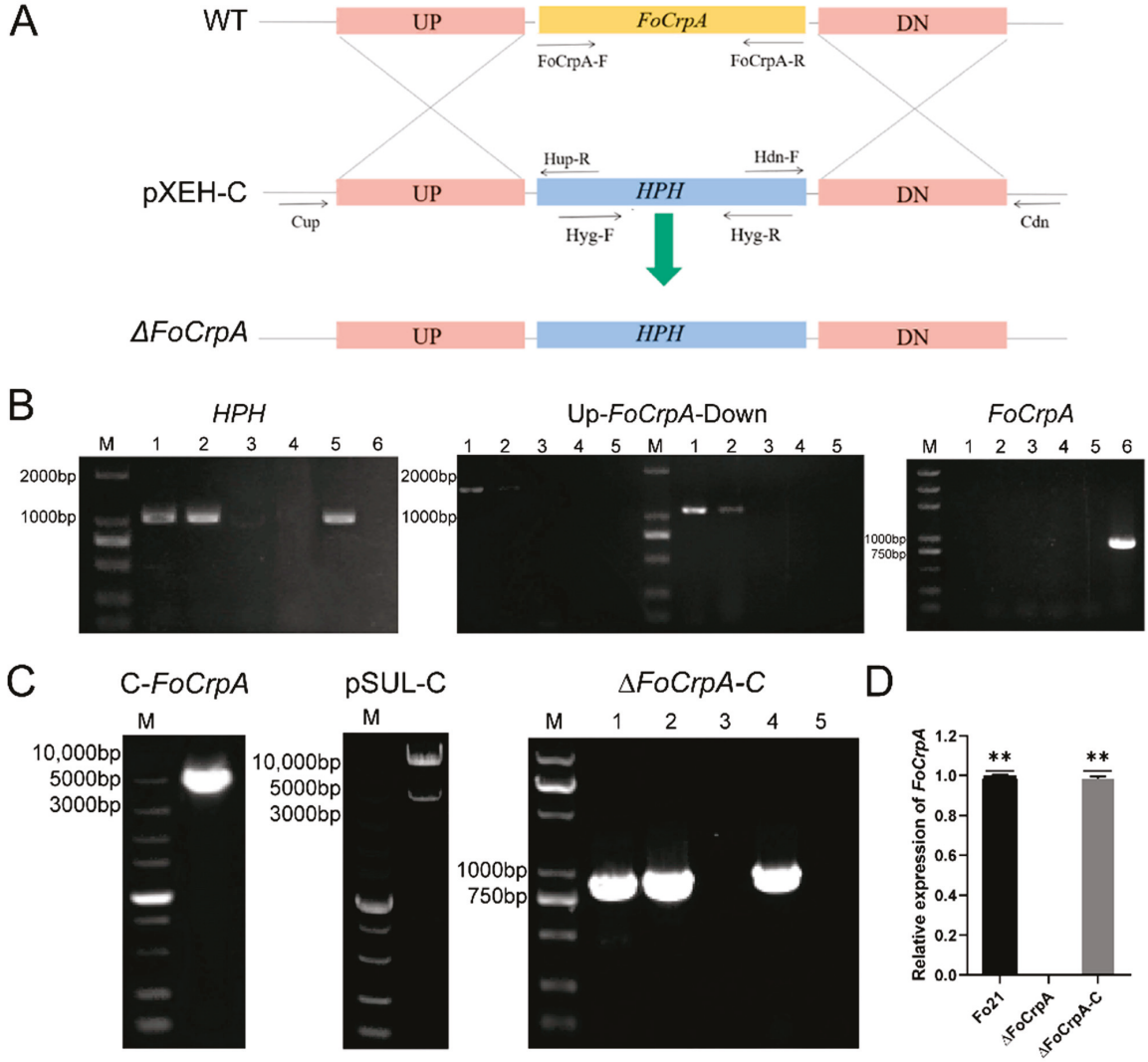


Figure 2. *FoCrpA* gene knockout strategy; PCR and qRT-PCR validation of knockout mutants and complementation strains. (**A**) *FoCrpA* gene knockout strategy. (**B**) PCR validation of *HPH* gene (M: DL2000 Ladder DNA Marker; 1–3: Mutant; 4: Fo21; 5: pXEH; 6: ddH_2O); PCR validation of the two side fragments of *FoCrpA* gene (M: DL2000 Ladder DNA Marker; 1–3: mutant; 4: Fo21; 5: ddH_2O); PCR validation of *FoCrpA* gene (M: DL5000 Ladder DNA Marker; 1–3: Mutant; 4: pXEH; 5: ddH_2O; 6: Fo21). (**C**) C-*FoCrpA* gene fragment (M: 1 kb Ladder DNA Marker); pSUL-C enzyme digestion validation (M: 1 kb Ladder DNA Marker); PCR validation of Δ*FoCrpA*-C (M: DL5000 Ladder DNA Marker; 1–2: complementation mutant; 3: Δ*FoCrpA*; 4: Fo21; 5: ddH_2O). (**D**) Expression analysis of *FoCrpA* in WT Fo21 and its mutants strains with qRT-PCR. Duncan's multiple range test was performed to determine significant difference, ** $p \leq 0.01$.

3.3. Effects of FoCrpA on Vegetative Growth and Conidiogenesis

Colony phenotypic characterization of *FoCrpA* and its mutant strains demonstrated that wild-type Fo21 and its mutant strains exhibited similar spreading growth patterns with comparable radial expansion rates, while Δ*FoCrpA* colonies displayed significant pigmentation

attenuation compared to the wild-type Fo21 and complemented strains, which showed indistinguishable colony coloration (Figure 3A). For the color of the liquid culture, Δ*FoCrpA* also produced visibly lighter extracellular pigments than wild-type and complemented strains (Figure 3B). Liquid cultures grown in PDB medium revealed no significant differences in mycelial biomass accumulation among strains (Figure 3C), demonstrating that *FoCrpA* deletion does not impair hyphal growth under standard nutrient conditions. Tolerance assays on $CuSO_4$-supplemented PDA (0–1 mM) demonstrated that Δ*FoCrpA* exhibited significant growth suppression at 0.5 mM and complete growth arrest at 1 mM $CuSO_4$, whereas wild-type and complemented strains maintained partial viability (Figure 3D). Conidial production and germination were similar between WT Fo21 and its mutant strains (Figure 3E,F). These results demonstrate that *FoCrpA* specifically modulates pigment biosynthesis and copper ion homeostasis in *F. oxysporum*, while exhibiting no significant regulatory effects on mycelial biomass accumulation, conidiogenesis, or conidial germination.

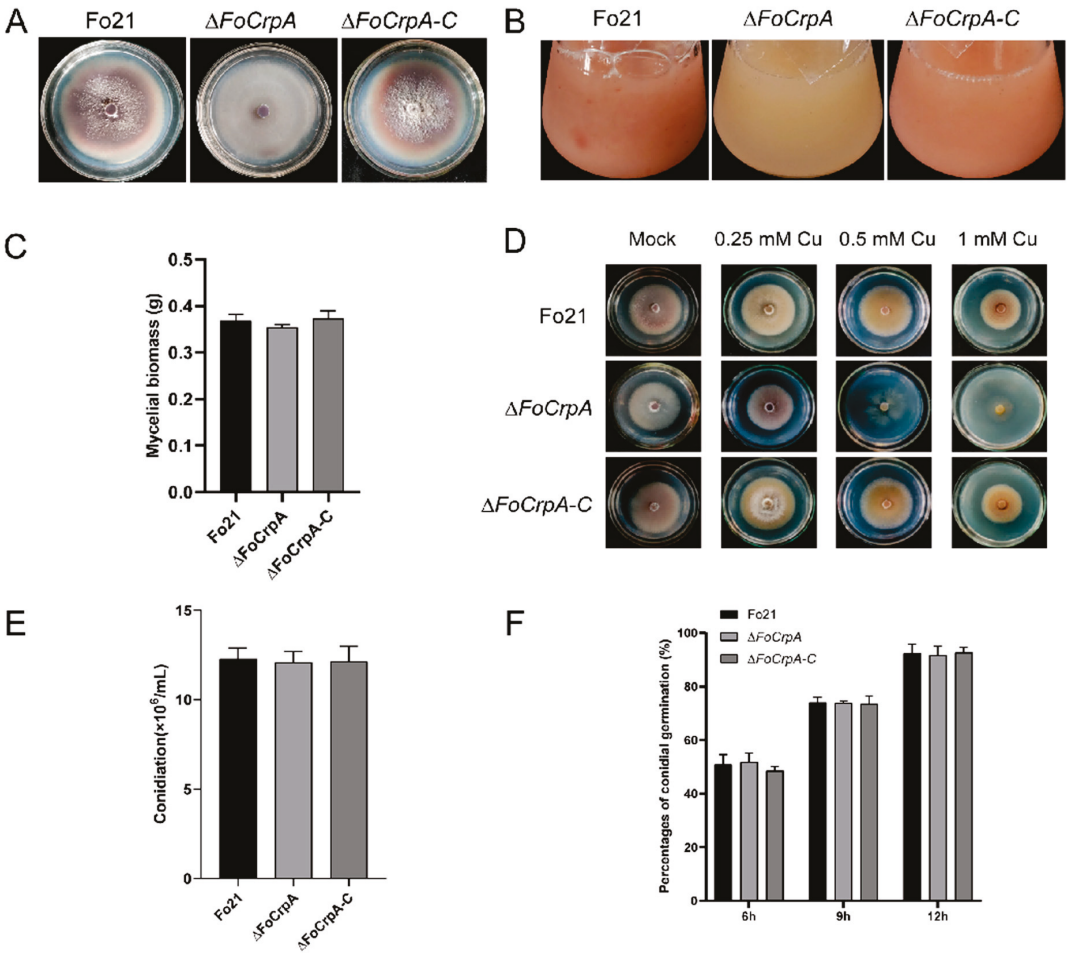


Figure 3. Phenotypic analysis of *FoCrpA* and its mutant strains. (**A**) Colony phenotypic characterization of Fo21, Δ*FoCrpA*, and Δ*FoCrpA-C* on PDA plates after incubation of 7 days at 25 °C. (**B**) Observing culture color of Fo21, Δ*FoCrpA*, and Δ*FoCrpA-C* strains grown in 100 mL PDB in a shaker at 180 rpm at 25 °C for 2 days. (**C**) Mycelial biomass was measured by determining the dry weight of Fo21, Δ*FoCrpA*, and Δ*FoCrpA-C* strains grown in 100 mL PDB in a shaker at 180 rpm at 25 °C for 3 days. (**D**) Colony morphology of Fo21, Δ*FoCrpA*, and Δ*FoCrpA-C* under Cu stress, amended with $CuSO_4$ at different concentrations indicated in the figure and cultured at 25 °C for 5 days. (**E**) Conidial production of Fo21, Δ*FoCrpA* and Δ*FoCrpA-C* grown in 50 mL PDB in a shaker at 180 rpm at 25 °C for 2 days. (**F**) Conidial germination was compared between Fo21 and its mutants by re-suspending the conidia in 40 mL liquid GM in a shaker at 180 rpm at 25 °C for 6 h, 9 h, and 12 h.

3.4. Response of FoCrpA to Stress Agents

To investigate the regulatory role of *FoCrpA* in environmental stress adaptation of *F. oxysporum*, comparative phenotypic analyses were performed using wild-type Fo21, Δ*FoCrpA*, and Δ*FoCrpA*-C on PDA plates supplemented with different stress agents, including NaCl and sorbitol (osmotic stresses), SDS and CR (cell wall stresses), and H_2O_2 (oxidative stress). After five-day incubation at 25 °C, the Δ*FoCrpA* mutant displayed significantly impaired growth under osmotic and oxidative stress conditions compared to the wild-type Fo21 and complemented strain Δ*FoCrpA*-C, while maintaining wild-type-level sensitivity to cell wall stressors (Figure 4A,B). These data collectively demonstrate that *FoCrpA* specifically modulates *F. oxysporum*'s tolerance mechanisms against osmotic and oxidative challenges.

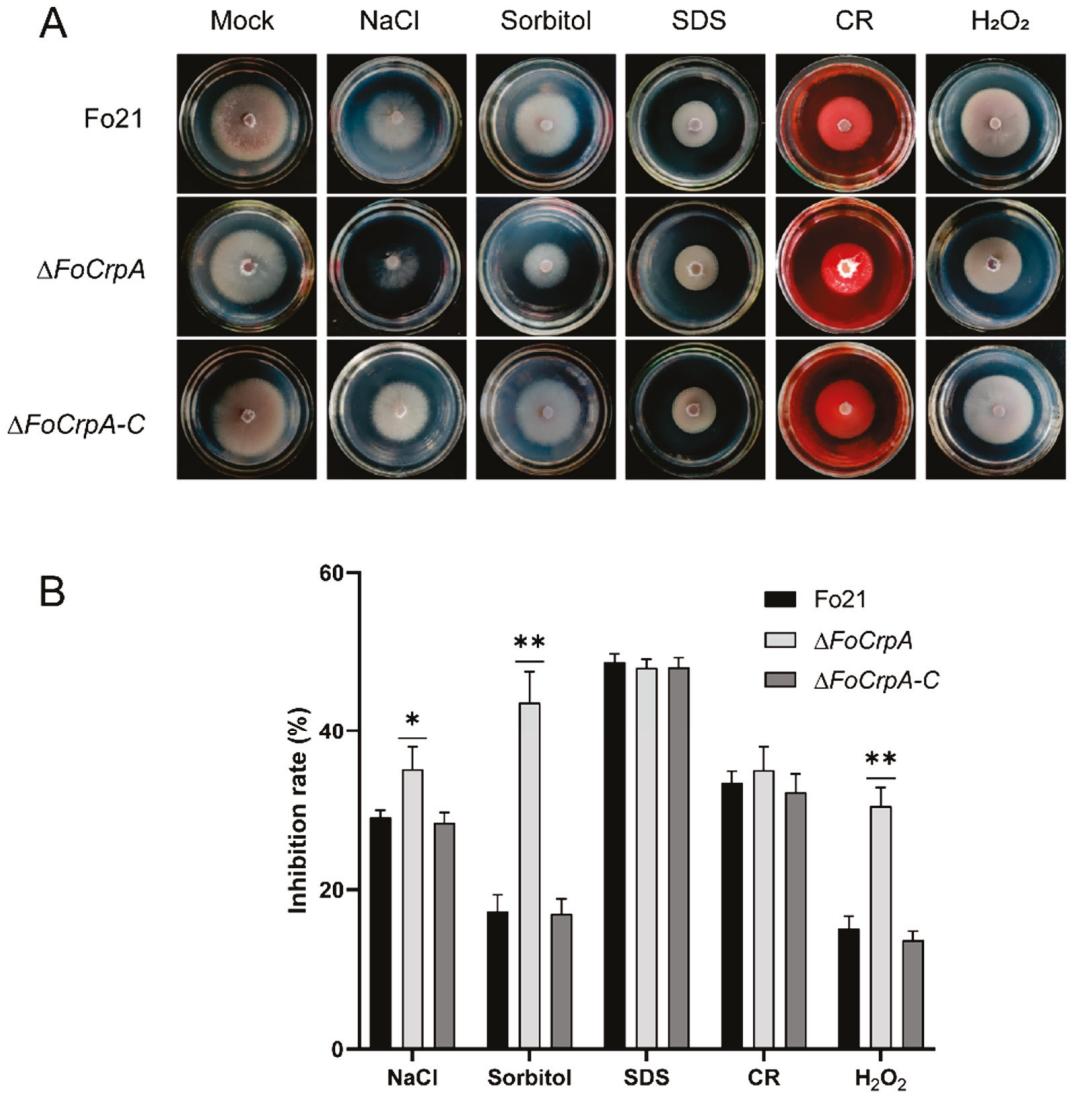


Figure 4. Deletion of *FoCrpA* affects various stress response. (**A**) Colony growth of Fo21, Δ*FoCrpA*, and Δ*FoCrpA-C* strains on PDA plates supplied with 0.5 M NaCl, 1 M sorbitol, 0.03% SDS, 1 mM Congo red, or 10 mM H_2O_2 after incubation of 5 days at 25 °C. (**B**) Inhibition rate of colony growth by different stress factors. Error bars represent the standard error of mean. Duncan's multiple range test was performed to determine significant difference,* $p \leq 0.05$,** $p \leq 0.01$.

3.5. Culture Filtrates Toxicity from FoCrpA Mutants

Toxicity assessment using culture filtrates from Fo21 and its mutants revealed significant suppression of rice seed germination and germ length compared to the PDB blank

control (Figure 5A). Notably, no statistically significant differences in these germination parameters were observed among filtrate-treated groups (Figure 5B,C). These findings demonstrate that *F. oxysporum* secretes germination-inhibitory metabolites into the extracellular milieu, while crucially establishing that *FoCrpA* does not participate in the biosynthesis or secretion of these toxic compounds.

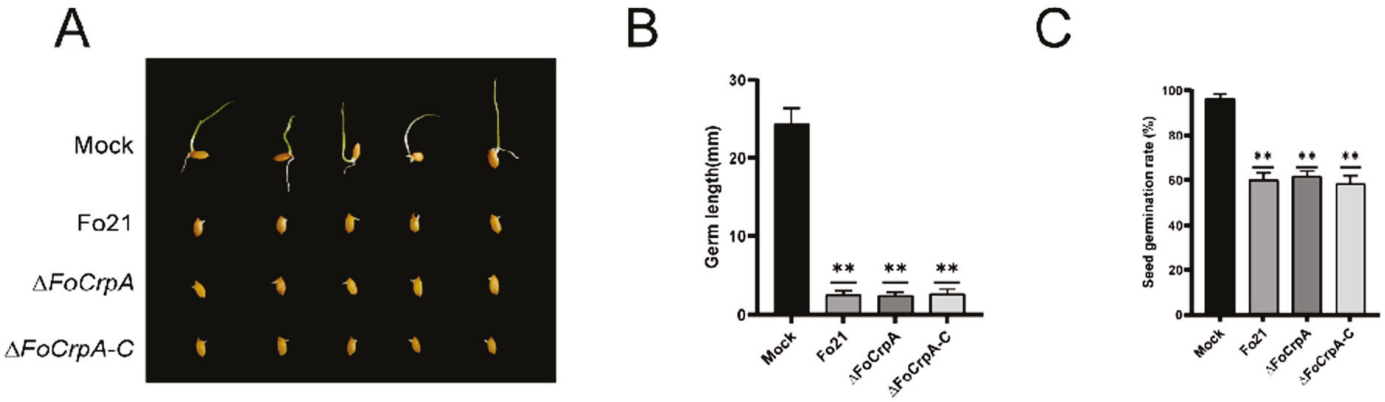


Figure 5. Toxicity of culture filtrates from Fo21 and *FoCrpA* mutants on the growth of rice seeds. (**A**) Culture filtrates of Fo21, Δ*FoCrpA*, and Δ*FoCrpA*-*C* strains caused defects in rice seeds growing. PDB medium without culture filtrates was used as the blank control. (**B**) Differences of germ length were examined after incubation under light at 25 °C for 5 days. (**C**) Seed germination rate was compared between WT Fo21 and its mutants after incubation under light at 25 °C for 5 days. Error bars represent the standard error of mean. Duncan's multiple range test was performed to determine significant difference,** $p \leq 0.01$.

3.6. Effect of FoCrpA Mutants on Pathogenicity

The infection–penetration assay conducted with Fo21, Δ*FoCrpA*, and Δ*FoCrpA*-C strains demonstrated comparable growth patterns across all strains when cultured on PDA plates overlaid with cellophane membranes. However, upon removal of the cellophane barrier followed by 24 h incubation, Fo21 and Δ*FoCrpA*-C strains exhibited normal tissue penetration capabilities, and Δ*FoCrpA* displayed significantly impaired colonization efficiency, as evidenced by reduced colony diameter (Figure 6A). This phenotypic divergence strongly suggests that *FoCrpA* plays a critical role in mediating host tissue invasion and penetration processes in *F. oxysporum*.

Pathogenicity assay results showed that most of the stems of rice seedlings inoculated with Fo21 and Δ*FoCrpA*-C strain turned brown, and some leaves turned yellow and wilted with a disease index of 74.30 and 76.37, respectively (Table 2). However, rice seedlings inoculated with Δ*FoCrpA* strain showed milder symptoms than those with Fo21 and Δ*FoCrpA*-C (Figure 6B,C). The results suggest that the deletion of *FoCrpA* reduces the pathogenicity of *F. oxysporum*.

Table 2. Disease index of the wild-type *F. oxysporum* Fo21 and mutant strains.

Stains	Disease Index
Fo21	74.30 ± 5.11 a
Δ*FoCrpA*	48.90 ± 4.85 b
Δ*FoCrpA*-C	76.37 ± 3.65 a

Mean ± SD was calculated from the results of three independent experiments. Values on the table followed by the same letter are not significantly different at $p \leq 0.01$ according to Duncan's multiple range test. Each experiment was replicated three times.

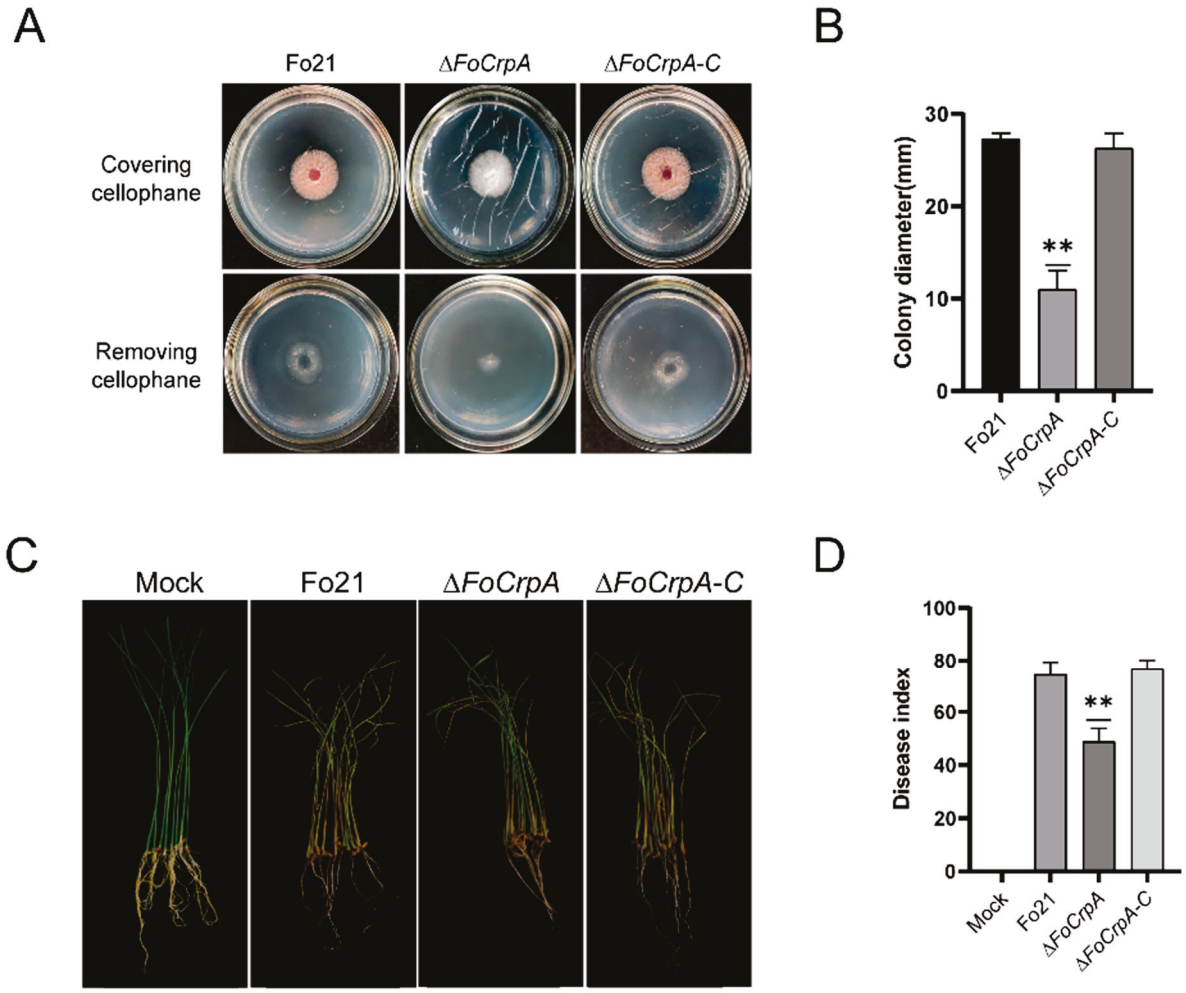


Figure 6. Pathogenicity of Fo21 and *FoCrpA* mutants on the stem base of rice seedlings. (**A**) Comparison of infection–penetration morphology caused by inoculation with Fo21, Δ*FoCrpA*, and Δ*FoCrpA-C* strains on cellophane membranes after 3 days of incubation at 25 °C. (**B**) Differences of colony diameter incubating 1 day at 25 °C after removing cellophane. (**C**) Disease symptoms on the stem base of rice seedlings observed at 14 dpi wtih Fo21, Δ*FoCrpA*, and Δ*FoCrpA-C* strains. (**D**) Disease index of rice seedlings was determined at 14 dpi wtih Fo21, Δ*FoCrpA*, and Δ*FoCrpA-C* strains. Fifty rice seedlings were inoculated per replication. Error bars represent the standard error of mean. Duncan's multiple range test was performed to determine significant difference,** $p \leq 0.01$.

4. Discussion

Copper performs a comprehensive and vital function in biological systems. It orchestrates the conformational and catalytic properties of numerous metalloproteins and enzymes, as typified by cytochrome oxidase and superoxide dismutase. Additionally, due to the propensity of copper to react with non-specific proteins and engender toxic manifestations, a highly intricate and elaborate system is requisite for the accomplishment of processes such as its assimilation, concentration regulation, translocation to specific protein-binding sites, and expulsion. This complex assemblage comprises small carriers, molecular chaperones, and active transporters [31]. From our established mutant library of *F. oxysporum*, a Cu-ATPase belonging to the HMA subfamily was discovered. It is speculated that it plays a role in the pathogenic process of *F. oxysporum*. The functional domain analysis of the encoded protein showed that the *FoCrpA* gene encoded protein belongs to the P-type heavy metal transport ATPase family, which is located on the plasma membrane. In *Aspergillus nidulans*, gene *CrpA* coordinates the transport of copper ions between the plasma membrane, endoplasmic reticulum, Golgi apparatus, and other organelles [32]. In

this study, by analyzing the biological functions of wild-type strain Fo21, knockout mutant Δ*FoCrpA*, and complementation mutant Δ*FoCrpA*-C, we investigated the function of the *FoCrpA* gene in *F. oxysporum*. It was found that Δ*FoCrpA* had no significant differences in mycelial dry weight, spore production, spore germination rate, and tolerance to cell membrane stress and cell wall stress compared to wild-type strains. However, compared with the wild-type strain, the colony and liquid color of Δ*FoCrpA* and its tolerance to high osmotic stress and oxidative stress decreased.

Cu-ATPase is involved in regulating the dynamic balance of copper metabolism, and copper is a cofactor for various copper-containing proteins, such as Cu/Zn superoxide dismutase (Cu/Zn SOD), laccase, etc. [33,34]. These enzymes are key enzymes in many biological reactions, such as Cu/Zn SOD, which can catalyze the decomposition of superoxide anions (O^{2-}) into less toxic hydrogen peroxide [35,36]. When pathogens invade host plants, it helps them resist the extracellular ROS produced by the host plants [37–39]. Moreover, laccase is involved in various biological processes such as fungal morphogenesis, pathogen infection, pigment synthesis, and stress response [40]. In this study, we found that compared with the wild-type strain Fo21, the colony and liquid color of the knockout mutant Δ*FoCrpA* and its tolerance to high osmotic stress and oxidative stress decreased, indicating that the *FoCrpA* gene can affect the pigment accumulation of *F. oxysporum* and its tolerance to exogenous osmotic stress and oxidative stress. Together with previous studies performed in other pathogenic fungi, such as in *Verticillium dahliae,* the knockout mutant Δ*VdSOD1* of the Cu/Zn *SOD* gene has reduced tolerance to oxidative stress [41]. In *Colletotrichum gloeosporiides,* the colony color of deletion mutant Δ*A2LAC1* changed from gray-black to nearly white, significantly reducing its pathogenicity to mangoes [42]. These results indicated that Cu-ATPase and other copper-containing proteins play a significant role in the growth and development of plant pathogenic fungi.

Our study also found that the deletion of the *FoCrpA* gene can lead to a decrease in the penetration ability of *F. oxysporum*, indicating that the *FoCrpA* gene plays an important regulatory role in the penetration ability of *F. oxysporum*. When *F. oxysporum* infects colonized host plants, it produces infection structures such as infection mats and attachment cells. In *Botrytis cinerea*, the deletion of the *BcCcc2* gene resulted in a diminished capacity to form attachment cells and infection mats, consequently impairing the fungus's ability to invade plant epidermal tissues [43]. It is hypothesized that the functionality of infection structures, including infection pads and attachment cells, might depend on unidentified and essential copper-containing proteins. Cu-ATPase potentially modulates the activity of these proteins. Similarly, the deletion of the *FoCrpA* gene can reduce the pathogenicity of *F. oxysporum*, indicating that the *FoCrpA* gene may affect the pathogenicity of *F. oxysporum* by reducing its invasion and penetration ability.

Excessive intracellular copper ions can affect cell structure, leading to disruptions in cell division and enzymatic systems, thereby affecting fungal growth. Cu-ATPase can eliminate excess copper ions from the cell and alleviate the inhibitory effect of excessive copper ions on fungal growth. For example, after knocking out Cu-ATPase *CrpA* in *Aspergillus fumigatus*, the strain is more sensitive to high concentrations of copper ions [44]. After knocking out the *FgCrpA* gene of *F. graminearum*, the knockout mutant showed inhibition of hyphal growth, decreased spore production and germination rate, reduced tolerance to reactive oxygen species, and decreased production of toxin deoxynivalenol under copper ion stress compared to the wild type [45]. Therefore, this study conducted colony growth experiments under copper stress on wild-type strains, Δ*FoCrpA* strains, and Δ*FoCrpA*-C strains. It was found that compared with the wild-type, Δ*FoCrpA* was more sensitive to copper ions, and the colony diameter of Δ*FoCrpA* under the same copper ion concentration was smaller, and the mycelial growth was sparser. When copper ions

increased to a certain concentration, Δ*FoCrpA* almost did not grow, while the wild-type strain could continue to grow. The deletion of the *FoCrpA* gene can exacerbate the inhibitory effect of excessive copper ions on fungus growth.

Overall, the *FoCrpA* gene is involved in osmotic and oxidative stress, affecting the invasion and penetration ability and pathogenicity of *F. oxysporum*. The *FoCrpA* study identifies copper homeostasis as a key vulnerability in *F. oxysporum*. Targeting this system—via Cu-ATPase inhibitors, optimized copper fungicides, or host-enhanced ROS—could reduce fungal virulence and improve crop resistance sustainably. *FoCrpA* also offers biotechnological potential: gene editing (e.g., CRISPR) or plant-derived inhibitors could engineer wilt-resistant crops, while structure-guided antifungal agents may selectively block fungal copper transport with minimal environmental impact. Crucially, *FoCrpA* regulates osmotic/oxidative stress adaptation and infection structures, making it pivotal for both understanding pathogenesis and developing control strategies for rice seedling blight. Future work should validate field applications, explore copper-immune synergies, and refine targeted inhibitors to bridge lab discoveries with agricultural practice.

Author Contributions: C.W., L.W. and J.Z. contributed to the study conception and design; C.W. and L.W. performed the experimental design; C.W. and L.W. wrote the manuscript draft; C.W., L.W., X.Z., L.H., Q.L., R.R., A.L., X.L., T.X. and P.G. conceived and performed all experiments; C.W., L.W., X.X., Z.N. and C.L. analyzed the results and corresponding data. All authors have read and agreed to the published version of the manuscript.

Funding: This research was funded by the Key Research and Development Program of Heilongjiang Province (GA23B010), National Key Research and Development Program Project (2023YFD1400205-3), Green Plant Protection Project in Heilongjiang Province (2130108), Key R&D Program Project of Heilongjiang Province (2023ZX02B0502), special project of central leading local science and technology development (ZY18C08), nature fund project of Heilongjiang (C2017032), Major Project of Heilongjiang Province Applied Technology Research and Development Plan (GA19B104) and the Natural Science Foundation of Heilongjiang Province of China (LH2022C022).

Institutional Review Board Statement: Not applicable.

Informed Consent Statement: Not applicable.

Data Availability Statement: The data presented in this study are available on request from the corresponding author.

Acknowledgments: We thank Zhang Shihong, Qin Qingming, and Li Guihua from Jilin University, for providing *Agrobacterium tumefaciens* AGL-1, *Escherichia coli* DH5α, plasmid pXEH and pSUL.

Conflicts of Interest: The authors declare no conflicts of interest.

References

1. Khepar, V.; Sidhu, A.; Sharma, A.B. Nanomaterized Zinc Sulfide-Meerschaum Biomatrix Efficiently Suppressed *Fusarium verticilloides* with Augmented Rice Seed Quality Benefits during Storage. *Pest Manag. Sci.* **2023**, *79*, 244–256. [CrossRef] [PubMed]
2. Gaire, S.P.; Zhou, X.G.; Zhou, Y.; Shi, J.; Jo, Y.K. Identification and distribution of fungal pathogens associated with seedling blight of rice in the southern United States. *Plant Pathol.* **2023**, *72*, 76–88. [CrossRef]
3. Li, Y.G.; Zhang, X.; Zhang, R.; Liu, J.X.; Ali, E.; Ji, P.; Pan, H.Y. Occurrence of seedling blight caused by *Fusarium tricinctum* on rice in China. *Plant Dis.* **2019**, *103*, 1789. [CrossRef]
4. Wang, S.; Sun, L.; Li, W.Q.; Liu, J.X.; Li, Y.G.; Wei, D. First report of seedling blight caused by *Fusarium redolens* on rice in northeast China. *Plant Dis.* **2019**, *103*, 1418. [CrossRef]
5. Wang, M.; Wei, P.; Cao, M.; Zhu, L.; Lu, Y. First Report of Rice Seedling Blight Caused by *Burkholderia plantarii* in North and Southeast China. *Plant Dis.* **2016**, *100*, 645. [CrossRef]
6. Gaire, S.P.; Zhou, X.-G.; Jo, Y.-K.; Shi, J. First Report of *Rhizoctonia solani* AG-4 Causing Seedling Disease in Rice. *Plant Dis.* **2020**, *104*, 1546. [CrossRef]

7. Gaire, S.-P.; Zhou, X.-G.; Jo, Y.-K. Sterile white basidiomycete fungus *Marasmius graminum*: A new pathogen causing seedling blight in rice. *Plant Dis.* **2021**, *105*, 702. [CrossRef] [PubMed]
8. Liu, J.; Zhang, R.; Xu, C.; Liu, C.; Zheng, Y.; Zhang, X.; Liu, S.; Li, Y. Characterisation of *Pythium aristosporum* Oomycete—A novel pathogen causing rice seedling blight in China. *J. Fungi* **2022**, *8*, 890. [CrossRef]
9. El-Shafey, R.A.S.; Attia, K.A.; Mostafa, F.A.; Elamawi, R.M. Incidence and molecular identification of *Cochliobolus carbonum* as causal organism of rice seedling blight. *Beni-Suef Univ. J. Basic Appl. Sci.* **2018**, *7*, 652–662. [CrossRef]
10. Liu, J.X.; Cai, Y.N.; Jiang, W.Y.; Li, Y.G.; Zhang, Q.F.; Pan, H.Y. Population structure and genetic diversity of fungi causing rice seedling blight in northeast China based on microsatellite markers. *Plant Dis.* **2020**, *104*, 868–874. [CrossRef]
11. Ma, B.; Wang, J.; Liu, C.; Hu, J.; Tan, K.; Zhao, F.; Yuan, M.; Zhang, J.; Gai, Z. Preventive effects of fluoro-substituted benzothiadiazole derivatives and chitosan oligosaccharide against the rice seedling blight induced by *Fusarium oxysporum*. *Plants* **2019**, *8*, 538. [CrossRef] [PubMed]
12. Ochi, A.; Konishi, H.; Ando, S.; Sato, K.; Yokoyama, K.; Tsushima, S.; Yoshida, S.; Morikawa, T.; Kaneko, T.; Takahashi, H. Management of bakanae and bacterial seedling blight diseases in nurseries by irradiating rice seeds with atmospheric plasma. *Plant Pathol.* **2017**, *66*, 67–76. [CrossRef]
13. Shenashen, M.; Derbalah, A.; Hamza, A.; Mohamed, A.; El Safty, S. Antifungal activity of fabricated mesoporous alumina nanoparticles against root rot disease of tomato caused by *Fusarium oxysporium*. *Pest Manag. Sci.* **2017**, *73*, 1121–1126. [CrossRef]
14. Cao, Y.; Ding, W.; Liu, C. Unraveling the metabolite signature of endophytic *Bacillus velezensis* strain showing defense response towards *Fusarium oxysporum*. *Agronomy* **2021**, *11*, 683. [CrossRef]
15. Ren, J.G.; Wang, J.L.; Cai, J. Effects of Fenaminosulf on Growth of Pepper (*Capsicum annuum* L.), Microbial Communities and Enzymatic Activities of the Soil Infested with *Fusarium oxysporum*. *Indian J. Pharm. Sci.* **2021**, *83*, 163–169. [CrossRef]
16. Yruela, I. Copper in Plants: Acquisition, Transport and Interactions. *Funct. Plant Biol.* **2009**, *36*, 409–430. [CrossRef] [PubMed]
17. Arredondo, M.; Núñez, M.T. Iron and Copper Metabolism. *Mol. Asp. Med.* **2005**, *26*, 313–327. [CrossRef]
18. Tapiero, H.; Townsend, D.M.; Tew, K.D. Trace Elements in Human Physiology and Pathology. Copper. *Biomed. Pharmacother.* **2003**, *57*, 386–398. [CrossRef]
19. Gao, T.; Shi, L.; Zhang, T.; Ren, A.; Jiang, A.; Yu, H.; Zhao, M. Cross talk between calcium and reactive oxygen species regulates hyphal branching and ganoderic acid biosynthesis in *Ganoderma lucidum* under copper stress. *Appl. Environ. Microbiol.* **2018**, *84*, e00438-18. [CrossRef]
20. Wang, C.; Xiao, X.Z.; Wei, F.; Qiu, J.; Wu, M.; Gao, H.H.; Yang, W.F.; Luo, S.Q. Cloning and expression analysis of copper transporter genes in rubber tree (*Hevea brasiliensis* Müll. Arg.). *Plant Physiol. J.* **2016**, *52*, 1389–1396. [CrossRef]
21. Burkhead, J.L.; Gogolin Reynolds, K.A.; Abdel-Ghany, S.E.; Cohu, C.M.; Pilon, M. Copper homeostasis. *New Phytol.* **2009**, *182*, 799–816. [CrossRef]
22. Boutigny, S.; Sautron, E.; Finazzi, G.; Rivasseau, C.; Frelet-Barrand, A.; Pilon, M.; Rolland, N.; Seigneurin-Berny, D. HMA1 and PAA1, two chloroplast-envelope PIB-ATPases, play distinct roles in chloroplast copper homeostasis. *J. Exp. Bot.* **2014**, *65*, 1529–1540. [CrossRef] [PubMed]
23. Seigneurin-Berny, D.; Gravot, A.; Auroy, P.; Mazard, C.; Kraut, A.; Finazzi, G.; Grunwald, D.; Rappaport, F.; Vavasseur, A.; Joyard, J.; et al. HMA1, a new Cu-ATPase of the chloroplast envelope, is essential for growth under adverse light conditions. *J. Biol. Chem.* **2006**, *281*, 2882–2892. [CrossRef] [PubMed]
24. Saitoh, Y.; Izumitsu, K.; Tanaka, C. Phylogenetic analysis of heavy-metal ATPases in fungi and characterization of the copper-transporting ATPase of *Cochliobolus heterostrophus*. *Mycol. Res.* **2009**, *113*, 737–745. [CrossRef] [PubMed]
25. Parisot, D.; Dufresne, M.; Veneault, C.; Laugé, R.; Langin, T. Clap1, a gene encoding a copper-transporting ATPase involved in the process of infection by the phytopathogenic fungus *Colletotrichum lindemuthianum*. *Mol. Genet. Genom.* **2002**, *268*, 139–151. [CrossRef]
26. Yang, K.; Shadkchan, Y.; Tannous, J.; Landero Figueroa, J.A.; Wiemann, P.; Osherov, N.; Wang, S.; Keller, N.P. Contribution of ATPase copper transporters in animal but not Plant virulence of the crossover pathogen *Aspergillus flavus*. *Virulence* **2018**, *9*, 1273–1286. [CrossRef]
27. Mullins, E.D.; Chen, X.; Romaine, P.; Raina, R.; Geiser, D.M.; Kang, S. Agrobacterium-Mediated transformation of *Fusarium oxysporum*: An efficient tool for insertional mutagenesis and gene transfer. *Phytopathology* **2001**, *91*, 173–180. [CrossRef]
28. Li, M.-H.; Xie, X.-L.; Lin, X.-F.; Shi, J.-X.; Ding, Z.-J.; Ling, J.-F.; Xi, P.-G.; Zhou, J.-N.; Leng, Y.; Zhong, S.; et al. Functional characterization of the gene FoOCH1 encoding a putative α-1,6-mannosyltransferase in *Fusarium oxysporum* f. sp. Cubense. *Fungal Genet. Biol.* **2014**, *65*, 1–13. [CrossRef]
29. Livak, K.J.; Schmittgen, T.D. Analysis of relative gene expression data using Real-Time Quantitative PCR and the $2^{-\Delta\Delta C}{}_{T}$ method. *Methods* **2001**, *25*, 402–408. [CrossRef]
30. Jiang, W.; Liu, J.; He, Y.; Payizila, A.; Li, Y. Biological control ability and antifungal activities of *Bacillus velezensis* Bv S3 against *Fusarium oxysporum* that causes rice seedling blight. *Agronomy* **2024**, *14*, 167. [CrossRef]

31. Inesi, G. Molecular features of copper binding proteins involved in copper homeostasis. *IUBMB Life* **2017**, *69*, 211–217. [CrossRef] [PubMed]
32. Antsotegi-Uskola, M.; Markina-Iñarrairaegui, A.; Ugalde, U. Copper resistance in *Aspergillus nidulans* relies on the P(I)-Type ATPase CrpA, regulated by the transcription factor AceA. *Front. Microbiol.* **2017**, *8*, 912. [CrossRef] [PubMed]
33. Probst, C.; Garcia-Santamarina, S.; Brooks, J.T.; Van Der Kloet, I.; Baars, O.; Ralle, M.; Thiele, D.J.; Alspaugh, J.A. Interactions between copper homeostasis and the fungal cell wall affect copper stress resistance. *PLoS Pathog.* **2022**, *18*, e1010195. [CrossRef] [PubMed]
34. Antsotegi-Uskola, M.; Markina-Iñarrairaegui, A.; Ugalde, U. New insights into copper homeostasis in filamentous fungi. *Int. Microbiol.* **2020**, *23*, 65–73. [CrossRef]
35. Li, C.; Li, Y.; Ding, C. The role of copper homeostasis at the host-pathogen axis: From bacteria to fungi. *Int. J. Mol. Sci.* **2019**, *20*, 175. [CrossRef]
36. García-Santamarina, S.; Thiele, D.J. Copper at the fungal pathogen-host axis. *J. Biol. Chem.* **2015**, *290*, 18945–18953. [CrossRef]
37. Robinson, J.R.; Isikhuemhen, O.S.; Anike, F.N. Fungal-metal interactions: A review of toxicity and homeostasis. *J. Fungi* **2021**, *7*, 225. [CrossRef]
38. Beauchamp, C.; Fridovich, I. Superoxide dismutase:improved assays and an assay applicable to acrylamide gels. *Anal. Biochem.* **1971**, *44*, 276–287. [CrossRef]
39. Broxton, C.N.; Culotta, V.C. SOD enzymes and microbial pathogens: Surviving the oxidative storm of infection. *PLoS Pathog.* **2016**, *12*, e1005295. [CrossRef]
40. Janusz, G.; Pawlik, A.; Świderska-Burek, U.; Polak, J.; Sulej, J.; Jarosz-Wilkołazka, A.; Paszczyński, A. Laccase properties, physiological functions, and evolution. *Int. J. Mol. Sci.* **2020**, *21*, 966. [CrossRef]
41. Tian, L.; Li, J.; Huang, C.; Zhang, D.; Xu, Y.; Yang, X.; Song, J.; Wang, D.; Qiu, N.; Short, D.P.G.; et al. Cu/Zn superoxide dismutase (VdSOD1) mediates reactive oxygen species detoxification and modulates virulence in *Verticillium dahliae*. *Mol. Plant Pathol.* **2021**, *22*, 1092–1108. [CrossRef] [PubMed]
42. Wei, Y.; Pu, J.; Zhang, H.; Liu, Y.; Zhou, F.; Zhang, K.; Liu, X. The laccase gene (LAC1) is essential for *Colletotrichum gloeosporioides* development and virulence on mango leaves and fruits. *Physiol. Mol. Plant Pathol.* **2017**, *99*, 55–64. [CrossRef]
43. Saitoh, Y.; Izumitsu, K.; Morita, A.; Tanaka, C. A copper-transporting ATPase BcCCC2 is necessary for pathogenicity of *Botrytis cinerea*. *Mol. Genet. Genom.* **2010**, *284*, 33–43. [CrossRef]
44. Cai, Z.; Du, W.; Zhang, Z.; Guan, L.; Zeng, Q.; Chai, Y.; Dai, C.; Lu, L. The *Aspergillus fumigatus* transcription factor AceA is involved not only in Cu but also in Zn detoxification through regulating transporters CrpA and ZrcA. *Cell. Microbiol.* **2018**, *20*, e12864. [CrossRef] [PubMed]
45. Liu, X.; Jiang, Y.; He, D.; Fang, X.; Xu, J.; Lee, Y.W.; Keller, N.P.; Shi, J. Copper tolerance mediated by *FgAceA* and *FgCrpA* in *Fusarium graminearum*. *Front. Microbiol.* **2020**, *11*, 1392. [CrossRef]

Disclaimer/Publisher's Note: The statements, opinions and data contained in all publications are solely those of the individual author(s) and contributor(s) and not of MDPI and/or the editor(s). MDPI and/or the editor(s) disclaim responsibility for any injury to people or property resulting from any ideas, methods, instructions or products referred to in the content.

Journal of Fungi

MDPI

Article

Omics-Based Comparison of Fungal Virulence Genes, Biosynthetic Gene Clusters, and Small Molecules in *Penicillium expansum* and *Penicillium chrysogenum*

Holly P. Bartholomew [1,2,*], Christopher Gottschalk [3], Bret Cooper [4], Michael R. Bukowski [5], Ronghui Yang [4], Verneta L. Gaskins [1], Dianiris Luciano-Rosario [1], Jorge M. Fonseca [1] and Wayne M. Jurick II [1]

[1] Food Quality Laboratory, U.S. Department of Agriculture, Agricultural Research Service, Beltsville Agricultural Research Center, Beltsville, MD 20705, USA
[2] Invasive Insect Biocontrol and Behavior Laboratory, U.S. Department of Agriculture, Agricultural Research Service, Beltsville Agricultural Research Center, Beltsville, MD 20705, USA
[3] Innovative Fruit Production, Improvement, and Protection, Appalachian Fruit Research Station, U.S. Department of Agriculture, Agricultural Research Service, Kearneysville, WV 25430, USA
[4] Soybean Genomics and Improvement Laboratory, U.S. Department of Agriculture, Agricultural Research Service, Beltsville Agricultural Research Center, Beltsville, MD 20705, USA
[5] Methods and Application of Food Composition Laboratory, U.S. Department of Agriculture, Agricultural Research Service, Beltsville Human Nutrition Research Center, Beltsville, MD 20705, USA
* Correspondence: holly.bartholomew@usda.gov

Abstract: *Penicillium expansum* is a ubiquitous pathogenic fungus that causes blue mold decay of apple fruit postharvest, and another member of the genus, *Penicillium chrysogenum*, is a well-studied saprophyte valued for antibiotic and small molecule production. While these two fungi have been investigated individually, a recent discovery revealed that *P. chrysogenum* can block *P. expansum*-mediated decay of apple fruit. To shed light on this observation, we conducted a comparative genomic, transcriptomic, and metabolomic study of two *P. chrysogenum* (404 and 413) and two *P. expansum* (Pe21 and R19) isolates. Global transcriptional and metabolomic outputs were disparate between the species, nearly identical for *P. chrysogenum* isolates, and different between *P. expansum* isolates. Further, the two *P. chrysogenum* genomes revealed secondary metabolite gene clusters that varied widely from *P. expansum*. This included the absence of an intact patulin gene cluster in *P. chrysogenum*, which corroborates the metabolomic data regarding its inability to produce patulin. Additionally, a core subset of *P. expansum* virulence gene homologues were identified in *P. chrysogenum* and were similarly transcriptionally regulated in vitro. Molecules with varying biological activities, and phytohormone-like compounds were detected for the first time in *P. expansum* while antibiotics like penicillin G and other biologically active molecules were discovered in *P. chrysogenum* culture supernatants. Our findings provide a solid omics-based foundation of small molecule production in these two fungal species with implications in postharvest context and expand the current knowledge of the *Penicillium*-derived chemical repertoire for broader fundamental and practical applications.

Keywords: apple; blue mold; *Penicillium expansum*; *Penicillium chrysogenum*; metabolomics; secondary metabolites; patulin; transcriptomics; whole genome sequencing; comparative genomics

1. Introduction

Blue mold decay, caused primarily by *Penicillium expansum*, is a major contributor to pome fruit losses, such as apple or pear, during postharvest storage [1]. Decay is initiated when conidia enter wounds or natural openings in the fruit. Once inside the fruit, the fungi cause watery, brown lesions that radiate from the initial wound. Additionally, mycotoxins like patulin are produced by the fungus during infection. Patulin is a genotoxic, cytotoxic, and carcinogenic compound, thus the mandatory limits in many countries are very low for fruit and fruit products [2–6]. Given that fungal rot negatively impacts the fruit quality and, in cases of mycotoxin producers, renders the fruit unsafe for human consumption, measures to mitigate rot are of utmost importance. However, current industry practices for fungal postharvest decay management are not sufficient in fully preventing blue mold decay. This issue is further compounded by increasing numbers of reports concerning fungicide resistance to all four fungicides utilized in the U.S. apple industry [7–12]. Moreover, many countries have lowered the allowable level of fungicide residues on imported fruit thus restricting their use. Additional mitigation strategies are needed to effectively address this growing agricultural challenge.

P. expansum causes blue mold decay through numerous virulence factors [1,13]. For example, patulin production impacts virulence, as demonstrated through experiments using genetically defined mutants in *P. expansum* and in pharmacologically-based studies [14–16]. Other virulence factors associated with blue mold include polygalacturonases (e.g., PepG1), pH modifiers (e.g., PacC), and effectors (e.g., PePrt, NLP1, Scp) [13,17–20]. Additionally, many proteins (e.g., Blistering1, LaeA, CreA, SntB, PacC, and VeA) are known to regulate these virulence factors, modulate secondary metabolite production, alter ambient pH, and impact general catabolism [14,20–25]. Together, these diverse activities act in an orchestrated manner to facilitate decay in the fruit host.

Penicillium spp. occupy different ecological niches and serve as human pathogens, saprophytes, and plant pathogens [26]. Unlike *P. expansum*, *Penicillium chrysogenum* does not cause decay when inoculated into wounded apple fruit [13,27]. *P. chrysogenum* has been exploited by industry for production of the widely used antibiotic, penicillin [28]. Indeed, the penicillin biosynthetic gene cluster was the first fungal biosynthetic gene cluster described, and extensive research has been performed to optimize its production and to understand *P. chrysogenum* metabolism [29].

Development of novel treatments to combat postharvest fungal phytopathogens is critical with the rise of fungicide resistance strains. One increasingly popular approach has been the use of biocontrol organisms and their natural products for the development of new biorationales. Biocontrol agents are successful through a variety of functional mechanisms, including direct microbial antagonism, reduction of nutrient availability and induction of host defense responses [30–32]. A recent study by our group found that two *P. chrysogenum* isolates, 404 and 413, were non-pathogenic in apple fruit, and significantly reduced blue mold decay when co-inoculated with two highly virulent *P. expansum* strains, Pe21 and R19 [27]. Because of these findings, there is great appeal to further understand the potential of these two isolates to antagonize *P. expansum*. However, investigation into their small molecule repertoire, toxin production potential, and virulence mechanism is necessary to determine their suitability for use in a postharvest context.

In this study, we investigated two *P. chrysogenum* isolates that cannot cause decay of apple fruit, 404 and 413, at the genomic, transcriptomic, and metabolomic levels in vitro, and compared them with two highly aggressive *P. expansum* R19 and Pe21 strains that cause significant blue mold decay. Through these comparative studies, insights into *P. expansum* virulence, patulin production, and unique genes and metabolites of both species were found. Further, the described strains may be useful for genetic manipulation and exploitation

to produce compounds of interest and/or as biocontrol antagonists that can outcompete pathogenic blue mold strains.

2. Materials and Methods

2.1. Fungal Isolate Propagation and Sample Inoculation

Four fungal strains, *Penicillium expansum* R19, *P. expansum* Pe21, *Penicillium chrysogenum* 404, and *P. chrysogenum* 413 were obtained from previous studies [27,33,34], Each were grown on potato dextrose agar (PDA; Thermo Fisher Scientific, Waltham, MA, USA) plates for 7 days at 25 °C. Conidia were washed from the plate using Tween-treated water (0.1% Tween-20, Sigma Aldrich, St. Louis, MO, USA) and adjusted to 1×10^6 conidia/mL. Flasks containing 50 mL of potato dextrose broth (PDB; Thermo Fisher Scientific, Waltham, MA, USA) were individually inoculated with 100 µL of conidial suspension. Cultures were grown for 7 days, shaking at 25 °C (125 RPM; Innova 42R, Eppendorf, Hamburg, Germany). Each flask was vacuum filtered through a sterile 0.2 µM cellulose acetate filter. The mycelial mat was aseptically transferred to a 50 mL conical tube. Filtered broth was transferred separately to 50 mL conical tubes. Mycelial mats were weighed for each sample, and pH was measured for each broth culture (Figure S1). All broth and mycelial mats were immediately submerged in liquid N_2 and stored at −80 °C. Broth samples were subsequently used for metabolite extraction for LC-MS and HPLC, whereas the mycelial mats were used for both DNA and RNA extractions for genomic DNA and RNA sequencing.

2.2. Fungal Genomic DNA Extraction

High-quality genomes of Pe21, 404, and 413, were produced to compare to each other and to the existing *P. expansum* R19 genome (NCBI GCA_004302965.1). Mycelial mats of Pe21, 404 and 413 were ground to a fine powder using a sterile mortar and pestle with liquid N_2. DNA was extracted using a phenol-chloroform extraction method (Pacific Biosciences, Menlo Park, CA) with an added RNAse (Thermo Fisher Scientific, Waltham, MA, USA) treatment for 30 min at 37 °C. DNA was resuspended in EB buffer, then visualized for quality via agarose gel electrophoresis (0.8% agarose, 90 volts for 45 min). Samples were quantified using Qubit (Invitrogen Qubit dsDNA H5, Waltham, MA, USA) And stored at −80 °C.

2.3. Oxford Nanopore Technology Sequencing

High-molecular weight (HMW) DNA obtained from the isolate samples of Pe21, 404, and 413 was used to prepare Oxford Nanopore Technologies (ONT; Oxford, UK) sequencing libraries using the V14 kit enabled with duplex reads (SQK-LSK114). Generated libraries were evaluated for quantity and quality using a TapeStation 4150 (Agilent, Santa Clara, CA, USA) with the genomic DNA ScreenTape and ladder for fragments >60 Kb. Libraries with >10–20 fmols of 50 Kb or greater fragments were chosen for sequencing on a ONT MinION device. All sequencing and preparation was done in-house. Each respective sample was sequenced on its own ONT R10.4.1 flow cell for ~72 h with reads <1000 bp filtered from the output using ONT sequencing software MinKNOW (v23.04.6). Real-time basecalling was disabled and POD5 files were the chosen output format. The resulting POD5 files were used as input into ONT pytorch basecaller, Dorado (v0.3.3), using the high accuracy (HAC) basecalling model dna_r10.4.1_e8.2_400bps_hac@v4.2.0 with default settings for the Pe21 sample and the super accurate (SUP) basecalling model dna_r10.4.1_e8.2_400bps_sup@v4.2.0 with default settings for the 404 and 413 samples. Additionally, all POD5s were rebasecalled for duplex reads using the Dorado duplex function. The resulting output bam files were sorted for duplex and simplex reads using samtools (v1.7) and converted into fastq files [35]. The fastq files were then evaluated for read length and base pair quality calls

using NanoPlot (v1.40.0) [36] and then processed for adapter sequences using Porechop (v0.2.4; https://github.com/rrwick/Porechop (accessed on 1 October 2023)) with default settings. Lastly, the adapter-removed fastq files were additionally filtered for reads ≥20 kb using NanoFilt (v2.8.0) [37].

2.4. Fungal Total RNA Extraction

Mycelial mats from four vacuum filtered liquid cultures of R19, Pe21, 404, and 413 were flash-frozen in liquid N_2, then ground with mortar and pestle. Each sample (approximately 0.1 mg/ powdered sample) was then processed with the TRIzol reagent protocol (Invitrogen) with slight modification. Briefly, a 25:24:1 phenol:chloroform:isoamyl alcohol (PCI; Sigma-Aldrich, St. Louis, MO, USA) step was added after the initial separation, where the aqueous layer from the TRIzol separation step was mixed 1:1 with PCI, incubated 5 min at 4 °C, centrifuged at 13,500× *g* for 15 min, and aqueous phase transferred for subsequent precipitation and washing steps per manufacturer's protocol. RNA was dissolved in 50 µL DEPC water and heated for 30 min at 65 °C. Initial quantification and quality of each sample was performed using a Nanodrop spectrophotometer (Thermo Fisher Scientific, Waltham, MA, USA) and by agarose gel electrophoresis (1% agarose, 90 volts, 30 min). Each sample was then stored at −80 °C until sequenced.

2.5. RNA Sequencing

RNA samples were sent for RNA sequencing at Novogene (Sacramento, CA, USA). Sample quality was assessed with Agilent 5400, then library prep (polyA enrichment), and finally short read (150 bp reads) paired-end sequencing was performed with a NovaSeq platform. Each strain had four individual RNA sequencing (RNA-seq) libraries generated.

2.6. Fungal Genome Assembly and Annotation

The sequencing provided opportunity to evaluate multiple assembly methods using the emergent duplex reads, simplex reads, and combined read types. For this, the focus was on 404 as it was the first sample sequenced. The first assembly was completed with Flye (v2.9.2) [38] using the --nano-hq parameter and only the simplex reads used. We also ran Flye in a module-based approach with the initial assembly from simplex reads used as input followed by the Flye -resume-from-polish module with the duplex reads. The second assembly was with HiFiasm (v0.19.5) [39] using the duplex reads the HiFi input and the simplex reads in the -UL input for ultra-long reads. The third method utilized Verkko (v1.4.1) [40] with the duplex reads used as --hifi inputs and the simplex reads as --nano inputs. If the assembler required estimated genome size, a value of 32.4 Mb was used as input. Comparisons of the resulting assemblies were performed using genometools seqstat (v.1.6.2; http://genometools.org/ (accessed on 1 October 2023)).

For the 413 genome, we followed the same approach of using Flye (v2.9.2), followed by Flye -resume-from-polishing step. However, the assembly was more fragmented than 404 and thus we performed homology-based scaffolding. The homology-based scaffolded utilized the RagTag software (v2.1.0) [41] with the 404 assembly used as a guide. For the Pe21 genome, ONT sequencing yielded few duplex reads and thus was assembled only from the simplex reads using Flye. We also used the homology based scaffolding approach for Pe21 with a separate assembly of a mutant Pe21 strain Pe_T1 (unpublished) followed by RagTag patch to gap fill using the NCBI GCA_000769735.1 accession (Pe21; synonym D1 strain) [34]. Genome and scaffolding stats were assessed using genometools seqstat and BUSCO (v5.3.1) [42] with the eurotiales_odb10 database. We further filtered all assemblies for sequencing artifacts and contig fragments with lengths <100 Kb and coverage that was >2 fold of the four longest contigs using seqtk (v1.4; https://github.com/lh3/seqtk (accessed on 1 October 2023)) prior to scaffolding.

In addition to the three genomes of Pe21, 404, and 413, we additionally set out to annotate the existing *P. expansum* R19 genome (NCBI GCA_004302965.1). The aim was to generate annotations for all four assemblies using the same extensive approach previously used for *Fusarium* and *P. fuscoglaucum* genomes [43,44]. The resulting assemblies were first annotated for transposable elements and other repetitive features using RepeatModeler (v.2.0.1) [45] and RepeatMasker (v.4.1.1) [46] hosted on the GenSAS server (v6.0) [47]. GenSAS' consensus repeat annotation was then invoked to generate a GFF file that combined the features identified by both RepeatModeler and RepeatMasker along with soft masked and hard masked fasta files. The RNA-seq files were first processed to trim adapter sequences and low-quality bases using fastp (v0.23.2) [48]. The processed reads files were then mapped to the hard masked sequences for each respective assembly using HiSAT2 (v2.2.1) [49] using the –max-intronlen setting of 2000 bp. The resulting alignment sam files were then sorted, indexed, and merged using SAMtools. The merged mappings were then used as input in StringTie2 de novo transcriptome assembled using default settings (v2.2.0) [50]. The resulting annotation file (gtf) was used as input into gffread (v0.12.7) [51] along with the hard masked sequence file to extract transcript sequences to serve as pseudo expression sequence tags (ESTs) evidence during ab initio gene annotation. For the ab initio gene annotation, we used the Maker (v.3.01.03) [52] pipeline with the pseudo-EST and protein evidence from *P. camemberti* from NCBI (GCA_000513335.1) [53] as inputs in the first round of annotation for Pe21 and 404. Following the first round of evidence-based Maker annotation, we trained Augustus (v.3.4.0) [54] and SNAP (v2006-07-28) [55]. We then ran a second round of Maker using the trained Augustus and SNAP models for ab initio annotation followed by a second round of training for each gene predictor. A final round of Maker annotation was performed, and the resulting predicted annotations were assigned functional annotation using BLASTP (v2.14.0) [56] and Interproscan (v5.61-90.3) [57]. For R19 and 413, we employed only a single round of Maker annotation using the Augustus and SNAP models generated for Pe21 and 404, respectively. We also included strain-specific pseudo-ESTs and the same *P. camemberti* protein fasta as additional evidence into the Maker pipeline. Non-coding genes (e.g., rRNA, tRNA) were annotated using the Infernal software suite (v1.1.4) [58] with default inputs. Lastly, annotation quality and descriptive statistics were calculated using BUSCO with the eurotiales_odb10 database and AGAT (v0.9.1; https://github.com/NBISweden/AGAT#publication-using-agat (accessed on 1 October 2023)), respectively.

2.7. Comparative Genomics

To determine regions of synteny and collinearity between the four assembled genomes, the python MCScanX pipeline (https://github.com/tanghaibao/jcvi/wiki/MCscan-(Python-version) (accessed on 1 October 2023)) [59] approach was employed. Here, the annotation gff files for each genome was converted to bed format using the MCScanX python version jcvi.formats.gff function. We then ensured that the fasta transcript files from each assembly were also of a compatible format using the jcvi.formats.fasta function. Then, synteny was classified in a pairwise fashion using the jcvi.compara.catalog function for R19 vs. Pe21, Pe21 vs. 404, and 404 vs. 413, then performed the jcvi.compara.synteny function using the --minspan = 30 and --simple parameters. Matching layout and seqids files were then created as directed in the protocol (https://github.com/tanghaibao/jcvi/wiki/MCscan-(Python-version)#workflow (accessed on 1 October 2023)). Finally, figures were generated using the jcvi.graphics.karyotype function. Additionally, Orthofinder (v2.5.5) was used to identify orthogroups between the four assemblies [60]. Orthogroups were identified by using the annotated protein fasta files generated during genome annotation as input into Orthofinder (v2.5.5) while invoking the -M msa command. Annotated virulence

genes from *P. expansum* were compiled from the primary literature (Table S1) and fastas were obtained from their respective NCBI accessions. These fastas were concatenated in a single fasta and used to identify their corresponding transcripts in the R19 transcript annotation using blastn. The blastn results were then used to identify single copy orthologues for each virulence gene across the four *Penicillium* samples using the Orthofinder results.

For secondary metabolite cluster identification, antiSMASH (v7.0.1) was run for each of the new 404, 413, and Pe21 genomic fasta files, and the re-annotated R19 genome (see Genome Annotation) [61]. Every "extra feature" was selected and executed using the 'relaxed' parameters within the fungal database.

2.8. Gene Expression Analysis

To compare gene expression profiles for each of the four samples, we used the RNA-seq mappings generated during genome annotation as input into StringTie2. StringTie2 was executed with the -B and -e commands to calculate expression statistics. The reference annotation for each respective sample was used as the -G input into the StringTie2 command. The resulting gtf files were then used as input in the PrepDE.py3 script provided by StringTie2 to extract hypothetical read counts per transcript information. Transcripts per million (TPM) measurements were then extracted as text files and used as input into R (v4.3.2) [62] for transcriptome visualization. TPM for each ortholog was then visualized using the heatmap function in R.

2.9. Metabolite Extraction

Filter-sterilized (0.2 µm) spent growth medium (50 mL; see 'Fungal isolate propagation and sample inoculation') from three independent cultures of Pe21, R19, 404, and 413 and uninoculated medium (five aliquots) was processed as previously described [21]. Each were centrifuged for 30 min at 15,000× *g* (rotor JA-12, Beckman Coulter, Brea, CA, USA). Chloroform was added to 3 mL medium at a 1:1 ratio before centrifuging again at 10,000× *g* for 10 min. The supernatant was transferred to a tube containing 3 mL 60% methanol:ddH_2O and vortexed for 2 min (Vortex Genie 2, Scientific Instruments, Schaumburg, IL, USA), then mixed with 5 mL of ethyl acetate. The top organic layer was transferred to a 15 mL conical tube and evaporated to dryness with continual flow of nitrogen gas using an N-EVAP nitrogen evaporator (Organomation, Berlin, MA, USA), then stored at −80 °C until resuspension.

2.10. Metabolomic Analysis

Three 404, 413, Pe21, and R19 sample residuals from the metabolite extraction were resuspended in 100 µL 50% methanol/0.1% formic acid. Twenty µL from each sample were pooled to make a quality control (QC) sample. Three samples of PDB without fungus were processed similarly but were not included in the QC. Five µL of the samples were separated on a 40 °C heated, 150 × 2.1 mm Hypersil GOLD VANQUISH HPLC column with 1.9 µm particles (Thermo Fisher Scientific, Waltham, MA, USA) coupled to a Vanquish HPLC pump (Thermo Fisher Scientific, Waltham, MA, USA) controlling a 10-min linear gradient from 0% to 95% acetonitrile and 0.1% formic acid at a flow rate of 0.2 mL per minute. Eluent was electrosprayed at 3.5 kV positive polarity into an Exploris 240 mass spectrometer (Thermo Fisher Scientific, Waltham, MA, USA) using an internal mass calibrant. Sheath gas was 35, auxiliary gas was 7, and sweep gas was 1 (arbitrary units). The ion transfer tube temperature was 325 °C and the vaporizer temperature was 275 °C. Advanced peak determination, mild trapping, and internal mass calibration was enabled. Default charge state was one and the expected peak width was 6 s. AcquireX software (accessed 1 July 2023) was used to create a background ion exclusion list from a blank sample consisting of 50% methanol/0.1% formic acid and an inclusion ion list from the QC

sample [63]. Subsequently, five injections of QC were performed to generate MS^2 spectra. After each of those injections, the resolved ions were appended to the exclusion list for the subsequent injection. Survey scans were recorded in the Orbitrap at 60,000 resolution over a mass range of m/z 70–800. The RF lens was 70%. Monoisotopic precursor selection was enabled, the minimum intensity was 5000, charge states were filtered to one and automated dynamic exclusion was enabled. Twenty precursors selected within a 1.0 Da isolation window were fragmented by high energy collision-induced dissociation (30%, 50%, 70% normalized stepped collision energy), and fragment ions were resolved in the Orbitrap at 30,000 resolution. Next, all test samples were analyzed alongside four intermittent injections of QC and blank consisting of 50% methanol/0.1% formic acid. Survey scans were recorded in the Orbitrap at 120,000 resolution over a mass range of m/z 70–800. The RF lens was 70%. The samples were also analyzed in negative ion mode at −2.5 kV but with the same other settings. These mass spectrometry data files can be retrieved from massive.ucsd.edu (MSV000095703). All samples were prepared and run in-house.

Result raw files were analyzed with Compound Discoverer version 3.3 (Thermo Fisher Scientific, Waltham, MA, USA). The ChromAlign node was used to align chromatographic peaks in all files to a QC replicate. The Detect Compounds node was used with 2 ppm mass tolerance, 10,000 minimum peak intensity, at least five scans per peak, 0.25 min maximum peak width, and compound detection of $[M + H]^{+1}$ ions (positive ion mode) or $[M - H]^{-1}$ ions (negative ion mode) to create peak areas. The Group Compounds node was used with 2 ppm mass tolerance, 0.25 min retention time (RT) tolerance, and a peak rating threshold of four for a minimum of five files. The Fill Gaps node was used with 2 ppm mass tolerance, the SERRF QC Correction node was used with 75% QC coverage to normalize the peak area results, and the Mark Background Components node was enabled. The Search mzCloud node was used to compare MS2 spectra to all compound classes at a precursor mass tolerance of 5 ppm and fragment mass tolerance of 5 ppm. The Search mzVault node was used to compare MS^2 spectra to the NIST_2020_MSMS High Resolution library at fragment mass tolerances of 10 ppm. The Predict Compositions nodes were used with 2 ppm mass tolerances. The software performed a one-way ANOVA to estimate compound peak area statistical differences and used the Benjamini and Hochberg method to estimate the false discovery rate (FDR). Filtering of results was performed to limit background ions, to use normalized peak areas, and to require MS^2 supporting spectra. Results were further filtered to require one match score greater than or equal to 70, R19/PDB compound peak area ratios greater than or equal to 2 $\log_2$ (with a similar increase in Pe21/PDB and almost no increase or a slight increase/decrease for both 404/PDB and 413/PDB) and have a FDR less than 5%. This yielded compounds with substantial increases for R19/404. A second result list was generated with 404/PDB compound peak area ratios greater than or equal to 2 $\log_2$ (with a similar increase in 413/PDB and almost no increase or a slight increase/decrease for both R19/PDB and Pe21/PDB). This yielded compounds with substantial increases in 404/R19. Results were examined by hand and discarded if the chromatographic peaks were substandard or if the MS^2 identifying spectrum did not fall within the assigned chromatographic peak area.

2.11. HPLC-High Resolution Mass Spectrometry

Filtered samples of supernatant were analyzed for patulin using an Agilent 1290 UHPLC coupled to an Agilent 6545XT hybrid quadrupole/time-of-flight mass spectrometer (Santa Clara, CA, USA). Samples were prepared and run in-house. Separations were performed on a Peek-lined AdvanceBio MS Spent Media column (2.1 × 100 mm, 2.7 µm) with a binary solvent gradient having an overall flow of 250 µL/min. Solvent A was

10 mM ammonium acetate in HPLC-MS grade water (Sigma Aldrich, St. Louis, MO, USA) and solvent B was 95:5 methanol: 200 mM ammonium acetate. Samples were separated using the following gradient: 0–5 min, 2% solvent B; 3–3.5 min, 10% solvent B; 3.5–4 min, 100% solvent B; 4–8 min, 100% solvent B; 8–8.2 min, 2% solvent B. Data were collected over a mass range of 100–1000 Da. Patulin was identified using three ions previously described [64]: m/z = 155.0339, $[M + H]^{+1}$; m/z = 169.0495, $[M—H_2O + CH_3OH]^{+1}$; m/z = 137.0233, $[M—OH]^{+1}$. Source parameters were optimized to increase detection of m/z = 137.0233, which was used as the quantitating ion, with m/z = 169.0495 used as a qualifying ion (Table S2). Quantitation was performed using a matrix-matched external calibration set with patulin concentrations of 0.5, 1, 5, 10, 25, 100, and 250 µg/mL. The calibration data was collected in triplicate and fit with second-order polynomial.

3. Results

3.1. Fungal Genome Sequencing and Assembly

Whole genome sequencing using nanopore technology was used to obtain improved quality of the available genomic resources for *Penicillium chrysogenum* 404, 413, and *Penicillium expansum* Pe21. We averaged 9.9 Gb of sequence for each sample with a mean phred score of Q16.9 (Table S3). Following filtering, the resulting sequence datasets had an average size of 2.2 Gb with read N_{50} between 22 Kb and 32 Kb. We also performed duplex basecalling where each dataset yielded between 0.34 Gb to 1.1 Gb of sequence. The duplex reads had an average N_{50} of 8175 bp and mean phred score of Q24.8. The duplex read output was 5% to 10% of the total sequence data (e.g., duplex efficiency) (Table S3). The duplex datasets were deemed too low in sequence amount for accurate de novo assembly. For the filtered simplex data, we achieved a minimum of 48× coverage for a genome of an estimated 32.4 Mb in length (Table S3). This resulting sequence was of sufficient coverage to proceed with de novo genome assembly. The 404-sequencing yielded sufficient coverage of duplex only reads to attempt duplex-based assembly and thus was a proof case for evaluation of different assembly methods and inputs. We utilized Flye with simplex only reads for the initial assembly and employed the Flye polishing module with the duplex reads. The initial N_{50} read length was 5.4, 9.1, and 6.4 Mb for Pe21, 404, and 413 respectively (Table 1).

Table 1. Whole genome sequencing and de novo assembly of *P. chrysogenum* 404 and 413, and *P. expansum* R19 and Pe21.

Genome	**R19** [1]	**Pe21**	**404**	**413**
Species	*P. expansum*	*P. expansum*	*P. chrysogenum*	*P. chrysogenum*
		Initial Assembly Statistics		
Sequencing Platform	PacBio	Oxford Nanopore	Oxford Nanopore	Oxford Nanopore
Length (bp)	-	32,558,303	32,571,984	32,551,633
Contig Number	-	10	6	9
N50	-	5,397,789	9,112,179	6,356,666
		Post-processing Assembly Statistics		
Length (bp)	32,896,497	32,468,381	32,569,297	32,630,660
Contig Number	16	5	4	4
N50	8,173,214	7,894,026	9,112,601	9,112,742
GC Content	47.28%	47.48%	48.81%	48.82%
Busco Complete	96.0%	96.5%	96.8%	96.8%
Busco Complete, single copy	95.9%	96.4%	96.4%	96.4%
Busco Complete, duplicated	0.1%	0.1%	0.4%	0.4%
Busco Fragmented	1.0%	0.7%	0.5%	0.5%
Busco Missing	3.0%	2.8%	2.7%	2.7%

[1] Using NCBI assembly accession PRJNA497398.

Comparing these two resulting assemblies, the polishing resulted in some "scaffolding" of shorter contigs and slight decreases in total length and N_{50} (Table 1). This suggests that the polishing with duplex reads was able to correct and place some contigs to increase the contiguity of the assembly. We also performed mixed assemblies with HiFiasm and Verkko using the duplex reads as a pseudo HiFi input. In both cases, the resulting assemblies were more fragmented suggesting Flye assembled superior genomes for this study (Table 2). We decided to move forward with Flye and duplex polishing as our primary assembly method except for Pe21 where not enough duplex reads were generated. We additionally employed some scaffolding and gap filling (i.e., patching) for the 413 and Pe21 assemblies.

Table 2. Genome assembly comparisons for *P. chrysogenum* 404.

Assembly Software	Flye	Flye (Duplex Polishing)	HiFiasm	Verkko
Simplex sequence used	Yes	Yes	Yes	Yes
Duplex sequence used	No	Yes	Yes	Yes
Number of contigs	6	6	99	24
Total contig length (bp)	32,621,534	32,571,904	36,183,816	33,335,027
Contigs > 500 bp	6	6	99	24
Contigs > 1 Kb	6	5	99	24
Contigs > 10 Kb	6	4	74	24
Contigs > 100 Kb	4	4	27	5
Contigs > 1 Mb	4	4	15	5
N50	9,113,167	9,112,179	1,734,376	6,357,403

Our final assemblies, following the polishing, scaffolding, and/or patching, resulted in highly contiguous genomes (Table 1). The assembly for Pe21 had a total length of 32.4 Mb, which is similar to the previously published R19 strain for *P. expansum* [65]. Moreover, GC content between the two only differed by 0.2%. Furthermore, BUSCO scores for both *P. expansum* genomes were above 96.0% complete with the Pe21 being 0.5% higher than R19 along with lower fragmented and missing BUSCOs. For the two *P. chrysogenum* genomes, 404 was more contiguous after the initial assembly step and thus served as a reference for the scaffolding of 413. Both assemblies were 32.5 Mb in length but 413 increased by another 100 Kb following scaffolding. The N50 for both post processed assemblies were nearly identical with values of 9.11 Mb and identical BUSCO scores. Overall, the assemblies for each species and two strains were highly similar in quality and contiguity, suggesting our assembly approaches were sound and effective (Table 1).

3.2. Penicillium spp. Genome Annotation

Using the three high quality genomes we assembled, in addition to the unannotated *P. expansum* R19 genomic resource available (NCBI accession PRJNA497398), we set out to thoroughly annotate each genome independently. For the *P. expansum* strains, we identified 9740 and 10,536 features of repetitive nature (e.g., transposable elements, simple repeats) (Table 3). Similarly, the *P. chrysogenum* yielded 10,111 to 10,400 repetitive elements. However, the total length of the repeats was >1 Mb more in *P. chrysogenum* than *P. expansum.* For the gene annotation, *P. expansum* had between 11,326 and 11,911 protein coding genes, whereas *P. chrysogenum* had between 12,246 and 12,774 protein coding genes. Average gene lengths between all the four assemblies were similar, with a range of 1661 bp for Pe21 to 1890 bp for R19. The average number of exons per gene was also similar with 3.2 for *P. expansum* and 3.1 for *P. chrysogenum.* Overall, all four genomes were thoroughly annotated with a BUSCO completeness score above 98.1% and a max of 1.2% missing BUSCOs (Table 3).

Table 3. Genome annotation of *P. chrysogenum* 404 and 413, and *P. expansum* R19 and Pe21.

Genome	R19 [1]	Pe21	404	413
Species	*P. expansum*	*P. expansum*	*P. chrysogenum*	*P. chrysogenum*
		Transposable Elements and Repeats		
RepeatMasker	7442	7071	7140	7163
RepeatModeler	3094	2669	2971	3237
Consensus Features	10,536	9740	10,111	10,400
Total Length (bp)	1,461,084	1,685,573	2,576,305	2,836,205
		Genes		
Number of gene	11,911	11,326	12,246	12,774
Average gene length (bp)	1890	1661	1743	1698
Average number of exons	3.2	3.2	3.1	3.1
Busco Complete	98.2%	98.1%	98.4%	98.2%
Busco Complete, single copy	95.4%	97.9%	96.2%	96.1%
Busco Complete, duplicated	2.8%	0.2%	2.2%	2.1%
Busco Fragmented	0.9%	0.7%	0.8%	1.0%
Busco Missing	0.9%	1.2%	0.8%	0.8%
		Non-coding Genes		
rRNA	63	37	51	65
tRNA	204	150	156	157

[1] Using NCBI assembly accession PRJNA497398.

3.3. Macro- and Micro-Synteny in Penicillium Species

To evaluate the synteny and collinearity of the genomes both inter- and intra-specifically, we performed ortholog block identification using MCScanX. The resulting analysis demonstrated high intra-specific collinearity between the strains, whereas the inter-specific synteny was highly decayed between the two species (Figure 1). The *P. chrysogenum* genomes were each composed of four chromosomes, whereas the *P. expansum* genomes spanned five, matching previously published numbers and sizes for each species [66,67]. Further, it appears the two *P. expansum* isolates also have an inversion in the fifth assembled contig. Many blocks of colinear genes were maintained between the species but were inverted, translocated, and/or rearranged to the point where chromosomes were no longer homologous (Figure 1).

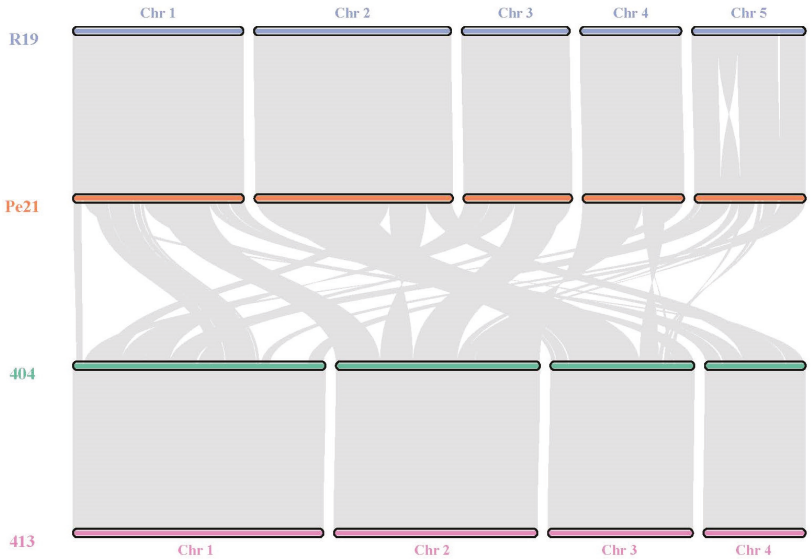


Figure 1. Genome macrosynteny between *P. expansum* R19 (blue), *P. expansum* Pe21 (orange) *P. chrysogenum* 404 (green), and *P. chrysogenum* 413 (pink) chromosomes (chr). Gray lines represent regions of synteny and connect to similar areas across chromosomal regions.

3.4. Secondary Metabolic Gene Clusters

The program antiSMASH was used to discover secondary metabolic (SM) gene clusters that are present in the four genomes. In strains 404 and 413, 56 SM clusters were identified, of which 21 were associated with known biochemical pathways (Table 4).

Table 4. Percent similarity of biosynthetic gene cluster in each *Penicillium* spp. isolate [1].

Type	Most Similar Known Cluster	404	413	R19	Pe21
Terpene	14-(N,N-dimethylleucyloxy)paspalinine/14-(leucyloxy)paspalinine/ 14-hydroxypaspalinine	30	30	n.d.	n.d.
T1PKS	4-oxomacrophorin A/macrophorin A/5′-epimacrophorin B	100	100	54	54
T1PKS, NRPS	AbT1	n.d.	n.d.	100	100
T1PKS	ACT-Toxin II	n.d.	n.d.	n.d.	100
T1PKS, NRPS	andrastin A	100	100	100	100
fungal-RiPP-like	ankaflavin/monascin/rubropunctatine/monascorubrin	n.d.	n.d.	12	8
T1PKS	azasperpyranone A/azasperpyranone B/azasperpyranone C/azasperpyranone D/azasperpyranone E/azasperpyranone F/azasperpyranone G/azasperpyranone H	12	12	12	12
NRPS-like	Choline	100	100	100	100
NRPS	chrysogine	83	83	n.d.	n.d.
NRPS	chrysoxanthone A/chrysoxanthone B/chrysoxanthone C	65 (8)	65 (8)	17	17
T1PKS, terpene	Citrinin	n.d.	n.d.	56	56
NRPS, indole	Clapurines	n.d.	n.d.	72	72
T1PKS, indole	communesin A/communesin B/communesin C/communesin D/communesin E/communesin G/communesin H	n.d.	n.d.	100	100
Terpene	Conidiogenone	100	100	n.d.	n.d.
NRPS	cyclo-(D-Phe-L-Phe-D-Val-L-Val)/cyclo-(D-Tyr-L-Phe-D-Val-L-Val)/cyclo-(D-Tyr-L-Trp-D-Val-L-Val)/cyclo-(D-Phe-L-Trp-D-Val-L-Val)/cyclo-(D-Phe-L-Phe-D-Val-L-Ile)/cyclo-(D-Phe-L-Phe-D-Ile-L-Val)/cyclo-(D-Tyr-L-Trp-D-Val-L-Ile)/cyclo-(D-Tyr-L-Trp-D-Ile-L-Val)/cyclo-(D-Tyr-L-Phe-D-Val-L-Ile)/cyclo-(D-Tyr-L-Phe-D-Ile-L-Val)	n.d.	n.d.	100	n.d.
T1PKS, NRPS	Equisetin	n.d.	n.d.	45	45
NRPS, T1PKS	flavichalasine F/flavichalasine G/aspochalasin C/aspochalasin E/aspochalasin M/TMC-169/aspergillin PZ	18	18	36 (18)	36
NRPS	Gliovirin	n.d.	n.d.	62	62
NRPS	gramillin A/gramillin B	17	17	17	17
NRPS-like, NRPS, terpene	hancockiamide E/hancockiamide B/hancockiamide C/hancockiamide D/hancockiamide A/hancockiamide F	25	25	n.d.	n.d.
T1PKS	harziphilone/t22azaphilone/isoharziphilone-1/isoharziphilone-2/ compound 4/compound 1	n.d.	n.d.	40	40
T1PKS	HEx-pks1 polyketide	n.d.	n.d.	60	60
NRPS, indole	histidyltryptophanyldiketopiperazine/dehydrohistidyltryptophanyldiketopiperazine/ roquefortine D/roquefortine C/glandicoline A/glandicoline B/meleagrine	100	100	57	57
NRPS	loline/N-acetylnorloline/N-formylloline	n.d.	n.d.	66	66
T1PKS, NRPS	metachelin C/metachelin A/metachelin A-CE/metachelin B/dimerumic acid 11-mannoside/dimerumic acid	50 (25)	50 (25)	n.d.	n.d.
T1PKS, terpene	Neosartorin	n.d.	n.d.	57	57
NRPS	nidulanin A	75	75	n.d.	75
T1PKS	Patulin	40	40	86	86
NRPS	Penicillin	87	93	n.d.	n.d.
NRPS	Penitremane	n.d.	n.d.	17	17
NRPS, T1PKS	Phomasetin	n.d.	n.d.	85	85
NRPS, T1PKS	phyllostictine A/phyllostictine B	n.d.	n.d.	20	20
Terpene	PR-toxin	100	100	n.d.	n.d.
T1PKS	Sorbicillin	100	100	n.d.	n.d.
terpene, T1PKS	squalestatin S1	60	60	60	60
NRPS-like	viridicatumtoxin/previridicatumtoxin/5-hydroxyanthrotainin/ 8-O-desmethylanthrotainin	n.d.	n.d.	27	27
T1PKS	YWA1	100	100	100	100
T1PKS	Zopfiellin	16	16	n.d.	n.d.

[1] Percentage and identification determined using the antiSMASH program. n.d. = no data result for that cluster and isolate. Parentheses indicate a second match to the same cluster was detected.

The Pe21 and R19 genomes had a total of 66 and 67 secondary metabolite clusters, respectively, with 28 and 27 annotated with known metabolite production. The identified biosynthetic gene clusters were classified as (or like) non-ribosomal protein synthetases (NRPS), type 1 polyketide synthases (T1PKS), indoles, terpenes, or fungal ribosomally synthesized and post-translationally modified peptides (fungal-RiPP-like). Many instances of identified clusters showed only partial matches, suggesting the potential for metabolite

production may be varied despite some nucleotide sequence homology. Pe21, R19, 404, and 413 only matched 7, 6, 8, and 8 clusters at 100%, with lowered stringency of 50% cluster matches for 18, 17, 14, and 14, respectively. Of the annotated clusters, seven were present in all four isolates above 50%. Only three SM clusters, andrastin A, choline, and YWA1 (2,5,6,8-tetrahydroxy-2-methyl-2,3-dihydro-4*H*-naphtho [2,3-*b*]pyran-4-one), had a 100% match in all four isolates, demonstrating that most of the secondary metabolic capacity is distinct between the two species. For example, the *P. expansum* isolates had clusters with at least 50% identity for AbT1, communesins, citrinin, clapurines, gliovirin, phomasetin, Hex-pks1 polyketide, and neosartorin. The *P. chrysogenum*-specific SM clusters included conidiogenone, chrysogine, macrophorin A, PR-toxin, sorbicillin, penicillin, and metachelin/dimerumic acids. Two isolate-specific SM clusters were also exclusively detected in the *P. expansum* genomes, which were ACT-Toxin II in Pe21, and cyclo-peptides in R19.

3.5. Conserved Expression for Virulence Gene Orthologues in Penicillium spp.

In addition to transcriptomic guidance to aid high-quality genomic annotation, we sought to compare transcriptomic profiles across the species to further understand their similarities and unique traits. A full list of conserved, single-copy gene orthologues was generated across the four *Penicillium* genomes. The expression of the orthologues across all isolates showed species-specific clustering with a principal component analysis (PCA; Figure 2). Further, 404 and 413 isolates clustered much closer together than the two *P. expansum* isolates, demonstrating less gene expression variability within the *P. chrysogenum* isolates in culture.

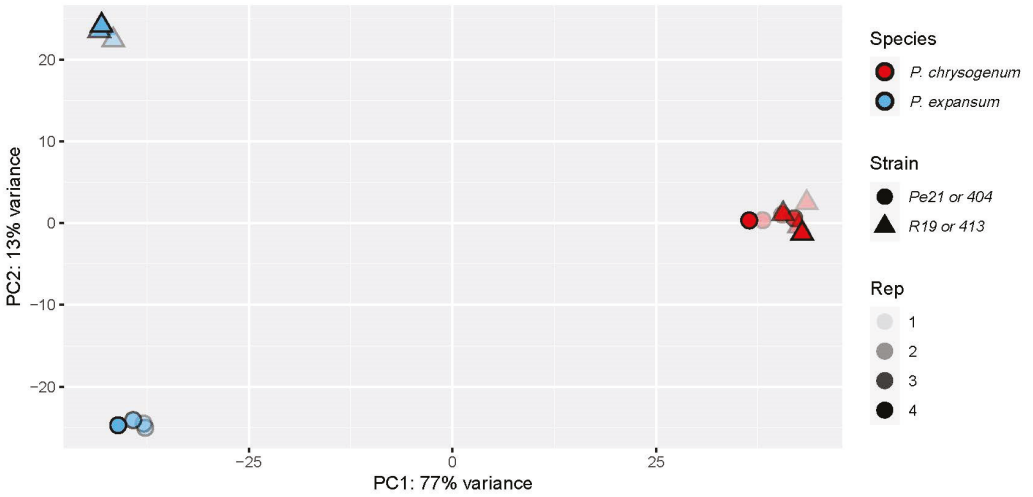


Figure 2. Principal Component analysis of transcriptomic data for each *Penicillium* spp. isolate. *P. chrysogenum* isolates 404 (red circles) and 413 (red triangles), *P. expansum* isolates R19 (blue triangles) and Pe21 (blue circles) across four replicates.

3.6. P. chrysogenum Isolates Share P. expansum-Associated Virulence Gene Orthologues

A select number of *P. expansum* genes have been experimentally verified via gene functional analysis to contribute to virulence during pome fruit decay (Table S1). Therefore, the 404, 413, R19, and Pe21 genomes were comprehensively searched for virulence gene orthologues to investigate the observed non-virulent phenotype of *P. chrysogenum* in apple fruit. Thirty-nine single-copy orthologues were found within each of the four genomes (Table S1). The *P. chrysogenum* genomes did not have any orthologues for four genes encoding PeLysM5, PeLysM8, PeLysM11, and PeLysM16. PeLysM7 was found in each genome except in 404. The remaining 12 orthologues were identified with multiple copy numbers within at least one of the genomes. Expression (log2 TPM) of the 39 single copy orthologues was evaluated (Figure S2). Most of the genes were similarly expressed in

culture within and between species, with little transcript detected for the gene encoding PeLysM15 in all isolates, and PeLysM14 in *P. expansum* isolates grown in culture (Figure S2).

3.7. Penicillium spp. Produce an Array of Metabolites In Vitro

Untargeted metabolomic profiling was performed on the spent liquid culture broth for each isolate. Across all samples, 4478 and 4448 compound features (by m/z and RT) were detected in positive and negative ion modes, respectively. PCA revealed species-level differences in the metabolomic profiles like the transcriptomic PCA, with 404 and 413 clustering tightly with each other but separately from R19 and Pe21 (Figure 3). These patterns indicate congruence between gene expression and small molecule production at a global level.

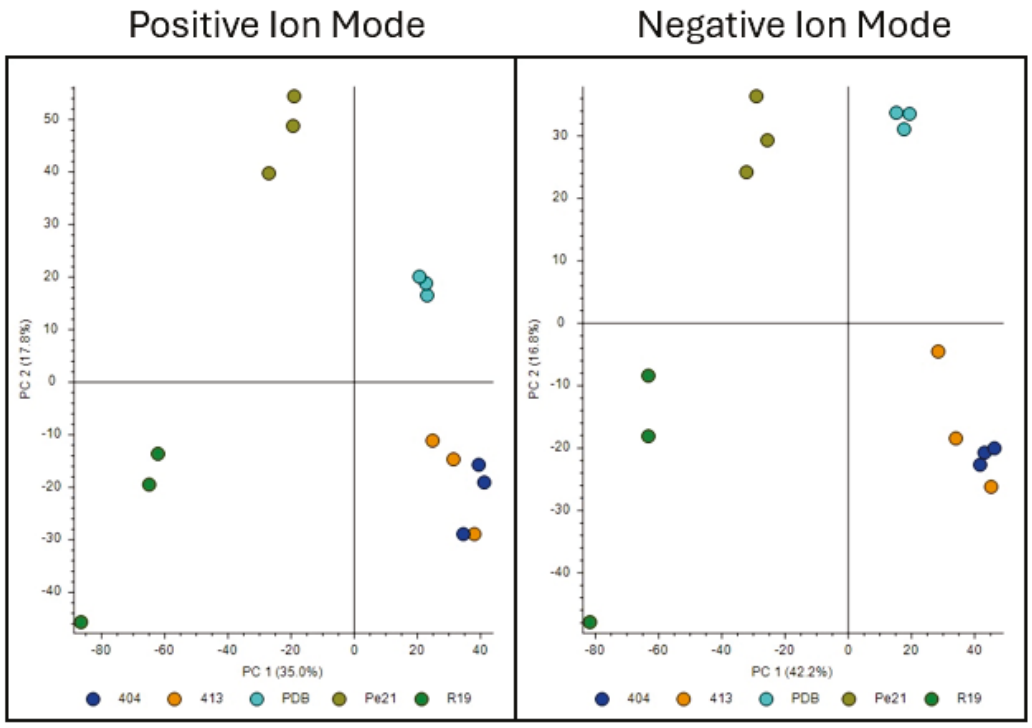


Figure 3. Principal Component analysis of metabolomic data for each *Penicillium* spp. isolate. *P. chrysogenum* isolates 404 (navy blue) and 413 (orange), *P. expansum* isolates R19 (green) and Pe21 (brown), and the PDB control samples (teal). Samples were analyzed in both positive ion mode (**left**) and negative ion mode (**right**).

Individual compounds were selected based on their spectral library match scores (>70) and accumulation differences (peak area significance $p < 0.05$) compared to the PDB control samples and higher abundance in one or both *P. chrysogenum* (Table 5) or *P. expansum* isolates (Table 6).

Many of the compounds identified can be grouped into one or more category based on potential biological activity. For example, multiple abundant compounds in *P. chrysogenum* have possible pharmacological activity, including anticancer and anti-inflammatory compounds like luteolin, rubiadin, citreorosein, and N-acetyltyramine, or other potential functions, like 6-methoxy-2-oxo-2H-1-benzopyran-3-carboxylic acid, a diuretic. Another subset in *P. chrysogenum* was previously shown to be antibacterial, antiviral, or antifungal, such as penicillin G, 5-methyl-L-uridine, 5-methylcytidine, and scopoletin. It should be noted that many of the preceding compounds have several known biological activities that may depend on biological context.

Table 5. Selected abundant matched compounds in *P. chrysogenum* 404 and 413 versus *P. expansum* R19 and Pe21 culture broth (compared to control PDB) [1].

Compound	Formula	Chemical Class	Mono-Isotopic Mass	Retention Time (min)	Library Match Score	Reference Ion	Peak Area 404/PDB	Peak Area 413/PDB	Peak Area Pe21/PDB	Peak Area R19/PDB
3,8-Dihydroxy-6-methyl-9-oxo-9H-xanthene-1-carboxylic acid	C15 H10 O6	Xanthone	286.05	7.684	80	–	**931.83**	1055.25	0.96	2.75
3-Phenyllactic acid	C9 H10 O3	Phenylpropanoic acid	166.06	6.515	99.3 †	–	**6.58**	7.02	0.34	0.16
4-(7-Hydroxy-4-oxo-4H-chromen-3-yl)phenyl hydrogen sulfate	C15 H10 O7 S	Isoflavone	334.01	7.811	91.6	–	**7998.47**	**6071.54**	19.79	4.76
5-Methylcytidine	C10 H15 N3 O5	Nucleoside	257.10	3.094	91.6	+	**15.36**	10.94	0.79	0.74
5-methyl-L-uridine	C10 H14 N2 O6	Nucleoside	258.09	4.331	87.9	+	**20.08**	**14.43**	1.09	1.77
6-methoxy-2-oxo-2H-1-benzopyran-3-carboxylic acid	C11 H8 O5	Coumarin	220.04	7.762	72.1	–	**275.72**	**358.32**	2.14	9.94
Archin	C15 H10 O5	Flavenoid	270.05	9.737	96.1	–	**54.73**	**29.23**	0.86	0.78
Chrysophanic acid	C15 H10 O4	Anthraquinone	254.06	10.582	70.3	–	**40.34**	12.37	0.61	0.81
Citreorosein	C15 H10 O6	Hydroxyanthraquinone	286.05	7.172	84.5	–	**412.60**	**359.93**	27.79	3.36
Luteolin	C15 H10 O6	Flavone	286.05	8.044	88.3 †	–	**222.00**	**209.18**	1.48	3.98
N-Acetyldopamine	C10 H13 N O3	Catechol	195.09	5.194	98.8 †	+	**16.89**	**18.05**	1.64	1.06
N-Acetyltyramine	C10 H13 N O2	Tyramine	179.09	6.122	87.7	–	**1337.65**	**1373.87**	2.08	4.48
Penicillin G	C16 H18 N2 O4 S	Beta-lactam antibiotic	334.10	7.735	94.8 †	+	**366.49**	134.66	1.15	2.49
Rubiadin	C15 H10 O4	Anthraquinone	254.06	7.811	76.1 †	–	**273.48**	**198.02**	1.44	3.37
Scopoletin	C10 H8 O4	Coumarin	192.04	7.918	79	+	72.25	67.67	1.53	1.71

[1] Bold indicates adj. $p < 0.05$. "+" = [M + H] + 1; "−" = [M − H] − 1. Match to NIST library or to mzCloud library ("†" demarcation).

Table 6. Selected abundant matched compounds in *P. expansum* Pe21 and R19 versus *P. chrysogenum* 404 and 413 culture broth (compared to control PDB) [1].

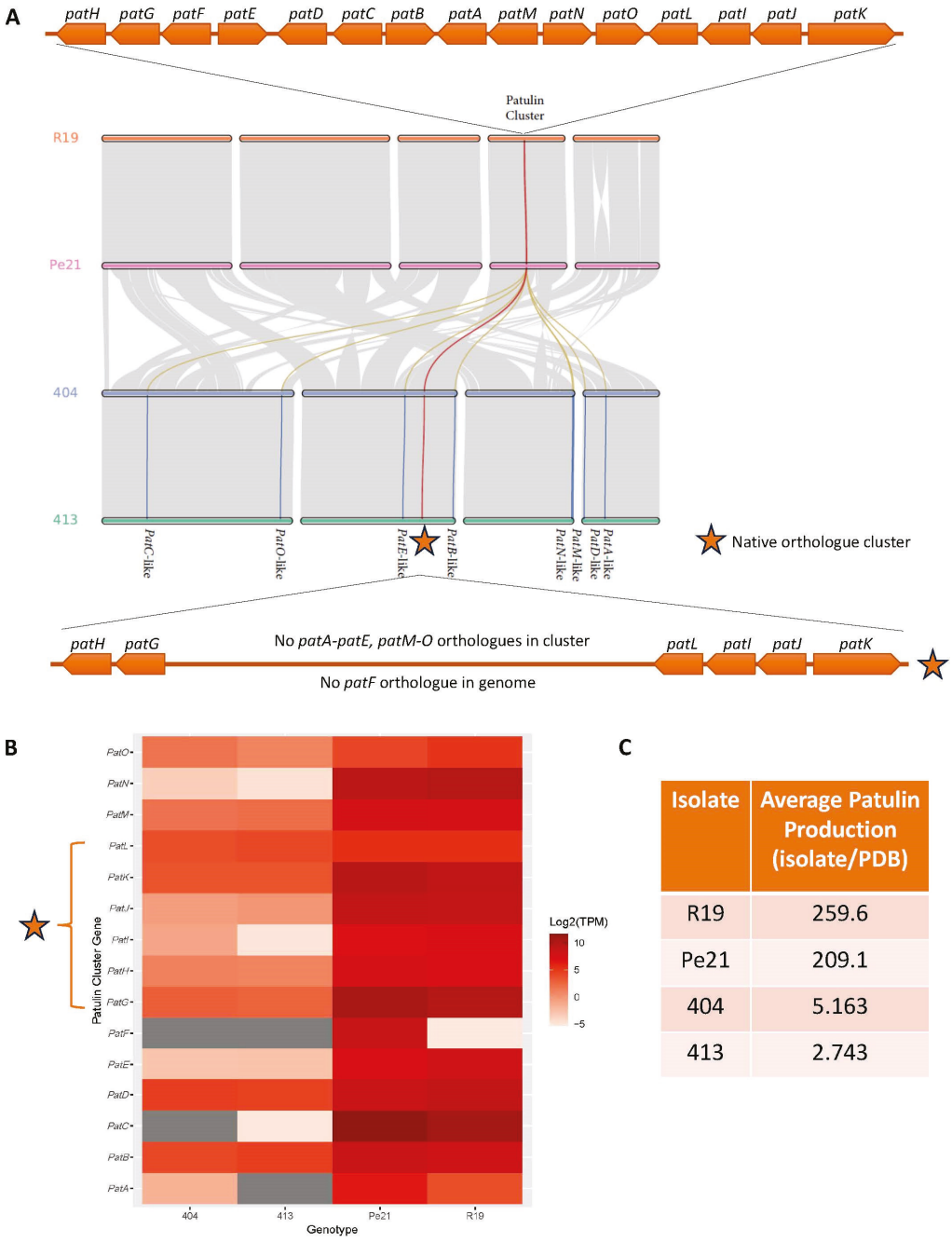
Compound	Formula	Chemical Class	Mono-Isotopic Mass	Retention Time (min)	Library Match Score	Reference Ion	Peak Area 404/PDB	Peak Area 413/PDB	Peak Area Pe21/PDB	Peak Area R19/PDB
12-Oxo phytodienoic acid	C18 H28 O3	Oxylipin	292.20	7.153	86.2 †	+	4.11	3.51	32.80	**349.47**
3,5-dimethylorsellinic acid	C10 H12 O4	Dihydroxybenzoic acid	196.07	7.542	92.1	+	0.85	1.00	22.00	**324.74**
3-carboxy-4-methyl-5-propyl-2-furanpropionic acid	C12 H16 O5	Fuanoid fatty acid	240.10	6.72	79.2	–	0.27	1.58	1.80	**842.44**
4-Methoxycinnamic acid	C10 H10 O3	Cinnamic acid	178.06	7.54	91.8 †	+	0.98	0.71	5.06	**73.42**
Citraconic acid	C5 H6 O4	Dicarboxylic acid	130.03	4.296	99.6 †	–	1.84	1.48	11.64	**17.88**
Corchorifatty acid F	C18 H32 O5	Oxylipin	328.23	7.171	72.7	–	3.09	2.81	19.39	**134.01**
Gallic acid	C7 H6 O5	Trihydroxybenzoic acid	170.02	4.972	86.7	+	1.40	1.18	**513.84**	**1189.03**
Gentisic acid	C7 H6 O4	Hydroxybenzoic acid	154.03	5.534	99.6 †	–	1.25	3.21	**406.10**	**716.38**
Indole-3-acetic acid	C10 H9 N O2	Carboxylic acid	175.06	5.89	84.1 †	+	2.67	1.60	**14.95**	**28.70**
Patulin	C7 H6 O4	Polyketide	154.03	4.907	85	–	5.16	2.74	209.10	**259.56**
Perillic acid	C10 H14 O2	Cyclohexenecarboxylic acid	166.10	5.227	73 †	–	1.54	1.42	11.16	**244.80**
Phenol	C6 H6 O	Aromatic	94.04	5.921	99.9 †	–	1.24	1.29	**41.53**	**39.81**
Sorbic acid	C6 H8 O2	Hexadianoic acid	112.05	4.175	76	+	0.27	0.59	**7.58**	**9.45**

[1] Bold indicates adj. $p < 0.05$. "+" = [M + H] + 1; "−" = [M − H] − 1. Match to NIST library or to mzCloud library ("†" demarcation).

In *P. expansum*, a completely different set of antimicrobials was produced, including the mycotoxin patulin, 3,5-dimethylorsellinic acid, perillic acid, 4-methoxycinnamic acid, and gentisic acid. A subset of compounds produced by *P. expansum* may also act as plant metabolites, including gallic acid, gentisic acid, and an isomer of indole-3-acetic acid (IAA).

3.8. Linking Patulin and Penicillin G Gene Clusters, Expression and Metabolite Production

The biosynthetic pathways for penicillin G, produced by the *P. chrysogenum* isolates, and patulin, produced by the *P. expansum* isolates, are characterized. To exemplify the utility of the multi-omics approach, we compiled the gene, expression, and metabolite production data for patulin and penicillin G from all isolates (Figures 4 and 5).

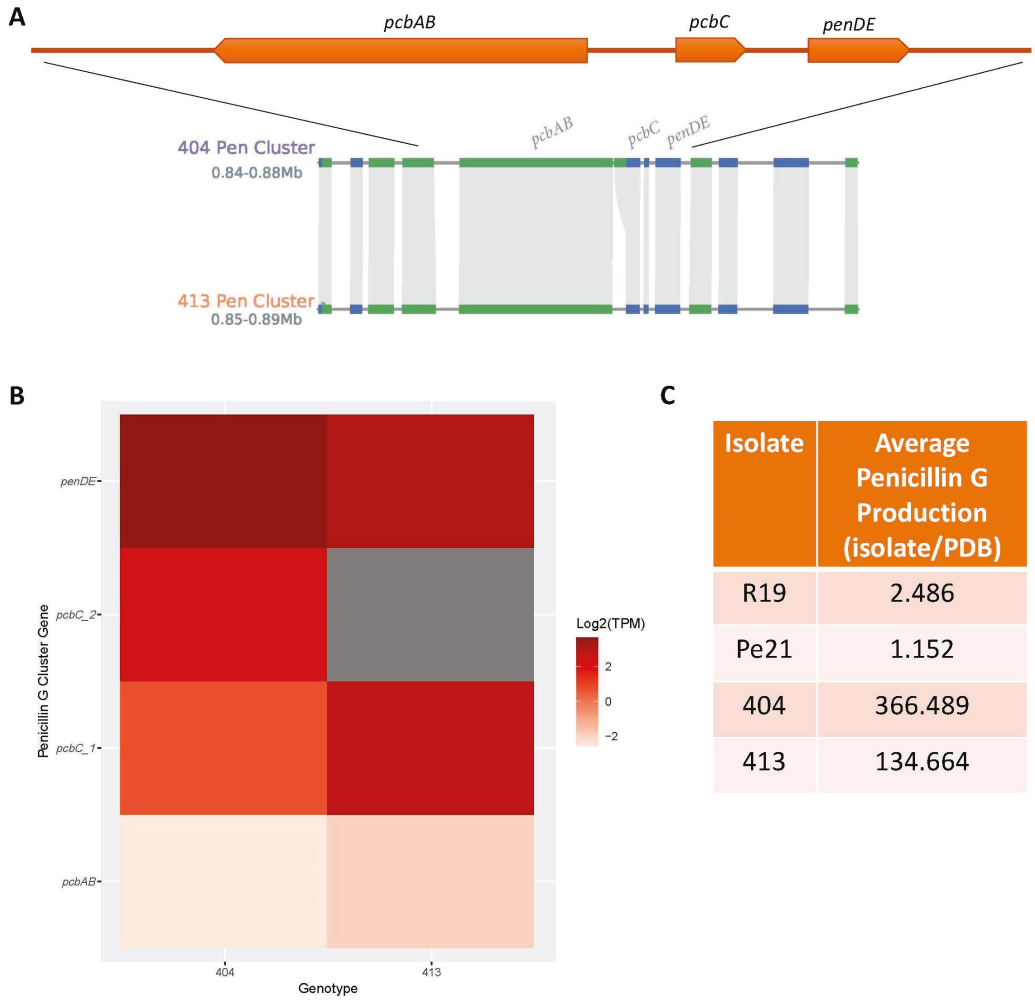


Isolate	Average Patulin Production (isolate/PDB)
R19	259.6
Pe21	209.1
404	5.163
413	2.743

Figure 4. Patulin genomic, transcriptomic, and metabolomic presence in each *Penicillium* isolate. (**A**) Complete 15-gene patulin biosynthetic gene cluster in *P. expansum* found localized to one location in R19 and Pe21 (top, orange line). In 404 and 413, the native orthologous cluster only contains 6 genes (bottom, star), with the remaining orthologues found across the four chromosomes (blue lines). (**B**) Expression (Log2 TPM) of each patulin cluster gene orthologue across the four isolates. Darker red indicates higher expression, and gray means transcript levels were below the threshold. TPM = transcripts per million. (**C**) Average patulin production detected in each isolate over the average potato dextrose broth (PDB) control. Values are average peak area ratios across replicates.

The patulin biosynthetic cluster was identified in R19 and Pe21 with an 86% homology match, whereas only 40% of the cluster was found in 404 and 413 using AntiSMASH. Microsynteny analysis confirmed that R19 and Pe21 have the entire 15-gene cluster in one location within each genome. However, 404 and 413 only have a partial cluster in one location, containing the six gene orthologues for *patH*, *patG*, *patL*, *patI*, *patJ*, and *patK* (Figure 4A). The

remaining orthologues with partial similarities were identified and were scattered across the other *P. chrysogenum* chromosomes (Figure 4A). There was no orthologue identified for *patF* in 404 or 413. All patulin cluster genes were expressed in R19 and Pe21 at higher levels than for any of the existing 404 and 413 orthologues (Figure 4B). The 404 *patC* orthologue did not have a corresponding transcript, and the 413 *patA* ortholog did not have corresponding transcript. The expression data for the gene clusters correlated with the patulin production in R19 and Pe21. The lack of patulin production in 404 and 413 can be definitively explained by reduced gene expression and absence of *patF* (Figure 4C). Targeted mass spectrometry confirmed patulin production for R19 and Pe21; patulin was not found at levels significantly above baseline in 404 and 413 growth media (Figure S3). Indeed, patulin peak areas were observed for each individual sample, and it can be confirmed the mean peak area shown for 404 and 413 have poor resolution and are likely isomers, adjacent peak tails, or background.



Isolate	Average Penicillin G Production (isolate/PDB)
R19	2.486
Pe21	1.152
404	366.489
413	134.664

Figure 5. Penicillin G genomic, transcriptomic, and metabolomic presence in each *Penicillium* isolate. (**A**) Penicillin G biosynthetic gene cluster in *P. chrysogenum* (top, orange line) chromosome 1, which were absent in R19 and Pe21. The 404 *pcbC* gene shows a larger segment that suggests a tandem repeat compared to the 413 genome. (**B**) Expression (Log2 TPM) of each penicillin G cluster gene orthologue across the two isolates. Darker red indicates higher expression, and gray means transcript levels were below the threshold. TPM = transcripts per million. (**C**) Average penicillin G production detected in each isolate over the average potato dextrose broth (PDB) control. Values are average peak area ratios across replicates.

The penicillin G three-gene cluster was present in both *P. chrysogenum* isolates but absent in R19 and Pe21 (Table 4). Further analysis of the micro-synteny revealed that 404 has a possible tandem duplication for the *pcbC* gene (Figure 5A). All of the genes were expressed in 413, while 404 lacked expression of the duplicated *pcbC* region (Figure 5B). Finally, both 404 and 413 produced penicillin G (Figure 5C). Penicillin G could not be significantly resolved above baseline in R19 and Pe21 growth medium (Figure 5C), and peaks examination individually confirmed off-target readings.

4. Discussion

Postharvest decay and mycotoxin contamination are a major economic challenge for the pome fruit industry, especially with the rise of fungicide resistance. Recent advances have been made to improve alternative control options to mitigate postharvest disease, including the use of biocontrol products like Bio-Save®, formulated from *Pseudomonas syringae* [68]. The two *P. chrysogenum* isolates examined in this study, 404 and 413, were recently shown to successfully reduce blue mold decay in apple if applied prior to the aggressive *P. expansum* isolates [27]. A comparative omics-based approach was implemented to provide resources to guide future studies in fungal-fungal interactions in postharvest systems, further understand the mode of action behind the previously observed decay reduction, and to explore the production of industrially useful compounds. Genomic, transcriptomic, and metabolomic data was generated from in vitro cultures and revealed a swath of differences between the two *Penicillium* species. The results expand on differences in fungal virulence genes and SM clusters and SM production between the two *Penicillium* spp.

A recent study confirmed that *P. chrysogenum* isolates 404 and 413 cause minimal decay in apple fruit, which provides a unique opportunity to study disparities concerning infection biology using an aggressive blue mold causing species like *P. expansum* [27]. Of all the *P. expansum* virulence factors that have been confirmed to be involved in apple fruit decay via functional genetics (e.g., *creA, veA, pacC*) or enzymatic activity (e.g., PEPG1 = polygalacturonase), only four loci of the *lysM* gene family (5, 8, 11, and 16) did not have homologues in either 404 or 413. None of the missing genes have been shown to manifest in non-virulent phenotypes in *P. expansum* when deleted. Instead, the four *lysM* genes showed an increase in *P. expansum* decay when deleted, suggesting they could be negative regulators of virulence [69]. Therefore, it is unlikely that the absence of these genes is the primary contributing factor behind the observed 404 and 413 avirulence phenotype in apple fruit. Indeed, most of the *P. expansum* virulence factors had orthologues in *P. chrysogenum* which evidently do not equate to conserved functionality in *P. chrysogenum*. As expected, the in vitro data did not show stark differences in expression of the known *P. expansum* virulence genes, as growth in axenic culture does not mimic the specific apple host environment nor does it mimic apple cell physiology. However, due to the lack of growth exhibited by *P. chrysogenum* in apple, axenic culture serves as the most appropriate milieu to study differences in small molecules produced by each species that may mediate fungal-fungal interactions and/or facilitate apple fruit decay. Taken together, we hypothesize that the simple model of presence or absence of fungal virulence genes is likely not a major underpinning of *P. expansum*'s aggressive nature. Instead, the ability of *P. expansum* to aggressively decay fruit is likely due to complex gene regulation and peptide or small molecule production during apple infection, which is the subject for future investigation.

The genome sequences generated in this study are improved resources for the fungal genetics community due to their contiguous, near-chromosomal level assemblies, high read quality and sequencing depth, and improved annotation accuracy/calling due to

the corresponding RNA-Seq dataset. All of the -omics data generated in this study was derived from the same culture conditions (e.g., mycelial mats from same flask were used to isolate gDNA, total RNA and broths used for metabolomics analysis), allowing accurate, streamlined comparison between data types and across fungal isolates. These genomic resources provide a strong foundation for understanding biology of two *Penicillium* spp. with contrasting fungal lifestyles. For example, it was previously found that isolates 404 and 413 had a missing gene homologue from the patulin cluster, *patF*, while R19 and Pe21 had complete patulin biosynthesis clusters [27]. However, the short-read genomes did not allow the level of resolution required for determining synteny when assembled de novo. Further, patulin production was not experimentally determined for the *P. chrysogenum* 404 and 413 isolates in that study. Here, genome mining via SM cluster analysis confirmed partial, localized patulin biosynthetic gene clusters in 404 and 413 on chromosome 2, while R19 and Pe21 had high homology of the entire, intact 15-gene cluster on *P. expansum* chromosome 4. Visualization of the partial cluster synteny in 404 and 413 supported the initial SM cluster match, as only six genes (*patGHIJKL*) were identified in a localized area. Expression of the cluster orthologues exhibited relatively higher abundance for the two *P. expansum* isolates for most of the genes. Subsequent metabolomics analyses demonstrated that both 404 and 413 do not produce patulin, whereas both *P. expansum* isolates produced copious amounts of the toxin in culture. Taken together, the integration of omics-based data for the patulin biosynthetic gene cluster provides definitive support that *P. chrysogenum* does not produce patulin, while *P. expansum* does, corroborating previous findings in the literature [27,34]. In addition, we show here for the first time the chromosomal location(s) of the patulin gene cluster in both *Penicillium* species and hypothesize that *P. chrysogenum* lost the central portion of the cluster to a recombination event during evolutionary divergence of the species that resulted in retention of only the flanking cluster genes, *patGHIJKL*.

Published *P. chrysogenum* genomic studies have shown bioinformatically and experimentally (e.g., pulse-field gel electrophoresis) that the genome is comprised of four chromosomes, consistent with the 404 and 413 assemblies in this study [66]. Further, previous comparative genomics of *P. chrysogenum* isolates showed a larger number of genetic duplications and overall larger chromosomes than other *Penicillium* species, with 13% of the gene families in *P. chrysogenum* found to be species-specific [34]. Similarly, 404 and 413 had larger chromosomes, almost 1000 more identified protein coding sequences, longer repeats (>1 Mb), and unique SM clusters identified than the R19 and Pe21 assemblies. However, many discrepancies have been observed across published representatives of *P. chrysogenum*, likely attributed, in part, to intentional selection pressure and mutagenic approaches to generate strains with high production of penicillin [66]. Here, the high similarity between the 404 and 413 isolates in genomic composition, SM cluster identification, expression, and small molecule production could be attributed to their identical geographical origin. The new R19 and Pe21 genome-level sequence assemblies also match the contig number of a recently available *P. expansum* isolate, IBT 35385, with 10 genomic contigs; however to our knowledge, no experimental confirmation of chromosome number has been demonstrated for this species (NCBI GenBank: GCA_028827855.1). Nonetheless, there were clear differences between the R19 and Pe21 expression profiles and metabolites produced in culture. Considering R19 was isolated from Pennsylvania, USA in 2011 and Pe21 from Israel in 2012 (NCBI BioSample: SAMN02928572), likely from apples with differing physiology (i.e., cultivars, maturity, storage regimens), the intraspecies differences may indicate evolutionary divergence. Indeed, as both are successful apple pathogens, the dissimilarities may further highlight niche pressures or biological variation amongst strict necrotrophs but may not represent necessities for virulence in apple fruit.

An untargeted metabolomics approach was used to putatively identify compounds produced by these two *Penicillium* species in culture. It should be noted misidentifications (e.g., isomers) could be indicated despite careful measures taken to ensure compound accuracy, as many of these molecules were not verified with purified chemical standards, nor examined for biological activity within each fungal species. Even so, many metabolites found suggest a unique fungal chemical repertoire for each of the species. For instance, multiple phytohormone-like compounds were detected exclusively in the *P. expansum* broth cultures. The capacity of the fungus to produce phytohormones, including an isomer of indole 3-acetic acid (IAA), phloroglucinol-related compounds (auxin and cytokinin-like activity), gallic acid (jasmonic acid (JA) and phenylpropanoid pathway induction), and gentisic acid (associated with salicylic acid (SA) pathway), as well as the JA precursor, 12-oxo phytodienoic acid, could suggest that the pathogen may manipulate the apple metabolism and defense response. To the best of our knowledge, this is the first indication of production of these compounds by *P. expansum* in axenic culture. Studies have shown that plant pathogens may produce phytohormones to help evade plant immune response, and to improve fungal virulence [70,71]. For example, it was confirmed that *Penicillium digitatum* can produce IAA, JA, 12-oxo phytodienoic acid, and SA, and that phytohormones are altered to facilitate infection in citrus [72]. Further, more mature apples with physiological shifts (i.e., reduced firmness, higher available sugar, etc.) have been linked to increased *P. expansum* tissue colonization [73], and *P. expansum* colonization appears to enhance ripening during infection as evidenced by increased ethylene detection [74]. Considering IAA and JA have previously been shown to stimulate ethylene production and ripening in apple fruit [75], it seems plausible that production of these compounds by *P. expansum* could aid the fungus in altering the apple fruit physiology. During *P. expansum* apple infection, ethylene-mediated defense responses are altered compared to a non-host interaction with *P. digitatum* [70]. Additionally, gallic acid levels increase in *P. expansum*-infected apples and have a concomitant increase in patulin [76]. Whether these compounds are produced to behave as or mimic phytohormones in vivo by *P. expansum*, by the apple, or both in concert during infection has yet to be determined but could significantly shift existing postharvest fungal-plant interactions paradigms to possibly leverage for new decay control mechanisms.

Among some of the most abundantly produced antimicrobials by *P. expansum* were corchorifatty acid F, perillic acid, and sorbic acid. Corchorifatty acid F is a lineolic acid derivative originally identified from *Corchorus olitorius L.* leaf tissue, and is a potential antifungal compound [77,78]. Perillic acid is a cyclohexenecarboxylic acid with antimicrobial activity against Gram-positive bacteria (*Staphylococcus aureus, Bacillus subtilis*), yeast (*Candida albicans*), and fungi (*Aspergillus brasiliensis*) that is commonly used as an antimicrobial in cosmetics [79]. Sorbic acid is a weak acid used as a food preservative with fungistatic activity that has been shown to delay germination in *Aspergillus niger* due to lowered cytosolic pH [80,81]. It is possible that *P. expansum* produces sorbic acid to compete against acid-sensitive species or utilizes sorbic acid production to stimulate the production of patulin [82]. Overall, these compounds may benefit the pathogen through competitive advantage against other sensitive organisms in the postharvest infection court. Furthermore, future biocontrol organisms used against *P. expansum* must have tolerance to these compounds, if found to be produced by the fungus during decay. Notwithstanding, utilizing *P. expansum* strains as a source of these compounds in scale up fermentation processes and/or by mining their genomes for biosynthetic clusters to move them into other organisms (e.g., yeast) for industrial scale production is of high value.

Industry has used *P. chrysogenum* for many years as a "biofactory" due to the heightened capacity of the species to produce the antibiotic penicillin [28]. Confirmation of an

intact penicillin SM cluster, gene expression, and production of penicillin G was observed in 404 and 413 presented in this work. Expanding the utility of *P. chrysogenum* to produce more compounds of interest beyond penicillin could be useful to the broader fungal scientific community and industry alike [28]. The untargeted metabolomics data was mined to find additional metabolites produced by *P. chrysogenum* with natural product potential. Many metabolites with therapeutic potential were produced by *P. chrysogenum* in these conditions, including 3,8-dihydroxy-6-methyl-9-oxo-9H-xanthene-1-carboxylic acid (anticancer), 6-methoxy-2-oxo-2H-1-benzopyran-3-carboxylic acid (diuretic), archin (anti-inflammatory, antitumor), luteolin (anticancer), N-acetyldopamine (anti-inflammatory), N-acetyltyramine (antitumor), and chrysophanic acid (anticancer). Other produced antimicrobial compounds besides penicillin may contribute toward a potential role of *P. chrysogenum* as an effective biocontrol agent against a variety of microbial pathogens. For example, n-acetyltyramine has been shown to inhibit acyl-homoserine lactone-based quorum sensing systems [83] and has also demonstrated mild antifungal activity [84]. Scopoletin is a coumarin that has antioxidant and antifungal properties [85]. When produced by *Penicillium janthinellum*, it has been shown to be effective against soybean nematode while simultaneously improving soybean health [86]. Finally, some *P. chrysogenum*-produced compounds may allow for apple host recognition or induction of defense that would normally be undetected or unstimulated when *P. expansum* is present alone. Daidzein 4′-sulfate (4-(7-hydroxy-4-oxo-4H-chromen-3-yl) phenyl hydrogen sulfate), a highly abundant compound produced by isolates 404 and 413 is an isoflavone. Isoflavones, like daidzein, are linked to phenylpropanoid metabolism and defensive phytoalexins in legume plants against fungal phytopathogens, though little is known of their role in apple fruit [87,88]. This explanation does support the observed efficacy of *P. chrysogenum* correlated with advanced establishment in the apple fruit [27], however, more functional work with the compounds is warranted. The list of desirable bioactive compounds could be further expanded with changes to production conditions, such as fermentation or induction of desired biosynthesis pathways. Further, some metabolites have more than one identified biological function, further supporting production interest and need for in-depth analysis in multiple biological contexts. The prospect of metabolomic production and manipulation is now further substantiated by the plethora of omics-based resources and functional genetic tools to optimize these strains in the laboratory and at an industrial level.

Degradation, inhibition, or sequestration of virulence factors could also reduce rot and postharvest decay incited by *P. expansum*. For instance, the antifungal activity that can be overcome by some fungi (e.g., *Penicillium* spp.), and degradation of this known virulence factor was shown in vitro with *Monolinia fructicola* [16,27,89]. As isolates 404 and 413 can tolerate patulin and have partial genetic similarity to the patulin biosynthetic cluster, it is plausible they too have an existing mechanism to reduce or disable patulin [27]. Hence, *P. chrysogenum* can be explored and manipulated for use as a model system to understand genus-level patulin tolerance mechanisms in the fungus. Further, the lack of patulin production shown here in conjunction with toxin tolerance and absence of decay symptoms highlight this species as a prime candidate for biocontrol agent development against patulin-producing pathogens like *P. expansum*.

5. Conclusions

Blue mold is a major problem for the postharvest pome fruit storage, packing and processing industries. Current mitigation strategies are not sufficient in eliminating the disease, nor to abate the production and accumulation of the mycotoxin patulin in processed pome fruit products. Understanding the omics-based differences between virulent and nonvirulent species of *Penicillium* is one way to determine fungal genetic requirements,

signaling mechanisms, and metabolomic suites necessary for apple-fruit infection. These factors can then be the main targets to serve for the development of novel decay control strategies. Additionally, through the integrated study of metabolomics, genomics, and exploring phenotypic differences between the species, the *P. chrysogenum* strains in this study have the potential to be optimized as biocontrol antagonists against blue mold decay, as contemporary laboratory tools for studying *Penicillium* spp. virulence factors, and as "fungal biofactories" to produce compounds of industrial importance.

Supplementary Materials: The following supporting information can be downloaded at: https://www.mdpi.com/article/10.3390/jof11010014/s1, Figure S1: Mean mycelial weight and pH of each fungal broth culture after 7 days postinoculation; Figure S2: Transcriptional heat map of single-copy virulence gene orthologues in each isolate; Figure S3: Patulin production by *P. expansum* and *P. chrysogenum* isolates in vitro; Table S1: Virulence genes within *P. expansum* and *P. chrysogenum* genomes [90–109]; Table S2: Source parameters for patulin measurement using HPLC-high resolution mass spectrometry; Table S3: Genome sequencing statistics.

Author Contributions: Conceptualization, H.P.B., C.G., B.C. and W.M.J.II; Data curation, C.G. and B.C.; Formal analysis, H.P.B., C.G., B.C., M.R.B. and W.M.J.II; Funding acquisition, W.M.J.II; Investigation, H.P.B., C.G., M.R.B., R.Y., V.L.G. and D.L.-R.; Methodology, H.P.B., C.G., B.C., M.R.B. and W.M.J.II; Project administration, W.M.J.II; Resources, C.G., B.C., M.R.B., V.L.G. and W.M.J.II; Software, C.G.; Supervision, J.M.F. and W.M.J.II; Validation, H.P.B., C.G., B.C., M.R.B., R.Y., V.L.G. and D.L.-R.; Visualization, H.P.B., C.G., B.C. and M.R.B.; Writing—original draft, H.P.B., C.G., B.C., M.R.B. and W.M.J.II; Writing—review & editing, H.P.B., C.G., B.C., M.R.B., V.L.G., D.L.-R., J.M.F. and W.M.J.II. All authors have read and agreed to the published version of the manuscript.

Funding: This research was supported by USDA-ARS National Program 303 Plant Diseases, project number 8042-42430-003-000-D, to Lead Scientist WMJ II and in part by two appointments to the Agricultural Research Service (ARS) Research Participation Program administered by the Oak Ridge Institute for Science and Education (ORISE) through an interagency agreement between the U.S. Department of Energy (DOE) and the U.S. Department of Agriculture (USDA). ORISE is managed by ORAU under DOE contract number DE-SC0014664. Additional support was from USDA-ARS National Program 301 Plant Genetic Resource, Genomics and Genetic Improvement project number 8080-21000-033-000-D, USDA-ARS National Program 304 Crop Protection and Quarantine, project number 8042-22000-315-000-D, and USDA-ARS National Program 107 Human Nutrition, project number 8040-10700-003 (MB). All opinions expressed in this manuscript are the authors' and do not necessarily reflect the policies and views of USDA, DOE, or ORAU/ORISE.

Institutional Review Board Statement: Not applicable.

Informed Consent Statement: Not applicable.

Data Availability Statement: The whole genome sequencing data generated in this study for *P. chrysogenum* 404, 413, and *P. expansum* Pe21 are openly available in the NCBI Sequence Read Archive (SRA) with BioProject Accession PRJNA1170244. The *P. expansum* R19 whole genome sequencing data used in this study was from the existing NCBI GenBank accession GCA_004302965.1. Complete assemblies and annotations for all four genomes presented in this study are available in a Zenodo Repository DOI 10.5281/zenodo.13904012. The metabolomics mass spectrometry data files can be retrieved from massive.ucsd.edu (MSV000095703).

Conflicts of Interest: The authors declare no conflicts of interest.

References

1. Louw, J.P.; Korsten, L. Pathogenic *Penicillium* spp. on Apple and Pear. *Plant Dis.* **2014**, *98*, 590–598. [CrossRef] [PubMed]
2. Liu, B.H.; Yu, F.Y.; Wu, T.S.; Li, S.Y.; Su, M.C.; Wang, M.C.; Shih, S.M. Evaluation of genotoxic risk and oxidative DNA damage in mammalian cells exposed to mycotoxins, patulin and citrinin. *Toxicol. Appl. Pharmacol.* **2003**, *191*, 255–263. [CrossRef]

3. Pal, S.; Singh, N.; Ansari, K.M. Toxicological effects of patulin mycotoxin on the mammalian system: An overview. *Toxicol. Res.* **2017**, *6*, 764–771. [CrossRef]
4. Zhou, S.M.; Jiang, L.P.; Geng, C.Y.; Cao, J.; Zhong, L.F. Patulin-induced oxidative DNA damage and p53 modulation in HepG2 cells. *Toxicon* **2010**, *55*, 390–395. [CrossRef] [PubMed]
5. U.S. Food and Drug Administration [USFDA]. Compliance Policy Guidance Sec. 510.150 Apple Juice, Apple Juice Concentrates, and Apple Juice Products-Adulteration with Patulin. 2005. Available online: https://www.fda.gov/regulatory-information/search-fda-guidance-documents/cpg-sec-510150-apple-juice-apple-juice-concentrates-and-apple-juice-products-adulteration-patulin (accessed on 21 October 2024).
6. European Commission (EC), Regulation No 1425/2003. *Off. J. Eur. Union L 203* **2003**, 1–3. Available online: http://data.europa.eu/eli/reg/2003/1425/oj (accessed on 1 October 2023).
7. Samaras, A.; Ntasiou, P.; Myresiotis, C.; Karaoglanidis, G. Multidrug resistance of *Penicillium expansum* to fungicides: Whole transcriptome analysis of MDR strains reveals overexpression of efflux transporter genes. *Int. J. Food Microbiol.* **2020**, *335*, 108896. [CrossRef] [PubMed]
8. Malandrakis, A.A.; Vattis, K.N.; Markoglou, A.N.; Karaoglanidis, G.S. Characterization of boscalid-resistance conferring mutations in the SdhB subunit of respiratory complex II and impact on fitness and mycotoxin production in *Penicillium expansum* laboratory strains. *Pestic. Biochem. Physiol.* **2017**, *138*, 97–103. [CrossRef]
9. Ali, E.M.; Amiri, A. Selection Pressure Pathways and Mechanisms of Resistance to the Demethylation Inhibitor-Difenoconazole in *Penicillium expansum*. *Front. Microbiol.* **2018**, *9*, 2472. [CrossRef] [PubMed]
10. Jurick, W.M., 2nd; Macarisin, O.; Gaskins, V.L.; Janisiewicz, W.J.; Peter, K.A.; Cox, K.D. Baseline Sensitivity of *Penicillium* spp. to Difenoconazole. *Plant Dis.* **2019**, *103*, 331–337. [CrossRef]
11. Yan, H.; Gaskins, V.L.; Vico, I.; Luo, Y.; Jurick, W.M., II. First report of *Penicillium expansum* isolates resistant to pyrimethanil from stored apple fruit in Pennsylvania. *Plant Dis.* **2014**, *98*, 1004. [CrossRef] [PubMed]
12. Gaskins, V.L.; Vico, I.; Yu, J.; Jurick II, W.M. First report of *Penicillium expansum* isolates with reduced sensitivity to fludioxonil from a commercial packinghouse in Pennsylvania. *Plant Dis.* **2015**, *99*, 1182. [CrossRef]
13. Luciano-Rosario, D.; Keller, N.P.; Jurick, W.M. *Penicillium expansum*: Biology, omics, and management tools for a global postharvest pathogen causing blue mould of pome fruit. *Mol. Plant Pathol.* **2020**, *21*, 1391–1404. [CrossRef] [PubMed]
14. Li, B.; Chen, Y.; Zong, Y.; Shang, Y.; Zhang, Z.; Xu, X.; Wang, X.; Long, M.; Tian, S. Dissection of patulin biosynthesis, spatial control and regulation mechanism in *Penicillium expansum*. *Environ. Environ. Microbiol.* **2019**, *21*, 1124–1139. [CrossRef] [PubMed]
15. Sanzani, S.M.; Reverberi, M.; Punelli, M.; Ippolito, A.; Fanelli, C. Study on the role of patulin on pathogenicity and virulence of *Penicillium expansum*. *Int. J. Food Microbiol.* **2012**, *153*, 323–331. [CrossRef]
16. Bartholomew, H.P.; Bradshaw, M.J.; Macarisin, O.; Gaskins, V.L.; Fonseca, J.M.; Jurick, W.M., II. More than a virulence factor: Patulin is a non-host specific toxin that inhibits postharvest phytopathogens and requires efflux for *Penicillium* tolerance. *Phytopathology* **2022**, *112*, 1165–1174. [CrossRef] [PubMed]
17. Yao, C.; Conway, W.S.; Sams, C.E. Purification and characterization of a polygalacturonase produced by *Penicillium expansum* in apple fruit. *Phytopathology* **1996**, *86*, 1160–1166. [CrossRef]
18. Levin, E.; Raphael, G.; Ma, J.; Ballester, A.R.; Feygenberg, O.; Norelli, J.; Aly, R.; Gonzalez-Candelas, L.; Wisniewski, M.; Droby, S. Identification and Functional Analysis of NLP-Encoding Genes from the Postharvest Pathogen *Penicillium expansum*. *Microorganisms* **2019**, *7*, 175. [CrossRef]
19. Prusky, D.; McEvoy, J.L.; Saftner, R.; Conway, W.S.; Jones, R. Relationship between host acidification and virulence of *Penicillium* spp. on apple and citrus fruit. *Phytopathology* **2004**, *94*, 44–51. [CrossRef]
20. Chen, Y.; Li, B.; Xu, X.; Zhang, Z.; Tian, S. The pH-responsive PacC transcription factor plays pivotal roles in virulence and patulin biosynthesis in *Penicillium expansum*. *Environ. Microbiol.* **2018**, *20*, 4063–4078. [CrossRef] [PubMed]
21. Jurick, W.M., 2nd; Peng, H.; Beard, H.S.; Garrett, W.M.; Lichtner, F.J.; Luciano-Rosario, D.; Macarisin, O.; Liu, Y.; Peter, K.A.; Gaskins, V.L.; et al. Blistering1 Modulates *Penicillium expansum* Virulence Via Vesicle-mediated Protein Secretion. *Mol. Cell Proteom.* **2020**, *19*, 344–361. [CrossRef]
22. El Hajj Assaf, C.; Snini, S.P.; Tadrist, S.; Bailly, S.; Naylies, C.; Oswald, I.P.; Lorber, S.; Puel, O. Impact of *veA* on the development, aggressiveness, dissemination and secondary metabolism of *Penicillium expansum*. *Mol. Plant Pathol.* **2018**, *19*, 1971–1983. [CrossRef]
23. Tannous, J.; Barda, O.; Luciano-Rosario, D.; Prusky, D.B.; Sionov, E.; Keller, N.P. New insight into pathogenicity and secondary metabolism of the plant pathogen *Penicillium expansum* through deletion of the epigenetic reader SntB. *Front. Microbiol.* **2020**, *11*, 610. [CrossRef] [PubMed]
24. Kumar, D.; Barad, S.; Chen, Y.; Luo, X.; Tannous, J.; Dubey, A.; Glam Matana, N.; Tian, S.; Li, B.; Keller, N.; et al. LaeA regulation of secondary metabolism modulates virulence in *Penicillium expansum* and is mediated by sucrose. *Mol. Plant Pathol.* **2017**, *18*, 1150–1163. [CrossRef]

25. Tannous, J.; Kumar, D.; Sela, N.; Sionov, E.; Prusky, D.; Keller, N.P. Fungal attack and host defence pathways unveiled in near-avirulent interactions of *Penicillium expansum creA* mutants on apples. *Mol. Plant Pathol.* **2018**, *19*, 2635–2650. [CrossRef] [PubMed]
26. Visagie, C.M.; Houbraken, J.; Frisvad, J.C.; Hong, S.B.; Klaassen, C.H.; Perrone, G.; Seifert, K.A.; Varga, J.; Yaguchi, T.; Samson, R.A. Identification and nomenclature of the genus *Penicillium*. *Stud. Mycol.* **2014**, *78*, 343–371. [CrossRef] [PubMed]
27. Bartholomew, H.P.; Luciano-Rosario, D.; Bradshaw, M.J.; Gaskins, V.L.; Peng, H.; Fonseca, J.M.; Jurick, W.M., 2nd. Avirulent Isolates of *Penicillium chrysogenum* to Control the Blue Mold of Apple Caused by *P. expansum*. *Microorganisms* **2023**, *11*, 2792. [CrossRef]
28. Guzmán-Chávez, F.; Zwahlen, R.D.; Bovenberg, R.A.L.; Driessen, A.J.M. Engineering of the Filamentous Fungus *Penicillium chrysogenum* as Cell Factory for Natural Products. *Front. Microbiol.* **2018**, *9*, 2768. [CrossRef]
29. Fierro, F.; Vaca, I.; Castillo, N.I.; García-Rico, R.O.; Chávez, R. *Penicillium chrysogenum*, a Vintage Model with a Cutting-Edge Profile in Biotechnology. *Microorganisms* **2022**, *10*, 573. [CrossRef]
30. Bartholomew, H.P.; Bradshaw, M.; Jurick, W.M., 2nd; Fonseca, J.M. The Good, the Bad, and the Ugly: Mycotoxin Production During Postharvest Decay and Their Influence on Tritrophic Host-Pathogen-Microbe Interactions. *Front. Microbiol.* **2021**, *12*, 611881. [CrossRef] [PubMed]
31. Legein, M.; Smets, W.; Vandenheuvel, D.; Eilers, T.; Muyshondt, B.; Prinsen, E.; Samson, R.; Lebeer, S. Modes of Action of Microbial Biocontrol in the Phyllosphere. *Front. Microbiol.* **2020**, *11*, 1619. [CrossRef]
32. Di Francesco, A.; Martini, C.; Mari, M. Biological control of postharvest diseases by microbial antagonists: How many mechanisms of action? *Eur. J. Plant Pathol.* **2016**, *145*, 711–717. [CrossRef]
33. Yu, J.; Jurick II, W.M.; Cao, H.; Yin, Y.; Gaskins, V.L.; Losada, L.; Zafar, N.; Kim, M.; Bennett, J.W.; Nierman, W.C. Draft genome sequence of *Penicillium expansum* strain R19, which causes postharvest decay of apple fruit. *Genome Announc.* **2014**, *2*, e00635-14. [CrossRef]
34. Ballester, A.R.; Marcet-Houben, M.; Levin, E.; Sela, N.; Selma-Lázaro, C.; Carmona, L.; Wisniewski, M.; Droby, S.; González-Candelas, L.; Gabaldón, T. Genome, Transcriptome, and Functional Analyses of *Penicillium expansum* Provide New Insights Into Secondary Metabolism and Pathogenicity. *Mol. Plant Microbe Interact.* **2015**, *28*, 232–248. [CrossRef] [PubMed]
35. Li, H.; Handsaker, B.; Wysoker, A.; Fennell, T.; Ruan, J.; Homer, N.; Marth, G.; Abecasis, G.; Durbin, R. 1000 Genome Project Data Processing Subgroup. The Sequence Alignment/Map format and SAMtools. *Bioinformatics* **2009**, *25*, 2078–2079. [CrossRef]
36. De Coster, W.; Rademakers, R. NanoPack2: Population-scale evaluation of long-read sequencing data. *Bioinformatics* **2023**, *39*, btad311. [CrossRef]
37. De Coster, W.; D'Hert, S.; Schultz, D.T.; Cruts, M.; Van Broeckhoven, C. NanoPack: Visualizing and processing long-read sequencing data. *Bioinformatics* **2018**, *34*, 2666–2669. [CrossRef]
38. Kolmogorov, M.; Yuan, J.; Lin, Y.; Pevzner, P.A. Assembly of long, error-prone reads using repeat graphs. *Nat. Biotechnol.* **2019**, *37*, 540–546. [CrossRef] [PubMed]
39. Cheng, H.; Concepcion, G.T.; Feng, X.; Zhang, H.; Li, H. Haplotype-resolved de novo assembly using phased assembly graphs with hifiasm. *Nat. Methods* **2021**, *18*, 170–175. [CrossRef] [PubMed]
40. Rautiainen, M.; Nurk, S.; Walenz, B.P.; Logsdon, G.A.; Porubsky, D.; Rhie, A.; Eichler, E.E.; Phillippy, A.M.; Koren, S. Telomere-to-telomere assembly of diploid chromosomes with Verkko. *Nat. Biotechnol.* **2023**, *41*, 1474–1482. [CrossRef]
41. Alonge, M.; Lebeigle, L.; Kirsche, M.; Jenike, K.; Ou, S.; Aganezov, S.; Wang, X.; Lippman, Z.B.; Schatz, M.C.; Soyk, S. Automated assembly scaffolding using RagTag elevates a new tomato system for high-throughput genome editing. *Genome Biol.* **2022**, *23*, 258. [CrossRef] [PubMed]
42. Simão, F.A.; Waterhouse, R.M.; Ioannidis, P.; Kriventseva, E.V.; Zdobnov, E.M. BUSCO: Assessing genome assembly and annotation completeness with single-copy orthologs. *Bioinformatics* **2015**, *31*, 3210–3212. [CrossRef]
43. Gottschalk, C.; Evans, B.; Collum, T.D. Improved Genome Assembly Resource of the Plant Pathogen *Fusarium avenaceum*. *PhytoFront* **2023**, *3*, 461–465. [CrossRef]
44. Luciano-Rosario, D.; Jurick, W.M., II; Gottschalk, C. The Near-Gapless *Penicillium fuscoglaucum* Genome Enables the Discovery of Lifestyle Features as an Emerging Post-Harvest Phytopathogen. *J. Fungi* **2024**, *10*, 430. [CrossRef] [PubMed]
45. Flynn, J.M.; Hubley, R.; Goubert, C.; Rosen, J.; Clark, A.G.; Feschotte, C.; Smit, A.F. RepeatModeler2 for automated genomic discovery of transposable element families. *Proc. Natl. Acad. Sci. USA* **2020**, *117*, 9451–9457. [CrossRef] [PubMed]
46. Smit, A.F.; Hubley, R.; Green, P. RepearMasker Open-4.0. 2013. Available online: http://repeatmasker.org (accessed on 1 October 2023).
47. Humann, J.L.; Lee, T.; Ficklin, S.; Main, D. Structural and Functional Annotation of Eukaryotic Genomes with GenSAS. *Methods Mol. Biol.* **2019**, *1962*, 29–51. [CrossRef]
48. Chen, S.; Zhou, Y.; Chen, Y.; Gu, J. fastp: An ultra-fast all-in-one FASTQ preprocessor. *Bioinformatics* **2018**, *34*, i884–i890. [CrossRef]
49. Kim, D.; Paggi, J.M.; Park, C.; Bennett, C.; Salzberg, S.L. Graph-based genome alignment and genotyping with HISAT2 and HISAT-genotype. *Nat. Biotechnol.* **2019**, *37*, 907–915. [CrossRef] [PubMed]

50. Kovaka, S.; Zimin, A.V.; Pertea, G.M.; Razaghi, R.; Salzberg, S.L.; Pertea, M. Transcriptome assembly from long-read RNA-seq alignments with StringTie2. *Genome Biol.* **2019**, *20*, 278. [CrossRef] [PubMed]
51. Pertea, G.; Pertea, M. GFF Utilities: GffRead and GffCompare. *F1000Research* **2020**, *9*, 304. [CrossRef]
52. Campbell, M.S.; Holt, C.; Moore, B.; Yandell, M. Genome Annotation and Curation Using MAKER and MAKER-P. *Curr. Protoc. Bioinform.* **2014**, *48*, 4.11.1–4.11.39. [CrossRef]
53. Cheeseman, K.; Ropars, J.; Renault, P.; Dupont, J.; Gouzy, J.; Branca, A.; Abraham, A.L.; Ceppi, M.; Conseiller, E.; Debuchy, R.; et al. Multiple recent horizontal transfers of a large genomic region in cheese making fungi. *Nat. Commun.* **2014**, *5*, 2876. [CrossRef] [PubMed]
54. Hoff, K.J.; Stanke, M. Predicting Genes in Single Genomes with AUGUSTUS. *Curr. Protoc. Bioinform.* **2019**, *65*, e57. [CrossRef] [PubMed]
55. Korf, I. Gene finding in novel genomes. *BMC Bioinform.* **2004**, *5*, 59. [CrossRef] [PubMed]
56. Camacho, C.; Coulouris, G.; Avagyan, V.; Ma, N.; Papadopoulos, J.; Bealer, K.; Madden, T.L. BLAST+: Architecture and applications. *BMC Bioinform.* **2009**, *10*, 421. [CrossRef] [PubMed]
57. Jones, P.; Binns, D.; Chang, H.Y.; Fraser, M.; Li, W.; McAnulla, C.; McWilliam, H.; Maslen, J.; Mitchell, A.; Nuka, G.; et al. InterProScan 5: Genome-scale protein function classification. *Bioinformatics* **2014**, *30*, 1236–1240. [CrossRef]
58. Nawrocki, E.P.; Eddy, S.R. Infernal 1.1: 100-fold faster RNA homology searches. *Bioinformatics* **2013**, *29*, 2933–2935. [CrossRef]
59. Wang, Y.; Tang, H.; Debarry, J.D.; Tan, X.; Li, J.; Wang, X.; Lee, T.H.; Jin, H.; Marler, B.; Guo, H.; et al. MCScanX: A toolkit for detection and evolutionary analysis of gene synteny and collinearity. *Nucleic Acids Res.* **2012**, *40*, e49. [CrossRef]
60. Emms, D.M.; Kelly, S. OrthoFinder: Phylogenetic orthology inference for comparative genomics. *Genome Biol.* **2019**, *20*, 238. [CrossRef]
61. Blin, K.; Shaw, S.; Augustijn, H.E.; Reitz, Z.L.; Biermann, F.; Alanjary, M.; Fetter, A.; Terlouw, B.R.; Metcalf, W.W.; Helfrich, E.J.N.; et al. AntisMash 7.0: New and improved predictions for detection, regulation, chemical structures and visualisation. *Nucleic Acids Res.* **2023**, *51*, W46–W50. [CrossRef]
62. R Core Team. *R: A Language and Environment for Statistical Computing*; R Foundation for Statistical Computing: Vienna, Austria, 2023. Available online: https://www.R-project.org/ (accessed on 1 October 2023).
63. Cooper, B.; Yang, R. An assessment of AcquireX and Compound Discoverer software 3.3 for non-targeted metabolomics. *Sci. Rep.* **2024**, *14*, 4841. [CrossRef]
64. Malysheva, S.V.; Diana Di Mavungu, J.; Boonen, J.; De Spiegeleer, B.; Goryacheva, I.Y.; Vanhaecke, L.; De Saeger, S. Improved positive electrospray ionization of patulin by adduct formation: Usefulness in liquid chromatography–tandem mass spectrometry multi-mycotoxin analysis. *J. Chromatogr. A* **2012**, *1270*, 334–339. [CrossRef]
65. Wu, G.; Jurick, W.M., II; Lichtner, F.J.; Peng, H.; Yin, G.; Gaskins, V.L.; Yin, Y.; Hua, S.; Peter, K.A.; Bennett, J.W. Whole-genome Comparisons of *Penicillium* spp. Reveals Secondary Metabolic Gene Clusters and Candidate Genes Associated with Fungal Aggressiveness during Apple Fruit Decay. *PeerJ* **2019**, *7*, E6170. [CrossRef]
66. Martín, J.F. Insight into the Genome of Diverse *Penicillium chrysogenum* Strains: Specific Genes, Cluster Duplications and DNA Fragment Translocations. *Int. J. Mol. Sci.* **2020**, *21*, 3936. [CrossRef]
67. Petersen, C.; Sørensen, T.; Nielsen, M.R.; Sondergaard, T.E.; Sørensen, J.L.; Fitzpatrick, D.A.; Frisvad, J.C.; Nielsen, K.L. Comparative genomic study of the *Penicillium* genus elucidates a diverse pangenome and 15 lateral gene transfer events. *IMA Fungus* **2023**, *14*, 3. [CrossRef] [PubMed]
68. Jet Harvest Solutions. Bio-Save. Available online: https://www.jetharvest.com/bio-save-1 (accessed on 1 October 2024).
69. Chen, D.; Li, G.; Liu, J.; Wisniewski, M.; Droby, S.; Levin, E.; Huang, S.; Liu, Y. Multiple transcriptomic analyses and characterization of pathogen-related core effectors and LysM family members reveal their differential roles in fungal growth and pathogenicity in *Penicillium expansum*. *Mol. Genet. Genom.* **2020**, *295*, 1415–1429. [CrossRef]
70. Vilanova, L.; Vall-Llaura, N.; Torres, R.; Usall, J.; Teixidó, N.; Larrigaudière, C.; Giné-Bordonaba, J. *Penicillium expansum* (compatible) and *Penicillium digitatum* (non-host) pathogen infection differentially alter ethylene biosynthesis in apple fruit. *Plant Physiol. Biochem.* **2017**, *120*, 132–143. [CrossRef]
71. Ma, K.W.; Ma, W. Phytohormone pathways as targets of pathogens to facilitate infection. *Plant Mol. Biol.* **2016**, *91*, 713–725. [CrossRef] [PubMed]
72. Lafuente, M.T.; González-Candelas, L. Phytohormones in the *Penicillium digitatum*-citrus fruit interaction. *Postharvest Biol. Technol.* **2024**, *209*, 112704. [CrossRef]
73. Kumar, D.; Barad, S.; Sionov, E.; Keller, N.P.; Prusky, D.B. Does the Host Contribute to Modulation of Mycotoxin Production by Fruit Pathogens? *Toxins* **2017**, *9*, 280. [CrossRef]
74. Gong, D.; Bi, Y.; Li, Y.; Zong, Y.; Han, Y.; Prusky, D. Both *Penicillium expansum* and *Trichothecim roseum* Infections Promote the Ripening of Apples and Release Specific Volatile Compounds. *Front. Plant Sci.* **2019**, *10*, 338. [CrossRef] [PubMed]
75. Ji, Y.; Wang, A. Recent Advances in Phytohormone Regulation of Apple-Fruit Ripening. *Plants* **2021**, *10*, 2061. [CrossRef] [PubMed] [PubMed Central]

76. Lončarić, A.; Šarkanj, B.; Gotal, A.-M.; Kovač, M.; Nevistić, A.; Fruk, G.; Skendrović, B.M.; Babić, J.; Miličević, B.; Kovač, T. *Penicillium expansum* Impact and Patulin Accumulation on Conventional and Traditional Apple Cultivars. *Toxins* **2021**, *13*, 703. [CrossRef]
77. Kim, S.; Chen, J.; Cheng, T.; Gindulyte, A.; He, J.; He, S.; Li, Q.; Shoemaker, B.A.; Thiessen, P.A.; Yu, B.; et al. PubChem 2023 update. *Nucleic Acids Res.* **2023**, *51*, D1373–D1380. [CrossRef]
78. Yoshikawa, M.; Murakami, T.; Shimada, H.; Yoshizumi, S.; Saka, M.; Yamahara, J.; Matsuda, H. Medicinal foodstuffs. XIV. On the bioactive constituents of moroheiya. (2): New fatty acids, corchorifatty acids A, B, C, D, E, and F, from the leaves of *Corchorus olitorius* L. (*Tiliaceae*): Structures and inhibitory effect on NO production in mouse peritoneal macrophages. *Chem. Pharm. Bull.* **1998**, *46*, 1008–1014. [CrossRef]
79. Rehdorf, J.; Kleber, A. Active Combinations of Perillic Acid and Activity Enhancing Substances. European Patent No. WO2017129338A1, 22 December 2016.
80. Plumridge, A.; Hesse, S.J.; Watson, A.J.; Lowe, K.C.; Stratford, M.; Archer, D.B. The weak acid preservative sorbic acid inhibits conidial germination and mycelial growth of *Aspergillus niger* through intracellular acidification. *Appl. Environ. Microbiol.* **2004**, *70*, 3506–3511. [CrossRef] [PubMed]
81. Moro, C.B.; Lemos, J.G.; Gasperini, A.M.; Stefanello, A.; Garcia, M.V.; Copetti, M.V. Efficacy of weak acid preservatives on spoilage fungi of bakery products. *Int. J. Food Microbiol.* **2022**, *374*, 109723. [CrossRef] [PubMed]
82. Podgórska, E. Effect of preservatives on patulin production by *Penicillium expansum*. *Acta Microbiol. Pol.* **1992**, *41*, 97–107. [PubMed]
83. Reina, J.C.; Pérez-Victoria, I.; Martín, J.; Llamas, I. A Quorum-Sensing Inhibitor Strain of *Vibrio alginolyticus* Blocks Qs-Controlled Phenotypes in *Chromobacterium violaceum* and *Pseudomonas aeruginosa*. *Mar. Drugs* **2019**, *17*, 494. [CrossRef] [PubMed]
84. Masi, M.; Castaldi, S.; Sautua, F.; Pescitelli, G.; Carmona, M.A.; Evidente, A. Truncatenolide, a Bioactive Disubstituted Nonenolide Produced by *Colletotrichum truncatum*, the Causal Agent of Anthracnose of Soybean in Argentina: Fungal Antagonism and SAR Studies. *J. Agric. Food Chem.* **2022**, *70*, 9834–9844. [CrossRef]
85. Antika, L.D.; Tasfiyati, A.N.; Hikmat, H.; Septama, A.W. Scopoletin: A review of its source, biosynthesis, methods of extraction, and pharmacological activities. *J. Biosci.* **2022**, *77*, 303–316. [CrossRef]
86. Yan, J.; Xing, Z.; Lei, P.; Sikandar, A.; Yang, R.; Wang, Y.; Zhu, X.; Liu, X.; Fan, H.; Xuan, Y.; et al. Evaluation of Scopoletin from *Penicillium janthinellum* Snef1650 for the Control of Heterodera glycines in Soybean. *Life* **2021**, *11*, 1143. [CrossRef] [PubMed]
87. Trush, K.; Pal'ove-Balang, P. Biosynthesis and role of isoflavonoids in legumes under different environmental conditions. *Plant Stress.* **2023**, *8*, 100153. [CrossRef]
88. Jiang, L.; Wu, P.; Yang, L.; Liu, C.; Guo, P.; Wang, H.; Wang, S.; Xu, F.; Zhuang, Q.; Tong, X.; et al. Transcriptomics and metabolomics reveal the induction of flavonoid biosynthesis pathway in the interaction of *Stylosanthes-Colletotrichum gloeosporioides*. *Genomics* **2021**, *113*, 2702–2716. [CrossRef]
89. Clemmensen, S.E.; Cowled, M.S.; Kromphardt, K.J.K.; Frisvad, J.C.; Larsen, T.O.; Frandsen, R.J.N. The role and fate of patulin in apple-associated fungal-fungal interactions. *Fungal Ecol.* **2024**, *69*, 101341. [CrossRef]
90. Chen, Y.; Zhang, Y.; Xu, D.; Zhang, Z.; Li, B.; Tian, S. PeAP1-mediated oxidative stress response plays an important role in the growth and pathogenicity of *Penicillium expansum*. *Microbiol. Spectr.* **2023**, *11*, e0380822. [CrossRef] [PubMed]
91. Zhang, F.; Zhang, X.; Gong, D.; Yu, L.; Prusky, D.; Sionov, E.; Bi, Y.; Zong, Y. ArfA and SarA small GTPases involved in growth, patulin biosynthesis and virulence of *Penicillium expansum*. *Postharvest Biol. Technol.* **2023**, *205*, 112506.
92. Xu, X.; Chen, Y.; Zhang, Z.; Chen, T.; Li, B.; Tian, S. Set1/COMPASS regulates growth, pathogenicity, and patulin biosynthesis of *Penicillium expansum* via H3K4 methylation and the interaction with PeVelB. *J. Adv. Res.* **2024**, *62*, 47–57. [CrossRef]
93. Zetina-Serrano, C.; Rocher, O.; Naylies, C.; Lippi, Y.; Oswald, I.P.; Lorber, S.; Puel, O. The *brlA* Gene Deletion Reveals That Patulin Biosynthesis Is Not Related to Conidiation in *Penicillium expansum*. *Int. J. Mol. Sci.* **2020**, *21*, 6660. [CrossRef] [PubMed]
94. Zhou, J.; Gong, W.; Tu, T.; Zhang, J.; Xia, X.; Zhao, L.; Zhou, X.; Wang, Y. Transcriptome Analysis and Functional Characterization Reveal That Peclg Gene Contributes to the Virulence of *Penicillium expansum* on Apple Fruits. *Foods* **2023**, *12*, 479. [CrossRef]
95. Zhu, Y.; Zong, Y.; Gong, D.; Wang, X.; Oyom, W.; Bi, Y.; Prusky, D. PacC mediates spatial regulation of the phospholipid metabolism in the apple fruit-*Penicillium expansum* interaction. *Postharvest Biol. Technol.* **2024**, *208*, 112666. [CrossRef]
96. Xu, M.; Godana, E.A.; Li, J.; Deng, Y.; Ma, Y.; Ya, H.; Zhang, H. Infection of postharvest pear by *Penicillium expansum* is facilitated by the glycoside hydrolase (*eglB*) gene. *Int. J. Food Microbiol.* **2024**, *410*, 110465. [CrossRef]
97. Luciano-Rosario, D.; Peng, H.; Gaskins, V.L.; Fonseca, J.M.; Keller, N.P.; Jurick, W.M., 2nd. Mining the *Penicillium expansum* Genome for Virulence Genes: A Functional-Based Approach to Discover Novel Loci Mediating Blue Mold Decay of Apple Fruit. *J. Fungi* **2023**, *9*, 1066. [CrossRef] [PubMed]
98. Luciano-Rosario, D.; Barda, O.; Tannous, J.; Frawley, D.; Bayram, Ö.; Prusky, D.; Sionov, E.; Keller, N.P. The histone demethylase KdmB is part of a trimeric protein complex and mediates virulence and mycotoxin production in *Penicillium expansum*. *Fungal Genet. Biol.* **2023**, *169*, 103837. [CrossRef]

99. Chen, Y.; Zhang, Z.; Li, B.; Tian, S. PeMetR-mediated sulfur assimilation is essential for virulence and patulin biosynthesis in *Penicillium expansum*. *Environ. Microbiol.* **2021**, *23*, 5555–5568. [CrossRef]
100. Levin, E.; Kishore, A.; Ballester, A.; Raphael, G.; Feigenberg, O.; Liu, Y.; Norelli, J.L.; Gonzales-Candelas, L.; Wisniewski, M.E.; Droby, S. Identification of pathogenicity-related genes and the role of a subtilisin-related peptidase S8 (PePRT) in authophagy and virulence of *Penicillium expansum* on apples. *Postharvest Biol. Technol.* **2018**, *149*, 209–220. [CrossRef]
101. Zhang, X.; Zong, Y.; Gong, D.; Zhang, F.; Yu, L.; Bi, Y.; Sionov, E.; Prusky, D. Small GTPase RacA is critical for spore growth, patulin accumulation, and virulence of *Penicillium expansum*. *Postharvest Biol. Technol.* **2022**, *191*, 111964. [CrossRef]
102. Zong, Y.; Zhang, X.; Gong, D.; Zhang, F.; Yu, L.; Bi, Y.; Sionov, E.; Prusky, D. Small GTPases RasA and RasB regulate development, patulin production, and virulence of *Penicillium expansum*. *Postharvest Biol. Technol.* **2023**, *197*, 112192. [CrossRef]
103. Xu, X.; Chen, Y.; Li, B.; Tian, S. Arginine Methyltransferase PeRmtC Regulates Development and Pathogenicity of *Penicillium expansum* via Mediating Key Genes in Conidiation and Secondary Metabolism. *J. Fungi* **2021**, *7*, 807. [CrossRef] [PubMed]
104. Zhang, J.; Meng, D.; Xia, X.; Sun, Y.; Zhao, L.; Zhou, X.; Wang, Y. Profiling the secretomes of *Penicillium expansum* reveals that a serine carboxypeptidase (PeSCP) is required for the fungal virulence on apple fruit. *Physiol. Mol. Plant Pathol.* **2022**, *122*, 101897. [CrossRef]
105. Levin, E.; Droby, S.; Wisniewski, M.; Dardick, C. Role of Effector Proteins in the Virulence of *Penicillium expansum* on Apple Fruit. In *Postharvest Pathology*; Spadaro, D., Droby, S., Gullino, M.L., Eds.; Springer: Cham, Switzerland, 2021; Volume 11, pp. 1–19. [CrossRef]
106. Sánchez-Torres, P.; Vilanova, L.; Ballester, A.R.; López-Pérez, M.; Teixidó, N.; Viñas, I.; Usall, J.; González-Candelas, L.; Torres, R. Unravelling the contribution of the *Penicillium expansum* PeSte12 transcription factor to virulence during apple fruit infection. *Food Microbiol.* **2018**, *69*, 123–135. [CrossRef] [PubMed]
107. Tahtah, N.; Zetina-Serrano, C.; Rocher, O.; Naylies, C.; Lippi, Y.; El Khoury, A.; Atoui, A.; Jamin, E.L.; Oswald, I.P.; Lorber, S.; et al. Implication of VelB in the development, pathogenicity, and secondary metabolism of *Penicillium expansum*. *Postharvest Biol. Technol.* **2023**, *195*, 112121. [CrossRef]
108. Zhao, L.; Hu, Y.; Liang, L.; Dhanasekaran, S.; Zhang, X.; Yang, X.; Wu, M.; Song, Y.; Zhang, H. WSC1 Regulates the Growth, Development, Patulin Production, and Pathogenicity of *Penicillium expansum* Infecting Pear Fruits. *J. Agric. Food Chem.* **2024**, *72*, 1025–1034. [CrossRef] [PubMed]
109. Zhang, X.; Zong, Y.; Zhang, F.; Liu, Q.; Gong, D.; Bi, Y.; Sionov, E.; Prusky, D. The small GTPase Ypt7 of *Penicillium expansum* is required for growth, patulin biosynthesis and virulence. *Food Microbiol.* **2024**, *119*, 104434. [CrossRef] [PubMed]

Disclaimer/Publisher's Note: The statements, opinions and data contained in all publications are solely those of the individual author(s) and contributor(s) and not of MDPI and/or the editor(s). MDPI and/or the editor(s) disclaim responsibility for any injury to people or property resulting from any ideas, methods, instructions or products referred to in the content.

Journal of *Fungi*

MDPI

Review

Research Progress and Management Strategies for the Common Mycotoxin Contamination of Traditional Chinese Medicines

Zhimin Yang [1], Huali Xue [2,*], Ye Han [3], Hui Ding [1] and Ying Zhang [1]

[1] Lanzhou Institutes for Food and Drug Control, Lanzhou 730050, China; yzmljh@163.com (Z.Y.); dhc467828@gmail.com (H.D.); 13609310016@163.com (Y.Z.)
[2] College of Science, Gansu Agricultural University, Lanzhou 730070, China
[3] College of Food Science and Engineering, Gansu Agricultural University, Lanzhou 730070, China; hanyest1989@163.com
* Correspondence: xuehual@gsau.edu.cn; Tel.: +86-931-7631212

Abstract: With rapid globalization and the increasing demand for traditional Chinese medicines, quality and safety has become a critical priority for both domestic and international markets. However, traditional Chinese medicines are susceptible to contamination by pathogenic microorganisms during the process of cultivation, growth, processing, storage, and transportation, which can lead to mycotoxin contamination that adversely affect the quality and safety of traditional Chinese medicines, and may pose potential threats to human health. This review summarizes mycotoxin contamination, the common detection methods, prevention and control measures, and regulatory recommendations, aiming to provide references for improving the quality standards and ensuring safety of these medications.

Keywords: traditional Chinese medicine; mycotoxin contamination; detection methods; regulatory recommendations

1. Introduction

Traditional Chinese medicines have been integral to health practices in China for over 2000 years. However, they are susceptible to contamination by pathogenic microorganisms during the process of cultivation, growth, processing, storage, and transportation, which lead to mycotoxin accumulation, posing potential health risks, including carcinogenicity, hepatotoxicity, and nephrotoxicity [1]. Mycotoxins are secondary metabolites produced by certain filamentous fungi under suitable temperature and humidity conditions [2,3]. As the world's largest producer, consumer, and exporter of traditional Chinese medicines, China plays a pivotal role in the global medicine sales market. In 2022, China's annual output of traditional Chinese medicinal materials exceeded 20 million tons, accounting for over 70% of global production. The domestic consumption scale reached approximately 1.1 trillion yuan in 2023. The export value of traditional Chinese medicine products (including Chinese medicinal materials, extracts, Chinese patent medicines and decoction pieces) amounted to $4.2 billion, with major market in Japan, South Korea, and Southeast Asia. Currently, the main exported medicinal materials, such as *Ginseng*, *Astragalus*, *Wolfberry*, *Angelica sinensis*, *Honeysuckle*, and *Licorice*, are highly sought after, yet the quality and safety of traditional Chinese medicines caused by mycotoxins has become a trade barrier. Although the Chinese Pharmacopoeia has updated and gradually included mycotoxin testing requirements for a variety of traditional Chinese medicines, as well as to add some detection methods and permissible limit values; however, the formulation of relevant standards and

management measures are still lacking. Significant gaps remain in standardization and regulatory oversight.

In this review, we focus on the current situation of mycotoxin contamination in traditional Chinese medicines, summarize the types of mycotoxin contamination in different kinds of medicinal materials, and present mycotoxin detection methods and regulatory recommendations.

2. Mycotoxin Contamination in Traditional Chinese Medicines

With increasing attention being paid to the quality and safety of traditional Chinese medicines by consumers, the issue of mycotoxin contamination in traditional Chinese medicines has also garnered widespread concern. The contamination level of mycotoxins is related to the types of traditional Chinese medicines and the species of fungi. Mycotoxins are produced by certain species of *Aspergillus*, *Fusarium*, *Alternaria*, and *Penicillium* under appropriate temperature and humidity conditions during growth, storage, processing, and transportation. These fungi have the ability to produce more than 400 mycotoxins; however, only a few mycotoxins have been detected in traditional Chinese medicines, including aflatoxins (AFs), ochratoxins (OTs), zearalenone (ZEN), deoxynivalenol (DON, also known as vomitoxin), fumonisins (FBs), and patulin (PAT) [4–8]. These mycotoxins exhibit carcinogenic, teratogenic, mutagenic, and immunosuppressive effects [9,10], among others, and pose unpredictable threats to the health of animals and humans, even at low dose levels [11,12].

The Chinese Pharmacopoeia has been paying increasing attention to the types of traditional Chinese medicines that are susceptible to mycotoxin contamination. The 2010 edition of the Chinese Pharmacopoeia included aflatoxin testing requirements for the first time, covering five types of traditional Chinese medicines: *Bombyx batryticatus*, *Citri reticulatae pericarpium*, *Ziziphi spinosae semen*, *Persicae semen*, and *Sterculiae lychnophorae semen*. On this basis, the 2015 edition of the Chinese Pharmacopoeia added 14 types of AF testing requirements for traditional Chinese medicines (including *Jujubae fructus*, *Hirudo*, *Pheretima*, *Myristicae semen*, *Scorpio*, *Cassiae semen*, *Hordei fructus germinatus*, *Polygalae radix*, *Quisqualis fructus*, *Platycladi semen*, *Nelumbinis semen*, *Scolopendra*, *Arecae semen*, and *Coicis semen*). Further expanding on the 2015 edition, the 2020 edition added five types of traditional Chinese medicines, including *Corydalis rhizoma*, *Eupolyphaga steleophaga*, *Aspongopus*, *Vespae nidus*, and *Strychni semen*. The 2025 edition of the Chinese Pharmacopoeia further strengthens the control of mycotoxins in traditional Chinese medicines and decoction pieces. The aflatoxin testing requirements now include bran-fried *Coix seed* decoction pieces. Additionally, the zearalenone testing requirements, which previously applied to *Coicis semen* in the 2020 edition, have been expanded to include bran-fried *Coix seed* decoction pieces. Furthermore, ochratoxin A testing requirements have been introduced for the first time for medicinal materials such as *Astragalus radix* and *Arecae semen* (Figure 1). With the continuous improvement and updates to the Chinese Pharmacopoeia, the mycotoxin contamination in traditional Chinese medicines remain a subject of concern for consumers.

The most common detected mycotoxins in traditional Chinese medicines include AFB_1, AFB_2, AFG_1, AFG_2, ZEN, DON, OTA, T-2 toxin, FB_1, FB_2, and PAT [13,14], which are contaminated by the fungal genera *Penicillium*, *Fusarium*, *Aspergillus*, and *Alternaria*. In general, aflatoxins and ochratoxins are primarily produced by the *Aspergillus* species (such as, *A. flavus*, *A. parasiticus*, *A. ochraceus*, *A. niger*, and *A. carbonarius*). *Fusarium* toxins are mainly produced by *Fusarium* spp. (including *F. graminearum*, *F. verticillioides*, *F. equiseti*, *F. culmorum*, and *F. asiaticum*), mainly including ZEN, DON, T-2 toxin, and FBs, among others. Patulin is primarily produced by *Penicillium expansum* [15,16]. Based on the carcinogenicity of mycotoxins, the International Agency for Research on Cancer

(IARC) classified mycotoxins into three groups in 1993. AFs were classified as Group 1 (carcinogenic to humans) due to their sufficient evidence of carcinogenicity in humans; OTs and FB_1 were classified as Group 2B (possibly carcinogenic to humans), for which there is limited but not conclusive evidence of carcinogenicity from human, experimental animal and/or mechanistic data. ZEN, DON, T-2 toxin, and PAT were classified as Group 3 (not classifiable as to its carcinogenicity to humans), for which there is limited and inadequate evidence, or no data in human and experimental animals to classify these [17] (Figure 2).

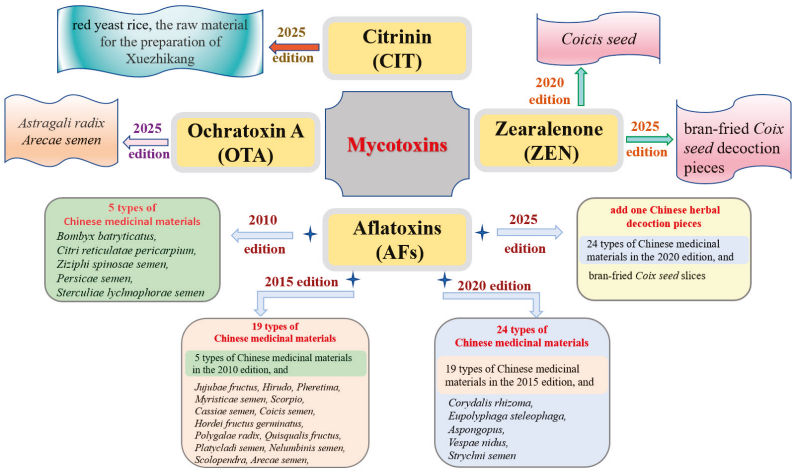


Figure 1. The varieties of traditional Chinese medicines tested for mycotoxins in the 2010 to 2025 editions of the Chinese Pharmacopoeia.

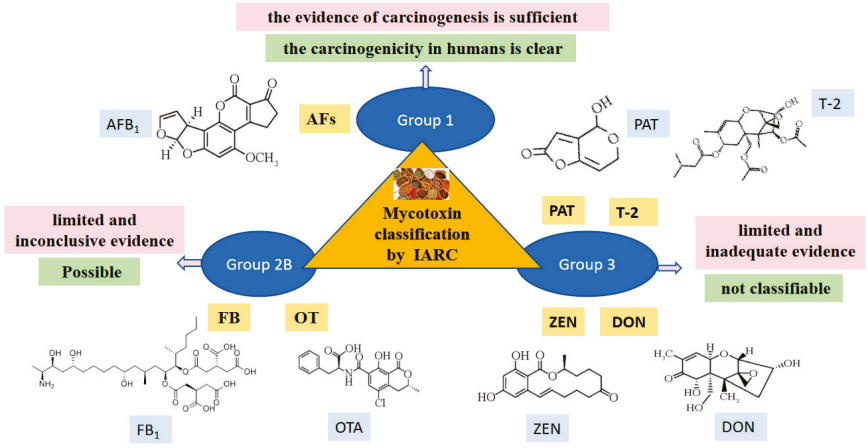


Figure 2. Classification and carcinogenicity of common mycotoxins in the Chinese medicinal material.

Group 1 mycotoxins (carcinogenic to humans), which includes aflatoxins (AFs), are secondary metabolites with a dihydrofuran coumarin structure, and are produced by *Aspergillus* spp., particularly *A. flavus* and *A. parasiticus* [4,18,19]. More than 20 kinds of aflatoxins with clearly defined structures have been found, including aflatoxin B_1, B_2, G_1, G_2, M_1, M_2, B_{2a}, G_{2a}, BM_{2a}, and GM_{2a}, among others [20]. AFB_1, AFB_2, AFG_1, and AFG_2 are the main aflatoxins contamination in traditional Chinese medicines, among which, AFB_1 is the most common and the most toxic aflatoxin. In recent years, there have been many reports about AF contamination in traditional Chinese medicines. Su et al. detected AFB_1 at a concentration of 4.54 μg/kg in *Astragalus membranaceus* infected by *Aspergillus* and *Penicillium* species [5]. Yang et al. detected AFs (AFB_1, AFB_2, AFG_1, and AFG_2) in 34 batches of traditional Chinese medicines, AFB_1 and AFB_2 were detected in 3 batches of *Semen ziziphi spinosae*, among them, the detection values of AFB_1 and AFB_2 were 0.41~1.47 μg/kg and 2.74~20.98 μg/kg, respectively. Yang et al. also reported the

presence of AFG_1 in *Paeoniae radix alba*, with a concentration of 0.45 μg/kg [21]. Wang et al. found that two batches of *Licorice root* samples and one batch of *Fritillary bulbs* tested positive for AFB_1. The AFB_1 content in the *Licorice root* was 12.56 μg/kg and 26.11 μg/kg, while the AFB_1 content in the *Fritillary bulbs* was 10.06 μg/kg, all of which exceeded the maximum limits of 5 μg/kg [22]. High levels of AFB_1, up to 52.0 μg/kg, were detected in *Platycladi* [23]. A total of 30.8% of *Nutmeg* samples were contaminated with AFB_1, at levels ranging from 0.73 to 16.31 μg/kg, and 23.1% of the analyzed samples were co-contaminated with at least two different mycotoxins (AFB_1, AFB_2, AFG_1, and AFG_2) [24]. AFs have been classified as Group 1 mycotoxins (carcinogenic to humans). They are hepatotoxic, mutagenic, teratogenic, carcinogenic and immunosuppressive, posing severe threats to human health [25–28].

Group 2B mycotoxins (possibly carcinogenic to humans), which include ochratoxins (OTs), are one of the most common naturally occurring mycotoxins produced by *A. ochraceus*, *A. niger*, *A. carbonarius*, *P. viridicatum*, and *P. verrucosum*, as well as other *Penicillium* species [29–31]. OTs are isocoumarin toxins, including seven structurally similar compounds, among which OTA, OTB, OTC, and OTD are the main varieties. OTA is the most widely found ochratoxin in traditional Chinese medicines, and it exhibits the highest toxicity within the ochratoxin group [32]. Yang et al. reported that, for 31 of the visibly moldy traditional Chinese medicines and for 26 of the not visibly moldy samples tested, 74.2% of the visibly moldy samples and 7.7% of the not visibly moldy were contaminated with OTA. Specifically, OTA contamination was detected in *Licorice root*, *Mongolian milkvetch root*, *Baikal skullcap root*, *Barley sprout*, *Medicated leaven*, *Common turmeric rhizoma*, *Upland cotton root*, and *Sowthistle tasselflower herb* at different levels in the range of 1.3~84.4 μg/kg, 87.7~158.7 μg/kg, 1.6~1.8 μg/kg, 10.7 μg/kg, 2.4 μg/kg, 10.6 μg/kg, 27.1 μg/kg, and 12.9 μg/kg, respectively [33]. High levels of OTA (92.3 μg/kg) were also detected in tangerine seeds [23]. OTA was detected in the *Massa medicata fermentata*, with the concentration ranging from 1.2 to 5.9 μg/kg [34]. OTA is known to be nephrotoxic, hepatotoxic, immunosuppressive, genotoxic, neurotoxic, carcinogenic, teratogenic, and embryotoxic, posing severe risks to human health [35–38].

Fumonisins (FBs) are a group of secondary metabolites produced by *Fusarium* spp., such as *F. verticillioides*, *F. proliferatum*, *F. oxysporum*, and other related species. They are classified into four categories (A, B, C, and P), with the B series being the most significant and widely studied [39,40]; among these, FB_1 and FB_2 are the most common toxins. FB_1 is the strongest level toxicity, with heat-stable and water-soluble properties [19]. Li et al. detected FB_1 and FB_2 in *Eupolyphaga steleophaga* and Chinese medicinal preparations containing *Eupolyphaga steleophaga*; among these samples, the content of FB_1 and FB_2 was 13.51 μg/kg and 6.31 μg/kg, respectively. In Chinese medicinal preparations containing *Eupolyphaga steleophaga*, the detection values of FB_1 and FB_2 ranged from 2.38 μg/kg to 17.87 μg/kg and from 3.01 μg/kg to 7.89 μg/kg, respectively [41]. Wang et al. established a determination method for 26 kinds of mycotoxins with UPLC-MS/MS in *Notoginseng radix et rhizoma*, and one batch sample detected FB_2, with a detection value of 1.2 μg/kg [42]. Among 20 batches of *Ophiopogonis radix* samples, FB_2 was detected in 14 samples, with the levels ranging from 4.99 to 378.99 μg/kg, and a positive detection rate of 70% [43]. FBs mainly damage the heart, lungs, liver, kidneys, and other organs of animals. Additionally, the exposure to FBs has been linked to human esophageal cancer and neural tube defects [39,44].

Group 3 mycotoxins (not classifiable as to its carcinogenicity to humans) include ZEN, DON, T-2 toxin, and PAT. ZEN is an estrogenic mycotoxin produced by *Fusarium* spp. (primarily including *F. graminearum*, *F. asiaticum*, *F. equiseti*, and *F. culmorum*) under specific environmental conditions, such as high humidity and moderate temperatures [45]. ZEN is also a non-steroidal estrogenic toxin [46], which often co-occurs with DON and

AFs [47]. The natural occurrence of ZEN has been reported in many countries [48–50]. ZEN contamination was detected in 107 tested *Coix seed* samples, with 55.6% of them exceeding the Chinese regulatory standards [51]. The detection rate of ZEN in *Coix seed* samples is relatively high, with the content of ZEN ranging from 0.343 μg/kg to 129.767 μg/kg [52]. ZEN contamination levels in the *Coicis semen* samples ranged from 2.77 μg/kg to 1076.18 μg/kg, with a detection rate of 84% and an over-standard rate of 6% [53]. Xu et al. detected ZEN in *Quisqualis indica L.*, with a detection rate of 1.52% [54]. Zhang et al. reported the levels of ZEN in *Massa medicata fermentata* ranging from 22.0 to 557.0 μg/kg [34]. ZEN mainly damages human endocrine and reproductive functions, leading to adverse effects, such as infertility, miscarriage, and other phenomena [55].

DON is one kind of trichothecene mycotoxin produced by the *Fusarium* species (mainly including *F. graminearum*, *F. culmorum*, *F. pseudograminearum*, and *F. sporotrichioides*) during the growth of agricultural crops [38]. It is the most common mycotoxin contaminating traditional Chinese medicines. DON is a representative of the type-B trichothecenes [56,57], and its contamination is widespread. In *Coicis semen* samples, DON contamination levels ranged from 1.54 to 360.12 μg/kg, with a detection rate of 36% [53]. Ten mycotoxins were detected in 483 traditional Chinese medicines, with a detection rate of 4.8%, and an average content of 52.9 μg/kg in positive samples [58]. DON mainly causes vomiting, diarrhea, gastrointestinal discomfort, headache, nausea, and other symptoms in humans and animals. In severe cases, DON can damage the hematopoietic system and even lead to death, and can often have synergistic effects with other mycotoxins [59,60].

T-2 toxin is a type A trichothecene mycotoxin primarily produced by certain *Fusarium* species, notably *F. sporotrichioides* and *F. langsethiae* under specific environmental conditions. It is a representative of the type-A trichothecene that is one of the most toxic mycotoxins among the type-A trichothecene. Li et al. reported T-2 contaminations in *Polygonum multiflorum* and *Panax notoginseng*, and the content level was 1.93 μg/kg [61]. Zhao et al. detected 10 mycotoxins in 30 batches of traditional Chinese medicines. Among them, the positive detection rates were 80%, 60% and 70%, and the average concentration levels were 1.19 ± 0.54 μg/kg, 0.86 ± 0.61 μg/kg, and 1.00 ± 0.45 μg/kg for *Polygalae radix*, *Coicis semen*, and *Eupolyphaga steleophaga*, respectively, which were all less than 2.0 μg/kg [62]. Although the contamination levels of T-2 toxin reported in traditional Chinese medicines were low, its toxicity should be paid attention to. T-2 toxin can directly stimulate the skin and mucosa, causing inflammation, and can also damage bone marrow hematopoietic tissue, enhance capillary permeability, and cause incomplete blood coagulation, resulting in visceral bleeding [15,63]. In addition, T-2 toxin can cause pathological changes in liver tissue and damage to the immune system [64].

PAT, also known as patulin, is a polyacetal lactone compound that is a secondary metabolite generated by *Penicillium*, *Aspergillus*, *Byssochlomys*, and *Paecilomyces* species under favorable conditions; it is usually found in pome fruits and their derivative products [65]. Zhang et al. found the blue mold tissues of Lanzhou Lily to be contaminated with patulin, produced by *P. gladioli* and *P. polonicum*, with a content of 2.38 μg/mL and 1.51 μg/mL, respectively [66]. PAT was detected in fresh *Codonopsis pilosula* infected by *P. expansum*, and HT-2 toxin and 15-acetyl-deoxynivalenol were also found in fresh *Codonopsis pilosula* infected by *F. acuminatum*, while DON, HT-2 toxin, and 15-acetyl-deoxynivalenol were detected in fresh *Codonopsis pilosula* infected by *Trichothecium roseum* [67]. PAT, sterigmatocystin, and 15-acetyl-deoxynivalenol were detected in fresh *Angelica sinensis* inoculated with *P. polonicum*, *Aspergillus versicolor*, and *F. solani*, respectively [68]. All the above results indicated that PAT existed widely in traditional Chinese medicines. PAT has broad toxicity, and exposure to PAT can cause a variety of symptoms in humans and animals, including nausea, vomiting, convulsions, and coma [69]. Furthermore, PAT has cytotoxicity,

teratogenicity, carcinogenicity, and mutagenicity toxicity, as well as immunotoxicity at high doses [70–72].

3. Detection Methods of Mycotoxins in Traditional Chinese Medicines

3.1. Detection Methods and Limited Standards of Mycotoxins in the Chinese Pharmacopoeia

The 2010 edition of the Chinese Pharmacopoeia stipulates the AF determination method to be high performance liquid chromatography (HPLC), including high performance liquid chromatography–iodine derivatization and high performance liquid chromatography–photochemical derivatization. The 2015 edition of the AF determination method adds high-performance liquid chromatography tandem mass spectrometry (HPLC-MS/MS). The 2020 edition of the AF determination method adds enzyme-linked immunosorbent assay (ELISA), as well as HPLC and HPLC-MS/MS for the determination of OTA, ZEN, and DON, HPLC-MS/MS for PAT, and high performance liquid chromatography with fluorescence detection (HPLC-FLD) for the determination of ZEN. The appendix includes HPLC-MS/MS for the determination of multiple mycotoxins, covering a total of seven categories and 11 types of toxins, namely AFB_1, AFB_2, AFG_1, AFG_2, OTA, DON, ZEN, PAT, FB_1, FB_2, and T-2 toxin.

The 2020 edition of the Chinese Pharmacopoeia stipulates a permissible limit of 5 μg/kg for AFB_1 and 10 μg/kg for the total AFs (the sum of AFB_1, AFB_2, AFG_1, and AFG_2) in 24 types of traditional Chinese medicines. It also adds a permissible limit of 500 μg/kg for ZEN in *Coicis semen* for the first time (Table 1). There are no detection methods developed for other mycotoxins, and there is no clear limit standard.

Table 1. The limit values of mycotoxins in the 2020 edition of the Chinese Pharmacopoeia.

Traditional Chinese Medicines	The Limit Value of Mycotoxins (μg/kg)		
	Total AFs	AFB_1	ZEN
Bombyx batryticatus, *Citri reticulatae pericarpium*, *Ziziphi spinosae semen*, *Persicae semen*, *Hirudo*, *Sterculiae lychnophorae semen*, *Jujubae fructus*, *Pheretima*, *Myristicae semen*, *Cassiae semen*, *Hordei fructus germinatus*, *Quisqualis fructus*, *Polygalae radix*, *Platycladi semen*, *Scorpio*, *Nelumbinis semen*, *Scolopendra*, *Arecae semen*, *Coicis semen*, *Corydalis rhizoma*, *Aspongopus*, *Eupolyphaga steleophaga*, *Vespae nidus*, and *Strychni semen*.	10	5	/
Coicis semen	/	/	500

3.2. The Process of Common Detection Methods for Mycotoxins

It is well known that traditional Chinese medicines have a complex matrix, which makes it extremely difficult to determine the contamination of mycotoxins. However, with the rapid and continuous development of detection technology and the diversification of detection techniques, it is possible to meet the needs of the detection of mycotoxins in complex matrices. In recent years, the major detection methods for common mycotoxins in traditional Chinese medicines mainly included HPLC, HPLC-MS/MS, rapid detection technology, and field real-time monitoring technology. A variety of pre-treatment methods have currently been implemented. The most commonly used methods for mycotoxin treatment are solid phase extraction (SPE), immune-affinity columns (IAC), multifunctional cleanup columns, column chromatography, and QuEChERS. A flow diagram of common

steps for mycotoxin analysis in traditional Chinese medicines is presented in Figure 3. These technologies have their own advantages and disadvantages, and should be selected according to different application scenarios to provide help for the detection, analysis, and quality safety control of mycotoxins in traditional Chinese medicines. The contamination status of mycotoxins detected by these instrumental methods in traditional Chinese medicines are shown in Table 2.

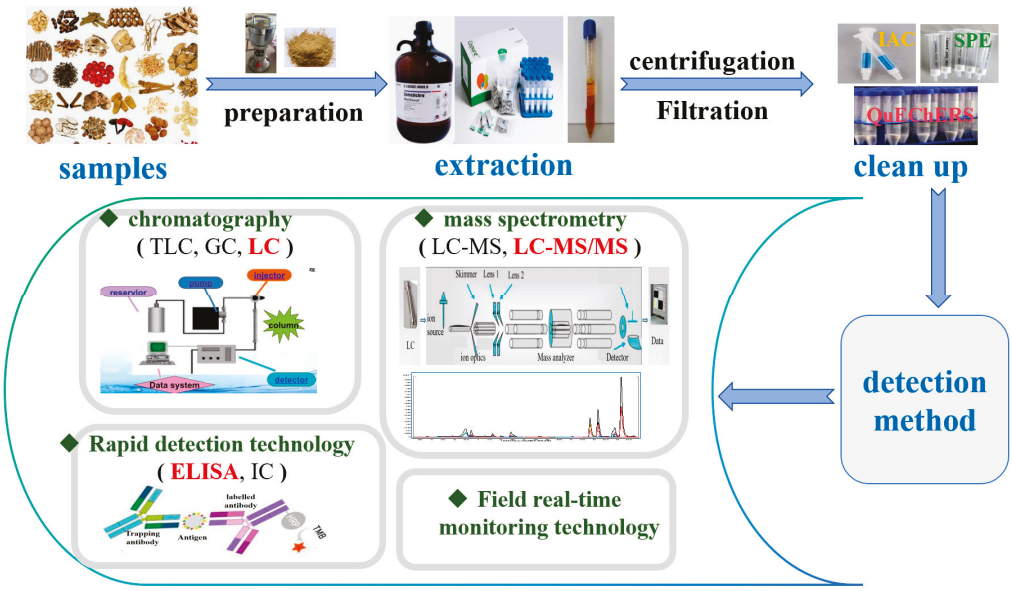


Figure 3. Flow diagram of common steps in mycotoxin analysis.

3.2.1. Liquid Chromatography

High performance liquid chromatography (HPLC) is based on the different retention time of different components in the chromatography column to be separated effectively, which places higher requirements on the sample, as most of the pretreatment requires immunoaffinity column to clean up and derivatization determination, including pre-column derivatizations [73], post-column derivatizations [21,74], photochemical derivatizations, and electrochemical derivatizations [75]. The pretreatment steps are complex, the detection cost is high, often only used to determine a single mycotoxin or a group of chemically related mycotoxins, and not suitable for the screening of large-batch samples. Yang et al. established HPLC methods combined with post-column photochemical derivatization after immunoaffinity column purification to determine aflatoxin B_1, B_2, G_1, and G_2 in 34 batches of traditional Chinese medicines. Among them, AFs were detected in three batches of *Semen ziziphi spinosae*, and AFB_1 in one batch exceeded the national standard limit (5 μg/kg) [21]. Yin et al. detected the content of four aflatoxins (AFB_1, AFB_2, AFG_1, AFG_2) in 21 kinds of traditional Chinese medicines by high performance liquid chromatography–post column iodine derivatization. All four batches of *Platycladi semen* and six batches of *Coicis semen* were contaminated by aflatoxins, with a positive detection rate of 100%. Moreover, the aflatoxin content in *Platycladi semen* and *Coicis semen* exceeded the legal standard limit, with an unqualified rate of 75% and 33%, respectively [76]. Kong et al. simultaneously determined the content of aflatoxins (AFB_1, AFB_2, AFG_1, AFG_2) and OTA in 13 batches of *Myristicae semen* using ultrasound-assisted solid–liquid extraction and immunoaffinity column clean-up combined with HPLC and on-line post-column photochemical derivatization–fluorescence detection (USLE-IAC-HPLC-PCD-FLD), and found that four batches of *Myristicae semen* were detected with contamination by AFs and one with OTA, the detection rate of AFB_1 was 30.8%, with the content levels of 0.73–16.31 μg/kg. Furthermore, at least two different mycotoxins co-occurred in three samples [24]. Yang et al. used immunoaffinity column

purification combined with HPLC-fluorescence detection (HPLC-FLD) to determine OTA in 57 batches of traditional Chinese medicines, such as *Licorice*, *Astragalus*, *Scutellaria baicalensis*, *Barley*, and *Angelica*, among others. The results showed that both moldy and non-moldy samples of traditional Chinese medicines may be contaminated by OTA, and the levels of contamination are different. A total of 23 of the visibly moldy samples and 2 of the not visibly moldy were contaminated with OTA levels in the range of 1.2–158.7 μg/kg and 2.5–5.6 μg/kg, respectively [33]. Yang et al. established a method of immunoaffinity column purification combined with HPLC-FLD to detect aflatoxins B_1, B_2, G_1, and G_2 in traditional Chinese medicines, such as *Herba ephedra*, *Platycladi semen*, *Corydalis rhizoma*, and *Coicis semen*, among others. The aflatoxin detection rate was 15.78%, with the content of the total aflatoxins ranging from 2.90 μg/kg to 32.18 μg/kg [77]. Zheng et al. determined AFs in 56 batches of 11 kinds of traditional Chinese medicines by HPLC, and found that AF contamination was more severe in *Bombyx batryticatus*, *Ziziphi spinosae semen*, *Coicis semen*, and *Sterculiae lychnophorae semen*; moreover, their group also suggested that samples with aflatoxins did not present apparent moldy symptom [78]. A total of 75 batches of traditional Chinese medicines were analyzed by the established method of immunoaffinity column purification–high performance liquid chromatography fluorescence detector (IAC-HPLC-FLD), the results showed that the positive detection rates of aflatoxins in *Platycladi seeds*, *Coix seed*, and *Cassia* were 77%, 29%, and 7%, respectively [79]. Wang et al. found the mycotoxin contamination level of AFB_1, AFB_2, and ZEN in *Coix seed* was different under different storage conditions (such as cryogenic seal, high temperature and humidity, aeration, and drying) by HPLC-FLD [80]. In brief, the contamination of mycotoxins in traditional Chinese medicines is related to the sample types or species.

3.2.2. Liquid Chromatography–Tandem Mass Spectrometry (LC-MS/MS)

High performance liquid chromatography–tandem mass spectrometry (HPLC-MS/MS) has become the mainstream method for the qualitative and quantitative analysis of mycotoxins and their metabolites in traditional Chinese medicines, due to its high separation performance in chromatography, its specificity and high sensitivity in mass spectrometry, and its simultaneous determination of multiple mycotoxins, which greatly improves the detection efficiency of samples. Moreover, the method of LC-MS/MS does not require too high a purity for test samples, and is suitable for large-scale sample screening and simultaneous determination of multi-component samples, which has certain advantages over samples with complex matrices especially.

Traditional Chinese medicines often contain various components, such as lipids, proteins, starch, tannins, and volatile oils, among other components. HPLC-MS/MS is more suitable for traditional Chinese medicines (rich in lipids, proteins, starch, and tannins) determination. Wu et al. employed HPLC-MS/MS to determine the traditional Chinese medicines that are rich in protein and lipid substrates, and found that the mycotoxin detection rate was higher in these traditional Chinese medicines, while the detection rate of mycotoxin was lower in traditional Chinese medicines containing high starch, volatile oils, and cellulose. It can be seen that the production of mycotoxins has a certain correlation with the composition of the matrix [1]. The complex matrix components can cause interferences to the detection; nevertheless, the advantages of LC-MS/MS can effectively reduce the matrix interference. Currently, numerous studies have reported on the simultaneous detection of multiple mycotoxins. It can be seen from Table 1 that there are multiple mycotoxin co-occurrences in a single kind of traditional Chinese medicines, such as *Myristicae semen* [81,82], *Eupolyphaga steleophaga* [41], *Angelica sinensis* [83], *Persicae semen* [84], *Coicis semen* [53], *Astragali radix* [85], *Notoginseng radix et rhizoma* [42,54], and *Platycladi semen* [54]; whereas LC-MS/MS can screen multiple mycotoxins simultaneously,

and will not be limited by the types of mycotoxin. Zhao et al. established a determination method for 10 mycotoxins using a multifunctional immune affinity column (multi-IAC) combined with HPLC-MS/MS for traditional Chinese medicine materials, and investigated a total of 30 samples (such as *Polygalae radix*, *Coicis semen*, and *Eupolyphaga steleophaga*) with mycotoxin contamination and co-occurrence. The results showed that all the samples in this study contained more than five mycotoxins, and AFB_1–AFs, AFB_1–DON, AFB_1–FBs, and AFB_1–T-2 are the most observed co-occurrences; a synergistic toxicity was also observed between AFB_1–OTA [62]. Li et al. established an analytical method for the determination of 16 mycotoxins in traditional Chinese medicine materials by isotope labeling–ultra performance liquid chromatography tandem mass spectrometry (UPLC-MS/MS), and found that 10 mycotoxins were detected in the 483 batches of samples, and ZEN has the highest detection rate, with an average content of positive samples of 71.2 μg/kg; among them, 3.11% of the samples exceeded the reference limit specified in the national standards [58]. Li et al. developed and established a UPLC-ESI-MS/MS method to simultaneously determine 12 mycotoxins (AFB_1, B_2, G_1, G_2, OTA, OTB, FB_1, FB_2, T-2 toxin, HT-2 toxin, DON, and ZEN) in *Polygoni multiflori radix*, and found that 8 kinds of mycotoxins, including AFB_1, AFG_2, FB_1, FB_2, OTA, OTB, T-2, and HT-2, were detected; their contents ranged approximately from 0.51 to 1643.2 μg/kg. Among them, AFB_1 in one batch of sample, with the content of 6.8 μg/kg, was beyond its limit standard [61]. Qin et al. determined 10 mycotoxins in 10 batches of *Dichondra micrantha UID* by UPLC-MS/MS, and the positive rate of the samples was 70% and 6 mycotoxins were detected; at the same time, the mycotoxins had a mixed contamination [86]. The types of mycotoxins contaminated in different traditional Chinese medicines are different [43,87,88]. The advantages of LC-MS/MS detection technology can meet the needs of the simultaneous determination of different kinds of toxins, and it is also a powerful technical means for confirming the mycotoxins in traditional Chinese medicines.

3.2.3. Rapid Detection Technology

To monitor and control the contamination by mycotoxins, rapid detection technology has become the research focus due to its relative simplicity, convenience, accuracy, and efficiency. Rapid detection techniques mainly include enzyme-linked immunosorbent assay (ELISA) and immunochromatography.

Enzyme-linked immunosorbent assay (ELISA) is a detection technique based on antigen and antibody specific binding reactions, which opens up a new field of rapid mycotoxin analysis. This technology has the advantages of simple pretreatment, rapid detection speed, strong specificity, high sensitivity, and convenience. ELISA can be used for the preliminary screening of mycotoxins in large numbers of samples, and is suitable for on-site rapid detection, both of which are commonly employed in the field. However, the method has some drawbacks, including numerous preparation steps, washing frequency, and long diffusion times required for antigen–antibody binding [89], thus it is time-consuming. The results have poor reproducibility, poor enzyme stability, and limited application in fast detection. Occasionally, it also produces false positive results [90]. Yang et al. determined AFB_1 in seven *Dendrobium candidum* samples with known concentrations by the ELISA method, and found that the results of AFB_1 content were basically consistent with those of HPLC [91]. Liu et al. determined the total AFs in *Ziziphi spinosae semen*, *Persicae semen*, *Hordei fructus germinatus*, *Polygalae radix*, *Cassiae semen*, and *Platycladi semen* by ELISA, and the results were basically consistent with those of HPLC [92]. Currently, using the ELISA method can specifically identify the contents of AFB_1 and the total AFs [93,94]. ELISA is commonly used for the detection of AFs, OTA, ZEN, and DON [90]. Among the established ELISA method for detecting mycotoxins in traditional Chinese medicines, AFB_1 is the most

mature and widely applied. The 2020 edition of the Chinese Pharmacopoeia first included the ELISA method, providing a technical option for the effective control of mycotoxins in traditional Chinese medicine materials.

Immunochromatographic assay (ICA) is a rapid immunoassay method that adopts colloidal gold or quantum dots as a labeled probe to detect multiple components by the specific binding reaction of antigen and antibody. IAC has the characteristics of rapid, simple, low cost, high sensitivity, and strong specificity, and is a research focus in the field of rapid detection. Huo et al. established a simultaneous and rapid detection method of mycotoxins (such as AFB_1, OTA, and ZEN) in *Ginseng*, *Astragalus*, and *Angelica* samples by fluorescent nanoparticle-based immunochromatography, and found that the coincidence rate of the results between the actual sample and the HPLC method was consistent [94]. Hou et al. employed colloidal gold immunochromatography to achieve the one-step rapid detection of FB_1, DON, and ZEN. The results were consistent with those of LC-MS/MS, which can verify the feasibility of this method [95]. However, the immunochromatographic detection technology also has some problems, such as poor stability, difficulty in long-term storage, and inaccurate quantification. Zhang et al. used IAC technology to capture and concentrate OTA in medicinal samples, and then determined it using ELISA technology. The two technologies were used in synergy for detection, and the sensitivity was significantly improved [96]. On one hand, by combining IAC with ELISA technology, it can improve the sensitivity of the method; on the other hand, it does not require that sensitivity to employ large-scale equipment to operate the detection. This method not only has good applicability, but is conducive to the preliminary screening of large quantities of samples, which can provide new ideas for the development of detection technology in the future.

3.2.4. Field Real-Time Monitoring Technology

Field real-time monitoring technologies include the spectroscopy method and sensor technology. The spectroscopic method is widely applied in the field of food for the determination of mycotoxins due to its unique advantages of no sample pretreatment, good reproducibility, and rapid detection. However, its application is rare in traditional Chinese medicines. The sensor method mainly includes immunosensors, aptamer sensors, enzyme sensors, and other sensors used for mycotoxin detection, all of which have the characteristics of rapid detection, simplicity and convenience, good specificity, high sensitivity, and low cost. They are suitable for the trace detection of small molecule substances and are an effective means for mycotoxin identification [97,98]. Fan et al. designed electrochemical biosensors for AFB_1 and OTA detection in Chinese herbal medicines [99]. Although the detection limit and recovery rate can meet the detection requirements of mycotoxins in Chinese herbal medicines, nevertheless, most sensors can only detect one toxin, and they are unable to meet the actual requirements of multiple mycotoxins at the same time. The rapid, convenient, low-cost, and high specificity of rapid detection technology has a driving effect on the preliminary screening of samples. Therefore, there are still some challenges in the practical application of these technologies.

Table 2. Detection technology and contamination status of mycotoxins in traditional Chinese medicines.

Detection Method	Sample	Pretreatment Technology	The Number of Toxins Detected	Toxin Species Detected	Ref.
LC (including fluorescence detector with post column photochemical derivatization, or post-column iodine derivatization)	*Ziziphi spinosae semen*, *Citri reticulatae pericarpium*, *Paeoniae radix alba*, *Angelica sinensis radix*, *Ophiopogonis radix*, *Schisandra chinensis fructus*, *Isatidis radix*, *Astragali radix*, *Bupleuri radix*, *Salviae miltiorrhizae radix et rhizoma*	IAC	4	AFB_1	[21]
	Sterculiae lychnophorae semen, *Ziziphi spinosae semen*, *Jujubae fructus*, *Scorpio*, *Sojae semen praeparatum*, *Arctii fructus*, *Euphorbiae semen*, *Platycladi semen*, *Coicis semen*, *Persicae semen*, *Citri reticulatae pericarpium*	IAC	4	AFB_1, AFB_2, AFG_1, AFG_2	[76]
	Myristicae semen	Ultrasound assisted solid–liquid extraction and IAC	5	AFB_1, AFB_2, AFG_1, AFG_2, OTA	[24]
	Astragali radix, *Scutellaria radix*, *Angelica sinensis radix*, *Glycyrrhizae radix et rhizoma*, *Morindae officinalis radix*, *Atractylodis rhizoma*, *Salviae miltiorrhizae radix et rhizoma*, *Panacis quinquefolii radix*	IAC	9	OTA	[33]
	Corydalis rhizoma, *Armeniacae semen amarum*, *Ephedrae herba*, *Platycladi semen*	IAC	4	Total AFs	[77]
	Jujubae fructus, *Angelica sinensis radix*, *Astragali radix*, *Bombyx batryticatus*, *Sterculiae lychnophorae semen*, *Ginseng radix et rhizoma*, *Notoginseng radix et rhizoma*, *Persicae semen*, *Coicis semen*, *Citri reticulatae pericarpium*, *Ziziphi spinosae semen*	IAC	4	Total AFs	[78]
	Platycladi semen, *Coicis semen*, *Cassiae semen*, *Codonopsis radix*	IAC	4	AFB_1, Total AFs	[79]
	Coicis semen	IAC	7	AFB_1, AFB_2, AFG_1, AFG_2, ZOL, ZEN	[80]
HPLC-MS/MS	*Myristicae semen*	IAC	12	OTA, AFB_1, AFB_2	[81]
	Myristicae semen	QuEChERS	21	AFB_1, AFB_2, AFG_1, AFG_2, AFM_1	[82]
	Eupolyphaga steleophaga	QuEChERS	9	FB_1, FB_2	[19]
	Angelica sinensis radix	SPE	9	AFB_1, AFB_2, AFG_1	[81]
	Persicae semen	QuEChERS	10	AFB_1	[82]
	Coicis semen	/	14	ZEN, AFB_1, AFB_2, DON, ST	[50]

Table 2. *Cont.*

Detection Method	Sample	Pretreatment Technology	The Number of Toxins Detected	Toxin Species Detected	Ref.
HPLC-MS/MS	*Astragali radix*, *Coicis semen*, *Eupolyphaga steleophaga*	SLE-SPE, QuEChERS	21	AFB_1, AFB_2, OTA, OTB, PA	[85]
	Notoginseng radix et rhizoma	SPE	26	FB_1	[42]
	Quisqualis fructus	SPE	22	AFB_1, AFB_2, AFM_1, OTA, OTB, ZEN	[54]
	Coicis semen, *Polygalae radix*, *Eupolyphaga steleophaga*, *Polygalae Radix*, *Eupolyphaga Steleophaga*	multi-IAC	10	AFB_1–AFs, AFB_1–FBs, AFB_1–DON, AFB_1–T-2, AFB_1–OTA	[85]
	Coicis semen, *Galli gigerii endothelium corneum*, *Hordei fructus germinatus*, *Persicae semen*, *Dioscoreae rhizoma*, *Poria*	multifunction clean-up columns	16	AFB_1, AFB_2, AFG_1, ZEN, DON, OTA, NIV, FB_1, FB_2, FB_3	[58]
	Polygoni multiflori radix	Modified QuEChERS	12	AFB1, AFG1, T-2, HT-2, OTA, OTB, FB_1, FB_2	[61]
	Dichondra micrantha Urb.	Modified QuEChERS	10	AFB_1, AFG_1, ZEN, OTA, DON, FB_1	[86]
	Glehniae radix, *Astragali radix*, *Codonopsis radix*	mPFC-QuEChERS	16	OTA, ST, 15-ACE	[87]
	Polygonati rhizoma, *Ophiopogonis radix*	SPE	10	FB_2, ZEN	[43]
	Lonicerae flos, *Puerariae lobatae radix*, *Hippophae fructus*	Accelerated solvent extraction (ASE)-QuEChERS	16	AFB_1, AFG_2, OTA, FB_1	[88]
Immunochromatographic detection technique	*Dendrobium candidum*	ELISA	1	AFB_1	[91]
	Ziziphi spinosae semen, *Persicae semen*, *Hordei fructus germinatus*, *Polygalae radix*, *Cassiae semen*, *Platycladi semen*	ELISA	4	Total AFs	[92]
	Ground beetle, *cockroach*, *Silkworm*, *Earthworm*	ELISA	1	AFB_1	[100]
	Jujubae fructus, *Nelumbinis semen*, *Coicis semen*, *Poria*, *Lilii bulbus*, *Euryales semen*, *Sojae semen nigrum*, *Pseudostellariae radix*, *Cinnamomi cortex*, *Phragmitis rhizoma*, *Dioscoreae rhizoma*, *Codonopsis radix*, *Crataegi fructus*, *Vignae semen*, *Prunellae spica*	ELISA	4	AFB_1, Total AFs	[91]

Table 2. *Cont.*

Detection Method	Sample	Pretreatment Technology	The Number of Toxins Detected	Toxin Species Detected	Ref.
Immunochromatographic detection technique	*Ginseng radix et rhizoma*, *Astragali radix*, *Angelica sinensis radix*	Lateral flow immunochromatography, LFIC	3	ZEN, AFB_1, OTA	[94]
	Lotus seed	ELISA	1	AFB_1	[101]
	Fallopia multiflora, *Codonopsis pilosula*, *Apricot kernel*, *Zingiber officinale*, *Wild jujube seed*, *Malt*, *Cassia obtusifolia*, *Red lotus seed*	immunochromatographic test strip (ICS)	6	AFB_1, ZEN, T-2	[102]
	Astragali radix, *Scutellariae radix*, *Glycyrrhizae radix et rhizoma*, *Atractylodis macrocephalae rhizoma*, *Bupleuri radix*, *Lonicerae japonicae flos*, *Phellodendri chinensis cortex*, *Chuanxiong rhizoma*, *Isatidis radix*, *Pinelliae rhizoma*, *Notoginseng radix et rhizoma*, *Polygonati rhizoma*, *polygoni multiflori radix*	IAC and ELISA	1	OTA	[96]
Field real-time monitoring technology	*Coicis semen*, *Jujubae fructus*, *Cassiae semen*	electrochemical biosensor	1	AFB_1	[98]
	Nelumbinis semen, *Panacis quinquefolii radix*	electrochemical biosensor	1	OTA	[99]

4. Comprehensive Prevention and Control Strategies for Mycotoxins in Traditional Chinese Medicines

Traditional Chinese medicines can be contaminated by mycotoxins under unfavorable conditions of growth, processing, storage, and transportation. The production of mycotoxins can be avoided by taking prevention and control strategies during the whole industry chain for the processing of traditional Chinese medicines. Thus, some strategies for controlling the mycotoxin contamination from the industrial chain need to be urgently proposed. Firstly, it is necessary to reduce the possibility of mycotoxin contamination from the source through to selecting the resistant variety of traditional Chinese medicines, and to standardize field operation technology and cultivation management procedures, to prevent traditional Chinese medicines from being infected by pathogenic fungi during planting.

To prevent and control the production of mycotoxins in traditional Chinese medicines throughout the entire process, the following steps should be taken. After harvesting, it is extremely crucial to keep traditional Chinese medicines dried in a timely manner, and to control the temperature and humidity to reasonable levels during stacking. At the same time, it is also necessary to standardize the drying, sterilization, and other operating methods during the processing of traditional Chinese medicines. Moreover, it is essential to strictly control the temperature, humidity, and the moisture content of products in storage and transportation. Furthermore, it is essential to select suitable packaging materials, and to establish processing and storage standards for traditional Chinese medicines.

In order to improve the quality and safety of traditional Chinese medicines, it is also necessary to strengthen the awareness of the relevant personnel in the prevention and control of mycotoxin contamination through training, which can improve the concept of standardized planting, the technical level and monitoring ability of planting personnel, as well as to collaborate with professionals from scientific research institutions to explore the prevention and control measures of mycotoxins.

5. Regulatory Recommendations for Mycotoxins Contamination in Traditional Chinese Medicines

5.1. Improve the Detection Standards

Mycotoxin contamination is one of the important risk factors affecting the quality and safety of traditional Chinese medicines. How to quickly, accurately, and efficiently detect mycotoxins in traditional Chinese medicines in large quantities has been the focus of researchers. Although the 2020 edition of the Chinese Pharmacopoeia has listed some detection methods for mycotoxins, it is still lacking for some research on mycotoxins in traditional Chinese medicines and their preparations. At present, an instrumental method is the main detection and analysis technology included in the Chinese Pharmacopoeia, which has some issues, such as high experimental costs, strong operability, high technical requirements for inspectors, and long inspection time. However, it is reliable in terms of the accuracy and stability of the qualitative and quantitative analysis. The field rapid detection and online monitoring technologies have great application prospects because of their characteristics of high sensitivity, good repeatability, and low cost. However, there are some challenges in practical applications. Currently, the rapid detection method has not been included in the Chinese Pharmacopoeia. Traditional Chinese medicines have complex matrix components, of which the chemical structure of some mycotoxins is similar. During the detection process, it is not only affected by matrix interference, but the chemical structures and chromatographic behaviors of most mycotoxins are similar, making it challenging for the efficient analysis of multiple mycotoxin residues in traditional Chinese medicines. It is urgent to establish an efficient, accurate, and reliable monitoring

system for multiple mycotoxins, and it is recommended to accelerate the formulation and improvement of relevant testing method standards.

5.2. Supplement Limit Regulations

At present, the limits of mycotoxins set for traditional Chinese medicines in the pharmacopoeia of many countries are relatively few, which cannot meet actual needs. The 2020 edition of the Chinese Pharmacopoeia only stipulates the limits for AFs and ZEN, and only includes 24 types of traditional Chinese medicines, which are far fewer than the actual number of medicinal materials found to be contaminated with mycotoxins. At the same time, the co-occurrence of multiple mycotoxins has not been given enough attention, and no limits have been established. The existing limit standards cannot meet the practical needs, making it difficult to evaluate and judge some test results for which there are no regulatory restriction standards on other traditional Chinese medicines susceptible to mycotoxins. Therefore, supervision work is also difficult to implement. It is suggested that temporary limit regulations should be set for traditional Chinese medicines susceptible to mycotoxin contamination, and for the mycotoxins frequently detected in traditional Chinese medicines. Afterwards, it is necessary to gradually solve the relatively lagging problem in the formulation of limit standards, and provide a basis for supervision and enforcement.

5.3. Strengthen Risk Monitoring Programs

At present, the monitoring data for mycotoxins in China are relatively scattered, and lack systematic monitoring. In addition, a database resource has yet to be formed. The monitoring of mycotoxin contamination levels in Chinese herbal medicine is relatively insufficient, and the role of safety supervision is limited. It is necessary to develop a reasonable risk monitoring plan for mycotoxins in traditional Chinese medicines, and to carry out routine monitoring in a directional manner. It is essential to establish a monitoring system and conduct a risk assessment, to identify high-risk varieties and mycotoxin factors, and to enhance risk warnings.

6. Conclusions and Future Perspectives

Mycotoxin contamination in traditional Chinese medicines is extremely universal and widespread, and poses severe health risks due to the multifaceted toxicity of these fungal metabolites. The most common mycotoxins in traditional Chinese medicines include aflatoxins, ochratoxins, zearalenone, deoxynivalenol, fumonisins and patulin, and T-2 toxin, which can affect the human exocrine and endocrine systems and suppress immune function, thus causing teratogenicity, carcinogenicity, and mutagenicity. Current detection methods for mycotoxins, including HPLC, HPLC-MS/MS, rapid detection technology, and field real-time monitoring technology, have played a crucial role in mycotoxin surveillance. However, these methods remain limited by high costs, variable sensitivity, false positives, or impractical field applicability. Thus, a rapid, accurate, highly-sensitive, cost-effective, and deployable, in a real-world setting, detection method for mycotoxins in traditional Chinese medicines still urgently needs to be developed. Moreover, it is essential to prevent and control the mycotoxin contamination from the source. Therefore, some suggestions should be put forward, such as to formulate uniform regulations for preharvest and postharvest, develop rapid and synchronous detection methods, increase legal limit regulations for common varieties of traditional Chinese medicines, as well as to strengthen public awareness of prevention, control, and management.

Author Contributions: Writing—original draft: Z.Y.; writing—review and editing: Z.Y., H.X., and Y.H.; project administration and supervision: Y.Z. project management: H.D. All authors have read and agreed to the published version of the manuscript.

Funding: This work was supported by the project of Lanzhou youth science and technology talent innovation project (grant number, 2023-QN-180), and Lanzhou science and technology development guidance plan project (grant number, 2023-ZD-234), Gansu provincial science and technology major special project (grant number, 23ZDFA013-1).

Institutional Review Board Statement: Not applicable.

Informed Consent Statement: Not applicable.

Data Availability Statement: The original contributions presented in this study are included in the article. Further inquiries can be directed to the corresponding author.

Conflicts of Interest: The authors declare no conflicts of interest.

References

1. Wu, R.S.; Ye, C.; Hu, Q.P.; Tong, P.Z.; Sun, D.M.; Chen, X.D.; Deng, C.Y.; Luo, W.H. Research progress on mycotoxin contamination of traditional Chinese medicine. *Guangdong Chem. Ind.* **2024**, *51*, 76–79.
2. Wei, G.F.; Guo, X.T.; Liang, Y.C.; Liu, C.S.; Zhang, G.Z.; Liang, C.L.; Huang, Z.X.; Zheng, Y.Q.; Chen, S.L.; Dong, L.L. Occurrence of fungi and mycotoxins in herbal medicines and rapid detection of toxin-producing fungi. *Environ. Pollut.* **2023**, *333*, 122082. [CrossRef]
3. Zheng, R.S.; Xu, H.; Wang, W.L.; Zhan, R.T.; Chen, W.W. Simultaneous determination of aflatoxin B_1, B_2, G_1, G_2, ochratoxin A and sterigmatocystin in traditional Chinese medicines by LC-MS-MS. *Anal. Bioanal. Chem.* **2014**, *406*, 3031–3039. [CrossRef]
4. Chen, X.Y.; Zhao, X.S.; Liu, X.M.; Yang, M.H. Composition and toxin-producing characteristics of exogenous contaminated fungi from *Codonopsis pilosula*. *Southwest China J. Agric. Sci.* **2021**, *34*, 66–70.
5. Su, C.Y.; Wei, J.C.; Hu, Y.J.; Luo, Y.; Gao, W.W. Optimization of isolation method of contamination fungi on three root medicinal herbs. *Mod. Chin. Med.* **2017**, *19*, 688–692.
6. Tan, H.X.; Zhou, H.Y.; Guo, T.; Zhou, Y.; Zhang, Q.; Zhang, Y.H.; Ma, L. Recent advances on formation, transformation, occurrence, and analytical strategy of modified mycotoxins in cereals and their products. *Food Chem.* **2023**, *405*, 134752. [CrossRef]
7. Zhang, X.; Wang, F.; Chen, H.P.; Liu, Y.P. Research status of fungal and mycotoxins pollution of Chinese medicinal materials. *World Sci. Technol. Mod. Tradit. Chin. Med.* **2015**, *11*, 2381–2388.
8. Alshannaq, A.; Yu, J.H. Occurrence, toxicity, and analysis of major mycotoxins in food. *Int. J. Environ. Res. Public Health* **2017**, *14*, 632–651. [CrossRef]
9. Huang, X.R.; Tang, X.Q.; Jallow, A.; Qi, X.; Zhang, W.; Jiang, J.; Li, H.; Zhang, Q.; Li, P.W. Development of an ultrasensitive and rapid fluorescence polarization immunoassay for ochratoxin A in rice. *Toxins* **2020**, *12*, 682. [CrossRef]
10. Zhu, B.; Ma, S.C.; Lin, R.C. A Survey of research on mycotoxins contamination of nature medicines. *Chin. Pharm. Aff.* **2009**, *23*, 1126–1132.
11. Omotayo, O.P.; Omotayo, A.O.; Mwanza, M.; Babalola, O.O. Prevalence of mycotoxins and their consequences on human health. *Toxicol. Res.* **2019**, *35*, 1–7. [CrossRef] [PubMed]
12. Da Rocha, M.E.B.; Da Chagas Oliveira Freire, F.; Feitosa Maia, F.E.; Florindo Guedes, M.I.; Rondina, D. Mycotoxins and their effects on human and animal health. *Food Control* **2014**, *36*, 159–165. [CrossRef]
13. Wang, L.L.; Kong, W.J.; Yang, M.H.; Han, J.P.; Chen, S.L. Safety issues and new rapid detection methods in traditional Chinese medicinal materials. *Acta Pharm. Sin. B* **2015**, *5*, 38–46. [CrossRef] [PubMed]
14. Qin, L.; Jiang, J.Y.; Zhang, L.; Dou, X.W.; Zhen, O.Y.; Wan, L.; Yang, M.H. Occurrence and analysis of mycotoxins in domestic Chinese herbal medicines. *Mycology* **2020**, *11*, 126–146. [CrossRef]
15. Wen, H.J.; Liao, Z.Q.; Jin, G.Y. Progress in detection methods for mycotoxin. *Drug Stand. China* **2023**, *24*, 465–475.
16. Nan, M.N.; Xue, H.L.; Bi, Y. Contamination, detection and control of mycotoxins in fruits and vegetables. *Toxins* **2022**, *14*, 309. [CrossRef]
17. Ostry, V.; Malir, F.; Toman, J.; Grosse, Y. Mycotoxins as human carcinogens-the IARC monographs classification. *Mycotoxin Res.* **2017**, *33*, 65–73. [CrossRef]
18. Wilson, D.M.; Mubatanhema, W.; Jurjevic, Z. Biology and ecology of mycotoxigenic *Aspergillus* species as related to economic and health concerns. *Adv. Exp. Med. Biol.* **2002**, *504*, 3–17.
19. Bennett, J.W.; Klich, M. Mycotoxins. *Clin. Microbiol. Rev.* **2003**, *16*, 497–516. [CrossRef]
20. Qu, X.M.; Wang, P.Y.; Zhu, K. Research progress in simultaneous detection of mycotoxins in traditional Chinese medicine. *SHS Web Conf.* **2023**, *179*, 05002. [CrossRef]
21. Yang, W.W.; Xiong, L.Y.; Wang, R.F.; Liu, Y.; Sun, Q.S.; Lei, Y.; Wang, Q. Determination of aflatoxin G_2, G_1, B_2, B_1 in 34 batches of Chinese herbs by HPLC associated with post column photochemical derivatization. *Res. Pract. Chin. Med.* **2013**, *27*, 43–47.

22. Wang, L.Z.; Wang, Z.; Gao, W.W.; Chen, J.; Yang, M.H.; Kuang, Y.; Huang, L.F.; Chen, S.L. Simultaneous determination of aflatoxin B_1 and ochratoxin A in licorice roots and fritillary bulbs by solid-phase extraction coupled with high-performance liquid chromatography-tandem mass spectrometry. *Food Chem.* **2013**, *138*, 1048–1054. [CrossRef] [PubMed]
23. Chen, A.J.; Jiao, X.L.; Hu, Y.J.; Lu, Z.H.; Gao, W.W. Mycobiota and mycotoxins in traditional medicinal seeds from China. *Toxins* **2015**, *7*, 3858–3875. [CrossRef]
24. Kong, W.J.; Liu, S.Y.; Qiu, F.; Xiao, X.H.; Yang, M.H. Simultaneous multi-mycotoxin determination in nutmeg by ultrasound-assisted solid-liquid extraction and immunoaffinity column clean-up coupled with liquid chromatography and on-line post-column photochemical derivatization fluorescence detection. *Analyst* **2013**, *138*, 2729–2739. [CrossRef] [PubMed]
25. Jafarzadeh, S.; Hadidi, M.; Forough, M.; Nafchi, A.M.; Khaneghah, A.M. The control of fungi and mycotoxins by food active packaging: A review. *Crit. Rev. Food Sci.* **2023**, *23*, 6393–6411. [CrossRef]
26. Zhu, Q.; Ma, Y.R.; Liang, J.B.; Wei, Z.W.; Li, M.; Zhang, Y.; Liu, M.; He, H.; Qu, C.F.; Cai, J.Q.; et al. AHR mediates the aflatoxin B_1 toxicity associated with hepatocellular carcinoma. *Signal Transduct. Target. Ther.* **2021**, *6*, 299. [CrossRef] [PubMed]
27. Ma, Z.K.; Zan, L.S. Advances in studies on hazards, detection methods and biodegradation of aflatoxins. *Prog. Vet. Med.* **2009**, *30*, 91–94.
28. Liu, Y.; Wu, F. Global burden of aflatoxin-induced hepatocellular carcinoma: A risk assessment. *Environ. Health Perspect.* **2010**, *118*, 818–824. [CrossRef]
29. Álvarez, M.; Rodríguez, A.; Peromingo, B.; Núñez, F.; Rodríguez, M. Enterococcus faecium: A promising protective culture to control growth of ochratoxigenic moulds and mycotoxin production in dry-fermented sausages. *Mycotoxin Res.* **2019**, *36*, 137–145. [CrossRef]
30. Cabañes, F.J.; Bragulat, M.R.; Castellá, G. Ochratoxin A producing species in the genus *Penicillium*. *Toxins* **2010**, *2*, 1111–1120. [CrossRef]
31. Malir, F.; Ostry, V.; Pfohl-Leszkowicz, A.; Malir, J.; Toman, J. Ochratoxin A: 50 years of research. *Toxins* **2016**, *8*, 191. [CrossRef] [PubMed]
32. Pitt, J.I. Toxigenic fungi and mycotoxins. *Br. Med. Bull.* **2000**, *56*, 184–192. [CrossRef] [PubMed]
33. Yang, L.; Wang, L.N.; Pan, J.Y.; Xiang, L.; Yang, M.H.; Logrieco, A.F. Determination of ochratoxin A in traditional Chinese medicinal plants by HPLC-FLD. *Food Addit. Contam. A* **2010**, *27*, 989–997. [CrossRef]
34. Zhang, W.; Yang, Z.; Jin, M.N.; Zhou, Y.; Liu, Y.W.; Wu, X.; Zhou, Y.H. Simultaneous determination of aflatoxin, zearalenone, and ochratoxin A in *Massa Medicata Fermentata* by high-performance liquid chromatography and fluorescence detection. *China Med. Pharm.* **2024**, *14*, 61–64.
35. Hohler, D. Ochratoxin A in food and feed: Occurrence, legislation and mode of action. *Eur. J. Nutr.* **1998**, *37*, 2–12.
36. Guan, X.; Feng, Y.C.; Suo, D.C.; Xiao, Z.M.; Wang, S.; Liang, Y.; Fan, X. Simultaneous determination of 11 mycotoxins in maize via multiple-impurity adsorption combined with liquid chromatography-tandem mass spectrometry. *Foods* **2022**, *11*, 3624. [CrossRef]
37. O'Brien, E.; Dietrich, D.R. Ochratoxin A: The continuing enigma. *Crit. Rev. Toxicol.* **2005**, *35*, 33–60. [CrossRef]
38. Mwabulili, F.; Xie, Y.L.; Li, Q.; Sun, S.M.; Yang, Y.H.; Ma, W.B. Research progress of ochratoxin a bio-detoxification. *Toxicon* **2023**, *222*, 107005. [CrossRef]
39. Gelderblom, W.C.A.; Marasas, W.F.O. Controversies in fumonisin mycotoxicology and risk assessment. *Hum. Exp. Toxicol.* **2012**, *31*, 215–235. [CrossRef]
40. Rheeder, J.P.; Marasas, W.F.O.; Vismer, H.F. Production of fumonisin analogs by *Fusarium* species. *Appl. Environ. Microbiol.* **2002**, *68*, 2101–2105. [CrossRef]
41. Li, Y.; Zhang, N.; Zhang, Y.F.; Sun, X.; Zhang, M.M.; Xie, Z.M. Simultaneous determination of nine mycotoxins in *Eupolyphaga steleophaga* and six kinds of Chinese medicinal preparations containing *Eupolyphaga steleophaga* by UHPLC-MS combined with QuEChERS. *Chin. Mod. Med.* **2022**, *24*, 142–146.
42. Wang, S.M.; Du, C.X.; Liu, X.X.; Liu, G.P.; Mao, D.; Liang, Y.F.; Huang, X.J.; Zhu, X.F.; Chen, K.; Ji, S. Simultaneous determination of 26 mycotoxins in *Notoginseng Radix et Rhizoma* by QuEChERS-ultra-high-performance liquid chromatograpty-tandem mass spectrometry. *World Chin. Med.* **2019**, *14*, 798–804.
43. Shen, L.; Tang, Y.; Chen, T.Z.; Cui, H.M.; Luo, H. Determination of 10 mycotoxins in *Polygonati rhizoma* and *Ophiopogonis radix* as a genuine regional drug of Sichuan by solid-phase extraction coupled with LC-MS/MS. *J. Pharm. Anal.* **2023**, *43*, 1369–1380.
44. Yang, L.M.; Su, J.M.; Lei, H.Y.; Ning, L.Z.; Zhao, Z.M. Progress in fumonisin research. *Prog. Vet. Med.* **2014**, *35*, 97–100.
45. Bhatnagar, D.; Yu, J.J.; Ehrlich, K.C. Toxins of filamentous fungi. *Chem. Immunol.* **2002**, *81*, 167–206.
46. Adejumo, T.O.; Hettwer, U.; Karlovsky, P. Survey of maize from southwestern Nigeria for zearalenone, alpha- and beta-zearalenols, fumonisin B_1 and enniatins produced by *Fusarium* species. *Food Addit. Contam.* **2007**, *24*, 993–1000. [CrossRef]
47. Yazar, S.; Omurtag, G. Fumonisins, trichothecenes and zearalenone in cereals. *Int. J. Mol. Sci.* **2008**, *9*, 2062–2090. [CrossRef]
48. Sohn, H.B.; Seo, J.A.; Lee, Y.W. Co-occurrence of Fusarium mycotoxins in mouldy and healthy corn from Korea. *Food Addit. Contam.* **1999**, *16*, 153–158. [CrossRef]

49. Briones-Reyes, D.; Gomez-Martinez, L.; Cueva-Rolon, R. Zearalenone contamination in corn for human consumption in the state of Tlaxcala, Mexico. *Food Chem.* **2007**, *100*, 693–698. [CrossRef]
50. Manova, R.; Ladenova, R. Incidence of zearalenone and fumonisins in Bulgarian cereal production. *Food Control.* **2009**, *20*, 362–365. [CrossRef]
51. Zhang, X.F.; Liu, W.K.; Logrieco, A.F.; Yang, M.G.; Ou-yang, Z.; Wang, X.; Guo, Q. Determination of zearalenone in tradtional Chinese medicinal plants and related products by HPLC-FLD. *Food Addit. Contam. A* **2011**, *28*, 885–893. [CrossRef] [PubMed]
52. Fang, J.H.; Pan, X.J.; Yin, F.; Zhang, S.F.; Gao, T.; Feng, T.H.; Zhang, C.J.; Cai, L.T.; Liang, Z.S.; Zhang, X.D. Simultaneous Determination of Eight Fungal Toxins in *Coix Seeds* by QuEChERS Ultra-High Performance Liquid Chromatography Tandem Mass Spectrometry. *J. Zhejiang Sci-Tech Univ.* **2025**, *53*, 254–262.
53. Zhang, H.X.; Jiang, W.K.; Yang, C.G.; Yuan, Q.S.; Guo, L.P.; Shen, Y.W.; Wen, N.T.; Zhang, J.Q.; Zhou, T. Contamination status and exposure risk of mycotoxins in *Coicis semen*. *China J. Chin. Mater. Med.* **2023**, *48*, 1491–1497.
54. Xu, L.; Huang, X.J.; Luo, X.; Dai, Q.; Wen, Y.S.; Zhao, X.Q. Simultaneous detection and risk assessment of 22 fungal toxins in *Quisqualis indica* L. using UHPLC-MS/MS. *Lishizhen Med. Mater. Med. Res.* **2021**, *32*, 984–987.
55. Mahato, D.K.; Devi, S.; Pandhi, S.; Sharma, B.; Maurya, K.K.; Mishra, S.; Dhawan, K.; Selvakumar, R.; Kamle, M.; Mishra, A.K.; et al. Occurrence, impact on agriculture, human health, and management strategies of zearalenone in food and feed: A review. *Toxins* **2021**, *13*, 92. [CrossRef]
56. McMullen, M.; Jones, R.; Gallenberg, D. Scab of wheat and barley: A re-emerging disease of devastating impact. *Plant Dis.* **1997**, *81*, 1340–1348. [CrossRef]
57. Mishra, S.; Srivastava, S.; Dewangan, J.; Divakar, A.; Kumar Rath, S. Global occurrence of deoxynivalenol in food commodities and exposure 581 risk assessment in humans in the last decade: A survey. *Crit. Rev. Food Sci.* **2020**, *60*, 1346–1374. [CrossRef]
58. Li, F.H.; Li, Z.H.; Yang, L.; Yuan, Y.C.; Wang, S.X.; Wang, A.X.; Li, W.; Zheng, F.J. Determination and analysis of 16 mycotoxins in medicinal and edible traditional chinese medicine. *Sci. Technol. Food Ind.* **2022**, *43*, 268–275.
59. Daenicke, S.; Keese, C.; Goyarts, T.; Döll, S. Effects of deoxynivalenol (DON) and related compounds on bovine peripheral blood mononuclear cells (PBMC) *in vitro* and *in vivo*. *Mycotox. Res.* **2011**, *27*, 49–55. [CrossRef]
60. Jiang, D.M.; Wang, H.; Wu, L.X.; Wang, L.Q.; Wang, D.; Wang, M. Research progress of deoxynivalenol in wheat. *J. Food Saf. Qual.* **2020**, *11*, 423–432.
61. Li, C.; Su, X.; Feng, W.H.; Li, R.R.; Liu, X.Q.; Li, P.Y.; Wang, Z.M. Simultaneous determination of 12 mycotoxins in *Polygoni Multiflori Radix* by UPLC-ESI-MS/MS combined with modified QuEChERS. *China J. Chin. Mater. Med.* **2016**, *41*, 1474–1479.
62. Zhao, D.T.; Gao, Y.J.; Zhang, W.J.; Bi, T.C.; Wang, X.; Ma, C.X.; Rong, R. Development a multi-immunoaffinity column LC-MS-MS method for comprehensive investigation of mycotoxins contamination and co-occurrence in traditional Chinese medicinal materials. *J. Chromatogr. B.* **2021**, *1178*, 122730. [CrossRef]
63. Dohnal, V.; Jezkova, A.; Jun, D.; Kuca, K. Metabolic pathways of T-2 Toxin. *Curr. Drug Metab.* **2008**, *9*, 77–82.
64. Zhou, G.X.; Zhang, H.X.; Hua, R.M. Research progress in toxicological effects and mechanism of T-2 toxin. *Asian J. Ecotoxicol.* **2011**, *6*, 121–128.
65. Paster, N.; Barkai-Golan, R. Mouldy fruits and vegetables as a source of mycotoxins: Part 2. *World Mycotoxin J.* **2008**, *4*, 385–396. [CrossRef]
66. Zhang, H.; Xi, J.H.; Liu, Z.G.; Chen, M.X.; Lu, Z.H.; Xue, H.L.; Bi, Y. Isolation and identification of pathogens causing blue mold of lanzhou lily during postharvest storage and control of disease and mycotoxin accumulation by ozone treatment. *J. Fungi* **2023**, *9*, 1091. [CrossRef] [PubMed]
67. Lv, B.R.; Yang, X.; Xue, H.L.; Nan, M.N.; Zhang, Y.; Liu, Z.G.; Bi, Y.; Shang, S.Q. isolation of main pathogens causing postharvest disease in fresh *Codonopsis pilosula* during different storage stages and ozone control against disease and mycotoxin accumulation. *J. Fungi* **2023**, *9*, 146. [CrossRef] [PubMed]
68. Xi, J.H.; Yang, D.Y.; Xue, H.L.; Liu, Z.G.; Bi, Y.; Zhang, Y.; Yang, X.; Shang, S.Q. Isolation of the main pathogens causing postharvest disease in fresh *Angelica sinensis* during different storage stages and impacts of ozone treatment on disease development and mycotoxin production. *Toxins* **2023**, *15*, 154. [CrossRef]
69. Zhou, Y.C.; Yang, M.H.; Xu, J. Research advance on patulin. *Guizhou Agric. Sci.* **2010**, *38*, 112–116.
70. Zhou, K.Q. Chemical detection methods for penicillin. *Foreign Med. Hyg. Vol.* **2001**, *28*, 29–32.
71. De Sales-Neto, J.M.; Rodrigues-Mascarenhas, S. Immunosuppressive effects of the mycotoxin patulin in macrophages. *Arch. Microbiol.* **2024**, *206*, 166. [CrossRef] [PubMed]
72. Sadok, I.; Stachniuk, A.; Staniszewska, M. Developments in the monitoring of patulin in fruits using liquid chromatography: An overview. *Food Anal. Methods* **2018**, *12*, 76–93. [CrossRef]
73. Zhao, S.R.; Xu, Y.X.; Xu, F.; Gao, W. High sensitive method for the detection of aflatoxins in extract from Chinese medicinal herb. *J. Cap. Med. Univ.* **2011**, *32*, 379–383.

74. Ran, C.C.; Chen, D.; Ma, H.Y.; Jiang, Y. Graphene oxide adsorbent based dispersive solid phase extraction coupled with multi-pretreatment clean-up for analysis of trace aflatoxins in traditional proprietary Chinese medicines. *J. Chromatogr. B* **2017**, *1044–1045*, 120–126. [CrossRef]
75. Zhang, X.H.; Liu, H.L.; Chen, J.M. Immunoaffinity column cleanup with liquid chromatography using post-column bromination for aflatoxins in medicinal herbs and plant extracts. *J. Chromatogr. Sci.* **2005**, *43*, 47–51. [CrossRef]
76. Yin, N.N.; Zhou, L.M.; Liu, J.T.; Hu, N.H. Simultaneous determination of content of four aflatoxins in 21 kinds of traditional Chinese medicine decocting pieces by high performance liquid chromatography. *Shandong J. Tradit. Chin.* **2019**, *38*, 1067–1071.
77. Yang, M.H.; Chen, J.M.; Zhang, X.H. Immunoaffinity column clean-up and liquid chromatography with post-column derivatization for analysis of aflatoxins in traditional Chinese medicine. *Chromatographia* **2005**, *62*, 499–504. [CrossRef]
78. Zheng, R.; Mao, D.; Wang, S.M.; Wang, K.; Ji, S. Determination of aflatoxin G_2, G_1, B_2, B_1 in eleven kinds of Chinese herbs by HPLC. *Chin. J. Pharm.* **2010**, *41*, 368–372.
79. Shan, L.N.; Wang, Y.D.; Dou, X.W.; Duan, Y.P.; Yang, S.M.; Wang, J.H.; Yang, M.H. Comparative study on the distribution of aflatoxins contamination status in four commonly used Chinese herbal pieces. *Mod. Tradit. Chin. Med. Materia-World Sci. Technol.* **2020**, *22*, 3718–3725.
80. Wang, X.H.; Dou, J.Y.; Xiao, Z.G. Study on the content changes of fungal toxin in *YiYiRen* under different storage conditions. *West. J. Tradit. Chin. Med.* **2018**, *31*, 20–23.
81. Mao, D.; Ye, L.L.; Wang, S.M.; Liu, X.X.; Chen, K.; Ji, S. Simultaneous determination of 12 mycotoxins in *Myristicae Semen* by LC-MS /MS. *China Pharm.* **2020**, *23*, 1311–1315.
82. Zhao, X.S.; Liu, D.; Zhang, L.; Zhou, Y.K.; Yang, M.H. Development and optimization of a method based on QuEChERS-dSPE followed by UPLC-MS/MS for the simultaneous determination of 21 mycotoxins in nutmeg and related products. *Microchem. J.* **2021**, *168*, 106499. [CrossRef]
83. Li, Y.F.; Jiao, J.; Huang, Z.; Xiao, F.; Huang, Y.F.; Wang, Q.; Liu, L.L.; Zhang, H. Simultaneous determination of 9 mycotoxins in *Angelica sinensis* by ultra high performance liquid chromatography-tandem mass spectrometry. *J. Cold-Arid Agri. Sci.* **2024**, *3*, 974–980.
84. Bao, H.Y.; Xiao, Z.G.; Xu, Q. Determination of 10 mycotoxins in *Peach kernel* by high performance liquid chromatography tandem mass spectrometry. *Cold Drought Agric. Sci.* **2024**, *2*, 72–76.
85. Wang, Y.; Zhang, C.; Zhang, L.; Zhao, M.; OuYang, Z.; Yang, M. A comprehensive strategy for screening and exploring multi-class mycotoxins contamination status in Astragali Radix. *Microchem. J.* **2020**, *158*, 105294. [CrossRef]
86. Qin, D.J.; Qiu, Y.; Wang, H.H.; Li, P.; Huang, H.L. Establishment of UPLC-MS/MS determination of 10 mycotoxins in *Dichondra micrantha Ulb*. *J. Southwest Minzu Univ. (Nat. Sci. Ed.).* **2023**, *49*, 530–536.
87. Xie, S.M.; Gu, S.Q.; Gu, L.H.; Li, J.M. Determination of 16 mycotoxins in three radix and rhizome Chinese herbal medicines by mPFC-QuEChERS with UPLC-MS/MS. *J. Instrum. Anal.* **2024**, *43*, 1003–1010.
88. Fang, Z.; Qu, L.; Gu, S.Q.; Chen, R.H.; Li, Y.; Deng, X.J.; Guo, D.H.; Feng, F. Determination of 16 mycotoxins in drug and food homologous products by ultra performance liquid chromatography-tandem mass spectrometry combined with accelerated solvent extraction and QuEChERS. *Chin. J Chromatogr.* **2020**, *38*, 782–790.
89. Zhang, Q.; Sun, Q.; Hu, B.S.; Shen, Q.; Yang, G.; Liang, X.; Sun, X.; Liu, F.Q. Development of a sensitive ELISA for the analysis of the organophosphorous insecticide fenthion in fruit samples. *Food Chem.* **2008**, *106*, 1278–1284. [CrossRef]
90. Urusov, A.E.; Zherdev, A.V.; Petrakova, A.V.; Sadykhov, E.G.; Koroleva, O.V.; Dzantiev, B.B. Rapid multiple immunoenzyme assay of mycotoxins. *Toxins* **2015**, *7*, 238–254. [CrossRef]
91. Yang, D.S.; Wang, L.L.; Ma, F.R.; Ye, Y.P.; Bi, Y.N.; Wang, L.X. Determination of aflatoxin B_1 in *Dendrobium candidum* of Yunnan province by enzyme linked immunosorbent assay method. *J. Food Saf. Qual.* **2020**, *11*, 7052–7056.
92. Liu, R.; Zhao, X.Y.; Mao, W.W.; Wang, Y.D.; Feng, H.; Zhang, D.H.; Zhang, L.L. Rapid detection of total aflatoxin in traditional herbal medicines by ELISA. *Chin. Tradit. Pat. Med.* **2020**, *42*, 2376–2381.
93. Zhou, Y.Q.; Xiong, Y.; Wu, S.Q. Study on the determination of aflatoxin in traditional Chinese medicine slices with the homology of medicine and food by enzyme linked immunosorbent assay. *Mod. Food.* **2022**, *28*, 163–168.
94. Huo, B.F.; Ma, B.; Li, J.L.; Mei, Q.; Zhou, Y.X.; Zhang, M.Z. Simultaneous and rapid detection of three mycotoxins in food and medicine homologous materials by fluorescent nanoparticle-based immunochromatography. *Mod. Food Sci. Technol.* **2024**, *40*, 227–235.
95. Hou, S.L.; Ma, J.J.; Cheng, Y.Q.; Wang, H.G.; Sun, J.H.; Yan, Y.X. One step rapid detection of fumonisin B_1, dexyonivalenol and zearalenone in grains. *Food Control* **2020**, *117*, 107107. [CrossRef]
96. Zhang, Y.Z.; Zhang, X.Z.; Yuan, Y.W.; Zhang, W. Detection of ochratoxin A using immunoaffinity chromatography combined with enzyme-linked immunosorbent assay. *Food Sci.* **2024**, *45*, 257–264.
97. Sun, C.N.; Liao, X.F.; Jia, B.Y.; Shi, L.C.; Zhang, D.K.; Wang, R.L.; Zhou, L.D.; Kong, W.J. Development of a ZnCdS@ZnS quantum dots-based label-free electrochemiluminescence immunosensor for sensitive determination of aflatoxin B_1 in lotus seed. *Microchim. Acta* **2020**, *187*, 236. [CrossRef]

98. Wei, X.H.; You, J.K.; Wang, T.Y.; Yu, Y.Y.; Zhang, H.Y. Electrochemical biosensor for rapid detection of AFB_1 in Chinese herbal medicine. *Chin. J. Anal. Lab.* **2021**, *40*, 130–134.
99. Fan, S.; Huang, R.F.; Mao, W.W.; Zhang, H.Y. Construction of electrochemical aptamer sensor for rapid detection of OTA in Chinese herbal medicine. *Chin. J. Anal. Lab.* **2024**, *43*, 18–23.
100. Wang, C.J.; Zhang, L.; Luo, J.Y.; Qin, J.A.; Jiang, J.Y.; Qin, L.; Zhao, Z.G.; Yang, S.H.; Yang, M.H. Development of a sensitive indirect competitive enzyme-linked immunosorbent assay for high-throughput detection and risk assessment of aflatoxin B_1 in animal-derived medicines. *Toxicon* **2021**, *197*, 99–105. [CrossRef]
101. Chu, X.F.; Dou, X.W.; Kong, W.J.; Yang, M.H.; Zhao, C.; Zhao, M.; Ou-yang, Z. Contamination level of aflatoxin B_1 in *Lotus seeds* rapid screening by indirect competitive ELISA method. *China J. Chin. Mater. Med.* **2015**, *40*, 704–709.
102. Zhang, J.Y.; Li, X.J.; Xie, J.H.; Huang, Z.B. Rapid and simultaneous detection of aflatoxin B_1, zearalenone, and T-2 toxin in medicinal and edible food using gold immunochromatographic test strip. *Foods* **2023**, *12*, 633. [CrossRef] [PubMed]

Disclaimer/Publisher's Note: The statements, opinions and data contained in all publications are solely those of the individual author(s) and contributor(s) and not of MDPI and/or the editor(s). MDPI and/or the editor(s) disclaim responsibility for any injury to people or property resulting from any ideas, methods, instructions or products referred to in the content.

MDPI AG
Grosspeteranlage 5
4052 Basel
Switzerland
Tel.: +41 61 683 77 34

Journal of Fungi Editorial Office
E-mail: jof@mdpi.com
www.mdpi.com/journal/jof



Disclaimer/Publisher's Note: The title and front matter of this reprint are at the discretion of the Guest Editors. The publisher is not responsible for their content or any associated concerns. The statements, opinions and data contained in all individual articles are solely those of the individual Editors and contributors and not of MDPI. MDPI disclaims responsibility for any injury to people or property resulting from any ideas, methods, instructions or products referred to in the content.





Academic Open
Access Publishing

mdpi.com

ISBN 978-3-7258-8170-3